BIOLOGICAL APPLICATIONS OF CHEMICAL PRINCIPLES: FROM AMINOGLYCOSIDE ANTIBIOTIC DERIVATIZATION TO GLYCOSIDASE AND GLYCOSYLTRANSFERASE ACTIVE SITE ANALYSIS

by

JONATHAN CHARLES KENNETH QUIRKE

(Under the Direction of David Crich)

ABSTRACT

Aminoglycosides have been widely recognized as critically important antimicrobials for treatment of multidrug resistant bacteria. As presented in Chapter 1, though effective against a wide range of Gram-positive and Gram-negative bacteria, aminoglycosides can induce reversible nephrotoxicity and irreversible ototoxicity and can be deactivated by aminoglycoside modifying enzymes (AMEs).

Chapter 2 details the synthesis of 5-*O*-furanosylated apramycin derivatives, prepared with the goal of increasing antibacterial activity while circumventing susceptibility to the aminoglycoside phosphoryl transferases (APH(3’,5’’)), all while maintaining the parent’s low toxicity. Ribosyl derivatives performed well compared to apramycin but suffered from APH(3’,5’’) susceptibility. Erythrosyl and 5-amino-5-deoxy-β-D-ribosyl derivatives overcame this hurdle and displayed greater activity and comparable toxicity to the parent. The most promising derivative, 5-*O*-[5-Amino-3-*O*-(2-aminoethyl)-5-deoxy-β-D-ribofuranosyl]apramycin, exhibited twofold decreased toxicity in cochlear explant studies and 2.5-fold increased efficacy in vivo compared to apramycin, and can be synthesized from the parent in six linear steps.

Chapter 3 discusses systematic 5’’-modifications of multiple 4,5-aminoglycosides in an attempt to generalize the results observed among the apralogs. Though most modifications were well-tolerated in neomycin, 5’’-deoxy, 5’’-amino, 5’’-acetamido, and erythrosyl derivatives of paromomycin, ribostamycin, and propylamycin all exhibited strongly reduced antibacterial activity. Installation of a 5’’-formamide, however, resulted in increased activity and reduced toxicity. These results will aid in the design of next-generation aminoglycoside antibiotics.

Chapter 4 presents the glycosylation reaction, a nucleophilic substitution between a glycosyl donor and acceptor and examines how glycosyl donor reactivity is significantly influenced by side chain conformation, where the most reactive *gauche,gauche* (*gg*) conformation strongly stabilizes the transition state. Chapter 5 illustrates through crystallographic analysis that glycosidases and glycosyltransferases have evolved to maximize reactivity of their substrates through side chain restriction. Glucoside, mannoside, and ulosonide processing enzymes strongly favor the most reactive *gg* conformation, while α-galactoside processing enzymes enforce the second-most reactive *gauche,trans* (*gt*) conformation, and β-galactoside processing enzymes favor the least reactive *trans,gauche* (*tg*) conformation. Some glycosidases maximize reactivity by binding their substrates in a superarmed conformation that strongly stabilizes the transition state. The results of this study will pave the way for the design of improved conformationally-locked inhibitors of carbohydrate-processing enzymes.

INDEX WORDS: Aminoglycoside antibiotics, antibiotic resistance, glycosylation, side chain conformation, glycoside hydrolases, glycosyltransferases

BIOLOGICAL APPLICATIONS OF CHEMICAL PRINCIPLES: FROM AMINOGLYCOSIDE ANTIBIOTIC DERIVATIZATION TO GLYCOSIDASE AND GLYCOSYLTRANSFERASE ACTIVE SITE ANALYSIS

by

JONATHAN CHARLES KENNETH QUIRKE

B.A., Oberlin College, 2016

A Dissertation Submitted to the Graduate Faculty of The University of Georgia in Partial Fulfillment of the Requirements for the Degree

DOCTOR OF PHILOSOPHY

ATHENS, GEORGIA

2021

BIOLOGICAL APPLICATIONS OF CHEMICAL PRINCIPLES: FROM AMINOGLYCOSIDE ANTIBIOTICS DERIVATIZATION TO GLYCOSIDASE AND GLYCOSYLTRANSFERASE ACTIVE SITE ANALYSIS

by

JONATHAN CHARLES KENNETH QUIRKE

Major Professor: David Crich

Committee: Rob Woods
Geert-Jan Boons

Electronic Version Approved:

Ron Walcott
Vice Provost for Graduate Education and Dean of the Graduate School
The University of Georgia
December 2021

DEDICATION

I dedicate this work to my parents, Esther Katzeff and Martin Quirke, and to my fiancée Aditi Gupta, for their endless love, support, and encouragement.

ACKNOWLEDGEMENTS

I would like to start by expressing my sincere gratitude to my advisor, Dr. David Crich, for his passion, patience, guidance, compassion, and support. He has always pushed me to live up to my potential and has hugely helped me prepare for obstacles to come. I genuinely cannot thank him enough.

I would like to thank our collaborators, Drs. Andrea Vasella and Erik Böttger, for their critical contributions to our work and their incredibly useful advice, as well as my committee members, Drs. Rob Woods and Geert-Jan Boons, for their time and their input. I would also like to acknowledge each of the members of the Crich lab with whom I overlapped: Dr. Oskar Popik, Dr. Suresh Dharuman, Dr. Takayuki Kato, Dr. Vikram Sarpe, Dr. Parasuraman Rajasekaran, Dr. Govind Singh, Dr. Kapil Upadhyaya, Dr. Rahul Bagul, Dr. Anura Wickramasinghe, Dr. Yagya Subedi, Dr. Santanu Jana, Dr. Samir Ghosh, Dr. Amr Sonousi, Dr. Harsha Amarasekara, Dr. Girish Sati, Dr. Philip Adero, Dr. Peng Wen, Dr. Bibek Dhakal, Dr. Sandeep Dhanju, Dr. Guanyu Yang, Dr. Xiaoxiao Liao, Dr. Mike Pirrone, Dr. Philemon Ngoje, Dr. Mohammed Hawsawi, Tim McMillan, Sameera Jayanath, Emmanuel Onobun, Asiri Hettikankanamalage, Jarvis Hill, Daniil Ahiadorme, Po-Sen Tseng, Courtney Kondor, Rukshana Jayawardana, Reza Samarbakhsh, Riku Ogasahara, Nicolas Osorio, Dean Jarois. In particular, I am genuinely grateful for Dr. Mike Pirrone for going above and beyond to help his coworkers and keep things running smoothly.

Finally, I would like to thank my father, Martin Quirke, for his ever-helpful advice, my mother, Esther Katzeff, for her patience and kindness, and my fiancée, Aditi Gupta, for her genuinely endless support. Thank you all.

TABLE OF CONTENTS

Page

LIST OF TABLES

Page

LIST OF FIGURES

Page

LIST OF SCHEMES

Page

LIST OF ABBREVIATIONS

A	Adenine
AA	Anchimeric Assistance
AAC	Aminoglycoside Acetyltransferase
Ac	Acetyl
AGA	Aminoglycoside Antibiotic
AME	Aminoglycoside Modifying Enzyme
ANT	Aminoglycoside Nucleotidyltransferase
APH	Aminoglycoside Phosphotransferase
Apra	Apramycin
A-Site	Aminoacyl Site
Ax	Axial
BAIB	Bis(acetoxy)iodobenzene
Bn	Benzyl
Bz	Benzoyl
C	Cytosine
CAZy	Carbohydrate Active Enzymes Database
Calcd	Calculated
CGTase	Cyclodextrin Glycosyltransferase
CIP	Contact Ion Pair

CMP	Cytidine Monophosphate
COSY	Correlation Spectroscopy
Cyt14	Human Cytosolic Decoding A-Site
DCM	Dichloromethane
DMAP	4-Dimethylaminopyridine
DMF	Dimethylaminoformamide
DNP	2,4-Dinitrophenyl
DOS	Deoxystreptamine
DNA	Deoxyribonucleic Acid
EDPI	Energy-Dependent Phase I
EDPII	Energy-Dependent Phase II
ENABLE	European Gram-Negative Antibacterial Engine
Eq	Equatorial
ESI	Electrospray Ionization
E-Site	Exit Site
ESKAPE	Pathogenic *Enterococcus faecium, Staphylococcus aureus, Klebsiella pneumoniae, Acinetobacter baumannii, Pseudomonas aeruginosa,* and *Enterobacter cloacae*
Et	Ethyl
FucT V	Human α-1,3-Fucosyltransferase V
G	Guanine
GalT	Galactosyltransferase
gg	Gauche,gauche

GH	Glycoside Hydrolase
GlcNAc	*N*-Acetylglucosamine
GT	Glycosyltransferase
gt	Gauche,trans
HEWL	Hen Egg White Lysozyme
HMBC	Heteronuclear Multiple Bond Correlation
HMDS	Hexamethyldisilazane
HRMS	High Resolution Mass Spectrometry
HSQC	Heteronuclear Single Quantum Coherence
Hν	Light
IC_{50}	Half-Maximal Inhibitory Concentration
IMI	Innovative Medicines Initiative
iPr	Isopropyl
KIE	Kinetic Isotope Effect
LD_{50}	Median Lethal Dose
MDR	Multidrug Resistant
Me	Methyl
MIC	Minimum Inhibitory Concentration
mRNA	Messenger Ribonucleic Acid
MRSA	Methicillin-Resistant *Staphylococcus aureus*
N_3	Azide
NDM-1	New Delhi Metallo-β-lactamase 1
NGO	Non-Governmental Organization

NGP	Neighboring Group Participation
NIS	*N*-Iodosuccinimide
NMR	Nuclear Magnetic Resonance
OHC	Outer Hair Cell
PDB	Protein Data Bank
Ph	Phenyl
Phth	Phthalimide
Ppm	Parts Per Million
Pr	*n*-Propyl
P-Site	Peptidyl Site
Py	Pyridine
RNA	Ribonucleic Acid
RND	Resistance Nodulation Division
ROS	Reactive Oxygen Species
rRNA	Ribosomal Ribonucleic Acid
RSCC	Real Space Correlation Coefficient
S_N1	Unimolecular Nuleophilic Substitution
S_N2	Bimolecular Nucleophilic Substitution
SSIP	Solvent-Separated Ion Pair
T6P	Trehalose-6-phosphate
TBS	*Tert*-butyldimethylsilyl
tBu	*Tert*-butyl
*t*dodec	*Tert*-dodecyl

TEMPO	(2,2,6,6-Tetramethylpiperidin-1-yl)oxyl
Tf	Triflyl
TFA	Trifluoroacetyl
THF	Tetrahydrofuran
tg	Trans,gauche
TLC	Thin Layer Chromatography
TMS	Trimethylsilyl
Tr	Triphenylmethyl
Tris	2,4,6-Triisopropylbenzenesulfonyl
Ts	*p*-Toluenesulfonyl
pTSA	*p*-Toluenesulfonic Acid
tRNA	Transfer Ribonucleic Acid
U	Uracil
UDP	Uridine Diphosphate
WHO	World Health Organization

CHAPTER 1

INTRODUCTION TO AMINOGLYCOSIDE ANTIBIOTICS

1.1. Introduction to Antibiotic Resistance

Antibiotic resistance is currently one of the most prominent threats to public health, with multidrug-resistant (MDR) bacteria responsible for over 2.8 million infections and over 35,000 deaths per year.[1] Despite the prominent mortality rates and tremendous contagious potential of these bacteria, antibiotic development by the pharmaceutical industry has remained comparatively stagnant, with only 37 new antibiotics developed between 2000 and 2020.[2, 3] In large part, this neglect stems from a lack of associated financial profit: not only do antibiotics become less potent over time due to the emergence of bacterial resistance mechanisms, but also the constantly changing regulations for market approval, sales limits, and inherently lower duration of use have led the pharmaceutical industry to favor other, more profitable types of drugs.[4] To combat the resistance crisis in spite of the above financial drawbacks, government agencies have implemented a series of regulations and strategies to address the root causes of resistance proliferation and mitigate further spread of bacteria, such as minimization of excess or unnecessary prescription of drugs and optimization of treatment regimens.[5, 6] However, these efforts do not preclude the critical need for additional drug candidates.

In light of the lack of support offered by the pharmaceutical industry for antibiotic development, it has fallen to academics and start-up companies to fill the void, with the support of non-governmental organizations (NGOs).[7] One such example is the Innovative Medicines

Initiative (IMI), an independent funding agency whose goal is to develop next-generation therapeutics such as vaccines.[8] IMI is responsible for foundation of the European Gram-Negative Antibacterial Engine (ENABLE), which seeks to develop antimicrobials for the treatment of Gram-negative pathogens.[9] Other independent funding sources include CARB-X[10] and GARDP,[11] nonprofits dedicated to developing new therapeutics for combating antibiotic resistant bacteria.

Antibiotics can be divided into four classes based on their mechanism of action: DNA replication inhibitors such as quinolones, cell wall synthesis inhibitors such as β-lactams, folic acid synthesis inhibitors such as sulfonamides, and protein synthesis inhibitors such as aminoglycoside antibiotics (AGAs).[12] Among these, AGAs present the distinct benefit of high activity against both Gram-negative bacteria, which have a characteristic protective lipopolysaccharide membrane, and Gram-positive bacteria, which lack this membrane. Gram-negative bacteria constitute the majority of MDR bacteria classified as threats by the WHO and are widely considered difficult to treat, so much so that no new antibiotics developed in the past decade target these bacteria.[1, 13-15] AGAs were first discovered in 1944 by Selman Waksman, who isolated the drug streptomycin **1** (Figure 1.1) and successfully implemented it in treatment of the formerly incurable tuberculosis.[16, 17] Though these drugs come with the significant drawbacks of reversible nephrotoxicity and irreversible ototoxicity and as such have suffered significant losses in the antibiotics market,[18] AGAs are still classed by the WHO as critically important antimicrobials[19] and have been the subject of renewed interest as targets for derivatization and conjugation to increase activity and decrease toxicity.[20-25]

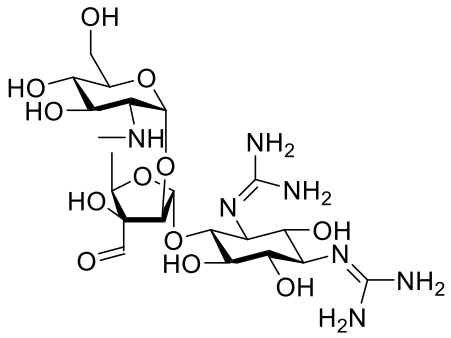

1

Figure 1.1. Structure of streptomycin

1.2. Aminoglycoside Antibiotic Structure

Aminoglycoside antibiotics are characterized by a central aminocyclitol ring, usually 2-deoxystreptamine (DOS) **2** or streptidine **3**, and are predominantly divided into two classes based on their substitution pattern: the 4,5-disubstituted series, exemplified by paromomycin **4** and neomycin **5**, and the 4,6-disubstituted series, exemplified by the gentamicins **6**. Among the few exceptions to the above trends is the promising *O*-4-monosubstituted aminoglycoside apramycin **7** which bears a bicyclic dialdose ring at *O*-4 instead of a standard pyranoside (Figure 1.2). The suffix of the drug indicates its natural source, with *micin* designating isolation from bacteria of the genus *Micromonospora* and *mycin* designating isolation from bacteria belonging to the genus *Streptomyces*. While the AGAs used in the clinic today predominantly belong to the 4,6-series, there is a great deal of interest in developing more drug candidates in the 4,5-series.

Due to both their low molecular weight and high polarity, AGA bioavailability through the gastrointestinal tract via oral intake is quite low, with < 1% absorption into the bloodstream, leaving intravenous injection as the preferred method of delivery for these drugs.[26]

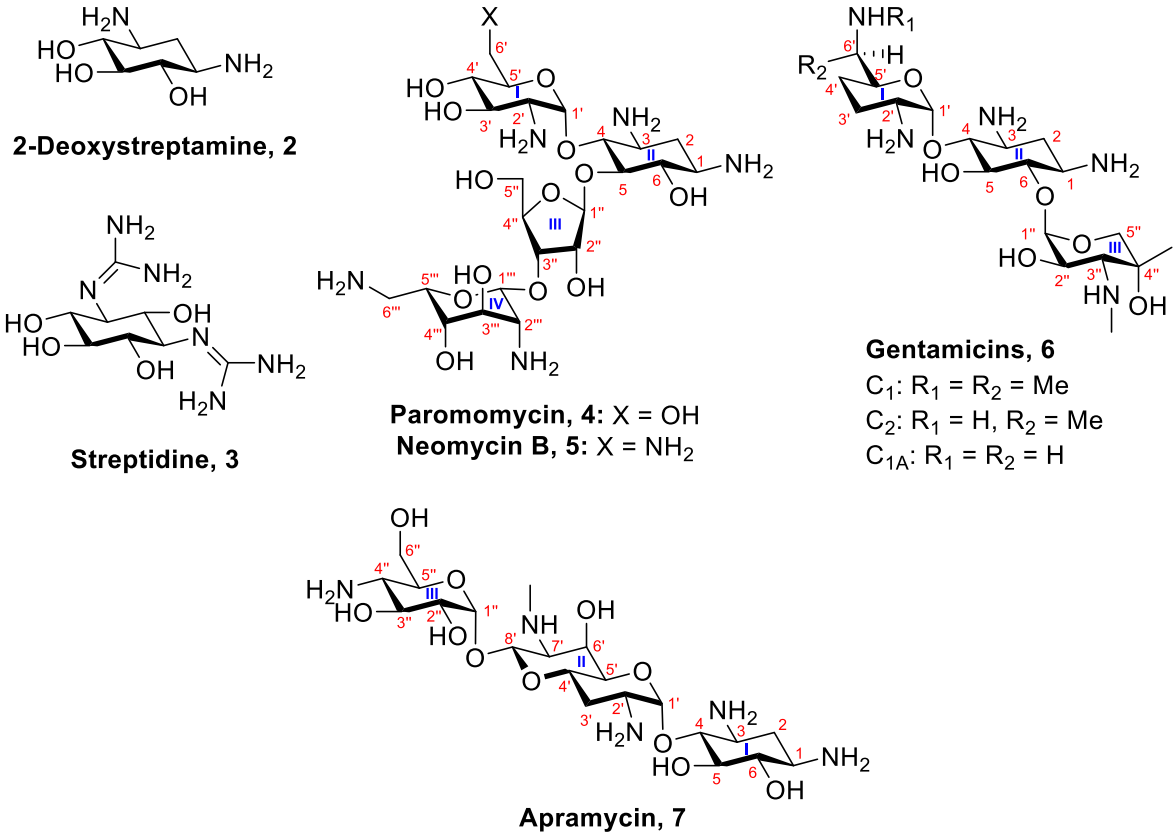

Figure 1.2. Representative AGA structures

1.3. AGA Mechanism of Action

One key advantage of AGAs is that their mechanism of action is well understood, meaning that rational modifications to the parent can be readily designed to achieve greater activity and/or lower toxicity. Uptake into the cell begins with electrostatic interaction between the positively charged AGA and the negatively charged lipopolysaccharides of the cell membrane. After initial attraction, the drug then slowly enters the cell during energy-dependent phase I (EDPI) uptake. The exact mechanism of this phase is still a subject of debate, as the drug can enter the cell either through diffusion across the cell membrane or through porins. In any case, this uptake phase is dependent on cellular respiration, rendering AGAs ineffective against anaerobic bacteria. After

entry into the cell, the drug undergoes energy-dependent phase II (EDPII) uptake, wherein the AGA rapidly binds to the 30S subunit of the bacterial ribosome and inhibits protein synthesis.[27, 28]

Protein synthesis can be broadly split into two distinct phases: transcription and translation. During transcription, messenger RNA (mRNA), which acts as a sequencing code for the protein, is synthesized from DNA in the nucleus. The newly generated mRNA is then extruded from the nucleus and subsequently binds to the two ribosomal subunits, denoted 50S and 30S in prokaryotes and 60S and 40S in eukaryotes, to initiate translation.[29] Once the ribosome-mRNA complex is formed, amino acid-bound transfer RNA (tRNA) can bind to individual sequences of three nucleotides in mRNA known as codons in the first of three ribosomal decoding sites known as the aminoacyl- (A-) site. Given that each tRNA molecule is bound to a specific amino acid based on a three-nucleotide binding sequence known as an anticodon, amino acid sequence fidelity is ordinarily well-maintained. tRNA binding causes the nucleobases A1492 and A1493 in the A-site to flip outwards, which through subsequent enforcement of additional conformational changes causes the tRNA-mRNA complex to shift to the adjacent peptidyl- (P-) site. This shift allows a second amino acid-bearing tRNA molecule to bind to the now empty A-site.[30] The P-site-bound tRNA then transfers its amino acid (or amino acid sequence) to that of the newly attached tRNA at the A-site, generating a lengthening polypeptide chain. After amino acid transfer, the P-site-bound tRNA shifts to the exit- (E-) site of the ribosome, wherein it is immediately released into the cytosol (Figure 1.3). This process continues until a sequence known as the stop codon in the mRNA is reached and a fully formed peptide skeleton is generated, which can then undergo proper folding and post-translational modification to give the final protein. Given that the translation process is conserved between humans and bacteria, any drug that inhibits translation must selectively bind to the bacterial ribosome over the human ribosome to avoid undesired toxicity.

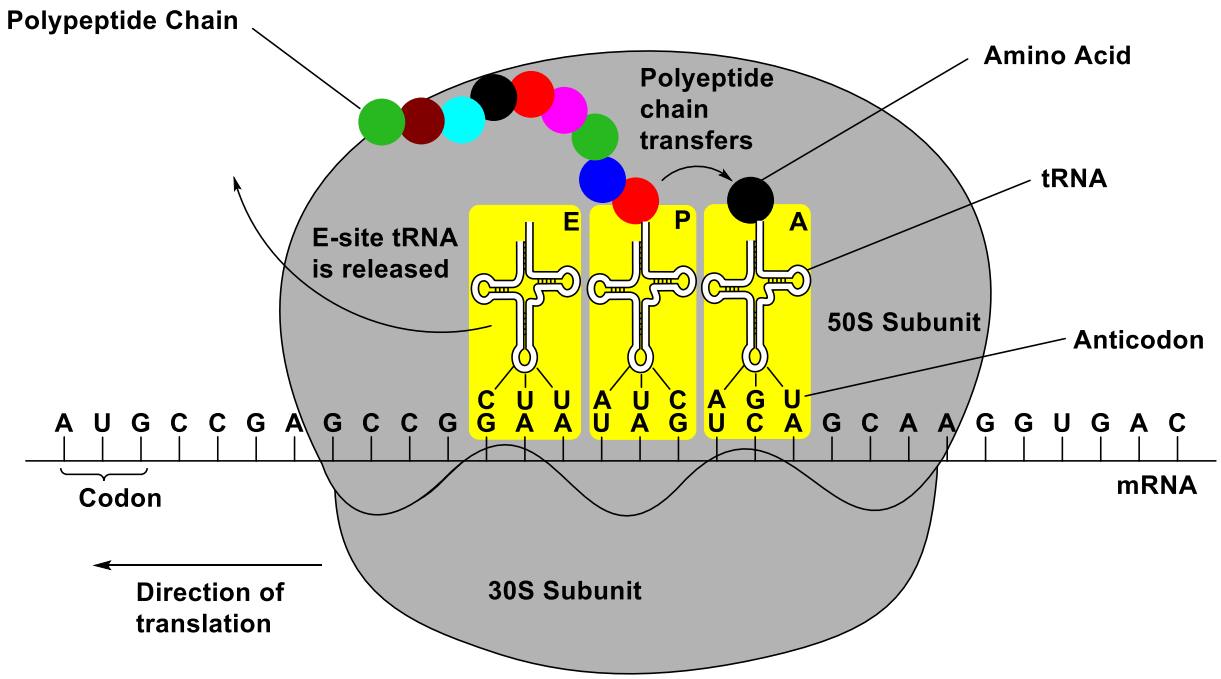

Figure 1.3. Overall schematic of the ribosome during translation

During EDPII, the AGA binds to helix 44 of the smaller ribosomal subunit, located at the decoding A-site, both through electrostatic interactions between the protonated amines of the AGA and the negatively charged phosphate backbone of the ribosomal RNA (rRNA), and through hydrogen bonding interactions between key nucleobases of the ribosome and hydroxyl groups/amines of the AGA.[31, 32] While many H-bonds with the ribosome will be specific to a given AGA or a subset thereof, certain interactions are common across most AGAs, such as pseudo-base pair interactions between A1408 and ring I, and H-bonds between the 2-DOS ring and both G1494 and U1495 (Figure 1.4a).[33] In most cases, AGA binding causes the nucleobases of A1492 and A1493 to fully flip outwards in a similar manner as that observed in translation (Figure 1.4b). This not only hinders further translation by increasing tRNA affinity for the A-site, but also reduces the energetic cost of binding of both correct and incorrect tRNA molecules, resulting in incorporation of incorrect amino acids in a process known as translational misreading.[34-38] Incorporation of

improper amino acids will cause misfolding and thereby render the polypeptide nonfunctional, which in turn will eventually lead to cell death either through generation of reactive oxygen species (ROS) and/or free radicals or through destabilization of the inner bacterial membrane.[39-41] For some AGAs such as apramycin, binding instead results in a partially flipped out conformation of A1492 and 1493 that fully inhibits translation instead of provoking misreading, resulting in cell death.[42]

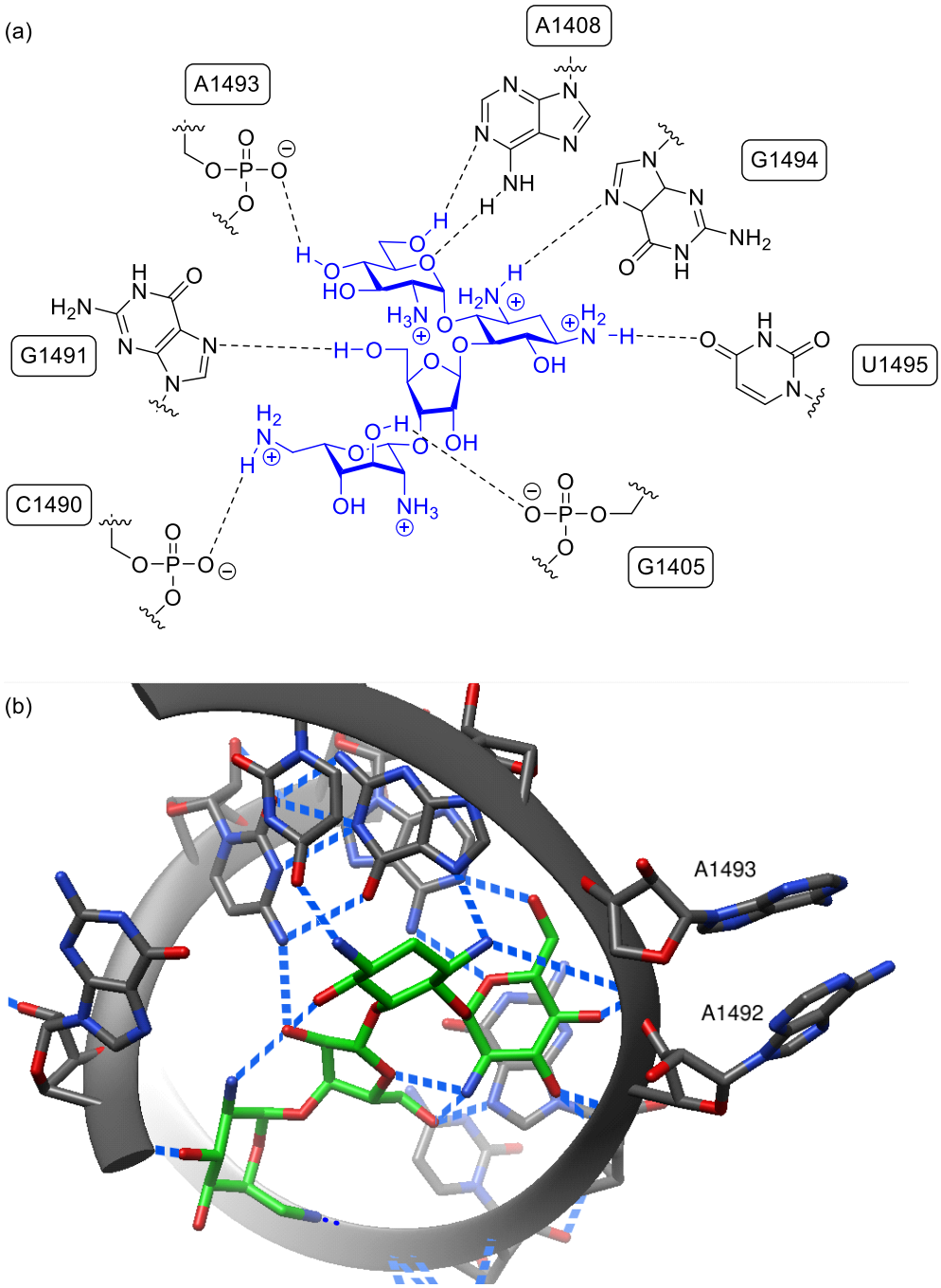

Figure 1.4. (a) Hydrogen bonding interactions between paromomycin and the decoding A-site (b) Flipped out conformation of A1492 and A1493 on binding of paromomycin to the *Thermus thermophilus* decoding A-site (PDB ID 1FJG)

1.4. Toxicity

The two primary drawbacks of use of AGAs in the clinic are reversible nephrotoxicity (kidney damage) and irreversible otoxicity (hearing loss). At present, the exact mechanism of nephrotoxicity is not fully understood. When the drug is administered through IV, >90% of the dose is excreted in the urine over 3-4 hours, while 5% of the administered dose is reabsorbed into kidney cells over time through endocytosis.[43] Once the drug has accumulated in the kidney cell lysosomes through electrostatic interactions with their phospholipids, it can inhibit lysosomal phospholipases and eventually lead to cell death through generation of ROS.[44, 45] Fortuitously, nephrotoxicity can be circumvented through administration of the drug in a once-daily dose instead of as several sporadic daily doses; given their low saturation threshold for AGAs, kidney cells are not readily able to accumulate lethal amounts of the drug when only one dose is administered.[46] Likewise, nephrotoxicity can be further mitigated by hydration therapy and co-treatment with polyaspartic acid to reduce the degree of AGA binding to the phospholipid.[12, 47]

Though its mechanism is better understood, irreversible ototoxicity poses a much greater hindrance to widespread use of AGAs in the clinic, impacting roughly 20% of the patient population. Ototoxicity can be divided into two classes, each of which can be observed among AGA patients: vestibulotoxicity, which results in loss of balance through vestibular cell death, and cochleotoxicity, which results in loss of hearing through cochlear hair cell death. In the latter case, the first cells to die are the basal cells, which detect high frequency sounds, followed by the apical cells which detect low frequency sounds.[48] Certain AGAs come with a predilection for one of these two types of toxicities, with neomycin leading to greater cochloetoxicity and streptomycin and gentamicin resulting in higher vestibulotoxicity. In each case, toxicity is irreversible due to the non-regenerative nature of the cells in question.[12, 32]

Uptake of the drug into the inner ear takes place within minutes of administration, with toxicity setting in as early as four hours after the initial dose. While the half-life of AGAs in serum is only 3-5 hours, these drugs can last as long as 30 days in the inner ear, though given that drug concentrations in the inner ear are comparable to those in other organs and are consistently lower than that in plasma, AGA accumulation has conclusively been ruled out as a cause of toxicity.[49, 50] As observed in both nephrotoxicity and in action against bacteria, cochlear cell death has been attributed to generation of ROS. While there are some competing theories over the generation of these species, such as complexation with iron and arachidonic acid or formation of superoxide radicals through an activation cascade of Rho-GTPase,[51, 52] the current prevailing theory is that ROS are generated through protein synthesis inhibition via binding of the AGA to the human mitochondrial ribosome, given that the nucleotide sequence of the decoding A-site is heavily conserved across both humans and bacteria (Figure 1.5).[53-55] Comparison between the human cytosolic ribosome and the wild type *Mycobacterium smegmatis* ribosome reveals two key amino acid differences in the AGA binding site: A1408 is replaced by guanine and G1491 is replaced by adenine (for convenience, bacterial numbering will be used throughout). Given that these two residues play key roles in aminoglycoside binding, the affinity of the drug for the human cytosolic ribosome is significantly less than that for the bacterial ribosome. In the human mitochondrial ribosome, however, A1408 is conserved, whereas the U1410-A1490 Watson-Crick base pair is replaced by a C-A non-canonical base pair. Though the latter renders partial difference in the three-dimensional shape of the decoding A-site, the presence of the critical A1408 residue renders the human mitochondrial ribosome distinctly susceptible to AGA binding. Analysis of the A-site structure of the A1555G mutant of the human mitochondrial ribosome, where A1490 (using bacterial numbering) is mutated into guanine, reveals that the overall three-dimensional shape of

the mutated human A-site becomes much more similar to that of the bacterial site due to the resulting Watson-Crick base pair interaction.[56, 57] Given that individuals with this otherwise benign mutation are rendered strongly susceptible to hearing loss, it is clear that binding of the drug to human ribosomes plays a strong role in AGA-induced ototoxicity.

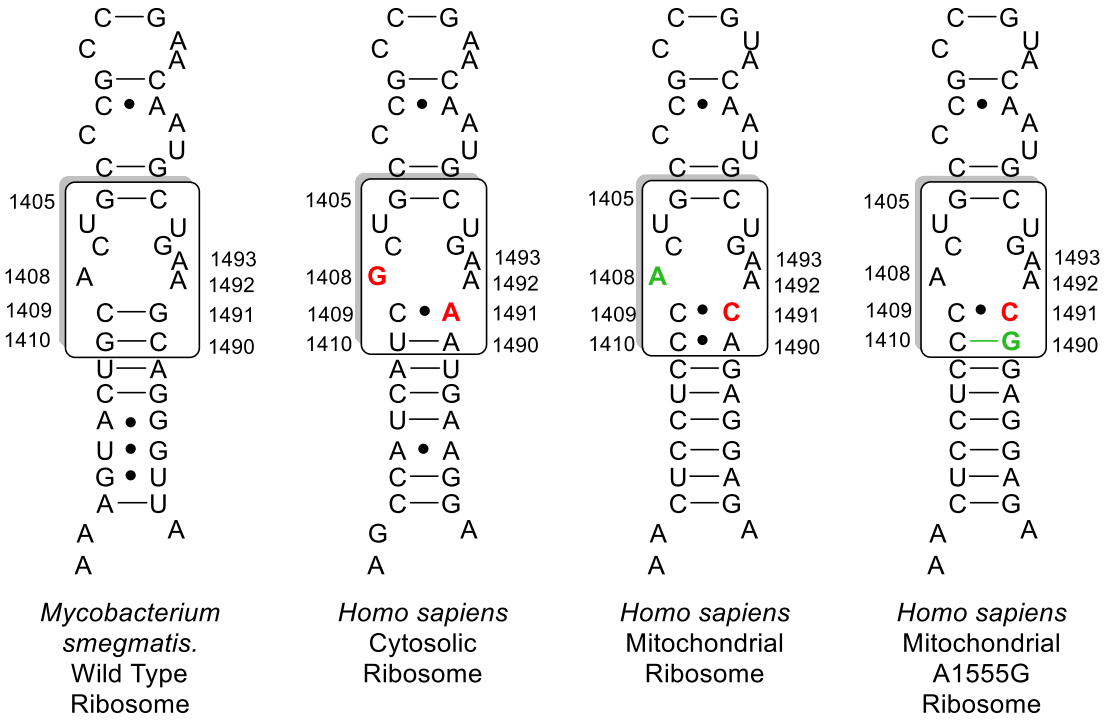

Figure 1.5. Comparison of decoding A-sites of bacteria and humans

1.5. Mechanisms of Resistance

Bacteria have developed three distinct mechanisms of resistance against AGAs: concentration reduction, ribosomal modification, and AGA modification. In the first case, some strains of bacteria alter their influx and efflux pathways to reduce intracellular concentration of the aminoglycoside. To reduce uptake of the AGA into the cell, different strains of bacteria will incorporate additives such as phosphoethanolamine or 4-amino-4-deoxy-L-arabinose into their

cell membranes, which reduce the negativatively charged character of the phospholipid bilayer and thus lower the degree of initial electrostatic interaction with the AGA.[58-60] Likewise, some strains of Gram-negative bacteria such as *Pseudomonas aeruginosa* and *Escherichia coli* express efflux pumps to remove antibiotics from the cell. The most common class of efflux pump is the resistance nodulation division (RND), whose machinery consists of a pump, a membrane fusion protein, and an outer-membrane factor. The efficacy of individual pump systems against AGAs is quite variable. For example, while the *Pseudomonas aeruginosa* efflux system MexAV-OrpM affords minimal resistance against AGAs, the efflux system MexY in the same strains of bacteria is effective against these drugs.[61-63]

Predominantly observed in AGA-producing bacteria, some strains modify the decoding A-site to reduce AGA susceptibility through either point mutation or methylation. The most common example of a resistance-inducing point mutation is A1408G, which strongly reduces ribosomal affinity of gentamicin and other 6'-NH_2-bearing AGAs.[64, 65] Methylation (predominantly at G1405) is carried out by methyl transferases in the *Rmt* or *arm* families and strongly reduces activity of 4,6-disubstituted AGAs, while minimally impacting 4,5-AGA binding.[21, 66, 67]

By far the most common mechanism of resistance is deactivation of the drug through aminoglycoside modifying enzymes (AMEs). These enzymes are classed as either aminoglycoside acetyltransferases (AACs), which acetylate amines, aminoglycoside phosphotransferases (APHs), which phosphorylate hydroxy groups, or aminoglycoside nucleotidyltransferases (ANTs), which adenylate hydroxy groups. All AMEs are denoted by their three-letter abbreviation followed by a parenthetical number indicating the site of the target heteroatom, with some specific AMEs also including roman numerals to indicate their phenotype and a letter denoting their gene of origin (Figure 1.6). In each case, the modification afforded by the AMEs prevents proper binding of the

AGA to the ribosome either through simple steric blockage or through removal of a key H-bonding interaction. Given that AMEs are encoded on plasmids, they are readily able to spread across various bacterial populations and are by far the most prolific mechanism of resistance acting against AGAs.[68-71] Of the three AME classes, AACs are the most abundant and predominantly target the 1, 3, 2', and 6' amines, though AAC(1) does not significantly deactivate AGAs and is thus not clinically relevant.[72] APHs target hydroxyl groups at positions 4, 6, 9, 3', 2'', 3'', and 7'' of the AGA, with some members of the most abundant APH(3') class impacting other denoted positions as well.[69] The phosphate group installed by APHs adds a negative charge to the drug and thus decreases the electrostatic interactions between the AGA and the nucleotide backbone in addition to providing steric blockage. ANTs, the least abundant of the three AME classes, act on the 9, 3', 4', 6', and 2'' hydroxyl groups, with ANT(2'')-Ia conferring significant resistance against 4,6-AGAs such as gentamicin.[73]

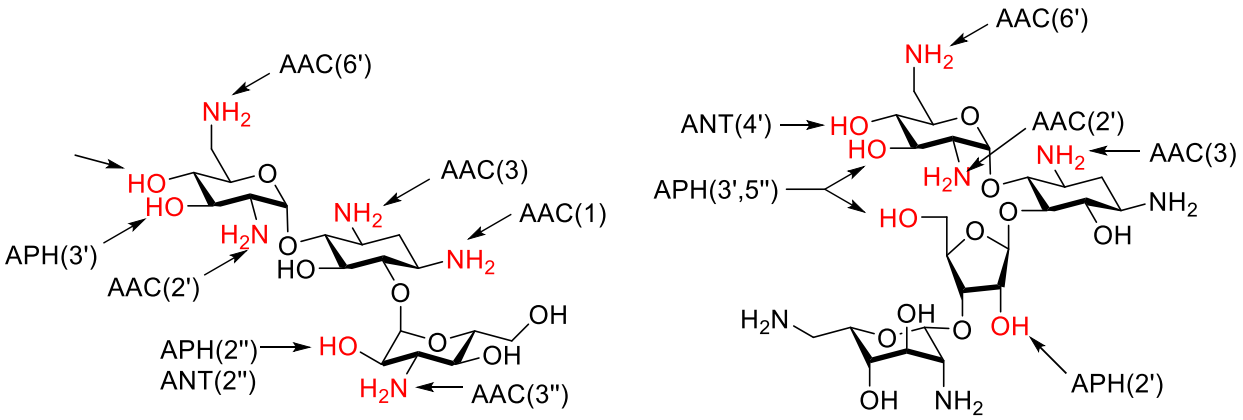

Figure 1.6. AME susceptibilities of kanamycin B and neomycin B

An ever-looming public health is the dissemination of plasmids encoding AMEs and RMTs across multiple strains of bacteria.[74] To this end, the worst case scenario is the evolution and spread of strains of bacteria against which no antimicrobials are effective.[75] Recently, there have been outbreaks of carbapenem-resistant strains of *Enterobacteriaceae* expressing New Delhi metallo-β-lactamase 1 (NDM-1) across many parts of the globe, originally constrained to Asia and South America but more recently spreading to Tuscany.[75, 76] Strains of bacteria expressing NDM-1, which can be spread across multiple strains through plasmids, were resistant to all antibiotics other than the last resort drugs tigecycline and colistin. Thus, it is critical to do whatever possible to circumvent bacterial resistance mechanisms, specifically AMEs in the case of aminoglycosides.

1.6. Combating Resistance and Recent Developments

There are currently two approaches to mitigating AME-induced resistance. The first involves co-administration of a small molecule AME inhibitor along with the drug itself, e.g. dosage with 7-hydroxytropolone to inhibit ANT(2'').[77] The second, more preferable approach is to modify the structure of the AGA such that the AMEs will be rendered nonfunctional, either by directly blocking the position targeted by the enzyme, by removing the targeted functional group itself, or by adding on steric bulk to the drug such that it will not fit properly in the enzyme active site (Figure 1.7). Sisomicin **9** and its semisynthetic derivative netilmicin **10**, for example, both avoid susceptibility to APH(3') and ANT(4') through omission of hydroxyl groups at these positions, with the steric influence of the netilmicin *N*-1-ethyl group additionally circumventing susceptibility to a range of other AMEs. Likewise, the presence of a 4-amino-2-(*S*)-hydroxybutyryl group on *N*-1, as is observed with the naturally occurring butirosin **11**, can strongly reduce susceptibility to AAC(1), AAC(3), APH(2''), and ANT(2''). This knowledge inspired the design

of AGAs such as the kanamycin derivative amikacin **12** and the sisomicin derivative plazomicin **13**, the most recently approved AGA for use in the clinic whose hydroxyethyl group at *N*-6' removes susceptibility to AAC(6').[78, 79] While plazomicin certainly circumvents most of the potential threats towards AGA function, it remains comparatively ototoxic and susceptible to action of *arm*A on the ribosome given its 4,6-disubstitution pattern.[80] In the 4,5-series, the recently developed and highly active paromomycin derivative propylamycin **14** takes advantage of the above principles through installation of a C-propyl group at C-4', which not only increases the basicity of O-5 to maximize its H-bonding interactions with A1408, but also sterically prevents activity of APH(3') and fully disables activity of ANT(4') due to omission of the target hydroxyl group.[21] Another promising AGA to combat antibiotic resistance is the relatively active and highly selective apramycin **7**, whose monosubstituted 2-DOS and unusual bicyclic dialdose ring render the drug susceptible only to AAC(3)-IV,[42, 81-83] and which is currently in clinical trials.[84, 85]

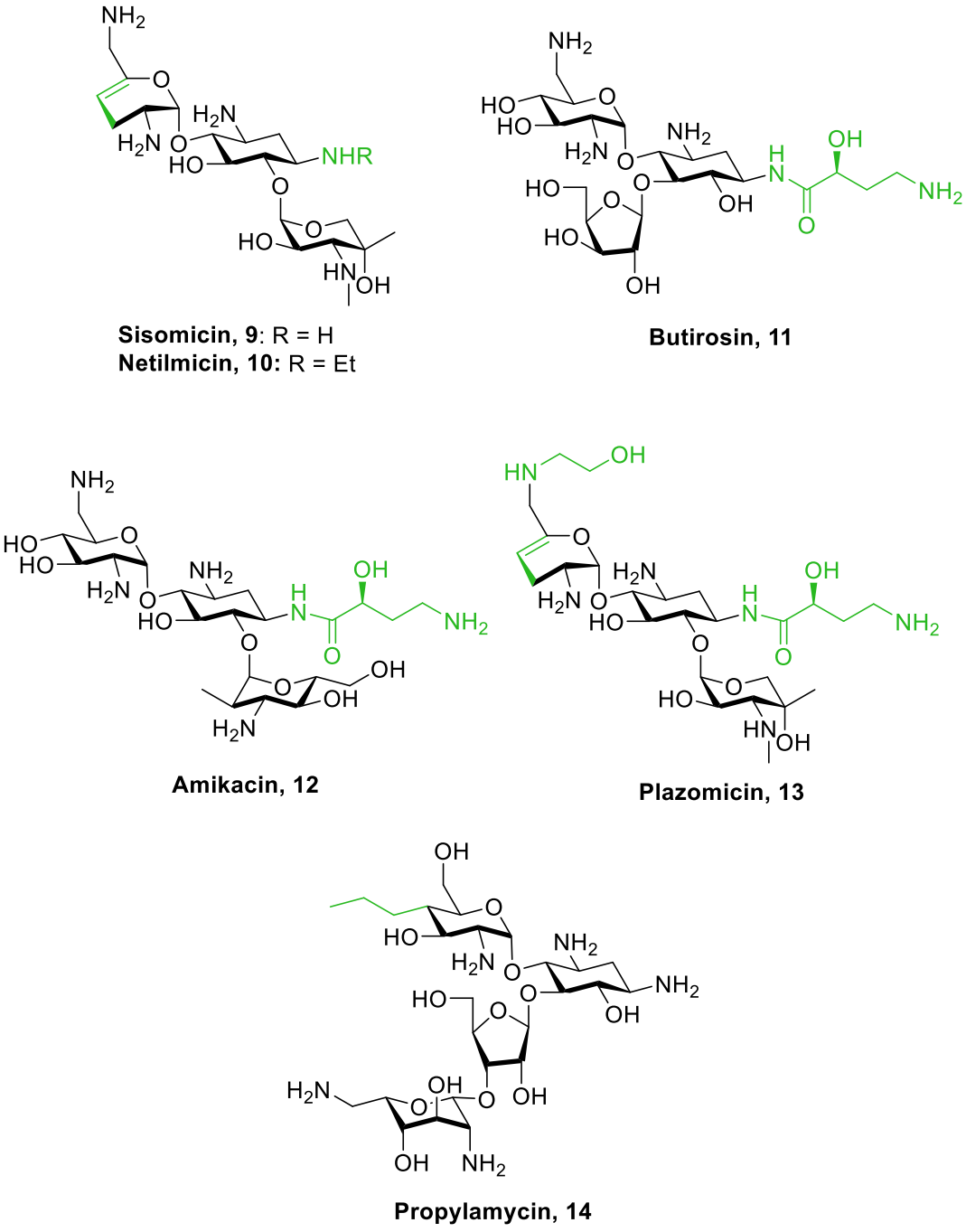

Figure 1.7. AGAs circumventing AMEs

1.7. Overall Goals

This work seeks to develop a series of new AGAs that are both more active and more selective for bacterial ribosomes than the parent drugs. Apramycin's low toxicity and low AME susceptibility render it a prime candidate for further functionalization to increase activity. The first project discusses the development of a series of 5-*O*-furanosylated apramycin derivatives, termed apralogs, which bear analogous structures to members of the 4,5-series of AGAs. Given that these compounds maintain the unusual bicyclic ring of the parent, and in light of promising preliminary results, the derivatives synthesized herein were expected to yield greater activity than the parent while maintaining both low toxicity and low AME susceptibility.

In view of both disparate reports in the literature and the results from the above apralog studies, the second project details the syntheses a series of simple 5''-derivatives of paromomycin, neomycin, and ribostamycin to conclusively determine the role of 5''-modifications on activity and selectivity while successfully circumventing of the prevalent APH(3',5'').

CHAPTER 2

SYNTHESIS OF APRAMYCIN DERIVATIVES

2.1. Introduction

The aminoglycoside antibiotic apramycin **7**, formerly referred to as nebramycin factor 2,[86] was first isolated by workers at Eli Lilly from *Streptomyces tenebrarius*.[87, 88] Though initially used only in veterinary medicine,[89, 90] apramycin is currently undergoing Phase 1 clinical trials for use in humans.[84, 85] Apramycin is structurally distinct from most other AGAs in that it is monosubstituted at O4 rather than disubstituted and contains a bicyclic dialdose ring instead of a simple pyranose ring at that position (Figure 2.1).

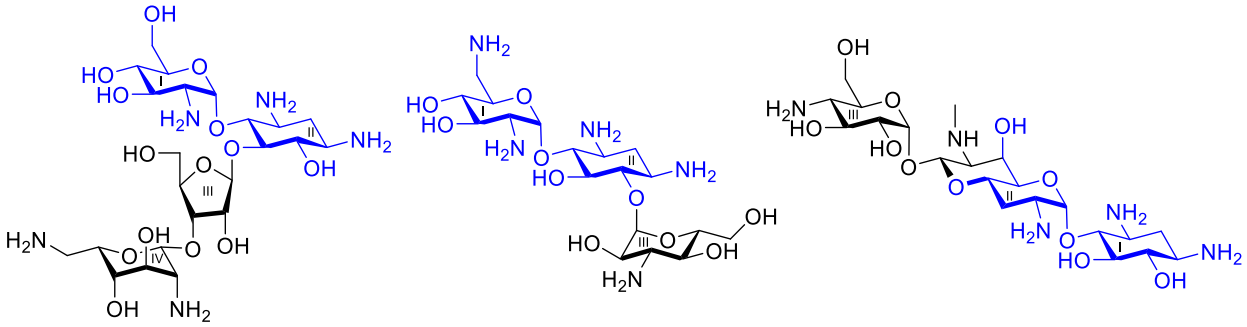

Figure 2.1. Structure of apramycin compared to other AGAs, with common structural elements colored blue

Figure 2.2 shows a crystal structure of apramycin bound to helix 44 of the 30S subunit of the *Thermus thermophilus* ribosome and a superimposed crystal structure with paromomycin bound in the same helix for comparison. As expected based on their common structural features shown in Figure 2.1a-b, rings I and II of apramycin bind in very similar positions to rings I and II of paromomycin. Of particular importance is the pseudo-base pair between ring II of apramycin and A1408 illustrated in Figure 2.2c, as evidenced by the sharp decrease in activity resulting from modifications at N7' and O6'.[91] Ring III of apramycin stabilizes a partially flipped out conformation of A1492 through H-bonding with the corresponding phosphate, which results in translational inhibition rather than misreading.[92] In AGAs such as aprosamine **15** that lack this ring (Figure 2.3), misreading is observed instead of inhibition, as the key binding interaction with A1492 that stabilizes the partially flipped out conformation of the apramycin complex is not present.[33, 93]

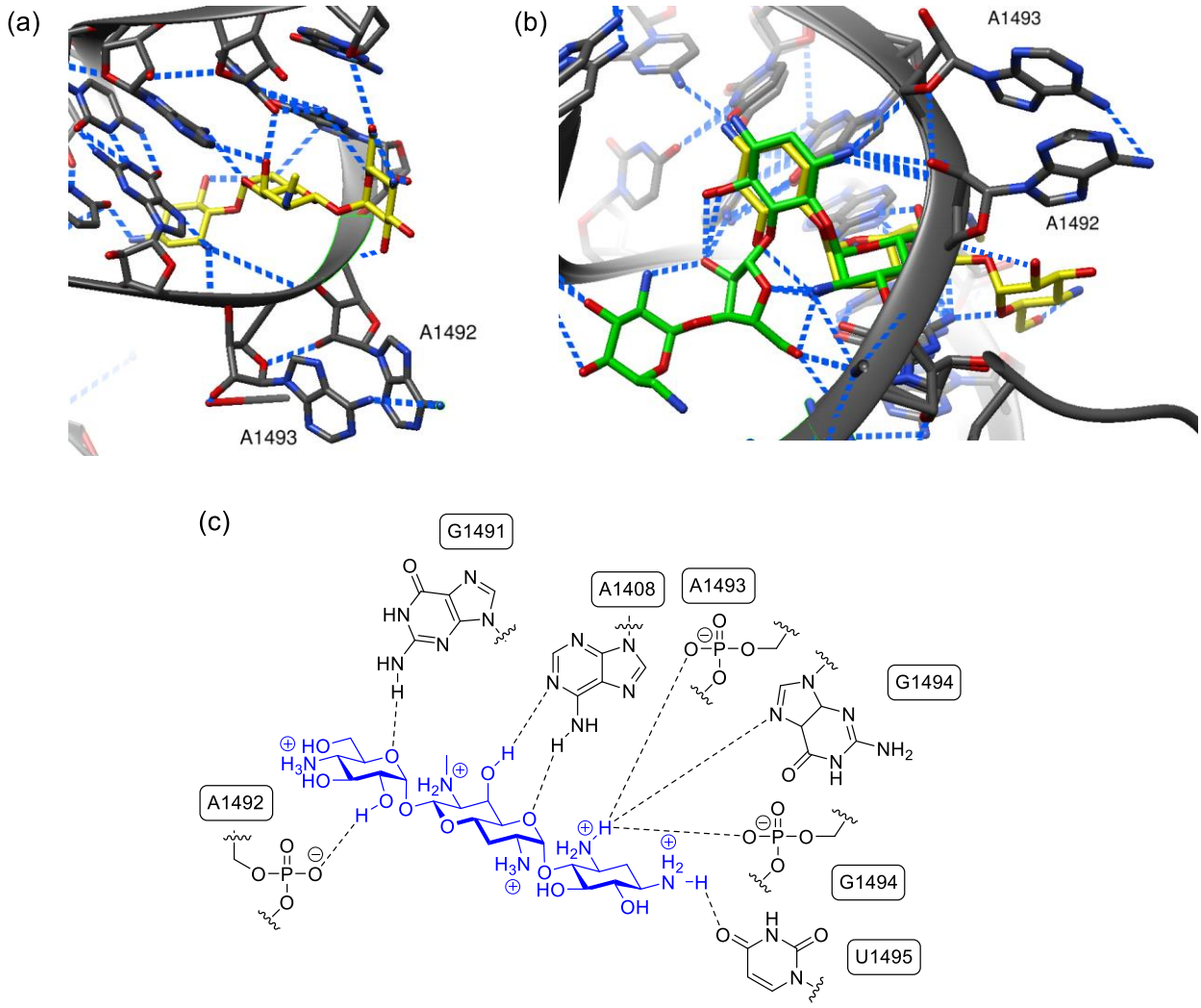

Figure 2.2. (a) Partial crystal structure of apramycin bound to the *Thermus thermophilus* decoding A-site (PDB ID 4AQY) with partially flipped out A1492 and A1493 (b) Superimposed crystal structures of the *T. thermophilus* decoding A site in complex with apramycin (PDB ID 4AQY, yellow) and paromomycin (PDB ID 1FJG, green) (c) Hydrogen bonding interactions between apramycin and the *T. thermophilus* decoding A-site

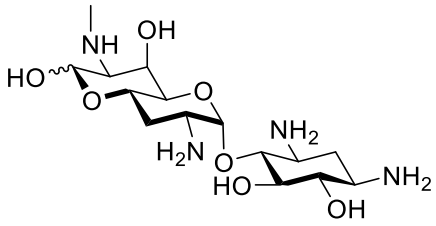

Figure 2.3. Structure of aprosamine **15**

As a result of its unusual structural features, apramycin circumvents susceptibility to all AMEs aside from the AAC(3)-IV isoform discussed in Chapter 1[82, 83, 92, 94] and to the ribosomal methyltransferases (RMTases), which deactivate every AGA currently used in the clinic.[66] In addition, apramycin exhibits both very low ototoxicity, as evidenced by cell-free ribosomal translation assays, cochlear explant studies, and in vivo guinea pig studies,[92, 95] and high activity against multidrug resistant Gram positive and Gram negative bacteria. The above benefits combined with its high availability through fermentation render apramycin a promising drug candidate for clinical use. Accordingly, apramycin can be considered a prime scaffold for derivatization to synthesize next generation AGAs, with the goal of increasing activity and reducing susceptibility to AAC(3)-IV while maintaining the low toxicity of the parent.[81, 96-100]

2.2. Targets

To date, the majority of studies on apramycin have involved rational modification of specific positions on apramycin, centering on N1,[101] N2',[102, 103] N4'',[104-107] N7',[91, 108] O8',[109] O6''[110], O6',[91] O5,[111, 112] or O6.[113] Though modification at the majority of these sites generally resulted in either comparable or lower antibacterial activity to the parent, select modifications at O5 and O6 were promising candidates for further examination. More specifically, and inspired by the greater activity exhibited by the 4,5- and 4,6-disubstituted AGAs compared to apramycin, Abe

and coworkers described 6-*O*-(3-amino-3-deoxy-α-D-glucopyranosyl) apramycin **16** and 5-*O*-(β-D-ribofuranosyl) apramycin **17β** in 1981, and found that glycosylation at O5 and O6 afforded increased antibacterial activity and decreased toxicity (Figure 2.4).[113] The ribofuranosyl ring of **17β** is structurally analogous to ring III of paromomycin, while the 3-aminoglucosyl ring of **16** resembles ring IV of kanamycin B. Given that rings I and II of apramycin, paromomycin, and kanamycin B all bind in similar positions in the ribosome, installation of the kanamycin and paromomycin ring III as in analogs **16** and **17β** allows them to benefit from additional H-bonding and electrostatic interactions not observed in the parent apramycin. Of note, in cases such as **17α** where the configuration of the newly installed glycosidic linkage did not match that of the 4,5-AGA, activity was sharply reduced.

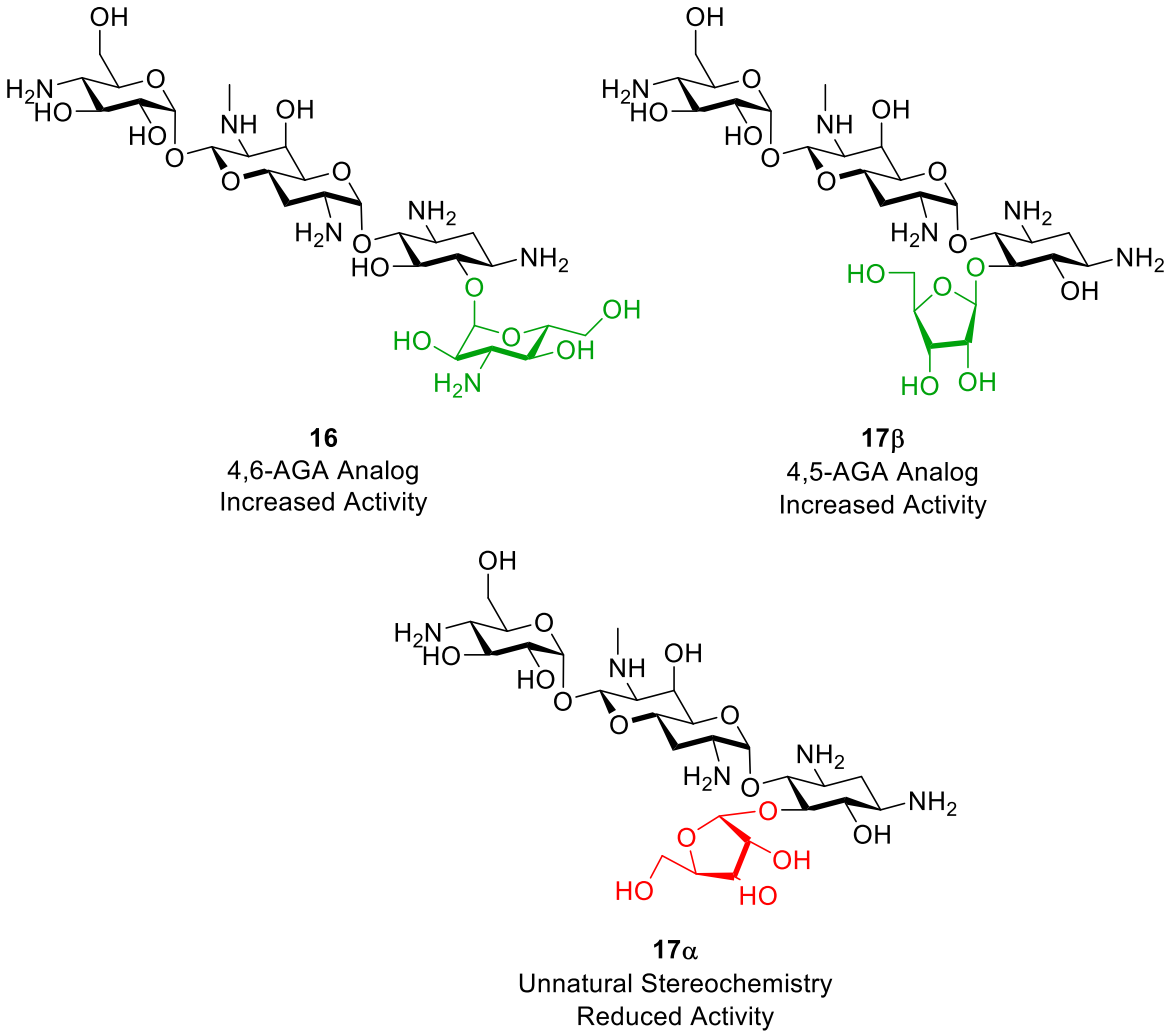

Figure 2.4. Previous apramycin derivatives 6-*O*-(3-amino-3-deoxy-α-D-glucopyranosyl) apramycin **16**, 5-*O*-(β-D-ribofuranosyl) apramycin **17β**, and 5-*O*-(β-D-ribofuranosyl) apramycin **17α**

In light of these promising preliminary studies, a series of 4,5-disubstituted apramycin derivatives, termed apralogs (Figure 2.5), were designed with the aim of further increasing antibacterial activity while minimizing susceptibility to AAC(3)-IV.[114, 115] It should be noted that analogs of the 4,6-disubstituted analogs such as **16** were avoided due to their anticipated susceptibility to the RMTases, which impact all 4,6-AGAs.[82, 92, 96] To further mimic the structural

features of the 4,5-AGAs, rings III and IV of paromomycin, termed parombiose, were appended to O5 of apramycin as shown in compound **18**, with the aim of achieving similar activity to the 4,5-AGA parent. In 1998, the Wong group probed the role of ring IV of neomycin in RNA binding and antibacterial activity through the design of a series of ribostamycin derivatives bearing simple aminoalkyl chains at O3'' to mimic the cationic nature of ring IV.[116] Wong and coworkers determined that these analogs exhibited significantly stronger binding to the decoding A site of *E. coli* than ribostamycin and similar antibacterial activity to neomycin, making them promising candidates for future examination. With these results in mind, simpler aminoethyl chain and hydroxyethyl chain were also installed at the 2-position of the furanose in compounds **19** and **20** respectively.

In the original studies carried out by Abe and coworkers, installation of a β-D-ribofuranosyl group at O5 gave rise to added susceptibility to APH(3',5''), which deactivates the AGA through phosphorylation the primary OH of the ribose ring. To circumvent this problem, Crich and coworkers designed a series of erythrofuranosyl (**21-26**), 5-deoxyribofuranosyl (**27**), 5-amino-5-deoxyfuranosyl (**28-31**) and 5-deoxy-5-formamidofuranosyl (**32-33**) derivatives, all of which lack the target hydroxyl group of phosphorylation. More specifically, a series of aminoalkyl chains were installed at O3'' of erythrose in derivatives **22-26** in an attempt to generalize the findings of Wong and coworkers as described above.[116] In the aminoribosyl series, flexible aminoalkyl chains were installed in **29** and **30** to determine whether the location of positive charge would influence activity. The syntheses of compounds **22-27** and **31** are described in this chapter; all other compounds in this collaborative effort having been made by coworkers in the Crich lab. The entire series of compounds are taken into consideration in the discussion of the biological activity.

5-*O*-Ribofuranosyl Series

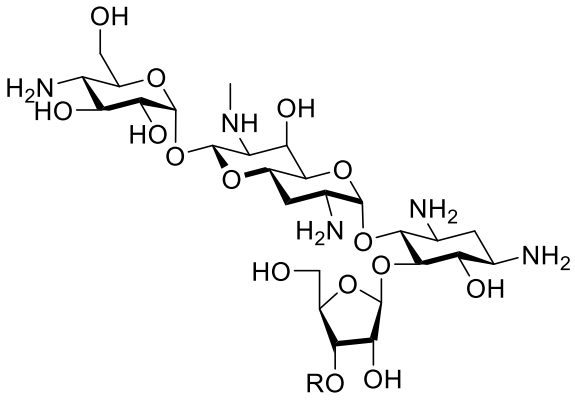

17: R = H
18: R = 2,6-diaminoidopyranosyl
19: R = $CH_2CH_2NH_2$
20: R = CH_2CH_2OH

5-*O*-Erythrofuranosyl Series

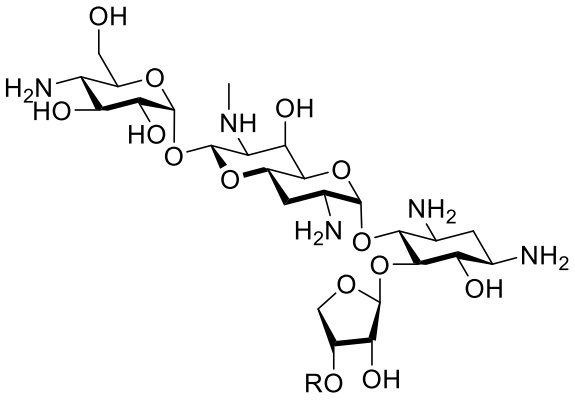

21: R = H
22: R = $CH_2CH_2NH_2$
23: R = CH_2CH_2OH
24: R = $CH_2CH_2NHCH_2CH_2NH_2$
25: R = $CH_2CH_2NHCH_2CH_2CH_2NH_2$
26: R = $CH_2CH_2NHCH_2CH_2CH_2NMe_2$

5-*O*-Deoxyribofuranosyl Apramycin

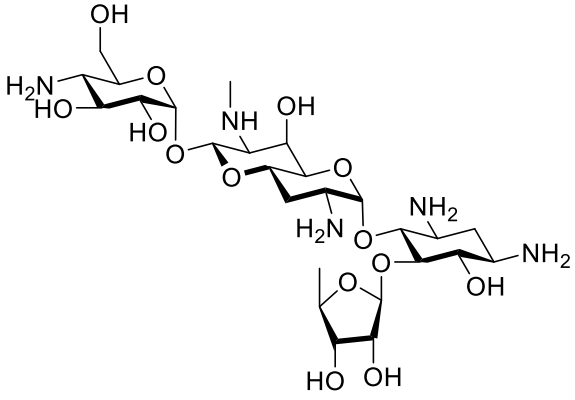

27

5-*O*-Aminoribofuranosyl Series

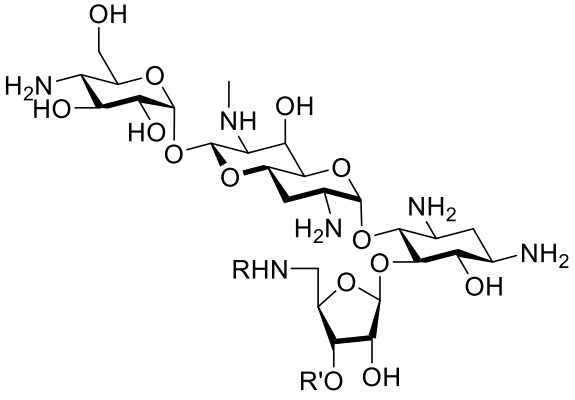

28: R = R' = H
29: R = $CH_2CH_2NH_2$, R' = H
30: R = $CH_2CH_2CH_2NH_2$, R' = H
31: R = H, R' = $CH_2CH_2NH_2$
32: R = CHO, R' = H
33: R = CHO, R' = $CH_2CH_2NH_2$

Figure 2.5. Structures of 5-*O*-furanosyl apralogs

2.3. Synthesis of Specific Apralogs

A common glycosyl acceptor was used for the synthesis of each of the targets below. Careful treatment of literature compound **34**, which is readily available from the parent compound in three steps,[91] with benzoyl chloride in pyridine at 0 °C gave the desired glycosyl acceptor **35** in 81% yield (Scheme 2.1).[112] Currently, the selectivity of benzoylation is only partially understood. Of the four secondary hydroxyl groups, O2'' and O5 are adjacent to a glycosidic linkage and are thus more electron deficient than O6 and O3'', meaning that the latter two positions are expected to react more readily. However, the cause of selective benzoylation of O2'' over O5 is not yet clear. Comparable selectivity was observed by coworkers in the Crich lab for acetylation with acetic anhydride and pyridine,[117] and was subsequently described by Fridman and coworkers.[118] This synthesis, which can be carried out in four linear steps from the parent apramycin in 33% overall yield, is a marked improvement on the original synthesis carried out by Abe and coworkers, which required five steps, proceeded in 16% overall yield, and involved use of benzyloxycarbonyl protecting groups making interpretation of NMR spectra difficult.[113]

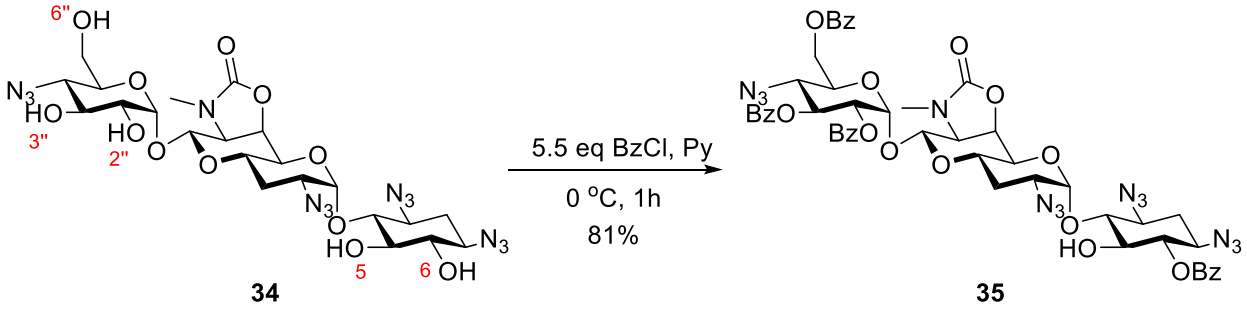

Scheme 2.1. Preparation of **35**

With glycosyl acceptor **35** in hand, glycosylations using a series of furanosyl donors were carried out to install the desired ring at O5. In all cases, given that the β-anomer is the desired

product, an acetate protecting group was installed at the 2-position of the furanosyl donor. During glycosylation, the acetate takes part in a process known as neighboring group participation (NGP, discussed in greater detail in Chapter 4), where the carbonyl oxygen will form a covalent linkage with the anomeric carbon. This bond is then cleaved in an S_N2 or S_N2-like fashion to preferentially afford the β-glycosylated product.

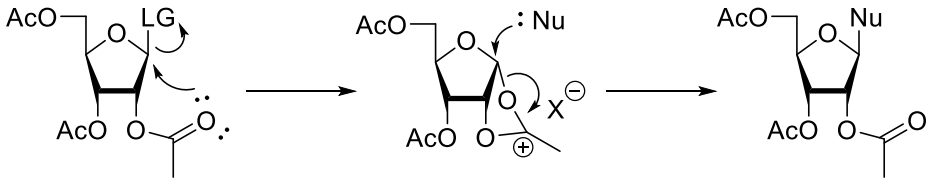

Scheme 2.2. Neighboring group participation by a vicinal acetate in glycosylations with furanosyl donors to give β-selectivity during glycosylation

Scheme 2.3 illustrates the preparation of the common glycosyl donor used to synthesize erythrosyl derivatives **22-26**. Starting with literature compound **36**,[119] an allyl group was installed using allyl iodide and sodium hydride to give the corresponding allyl ether **37** in 70% yield. Subsequent cleavage of the acetonide and installation of acetate groups generated a mixture of isomers **38** in 42% yield over two steps.

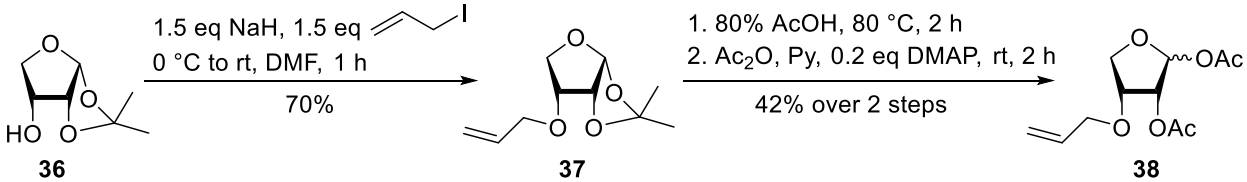

Scheme 2.3. Preparation of **38**

Using $BF_3{\cdot}OEt_2$ as an activator, glycosylation was carried out with acceptor **35** and donor **38** to exclusively give the β-anomer of **39** in 34% isolated yield as shown in Scheme 2.4. Here, the exquisite selectivity can be attributed to NGP by the acetate at the 2-position of the erythrosyl donor, as discussed above, in conjunction with the relatively low temperature. Stereochemistry at the newly generated glycosidic linkage was determined using ^{13}C NMR chemical shifts in accordance with established rules: the ^{13}C chemical shift of the anomeric carbon in β-furanosides is approximately 107 ppm, while that of α-furanosides is approximately 102 ppm.[120] The 1''-anomeric carbon of compound **39** exhibited a chemical shift of 107.1 ppm, indicating that the desired β-anomer was produced. Glycosylation product **39** was subsequently converted to aldehyde **40** in 97% yield over 2 steps through dihydroxylation with catalytic OsO_4 followed by cleavage of the diol using $NaIO_4$ suspended in silica gel.[121] The aldehyde was then subjected to reductive amination with a series of amines,[122] and the resulting intermediate was deprotected through basic hydrolysis of the esters and hydrogenolysis of azides. Each fully deprotected compound was passed through a column of Sephadex C25 ion exchange resin and lyophilized with AcOH to give the peracetate salts of **22-26** as shown in the tables of Scheme 2.4.

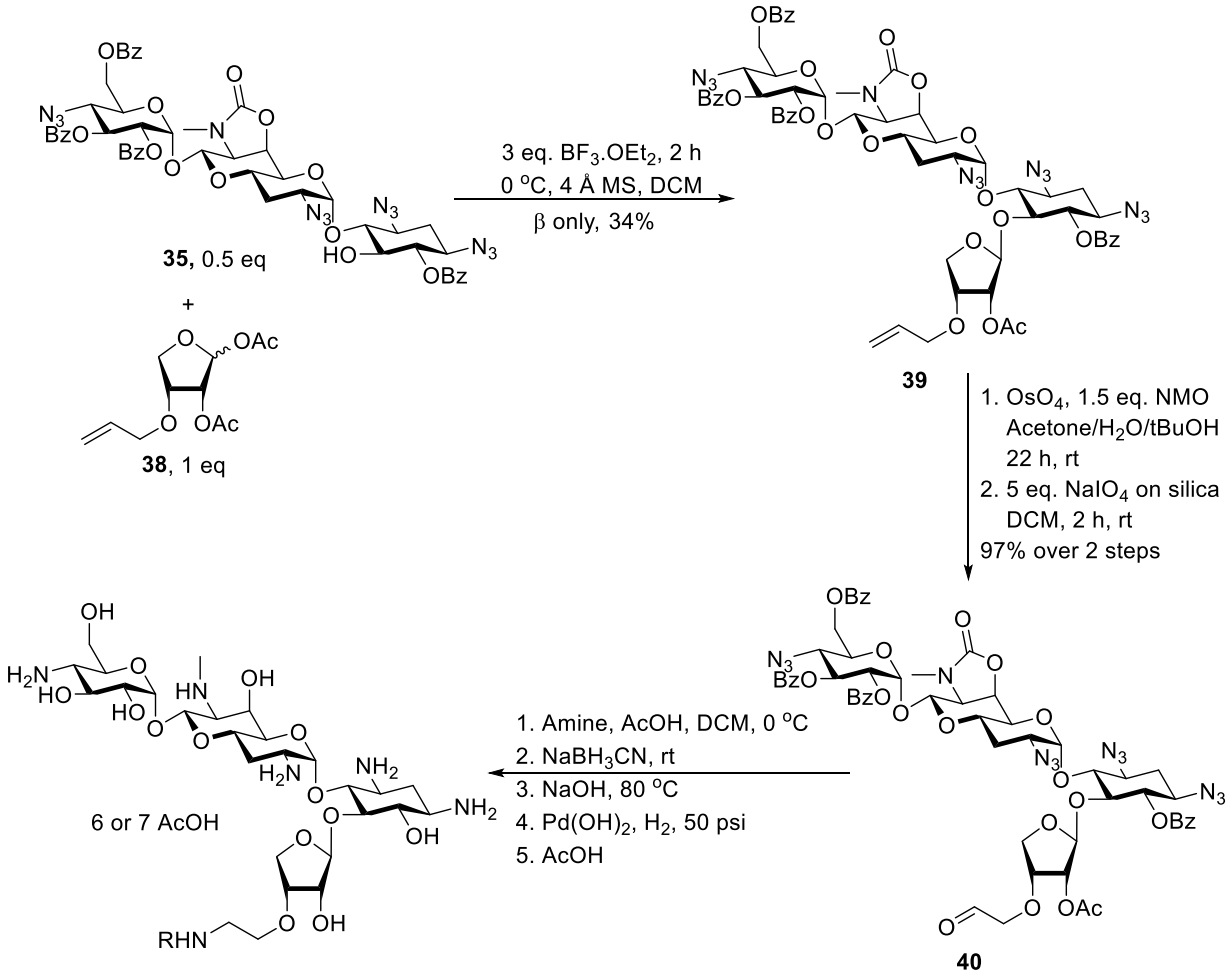

Amine	Product	Yield (% from 38)
$BnNH_2$	**22**	18
$H_2NCH_2CH_2OH$	**23**	3
$H_2NCH_2CH_2NH_2$	**24**	18
$H_2NCH_2CH_2CH_2NHCbz$	**25**	3
$H_2NCH_2CH_2CH_2NMe_2$	**26**	8

Scheme 2.4. Preparation of **22-26**

In the case of deoxyribosyl apramycin **21**, glycosylation was carried out using the commercial donor **41** and $BF_3.OEt_2$ as an activator at room temperature over two hours to give the desired product **42** in 27% isolated yield and an α:β ratio of 0.4:1 (Scheme 2.5). The stereochemistry at the newly installed anomeric center was confirmed on the basis of the ^{13}C NMR

anomeric chemical shifts; the observed ^{13}C chemical shift of 105.5 at the furanosyl anomeric carbon is consistent with formation of the desired β-anomer. The reduced selectivity in this glycosylation likely stems from the higher temperature needed to achieve reactivity. The glycosylation product was then deprotected through one-pot basic hydrolysis of the acetates followed by Staudinger reduction of the azides,[123] and the resulting solid was passed through Sephadex C25 ion exchange resin and lyophilized with AcOH to give the peracetate salt of **27** in 57% yield over 3 steps.

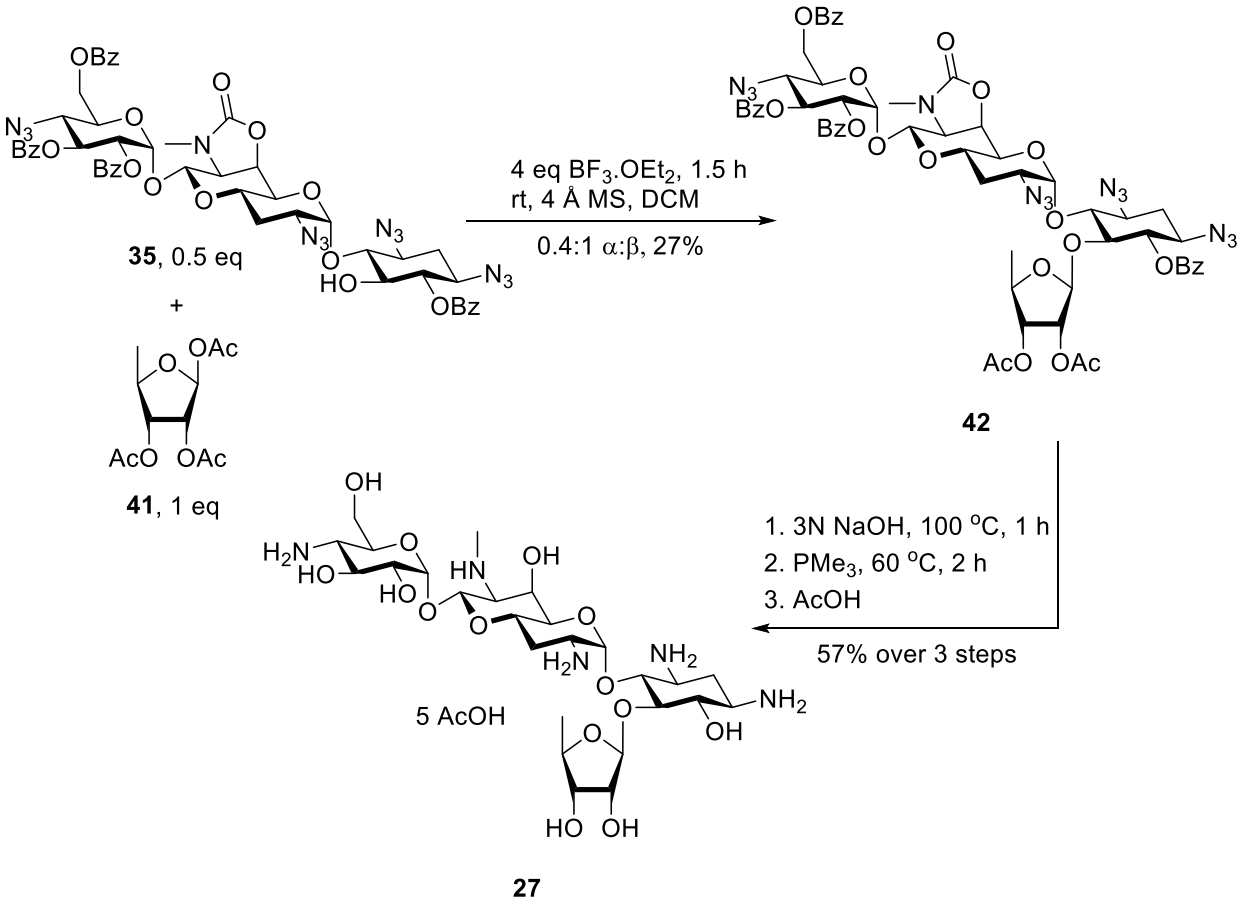

Scheme 2.5. Preparation of **27**

Compound **31** was prepared in a similar fashion to the above series. Treatment of literature compound **43**[124] with sodium hydride and 2-azidoethyl tosylate prepared by Sharpless' method[125] gave the azidoethyl compound **44** in 45% yield. Subsequent hydrolysis of the acetonide followed by acetylation of the free hydroxyl groups gave **45** as a mixture of anomers in 82% yield (Scheme 2.6).

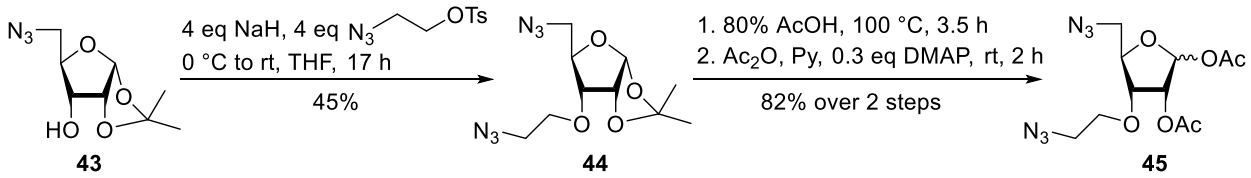

Scheme 2.6. Preparation of **45**

As shown in Scheme 2.7, glycosylation was carried out using donor **45** as a mixture of anomers and $BF_3{\cdot}OEt_2$ as a promoter to give **46** as a 0.3:1 ratio of α:β products in 34% isolated yield. As in the formation of **42**, the lowered selectivity is likely due to the higher temperatures needed to achieve activation. Stereochemistry at the newly synthesized glycosidic linkage was confirmed through ^{13}C chemical shift analysis; the observed ^{13}C chemical shift of 107.2 at the anomeric position of the furanoside is consistent with formation of the desired β-anomer. Compound **46** was deprotected in an analogous manner as glycosylation product **42**, through one-pot hydrolysis of the esters and oxazolidinone followed by Staudinger reduction of the azides. The resulting solid was passed through a column of Sephadex C25 ion exchange resin and lyophilized with acetic acid to give the peracetate salt of **31**.

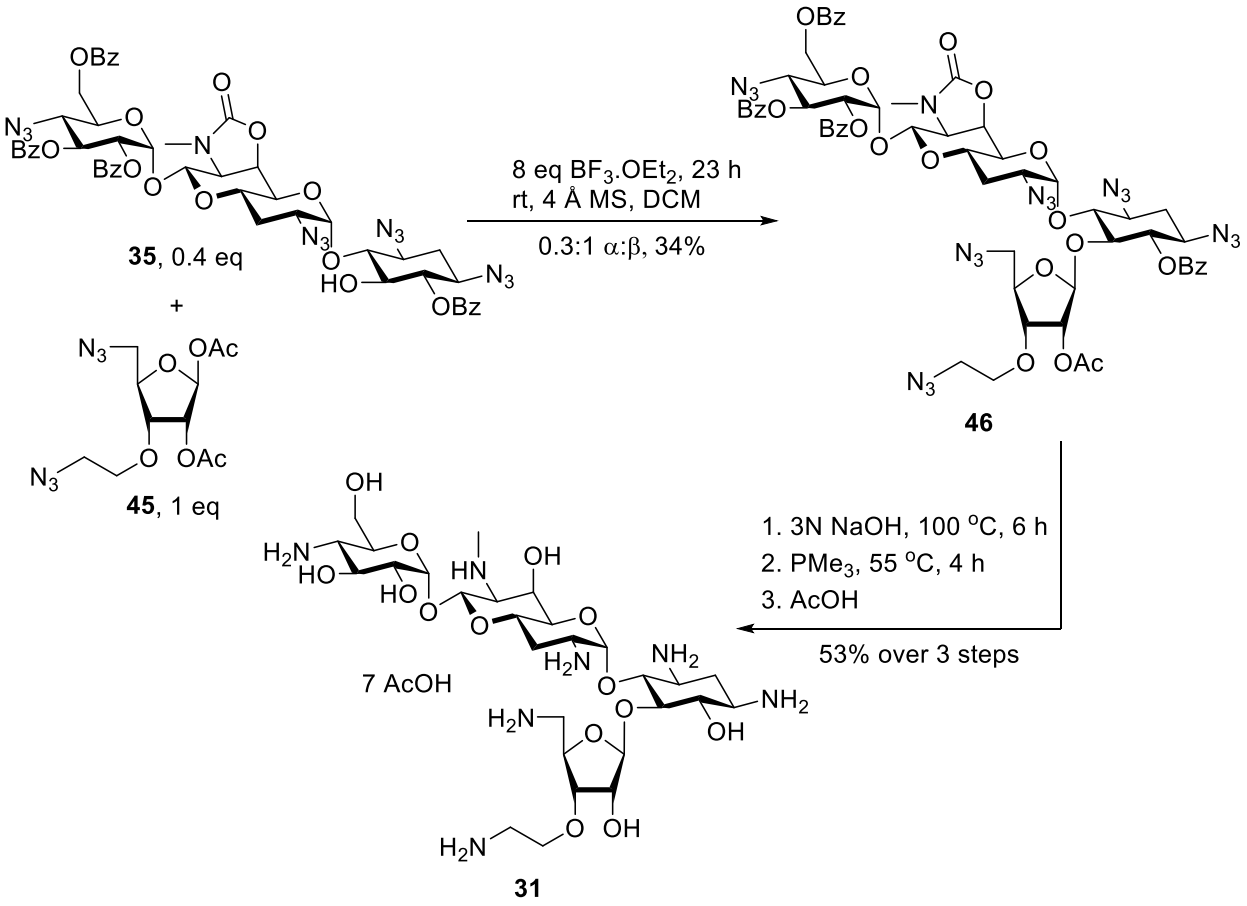

Scheme 2.7. Preparation of **31**

2.4. Antiribosomal Activity and Selectivity

Each apralog was subjected to the cell free ribosomal IC_{50} assays developed by the Böttger group, which measure the minimum amount of AGA needed to inhibit protein synthesis by 50%.[126] Here, Böttger and coworkers engineered a series of *Mycobacterium smegmatis* ribosomes to contain either the human cytosolic decoding A site (Cyt14), the human mitochondrial decoding A site (Mit13), or the human A1555G decoding A site (A1555G), and treated them alongside the wild type bacterial ribosome with the AGA.[56, 57, 93, 127]

Table 1 shows the IC_{50} values obtained for apralogs **17β-31** and for apramycin **7**, organized according to the structure of the appended motif. Selectivity metrics for each of the human A site

were calculated through division of the mutant ribosome IC_{50} value by that of the wild type IC_{50} value. As discussed in Chapter 1, high selectivity for bacterial ribosomal inhibition over the mitochondrial and A1555G A site inhibition is predictive of low AGA-induced ototoxicity, while high selectivity against the human cytosolic A site is predictive of low general toxicity. Additionally, a lower IC_{50} value against the wild type bacterial ribosome is predictive of greater activity. Thus, the most favorable derivatives would exhibit a lower IC_{50} for the wild type bacterial ribosome and greater selectivity factors across the board than those of apramycin.

Table 2.1. IC_{50} values of apralogs

		IC_{50} (μM)					Selectivity		
AGA	**Modification**	**wt**	**Mit13**	**A1555G**	**Cyt14**		**Mit13**	**A1555G**	**Cyt14**
Apra.	Parent	0.11	127 ± 29	134 ± 42	130 ± 3.5		1123	1186	1155
Ribosyl Series									
17β	Ribosyl	0.16	439	272	475		2815	1745	3045
18	Parombiosyl	0.12	2.7	0.47	22		22	4	184
19	3-*O*-Aminoethyl ribosyl	0.08	79	30	253		994	288	3173
20	3-*O*-Hydroxyethyl ribosyl	0.31	904	456	1227		2940	1483	3992
Erythrosyl and Deoxyribosyl Series									
21	Erythrosyl	0.11	329	208	474		2931	1857	4230
22	3-*O*-Aminoethyl erythrosyl	0.02	90	12	194		4471	573	9646
23	3-*O*-(Hydroxyethylaminoethyl) erythrosyl	0.14	180	65	495		1285	464	3536
24	3-*O*-(Aminoethylaminoethyl) erythrosyl	0.03	30	12	72		1010	397	2400
25	3-*O*-(Aminopropylaminoethyl) erythrosyl	0.07	46	7.4	204		657	106	2914
26	3-*O*-(*N',N'*-Dimethylaminopropylaminoethyl) erythrosyl	0.05	21	4.8	95		403	92	1827
27	5-Deoxyribosyl	0.28	562	323	462		2022	1162	1662
5-Aminoribosyl Series									
28	5-Amino-5-deoxyribosyl	0.12	113	109	81		949	916	679
29	5-*N*-Aminoethyl aminoribosyl	0.046	191	150	133		4152	3261	2829
30	5-*N*-Aminopropyl aminoribosyl	0.09	80	72	61		917	820	696
31	3-*O*-Aminoethyl aminoribosyl	0.032	43	21	40		1343	656	1250
32	5-Formamido-5-deoxyribosyl	0.307	572	232	567		1863	755	1847
33	3-*O*-Aminoethyl formamidoribosyl	0.085	93	11	142		1096	130	1669

As illustrated in Table 2.1, installation of a β-D-ribosyl ring at the 5 position of apramycin generally confers greater selectivity for the bacterial A site over each of the human A sites, indicating that these apralogs are likely less toxic than the parent drug. Likewise, antiribosomal activity is only slightly reduced compared to that of the parent drug. These observations are consistent both with the initial studies by Abe and coworkers[113] and with studies by the Fridman group in which a β-D-ribofuranosyl group was installed at the 5-position of 4,6-AGAs and resulted

in comparable activity but significantly increased selectivity for the bacterial ribosome.[31] Moreover, the above results are in accordance with recent studies by Fridman and coworkers who observed that **17β** displayed comparable activity and greater selectivity compared to the parent.[118] It should be noted that installation of a basic aminoethyl group at the 3-position of the furanosyl ring as in compound **19** resulted in a slight increase in activity. The apramycin-paromomycin hybrid **18**, however, shows strikingly high antiribosomal activity against the human mitochondrial and A1555G decoding A sites and thus shows extremely poor selectivity.

Interestingly, 5-*O*-erythrofuranosyl derivatives **21-26** which lack a hydroxymethyl side chain generally exhibit greater activity against the wild type bacterial ribosome than the parent, but with the exception of **21** are significantly less selective against the A1555G decoding A site. As observed in the ribosyl series, installation of an aminoethyl group at the 3-position of the furanose in **22** resulted in a sharp increase in activity, while installation of aminoalkylaminoethyl groups or hydroxyethyl groups at this position resulted in decreased selectivity and decreased activity, respectively. Addition of a 5-deoxyribosyl moiety to the 5-position of apramycin as observed in **27** affords high selectivity for the bacterial ribosome coupled with generally low antiribosomal activity.

Replacement of the primary hydroxyl group of ribose with a simple basic amine as observed in **28** resulted in a slight increase in antiribosomal activity. Installation of an aminoethyl group at *N*5 in **29** strongly increased antiribosomal activity only against the bacterial ribosome, resulting in extremely high selectivity, while the aminopropyl group at N5 in **30** and the 3-*O*-aminoethyl group of **31** each conferred a general increase in antiribosomal activity resulting in comparable selectivity to the parent apramycin. Interestingly, installation of a 5’’’-formamido group resulted in high selectivity at the cost of reduced activity compared to both the parent and

derivatives with a corresponding basic amine. In view of the results shown in Table 2.1, the 5-amino-5-deoxyribofuranosyl derivatives show the most promise, due to their high antiribosomal activities and selectivities, followed by the erythrosyl derivatives.

2.5. Antibacterial Activity

To determine their antibacterial activity, each apralog was administered to cultures of *Escherichia coli* and the ESKAPE pathogens *Klebsiella pneumoniae, Acinetobacter baumanii, Enterobacter cloacae, Pseudomonas aeruginosa*, and methicillin-resistant *Staphylococcus aureus* (MRSA) in a Minimum Inhibitory Concentration (MIC) assay, which determines the minimum amount of the compound needed to inhibit bacterial growth by 50%. Thus, the most promising derivatives would show lower MIC values than the parent apramycin against each strain of bacteria.

Table 2.2. Antibacterial activities against wild type bacterial strains

		MIC (μg/mL)					
	Strain	**AG001**	**AG215**	**AG290**	**AG225**	**AG220**	**AG038**
AGA	**Modification**	***E. coli***	***K. pneumoniae***	***E. cloacae***	***A. baumanii***	***P. aeruginosa***	**MRSA**
Apra.	Parent	4	1-2	2-4	4	4	4
Ribosyl Series							
17β	Ribosyl	4	2	4	16	64	64
18	Parombiosyl	2	1	2	4	16	2-4
19	3-*O*-Aminoethyl ribosyl	2-4	1-2	1-2	4-8	16-32	2-4
20	3-*O*-Hydroxyethyl ribosyl	32	4	8	16	>64	32
Erythrosyl and Deoxyribosyl Series							
21	Erythrosyl	8-16	4	4	8	32	16-32
22	3-*O*-Aminoethyl erythrosyl	1-2	0.5	2-4	4	16	2
23	3-*O*-(Hydroxyethylaminoethyl) erythrosyl	2-4	2	4	8	32	8
24	3-*O*-(Aminoethylaminoethyl) erythrosyl	1-2	1	2-4	4-8	4-8	1-2
25	3-*O*-(Aminopropylaminoethyl) erythrosyl	2	1	1-2	4	8	2
26	3-*O*-(*N',N'*-Dimethylaminopropylaminoethyl) erythrosyl	1-2	0.5	1	4	16	2
27	5-Deoxyribosyl	8	8	8-16	16	64	4-8
5-Aminoribosyl Series							
28	5-Amino-5-Deoxyribosyl	4	1-2	1-2	4-8	4	2
29	5-*N*-Aminoethyl aminoribosyl	2	1	1-2	4-8	4-8	4
30	5-*N*-Aminopropyl aminoribosyl	2-4	2	4	4	2-4	2
31	3-*O*-Aminoethyl aminoribosyl	1-2	0.5-1	1	2	2	1
32	5-Deoxy-5-Formamidoribosyl	8	2-4	4-8	16	>64	8-16
33	3-*O*-Aminoethyl formamidoribosyl	2	1	1-2	4-8	16-32	4

Overall, the MIC values are consistent with the IC_{50} values for each apralog, as shown in Table 2.2. In the 5-*O*-ribofuranosyl series, while increased activity was observed against *E. coli*, *K. pneumoniae*, and *E. cloacae* across the board, all compounds showed a sharp decrease in activity against *P. aeruginosa*, and **17β** and **20** showed poor activity against *A. baumanii* and MRSA. In the erythrosyl series, installation of an additional basic amine as observed in **22-26**

results in a strong increase in activity from the parent against most of the tested pathogens with the exception of *P. aeruginosa*. Though still under examination, one possible explanation for this decreased activity could be susceptibility of the drugs to the efflux mechanism of resistance in *P. aeruginosa* discussed in Chapter 1.[61, 63] The role of additional basic amines is further exemplified by the 5-amino-5-deoxyribofuranosyl derivatives **28**-**30**, all of which exhibit comparable activity to the parent, and **31**, which exhibits greater activity against all strains of bacteria tested than both the parent and each of the other apralogs. Thus, **31** stands out as the most promising of the apralogs based on wild type antibacterial activity.

2.6. AME Susceptibility

As illustrated in Table 2.3, additional MIC assays were carried out with clinical isolates of *E. coli* known to express AAC(3) or APH(3',5'') resistance determinants (the latter of which is denoted below as APH(3')), to determine susceptibility to these AMEs.

Table 2.3. MIC assays against strains of *E. coli* bearing specific resistance determinants

		MIC (μg/mL)				
	Strain	**AG001**	**AG170**	**AG173**	**AG164**	**AG166**
AGA	**Modification**	**WT**	**AAC(3)-IId**	**AAC(3)-IV**	**APH(3')-I**	**APH(3')-IIa**
Apra.	Parent	4	4-8	128-256	4-8	4-8
Ribosyl Series						
17β	Ribosyl	4	8	16-32	8-16	8
18	Parombiosyl	2	4-8	2	8-16	2-4
19	3-*O*-Aminoethyl Ribosyl	2-4	2	4	4	2
20	3-*O*-Hydroxyethyl Ribosyl	16	16	32-64	8-16	8
Erythrosyl and Deoxyribosyl Series						
21	Erythrosyl	8-16	16	128-256	8	8
22	3-*O*-Aminoethyl Erythrosyl	1-2	1	16-32	1	2
23	3-*O*-(Hydroxyethylaminoethyl) Erythrosyl	2-4	4	64	4-8	4
24	3-*O*-(Aminoethylaminoethyl) Erythrosyl	1-2	4	8	1-2	2
25	3-*O*-(Aminopropylaminoethyl) Erythrosyl	2	2-4	4	1-2	4
26	3-*O*-(*N',N'*-Dimethylaminopropylaminoethyl) Erythrosyl	1-2	1	4-8	1-2	2-4
27	5-Deoxyribosyl	8	-	>128	-	8-16
5-Aminoribosyl Series						
28	5-Amino-5-Deoxyribosyl	4	-	-	-	-
29	5-*N*-Aminoethyl Aminoribosyl	2	2	16	2	4
30	5-*N*-Aminopropyl Aminoribosyl	2-4	4	16	2-4	2-4
31	3-*O*-Aminoethyl Aminoribosyl	1-2	1-2	4	1-2	1-2
32	5-Deoxy-5-Formamidoribosyl	8	-	128	-	8-16
33	3-*O*-Aminoethyl formamidoribosyl	2	-	16-32	-	2-4

With the exception of erythrosyl apramycin **21** deoxyribosyl **27**, and 5’’’-formamido derivatives **32**, the apralogs show significantly reduced susceptibility to AAC(3)-IV, the only AGA acting against the parent apramycin. Interestingly, the particularly high activity observed by **18** and **19** against the AAC(3)-IV-expressing *E. coli* indicates that substitution at O3 of the furanosyl ring with either an aminoethyl group or ring IV of paromomycin circumvents susceptibility to

AAC(3), possibly through inhibition of AGA binding to the AME active site. In the erythrosyl seies, on the other hand, activity significantly drops against cultures of *E. coli* expressing AAC(3)-IV in compounds **22-26**, despite the presence of the aminoethyl chain. In conjunction with the relatively high susceptibility to AAC(3)-IV exhibited by **29**, **30**, and **33** and the low susceptibility of **31**, these results indicate that AAC(3)-IV susceptibility is best circumvented through the presence of both an aminoethyl chain at O3 and a primary OH or NH_2 at the 5-position of the furanosyl ring. Of note, only members of the ribosyl series bearing a primary hydroxyl group at the 5-position of the furanose ring showed heightened susceptibility to the APH(3') enzymes; omission of the side chain or replacement of the 5-hydroxyl group with a basic amine bypassed susceptibility to this determinant as expected.

2.7. Cochlear Explant Studies to Determine Ototoxicity

With the above results in hand, further biological testing was carried out on compound **31**, which exhibited greater antibacterial activity across the board and comparable selectivity to the parent apramycin. In order to determine the relative ototoxicity of **31** to that of apramycin, the Sha group at Medical University of South Carolina incubated mouse cochlear explants with apralog **31** and the parent **7** over a 72 hour period, after which the outer hair cells (OHCs) were stained and counted.[114, 128] Greater ototoxicity would result in increased cell death, meaning that the OHC count would be reduced. Systematic variation of drug concentrations as shown in Figure 2.6 allowed for the determination of an LD_{50} value for each drug, a metric that denotes the dose of the drug needed to kill 50% of cells. Through these studies, LD_{50} values for apramycin **7** and derivative **31** were calculated to be 71 ± 1.8 μM and 175 ± 19.2 μM respectively, indicating that derivative **31** is roughly 2.5-fold less ototoxic than the already relatively non-toxic parent. It should be noted

that this sharp decrease in toxicity coincides with only a small increase in ribosomal selectivity as indicated in Table 2.1.

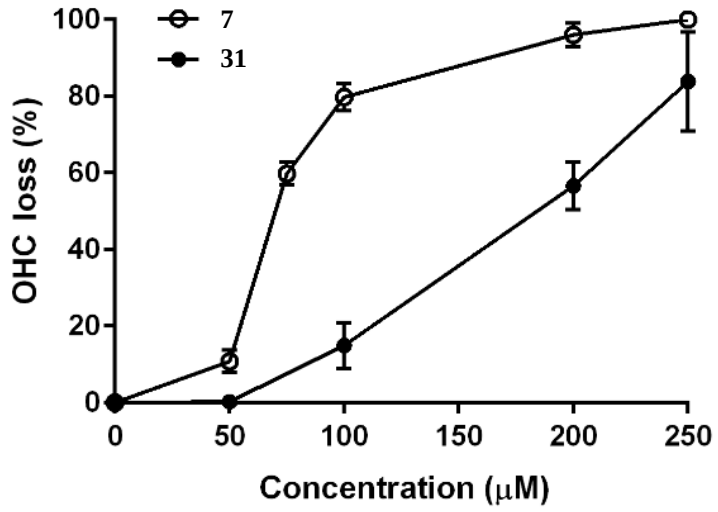

Figure 2.6. Plot of OHC loss as a function of drug concentration for apramycin **7** and **31**

2.8. In Vivo Efficacy Studies to Determine Antibacterial Activity

In vivo efficacy studies using a mouse thigh neutropenic thigh infection model were carried out by scientists at Evotech to determine the relative activity of **31** compared to **7**, as illustrated in Figure 2.7. Log CFU denotes a logarithmic scale of the bacterial burden in the blood of the mouse, where a greater log CFU value denotes a larger bacterial population. Initially, immunosuppressed mice were injected with *E. coli* and were then treated with either **7** or **31** using the doses listed in Figure 2.7. The SOT column denotes the initial bacterial burden on the mouse, while the vehicle column represents bacterial burden after inoculation with *E. coli*. The subsequent columns represent the resulting bacterial burden on the blood after treatment with either **7** or **31** at the specified dose. These studies indicate that roughly double the dose of the parent apramycin is

needed to achieve the reduction in bacterial population observed with administration of **31**; in effect, apralog **31** is roughly twice as active as the parent in addition to being roughly 2.5-fold less ototoxic.

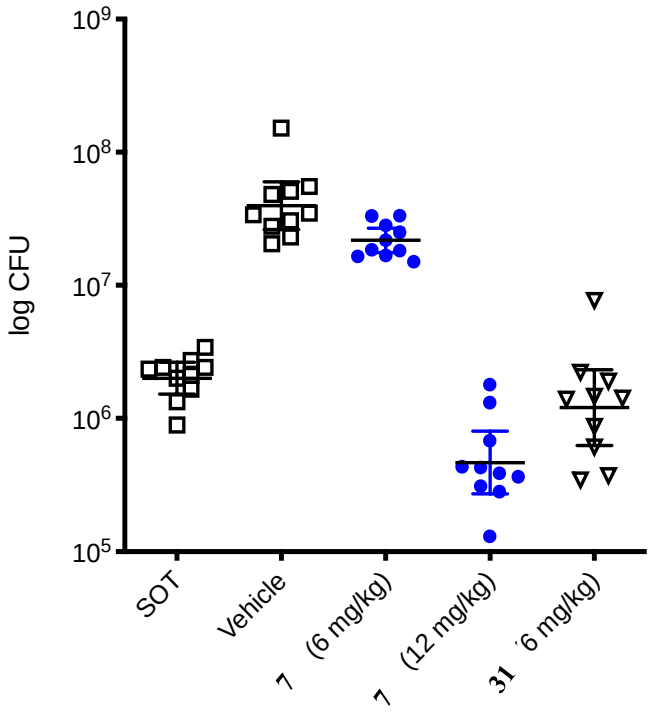

Figure 2.7. In vivo efficacy studies of apramycin **7** and **31** in a mouse thigh infection model

2.9. Conclusions

Through installation of a range of furanosyl groups at O5 of apramycin, a series of apramycin derivatives were prepared with greater antibacterial activity and/or lowered or comparable toxicity to the parent apramycin and resilience to AAC(3)-IV. Members the 5-β-D-ribofuranosyl series expressed generally lower toxicity than the parent compound while maintaining comparable activity, though these derivatives were susceptible to deactivation by the APH(3',5'') AMEs. This susceptibility was circumvented in both the erythrosyl series and the 5-

amino-5-deoxyribosyl series, whose members generally expressed greater antibacterial activity than the parent along with comparable toxicity. Overall, the 5-*O*-[5-amino-3-*O*-(2-aminoethyl)-5-deoxy-β-D-ribofuranosyl] apramycin derivative **31** is the most promising apramycin derivative described to date. It displays 2.5-fold reduced ototoxicity compared to apramycin in ex vivo cochlear explant studies and roughly twofold increased activity compared to apramycin in vivo efficacy studies. Moreover, **31** is strongly resilient against AAC(3)-IV and can be synthesized from the parent apramycin in six linear steps, making it a prime candidate for larger scale synthesis. These factors combine to make **31** an attractive candidate for further development.

CHAPTER 3

STRUCTURE-ACTIVITY RELATIONSHIPS FOR AMINOGLYCOSIDE MODIFICATION AT THE 5''-POSITION

3.1. Introduction

As described in Chapter 2, it was found that installation of a 5-deoxy-5-amino-β-ribofuranosyl moiety at O5 of apramycin in **28** and **31** resulted in excellent in vitro and in vivo antibacterial activity, while installation of a 5-deoxy-5-formamido-β-ribofuranosyl group in **32** resulted in decreased activity.[114, 115, 117] Attempting to generalize on the observations discovered there, a systematic study of simple modifications at the 5''-position was carried out on neomycin, paromomycin, and ribostamycin. Before entering into details of the work conducted, however, it is necessary to look at the extensive and checkered background on modification at the 5''-position.

One of the prominent AME classes that deactivates 4,5- and 4,6-disubstituted AGAs is APH(3'), which phosphorylates the 3'-position. Action of this enzyme series can often be circumvented through deoxygenation at the 3'-position, as is observed for example in the clinical drug tobramycin **47** (Figure 3.1), leading to widespread use of this modification both by Nature and by chemists.[129-131] Some isoforms of the APH(3') enzymes, however, will phosphorylate one or both of the 3' and 5'' positions of the 4,5-AGAs, as evidenced by the susceptibility of the 3'-deoxy-4,5-AGA lividomycins **48** and **49** to certain APH(3') isozymes.[132]

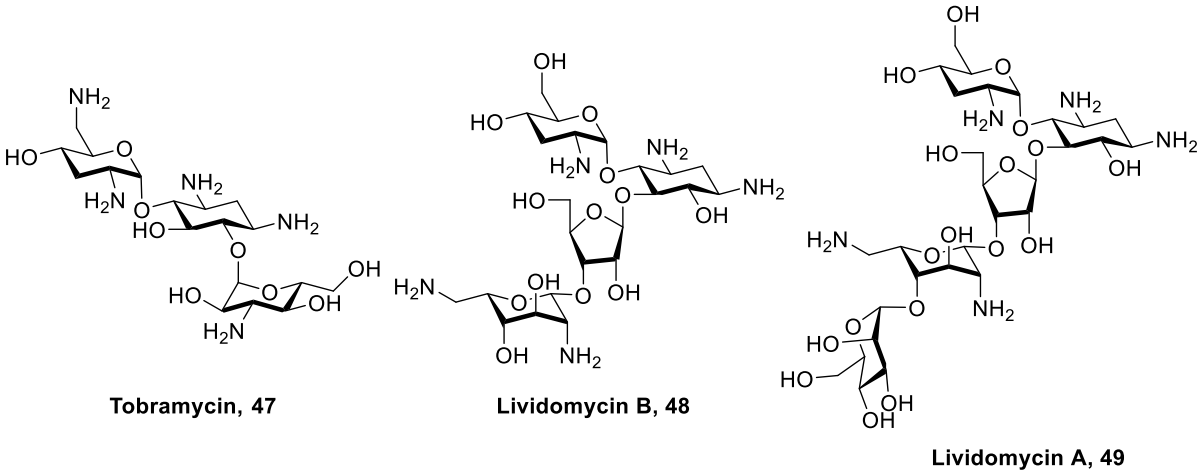

Figure 3.1. Structures of tobramycin **47,** lividomycin B **48**, and lividomycin A **49**

In order to fully circumvent susceptibility to all APH(3') isoforms, modifications must be made at both the 3' and 5'' positions of 4,5-AGAs. Unfortunately, though chemistry at the 5''-hydroxyl group is relatively straightforward given that it is one of only two primary alcohols in most 4,5-AGAs and the only one in some AGAs such as neomycin, early modifications to this group resulted in strongly diminished antibacterial activity, as summarized in Figure 3.2. Deoxygenation and halogenations at the 5''-position of lividomycin B (**50**-**52**), for example, all resulted in significant reductions in activity, as did deoxygenation and installation of a 5''-amino group in lividomycin A (**53** and **54**).[133, 134] In the neomycin series, installation of a range of pyranosamines at the 5''-position (**55-57**) led to a roughly tenfold decrease in antibacterial activity compared to the parent.[135] Moreover, though its antibacterial activity was not reported, 5''-deoxyneomycin (**58**) exhibited a tenfold drop in binding affinity to a 27-mer RNA fragment modeling the decoding A site.[136] In the paromomycin series, aminoalkylation (**59**) and fluorination (**60**) of the 5''-position resulted in significantly reduced activity compared to the parent,[137] as did installation of a 5''-carboxylic acid (**61**) and a 5''-carboxamide (**62**).[138] Likewise, cyclic

compounds such as **63-66** with bridging across the 2'- and 5''- positions or across the 3'- and 5''- positions exhibited sharply decreased antibacterial activity in comparison to the parent AGAs.[136, 139-141]

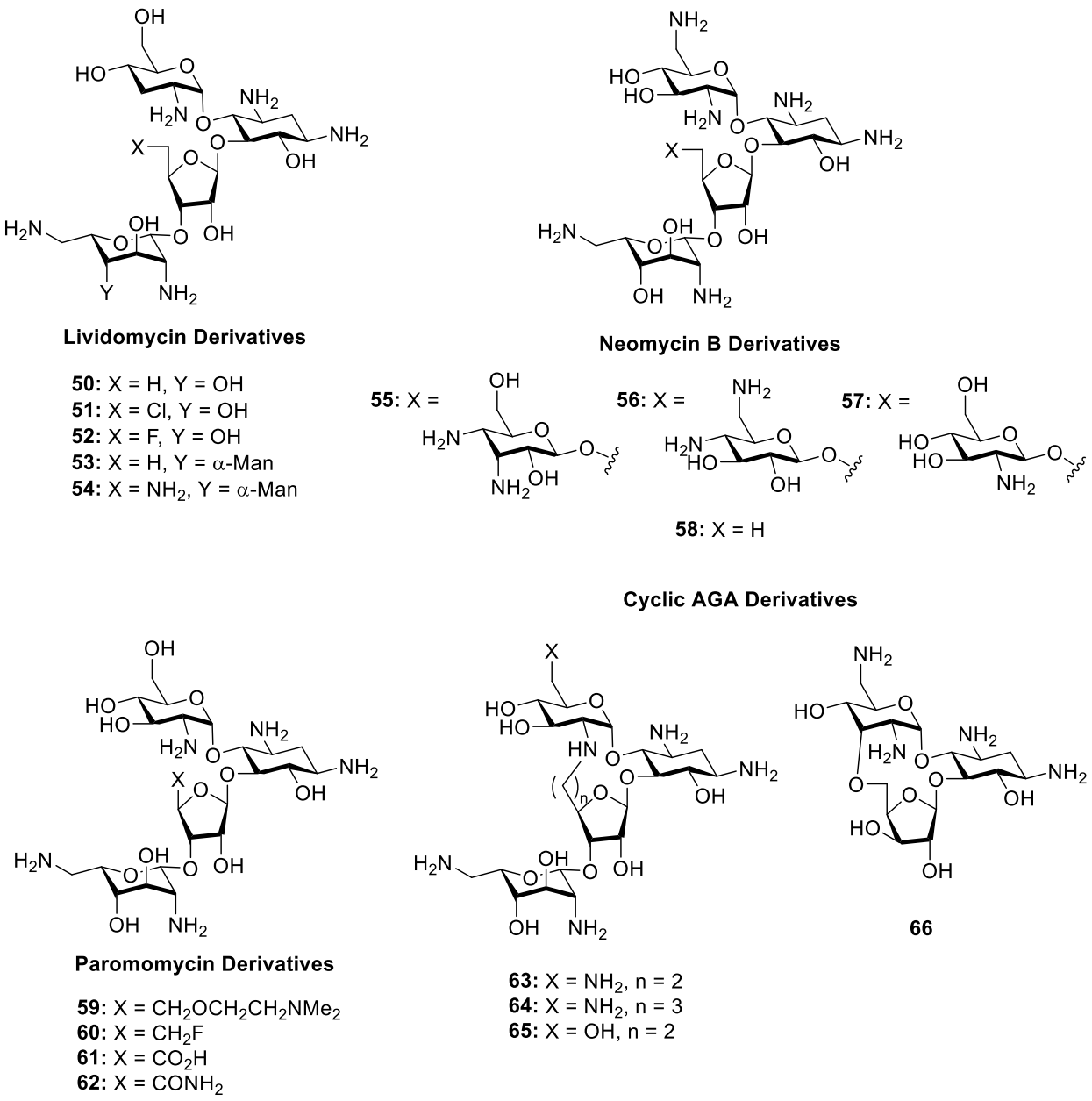

Figure 3.2. 5''-Modifications affording strongly reduced activity

Other modifications at the 5’’-position, however, yielded more promising results, as summarized in Figure 3.3. In the butirosin series, for example, 5’’-amino-5’’-deoxybutirosin **67** exhibited similar antibacterial activity to the parent **11**,[142] as did 5’’-amino- and 5’’-guanidino-4’,5’’-dideoxybutirosin **68** and **69**.[143] Though it showed worse antibacterial activity than the parent AGA ribostamycin **70** against most bacteria, 3’,4’,5’’-trideoxyribostamycin **71** was more active against strains of *E. coli* known to contain APH(3’) resistance determinants.[144] In the paromomycin and neomycin series, Hanessian and coworkers found that 5’’-amino-5’’-deoxy derivatives **72** and **73** show only a slight reduction in activity compared to the parent AGAs.[145] Unlike the pyranose conjugates shown in Figure 3.2, installation of a β-D-ribofuranose moiety at the 5’’-position of neomycin (**74**) afforded similar levels of antibacterial activity to the parent AGA.[135] Likewise, 5’’-deoxy-5’’-triazolyl derivatives **75** and **76** and a range of peptide derivatives such as **77-79** synthesized by Chang and coworkers showed similar MIC values to the parents against strains of *Escherichia coli* and *Staphylococcus aureus*.[146] In 2015, Watkins and coworkers found that neomycin dimer **80** displays greater activity than the parent against strains of *S. aureus* with APH(3’) and AAC(3) resistance determinants as well as lower susceptibility to a wide range of AMEs.[147] In fact, many derivatives of **80** have been prepared using of a wide range of linkers, though their activities strongly vary based on the chosen linker.[147-149]

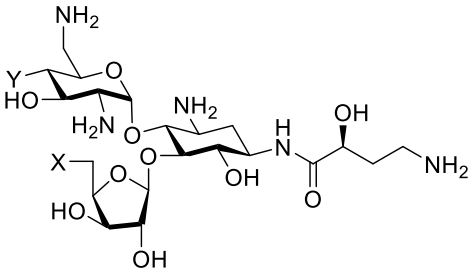

Butirosin Derivatives

67: X = NH_2, Y = OH
68: X = NH_2, Y = H
69: X = NHC(=NH)NH_2, Y = H

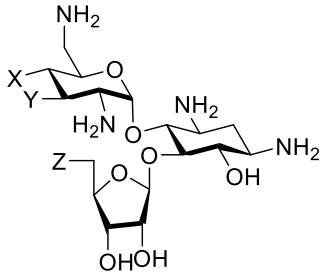

Ribostamycin, 70: X = Y = Z = OH
71: X = Y = Z = H

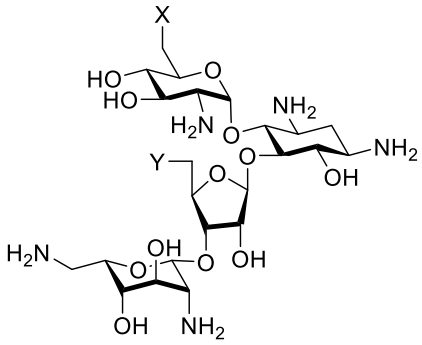

Paromomycin and Neomycin Derivatives

72: X = Y = NH_2
73: X = OH, Y = NH_2
74: X = NH_2, Y =

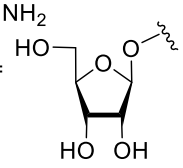

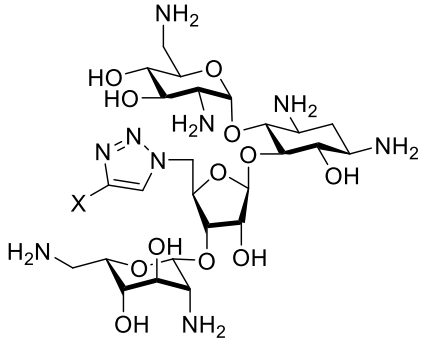

Triazolyl Neomycin Derivatives

75: X = CH_2NMe_2
76: X = CH_2NHMe

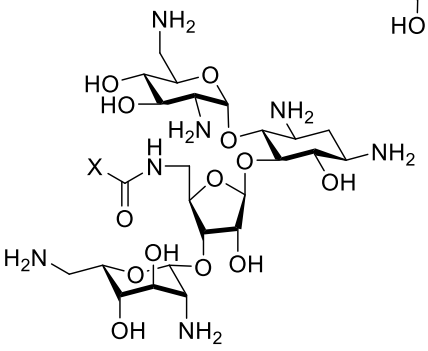

Neomycin Peptide Derivatives

77: X = CH_2NH_2
78: X = $CH_2NHC(=O)CH_2NH_2$
79: X = Palmitoyl

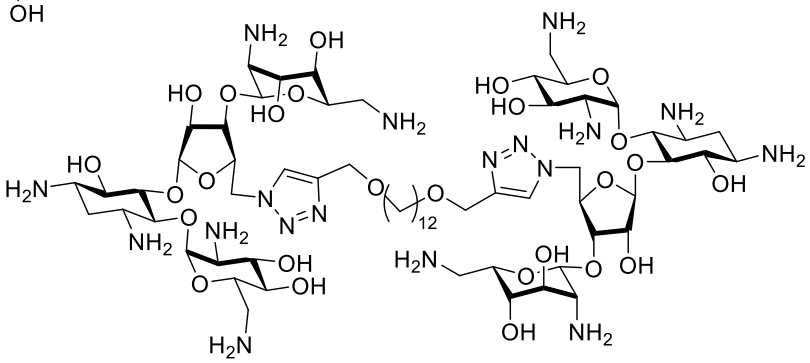

Neomycin Dimer 80

Figure 3.3. 5’’-Modifications affording promising antibacterial activity

Consistent with reports by Hanessian on paromomycin and neomycin,[145] recent studies carried out in the Crich group on the highly active propylamycin **14** show that the 5’’-deoxy-5’’-amino derivative **81** exhibits slightly lower antibacterial activity than the parent and increased toxicity. The corresponding formamido derivative **82**, on the other hand, displays comparable activity and reduced toxicity with respect to propylamycin (Figure 3.4).[150]

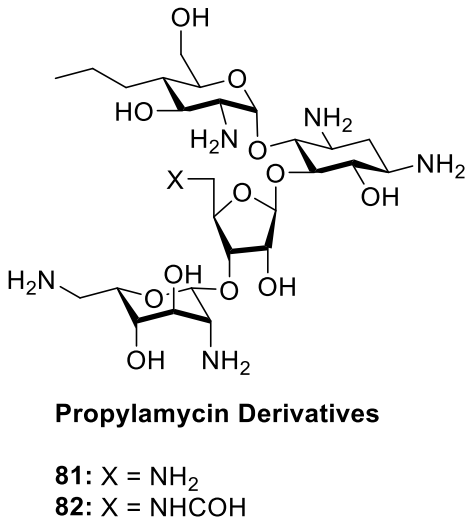

Figure 3.4. Structure of propylamycin derivatives

3.2. Target Modifications at the 5’’-Position

In view of the need to overcome the action of the APH(3’)s without loss of antibacterial activity, and of the many disappointing results observed by previous workers with simple substitutions at the 5’’-position, a systematic survey of modifications at the 5’’-position of neomycin, paromomycin, and ribostamycin was undertaken in the Crich lab, as shown in Figure 3.5. The high activity of erythrosyl apralog **21** inspired the examination of the erythrosyl modification in other 4,5-AGAs. Though 5’’-deoxygenation of neomycin was reported by previous workers to result in reduced binding strength to a RNA fragment,[136] the lack of published

antibacterial data led to inclusion of this modification in this series. Though installation of a 5’’-amino group was suggested by Hanessian[145] and Baasov[151] to reduce activity in paromomycin, neomycin, and ribostamycin as discussed above, the increased activity conferred by its inclusion in the apralog series inspired further investigation. Similarly, given that installation of a 5’’-formamido group in propylamycin analog **82** retained the high antibacterial of the parent while the corresponding modification in apralog **32** resulted in lower activity, the formamido group was selected as a 5’’-modification for further study. In view of the wide range of peptide derivatives tolerated at the 5’’-position of neomycin shown above, which indicate that steric bulk may be tolerated at this position, the simple 5’’-acetamido group was selected for examination. It is well established that the activity of a given AGA generally increases with the number of protonated amines due to electrostatic interaction between the positively charged AGA and the negatively charged binding site.[152-155] Thus, the AGAs neomycin, paromomycin, and ribostamycin, which contain six, five, and four basic amines respectively, were selected as parent compounds to determine how the number of basic amines influences tolerance of each 5’’-modification.

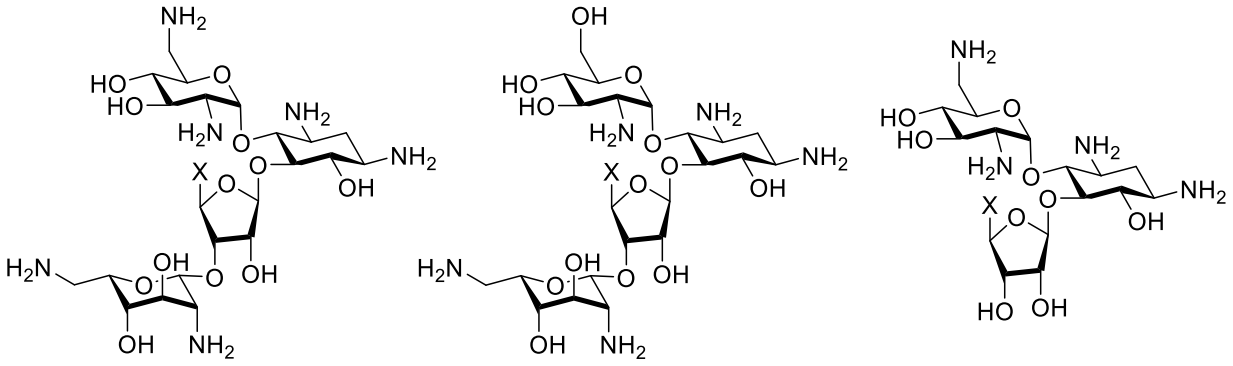

Neomycin Targets

83: X = H
58: X = CH_3
72: X = CH_2NH_2
84: X = CH_2NHCOH
85: X = $CH_2NHCOMe$

Paromomycin Targets

86: X = H
87: X = CH_3
73: X = CH_2NH_2
88: X = CH_2NHCOH
89: X = $CH_2NHCOMe$

Ribostamycin Targets

90: X = H
91: X = CH_2NH_2
92: X = CH_2NHCOH
93: X = $CH_2NHCOMe$

Figure 3.5. Targeted 5''-modifications of neomycin, paromomycin, and ribostamycin

The syntheses of compounds **58, 72, 73, 83-87**, and **91** are described in this chapter; all other compounds in this collaborative effort were made by coworkers in the Crich lab. The entire series of compounds is taken into consideration in the discussion of their biological activity.

3.3. Synthesis of 5''-Derivatives

As shown in Scheme 3.1, literature compound **94**[156] was treated with trityl chloride to selectively protect the primary 5''-OH, after which the compound was peracetylated in the same pot. The trityl group was subsequently deprotected using $FeCl_3 \cdot 6H_2O$[157] and the resulting primary alcohol was oxidized using BAIB and TEMPO[158] to form **95** in 33% yield over four steps. Compound **95** was subjected to Barton decarboxylation conditions[159] using 1-oxa-2-oxo-3-thiaindolizinium chloride to make an activated ester followed by photolytic cleavage with *tert*-dodecyl thiol as a hydrogen source to make erythrosyl derivative **96** in 42% yield. All acetates were selectively cleaved with $Mg(OMe)_2$[21] and all TFA groups were subsequently hydrolyzed in

NaOH. Initial cleavage of the acetates is crucial, as simultaneous cleavage of acetates and trifluoroacetamides can lead to migration of an acetate to a free amine, generating an acetamide that is difficult to cleave. The resulting solid was subsequently passed through Sephadex C-25 ion exchange resin and lyophilization with acetic acid gave the peracetate salt of **83** in 55% yield.

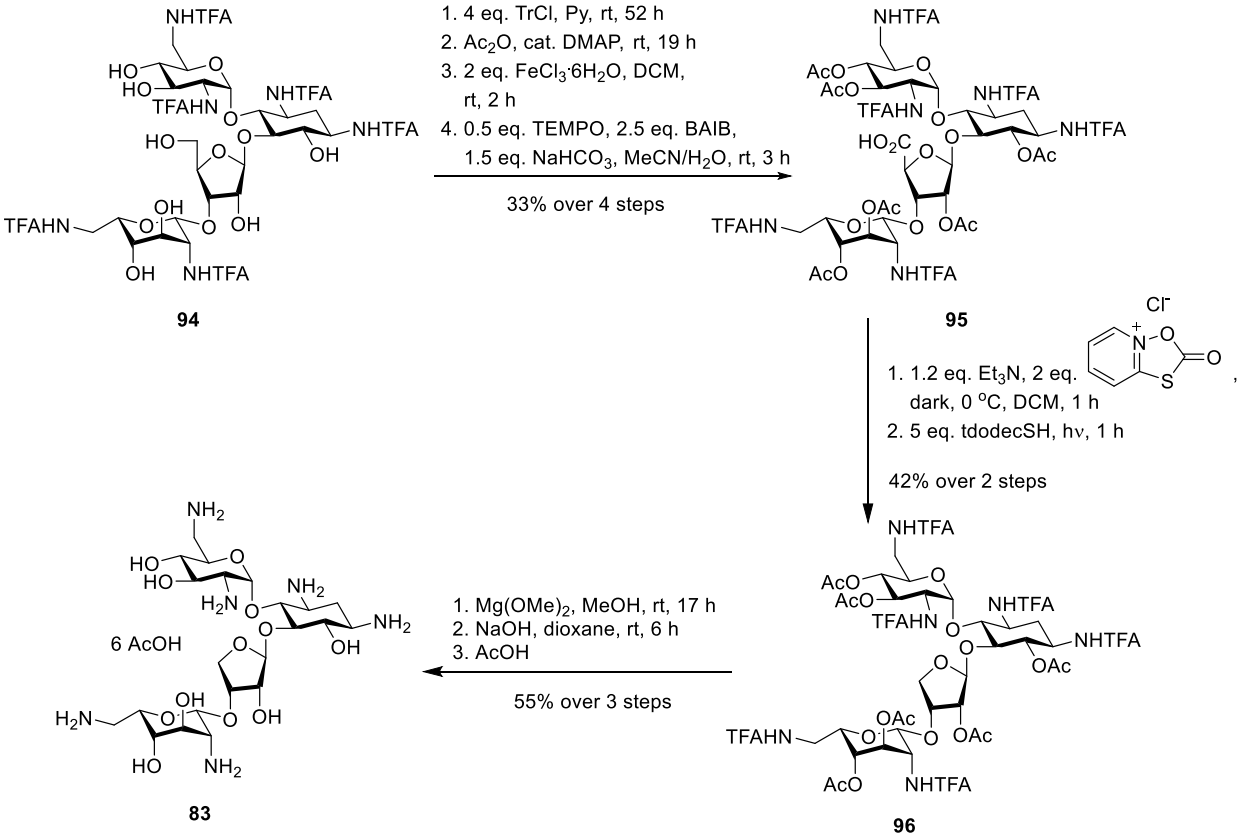

Scheme 3.1. Synthesis of **83**

As shown in Scheme 3.2, compounds **58**, **72**, **84**, and **85** were all prepared from the common intermediate **98**, generated through trisylation of literature compound **97**[160] in 61% yield. Displacement of the trisyl group using NaI gave the alkyl iodide **99** in 74% yield, and subsequent hydrogenolysis to cleave the azides and the C-I bond followed by elution through Sephadex C-25

ion exchange resin gave the peracetate salt of **58** in 33% yield. Displacement of the trisyl group in **98** with potassium phthalimide gave the phthalimido derivative **100** in 50% yield, which was subsequently deprotected with hydrazine hydrate[161] to give the free amine **101** in 73% yield. Hydrogenolysis of the azides followed by elution through Sephadex C-25 and lyophilization with acetic acid gave the peracetate salt of **72** in 70% yield. To install the 5''-formyl group, compound **101** was treated with excess formic acetic anhydride.[162] The resulting product was treated with methanol and $NaHCO_3$ to hydrolyze any *O*-formyl groups generated during acylation and subsequently subjected to hydrogenolysis to deprotect the azides. The fully deprotected compound was passed through a Sephadex-C25 column and lyophilized with acetic acid to give the peracetate salt of **84** in 41% yield. Similarly, compound **101** was treated with excess acetic anhydride in triethylamine to acetylate the free amine followed by sodium methoxide to hydrolyze any *O*-acetyl groups. Hydrogenolysis followed by elution through Sephadex C-25 and lyophilization with acetic acid gave product **85** in 24% yield.

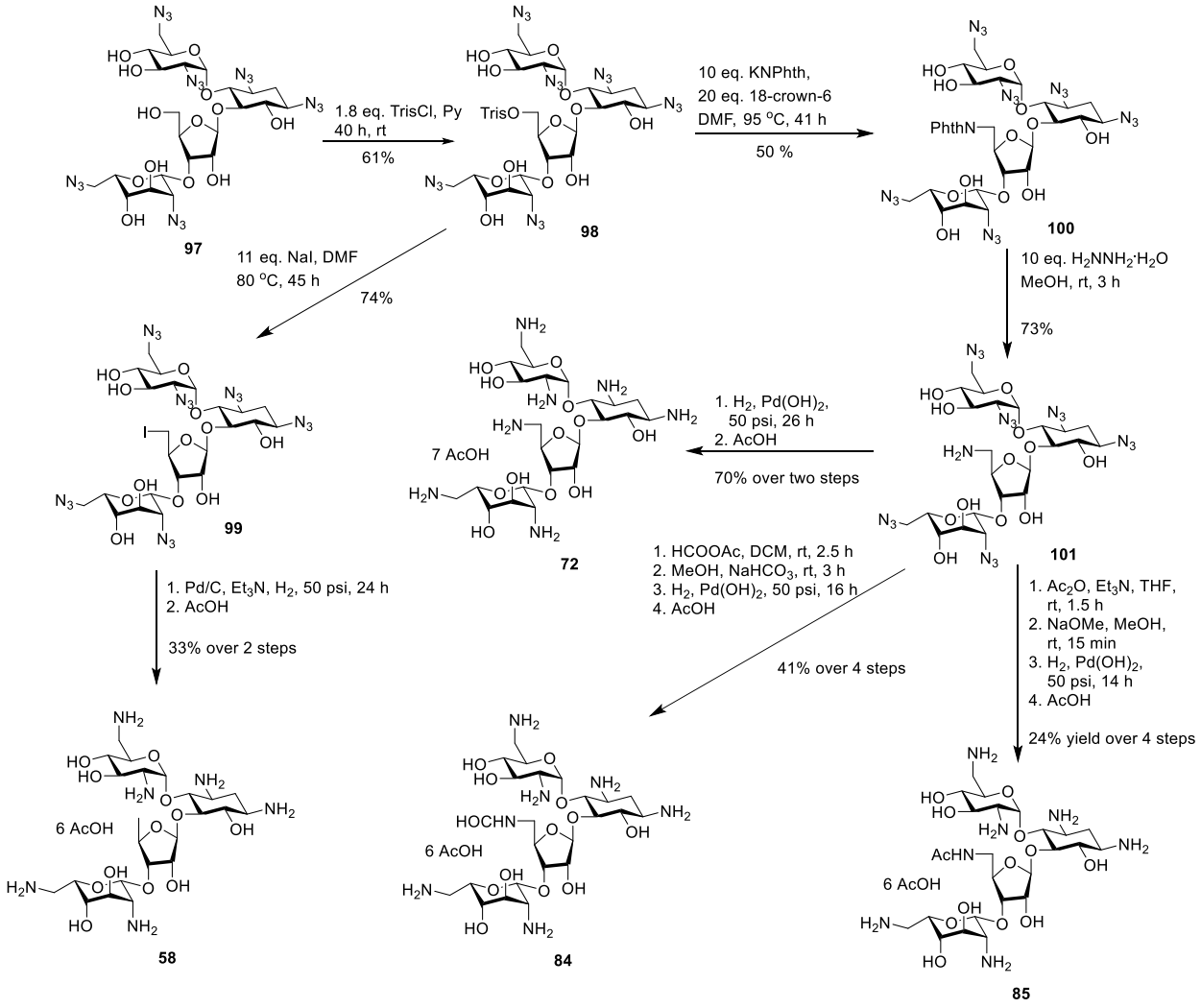

Scheme 3.2. Synthesis of **58**, **72**, **84**, and **85**

Interestingly, and unlike acetamido derivatives **85** and **89**, formamido derivatives **84** and **88** are found in solution as mixtures of two isomers: the major *Z* isomer and the minor *E* isomer. The major isomer of **84** exhibited $^{3}J_{H5'',\text{-CHO}}$ and $^{1}J_{\text{CHO-CO}}$ coupling constants of 2.3 and 197.5 Hz respectively, consistent with the *Z*-rotamer.[163, 164] As illustrated in Figure 3.6a, the *E* rotamer of acetamides is strongly disfavored due to the ensuing steric clash between the methyl group and the substituent at nitrogen. In formamides, however, a small percentage of the *E* rotamer is observed

because the clash between the formyl proton and the substituent at nitrogen is minimal.[165] Figure 3.6b shows the *E*/*Z* ratios of various *N*-monosubstituted amides.[164, 166]

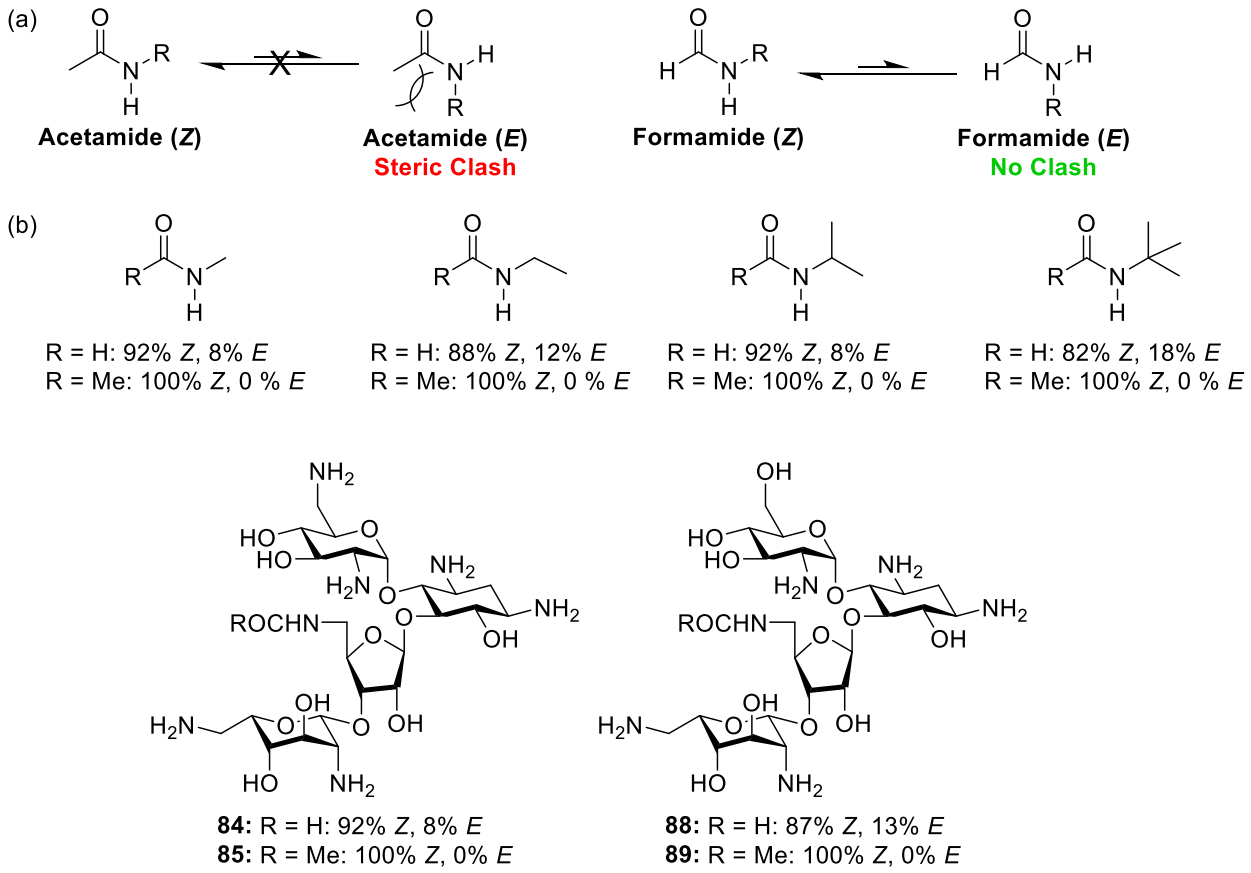

Figure 3.6. (a) Rotational isomerization in formamides versus acetamides (b) Populations of *E* and *Z* rotamers for monosubstituted amides and compounds **84**, **85**, **88**, and **89**

The synthesis of compound **86** strongly resembles that of **83** and is shown in Scheme 3.3. Literature compound **102**,[21] where all amines are protected as trifluoroacetamides and O4 and O6 are protected with a benzylidene acetal, was exposed to one-pot tritylation and acetylation, followed by deprotection of the trityl group with $FeCl_3 \cdot 6H_2O$ as above.[157] The resulting alcohol was oxidized according to protocols by Baasov and coworkers[167] using BAIB and TEMPO to give

acid **103** in 36% overall yield. Carboxylic acid **103** was then subjected to Barton decarboxylation[159] to make erythrosyl derivative **104** in 47% yield. After deprotection of the benzylidene acetal through acidic hydrolysis, all acetates were selectively cleaved with $Mg(OMe)_2$[21] and all TFA groups were subsequently hydrolyzed in NaOH. The deprotected compound was passed through a column of Sephadex-C25 ion exchange resin and lyophilized with acetic acid to give the peracetate salt of **86** in 83% yield.

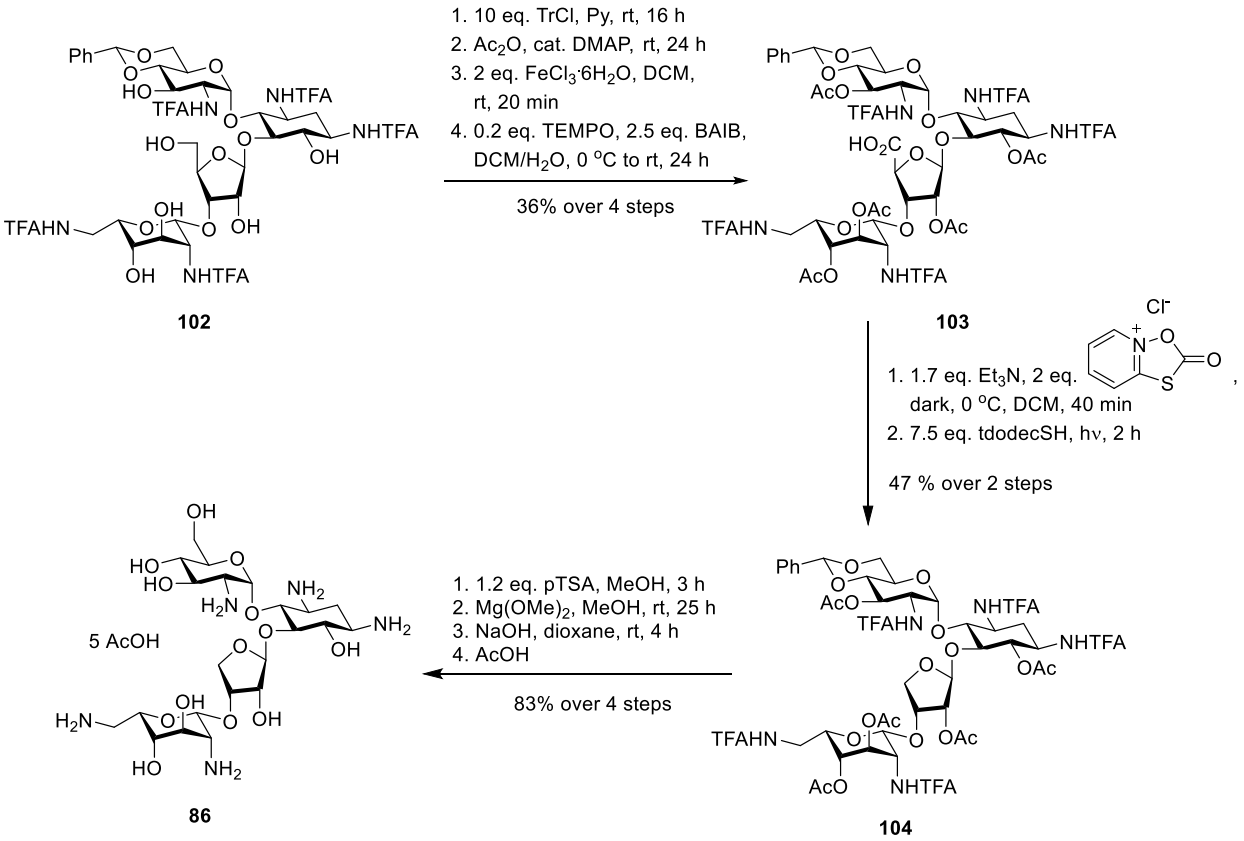

Scheme 3.3. Synthesis of **86**

Compounds **87** and **73** were synthesized using the common intermediate **106**, prepared from trisylation of literature compound **105** in 53% yield as shown in Scheme 3.4.[168] Displacement

of the trisyl group with NaI in acetone at reflux gave intermediate **107** in 68% yield, which was subsequently subjected to acidic hydrolysis to remove the benzylidene group and hydrogenolysis to cleave the azides. The fully deprotected compound was passed through a column of Sephadex C-25 ion exchange resin to generate the peracetate salt of **87** in 57% yield. Similarly, displacement of the trisyl group with NaN_3 gave the 5’’-azido derivative **108** in 78% yield, which was then subjected to hydrogenolysis, eluted through a column of Sephadex C-25 ion exchange resin, and lyophilized with acetic acid to give **73** in 54% yield.

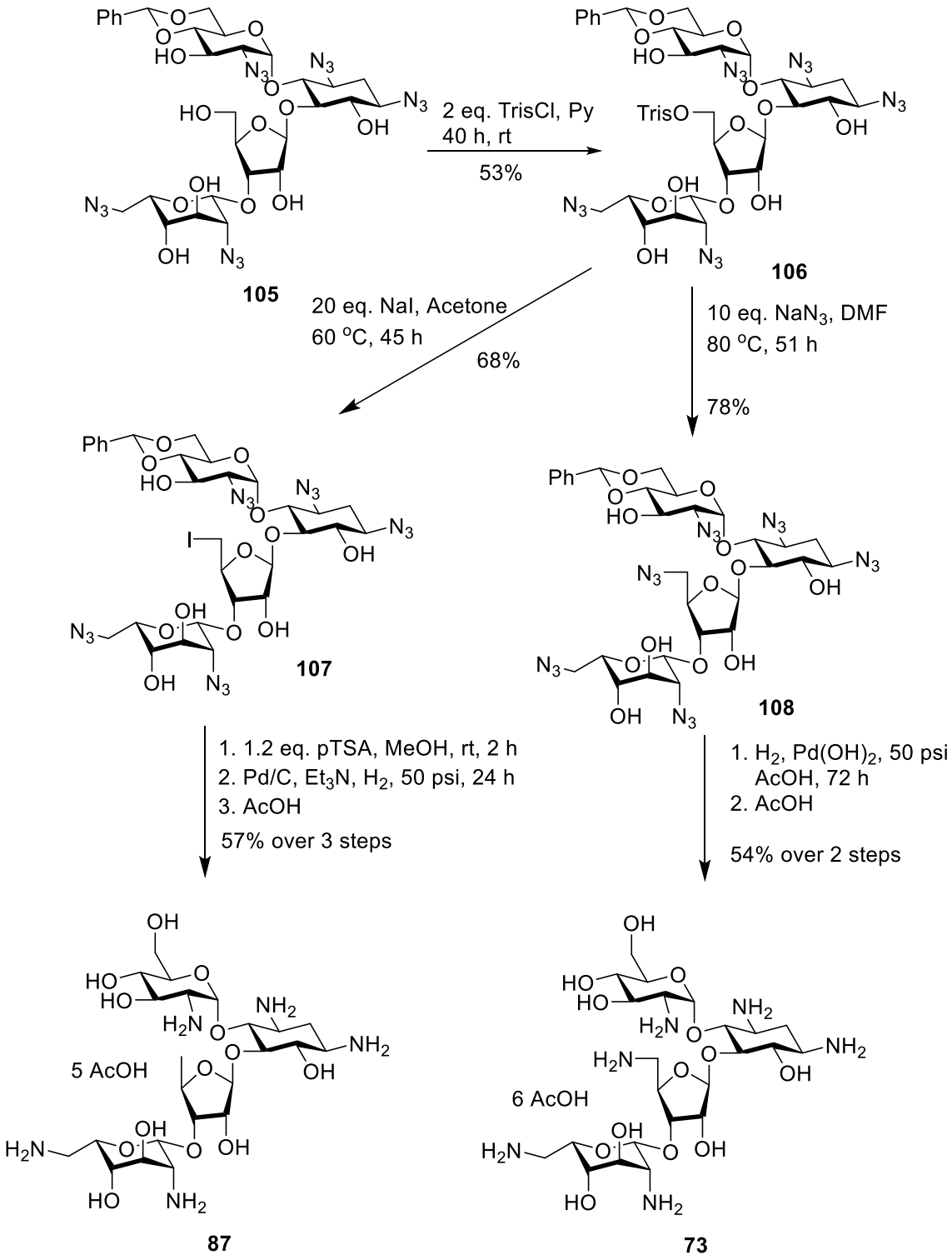

Scheme 3.4. Synthesis of **87** and **73**

To prepare derivative **91**, the free amines of ribostamycin **70** were protected as azides using triflyl azide and copper sulfate[156] to generate intermediate **109** in 57% yield. The primary hydroxyl group was then trisylated to give **110** in 41% yield. Subsequent displacement with sodium azide produced the 5’’-azido derivative **111** in 74% yield, which was then subjected to hydrogenolysis, passed through a Sephadex C-25 resin column, and lyophilized with acetic acid to give the peracetate salt of **91** in 31% yield (Scheme 3.5).

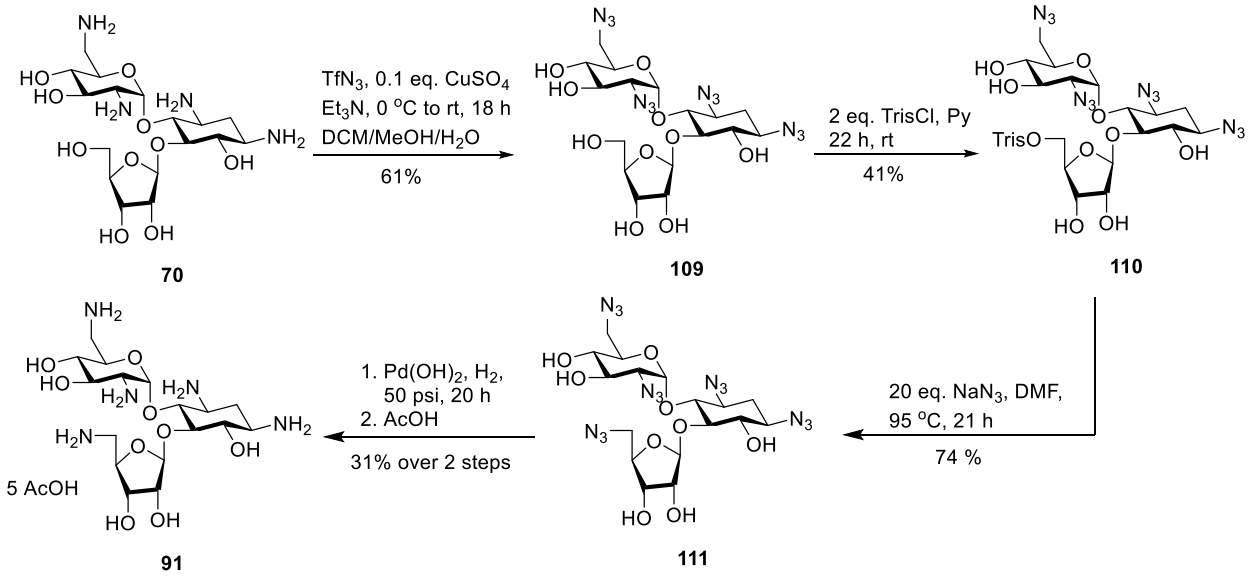

Scheme 3.5. Synthesis of **91**

3.4. Antiribosomal Activity and Selectivity

IC_{50} studies were carried out by the Böttger laboratory in Zurich on wild type *M. smegmatis* ribosomes and on mutant ribosomes containing the human cytoplasmic, mitochondrial, and A1555G decoding A sites, as illustrated in Table 3.1. Lower IC_{50} values indicate greater antiribosomal activity, while higher selectivity values are predictive of lower toxicity. In addition

to the neomycin, paromomycin, and ribostamycin derivatives discussed above, select apralogs and propylamycin derivatives are included to serve as points of comparison.

Table 3.1. IC_{50} assays on 5’’-derivatives of various AGAs

		IC_{50} (μM)					Selectivity		
Compound	**5’’-Substituent**	**wt**	**Mit13**	**A1555G**	**Cyt14**		**Mit13**	**A1555G**	**Cyt14**
Neomycin Series (6 basic amines in parent)									
Neomycin	OH	0.034	3.6	0.40	34		106	12	1000
83	Erythro	0.037	4.5	0.076	32		122	2	865
58	H	0.039	10.7	0.945	32		274	24	821
72	NH_2	0.023	17	0.578	32		739	25	1391
84	NHCHO	0.048	15	1.09	56		313	23	1167
85	NHAc	0.038	18	1.2	38		474	32	1000
Paromomycin Series (5 basic amines in parent)									
Paromomycin	OH	0.033	131	12	37		3970	364	1121
86	Erythro	1.059	302	5.7	25		285	5.4	24
87	H	1.092	236	134	288		216	123	264
73	NH_2	0.090	36	6.3	6.6		400	70	73
88	NHCHO	0.040	166	27	114		4150	675	2850
89	NHAc	0.513	270	17	146		526	33	285
Ribostamycin Series (4 basic amines in parent)									
Ribostamycin	OH	0.089	461	86	416		5180	966	4674
90	Erythro	1.612	502	122	451		311	76	280
91	NH_2	0.088	76	34	50		861	386	570
92	NHCHO	0.686	682	284	620		994	414	904
93	NHAc	3.542	629	560	616		178	158	174
Propylamycin Series (5 basic amines in parent)									
Propylamycin	OH	0.022	150	56	61		6818	2545	2773
81	NH_2	0.14	62	38	9.0		443	271	64
82	NHCHO	0.034	290	118	175		8529	3471	5147
Apralog Series (5 basic amines in parent)									
17β	OH	0.16	439	272	475		2815	1745	3045
21	Erythro	0.11	329	208	474		2931	1857	4230
27	H	0.28	562	323	462		2022	1162	1662
28	NH_2	0.12	113	109	81		949	916	679
32	NHCHO	0.307	572	232	567		1863	755	1847

In the neomycin series, all modifications were generally well-tolerated; antiribosomal activity was comparable in all cases and selectivity against the human mitochondrial ribosome increased with each modification. In the paromomycin series, however, erythrosyl paromomycin **86** and 5’’-deoxyparomomycin **87** exhibit sharp decreases in both antiribosomal activity against the wild type bacterial ribosomes and selectivity, as does 5’’-acetamido paromomycin **89**. Though not to the same degree, 5’’-amino-5’’-deoxyparomomycin **73** displays slightly reduced antiribosomal activity against the wild type ribosome and significantly reduced selectivity compared to the parent. The 5’’-formamido derivative **88**, however, demonstrates excellent antiribosomal activity against the bacterial ribosome and greater selectivity against the human A sites, especially the A1555G mutant. The trends observed in the paromomycin series are mirrored by propylamycin: introduction of a 5’’-amine reduces wild type antiribosomal activity and selectivity while introduction of a 5’’-formamide preserves activity against the bacterial ribosome while increasing selectivity. In the case of ribostamycin, erythrosyl derivative **90**, 5’’-formamido derivative **92**, and 5’’-acetamido derivative **93** all exhibit sharply reduced antiribosomal activity against the wild type bacteria and selectivity. Though 5’’-deoxy-5’’-aminoribostamycin **91** shows comparable activity to the parent, its selectivity against the human ribosome is strongly diminished. In light of the similar antiribosomal activity between the erythrosyl and deoxyribosyl derivatives in the paromomycin and neomycin series and the lack of antiribosomal activity displayed by erythrosyl ribostamycin **90**, 5’’-deoxyribostamycin was not prepared and is expected to be inactive.

The observations in the apralog series, however, strongly differ from the above trends. The 5’’-deoxy and 5’’-formamido apralogs **27** and **32** both show markedly decreased antiribosomal activity and selectivity compared to ribofuranosyl apralog **17β**. Introduction of a 5’’-amine in **28**

resulted in increased antiribosomal activity against the wild type ribosome at the cost of decreased selectivity, while erythrosyl derivative **21** exhibited both high activity and high selectivity.

The difference between the trends observed in the neomycin series, where 5''-modifications are broadly tolerated, and those observed in the paromomycin and ribostamycin series, where certain modifications result in strong reductions in antiribosomal activity, can be attributed to the difference in the number of basic amines in the parent AGAs. As discussed above, the correlation between the number of protonated amines on an aminoglycoside and antibacterial activity is well established;[152-155] of the parent AGAs examined in this study, neomycin is by far the most active due to its high number of basic amines. Thus, the tolerance for modifications at the 5''-position of the neomycin series can be rationalized by strong electrostatic stabilization of the neomycin-ribosome complex resulting from the six protonated amines, which can apparently outweigh potential destabilizing interactions at the 5''-position for the derivatives studied. Given that the coulombic stabilization of the AGA – ribosome complex is reduced in paromomycin and more so in ribostamycin, these AGAs are more susceptible to destabilizing interactions resulting from 5''-modification than neomycin.

In view of the well-documented correlation of the number of basic amino groups with affinity for the ribosome, the introduction of another basic amine at the 5''-position was expected to result in increased antiribosomal activity. Indeed, this was found to be the case with apralog **28**. With all other derivatives, however, installation of a 5''-amino group afforded reduced or comparable antiribosomal activity to that of the parent. Additionally, while an increase in positive charge generally correlates with greater toxicity,[152] as evidenced by the selectivities in the neomycin, paromomycin, and ribostamycin series, 5''-deoxy-5''-aminoneomycin **72** exhibits

greater selectivity against the human mitochondrial A site than the parent. At present, this observation is not well understood and is the subject of ongoing study.

3.5. Antibacterial Activity

As with the apralogs in Chapter 2, MIC assays were carried out with each 5’’-derivative on *Escherichia coli* and various ESKAPE pathogens to determine the effect of the modifications on antibacterial activity, presented in Table 3.2.

Table 3.2. MIC assays on ESKAPE pathogens and *E. coli*

		MIC (μg/mL)					
	Strain	**AG001**	**AG215**	**AG290**	**AG225**	**AG220**	**AG038**
Compound	**5''-Substituent**	***E. coli***	***K. pneumoniae***	***E. cloacae***	***A. baumanii***	***P. aeruginosa***	**MRSA**
Neomycin Series (6 basic amines in parent)							
Neomycin	OH	2	0.5	1	1-2	32-64	1
83	Erythro	4	0.5-1	1-2	2-4	>64	1
58	H	4	1-2	1-2	2-4	>64	1-2
72	NH_2	4-8	2	2-4	8	16-32	1-2
84	NHCHO	2-4	0.5-1	1-2	2-4	64	1-2
85	NHAc	2-4	0.5-1	1-2	2-4	>64	1
Paromomycin Series (5 basic amines in parent)							
Paromomycin	OH	2-4	1	2	2-4	>128	2
86	Erythro	16	4-8	8-16	16	>64	8
87	H	32-64	16-32	32	64	>64	16-32
73	NH_2	8	2-4	4	4-8	>64	2-4
88	NHCHO	4	1	2	2-4	≥128	2-4
89	NHAc	16	8	8-16	8-16	>128	8
Ribostamycin Series (4 basic amines in parent)							
Ribostamycin	OH	4-8	2	4	4	>128	4
90	Erythro	64-128	32	64	64	>128	32
91	NH_2	32-64	4	4	4	>32	8
92	NHCHO	16-32	8	8-16	16	>128	16-32
93	NHAc	128	32	32-64	128	>128	64-128
Propylamycin Series (5 basic amines in parent)							
Propylamycin	OH	1	0.25-0.5	0.5	1-2	8	1-2
81	NH_2	2	1	1	2	4	2
82	NHCHO	1	1	1	2	8	1
Apralog Series (5 basic amines in parent)							
17β	OH	4	2	4	16	64	64
21	Erythro	8-16	4	4	8	32	16-32
27	H	8	8	8-16	16	64	4-8
28	NH_2	4	1-2	1-2	4-8	4	2
32	NHCHO	8	2-4	4-8	16	>64	8-16

The antibacterial activities from the MIC assay generally match the trends in antiribosomal activity exhibited in Table 3.1. In nearly all cases, erythrosyl, 5''-deoxy, and 5''-acetamido

derivatives exhibit lower activity than the parent compounds, though for neomycin these decreases are not substantial. The exceptions lie in the apralog series, where erythrosyl derivative **21** and 5’’-deoxyribosyl derivative **27** show significantly greater activity than ribosyl apralog **17β** against strain AG038 of MRSA, which does not express any AMEs.

In the neomycin, paromomycin, ribostamycin, and propylamicin series, the installation of a 5’’-amino group appears to reduce antibacterial activity, while the 5’’-amino apralog **28** exhibits comparable or increased antibacterial activity (depending on the strain of bacteria) to that of ribosomal apralog **17β**. The slight reduction in activity of 5’’-amino derivatives **72, 73**, and **91** is consistent with the reduced activity observed by both Hanessian[145] and Baasov,[151] and can potentially be explained through analysis of the crystal structure of paromomycin bound to helix 44 of the 30S ribosomal subunit of *Thermus thermophilus* (Figure 3.7).[33] It is well established that intramolecular hydrogen bonding in AGAs aids in preorganization of the drug into a conformation that more closely resembles that observed when bound to the decoding A site; this preorganization reduces the entropic penalty of binding to the ribosome, thereby increasing AGA binding affinity.[136, 169] In the 4,5-series, intramolecular H-bonding is observed between N2’ and O5’’ and between N2’ and O4’ as shown in Figure 3.7.[31, 33, 170] When the 5’’-hydroxyl group is converted into a basic amine, hydrogen bonding between the 2’- and 5’’-positions is no longer possible, as both positions are protonated. As a result, the 5’’-amino derivatives do not benefit from preorganization arising from H-bonding between these positions. Moreover, given that both residues are positively charged, the electrostatic repulsion between N2’ and N5’’ likely causes the C5’’-N5’’ bond to take up a different conformation, thereby distancing N5’’ from G1491 and weakening any hydrogen bonding between these groups. It is not currently clear, however, why

the 5’’-amino modification in the apralog series confers increased activity that contrasts with the other 4,5-AGAs; this observation is still under investigation.

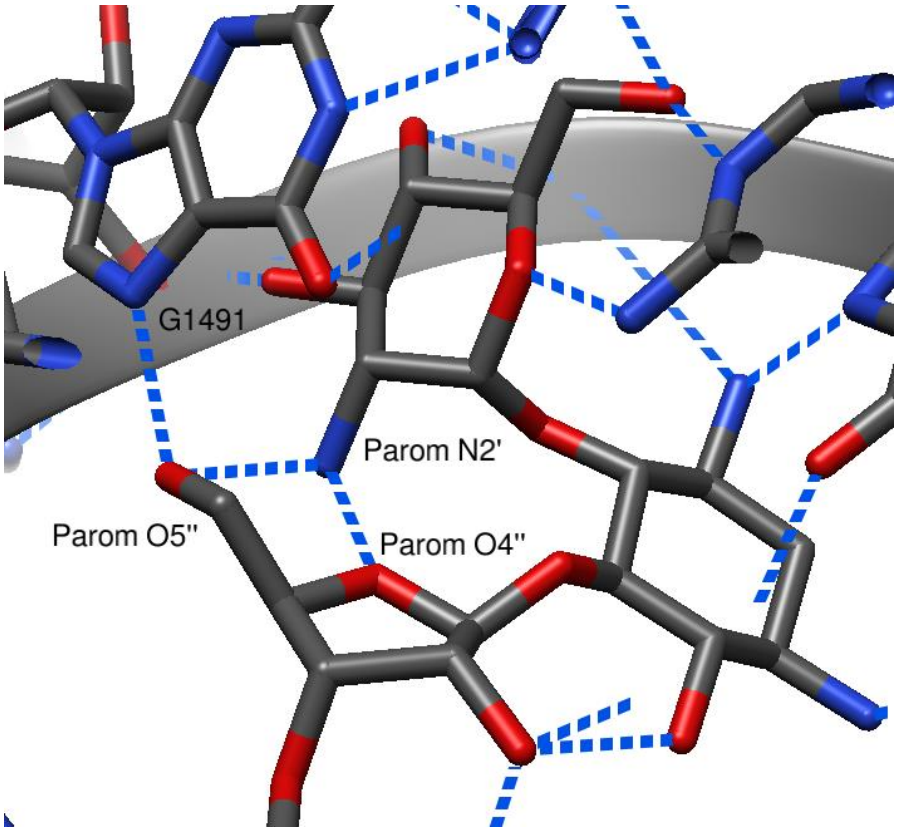

Figure 3.7. Partial crystal structure of paromomycin bound to the decoding A site of *Thermus thermophilus* (PDB ID 1FJG), with dashed blue lines denoting hydrogen bonds

Though the increased activity of the formamido derivatives of neomycin, paromomycin, and propylamycin is not fully understood, it is possible that their ability to populate the *E* conformer shown in Figure 3.6 could contribute to greater activity. According to early studies carried out by Huisgen,[171] the *E* isomer is expected to be slightly more polar than the *Z* isomer. As summarized in Table 3.3, Huisgen and coworkers measured the dipole moments of lactams of variable ring size, noting that the conformation of the amide changes from *E* to *Z* when ring size

is greater than 9. In almost all cases, lactams in the *E* configuration exhibit greater dipole moments than those in the *Z* configurations. Interestingly, the pKa of the N-H proton does not vary significantly between the *E* and *Z* isomers, as evidenced by studies of lactams and their acyclic analogs carried out by Bordwell and Fried.[172]

Table 3.3. Comparison of lactam dipole moments

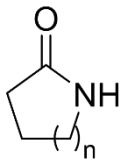

n	Rotamer	Dipole Moment (D)
0	*E*	3.55
1	*E*	3.83
2	*E*	3.88
3	*E*	3.86
4	*E*/*Z* Mixture	3.85
5	*Z*	3.79
6	*Z*	3.78
8	*Z*	3.64
9	*Z*	3.68
11	*Z*	3.69
12	*Z*	3.67
14	*Z*	3.67

If the minor *E* rotamer is more active than the *Z* rotamer to which the acetamides are restricted, the formamide derivatives would exhibit significantly greater antibacterial activity than the acetamide derivatives. Likewise, the rotational rigidity and steric bulk of the acetamides could contribute to their generally lower activity. Unlike the rest of the 4,5-AGAs, the 5’’-formamido apralog **32** shows decreased activity from both the parent and the 5’’-amino apralog **28**. Moreover, though installation of a 5’’-formamido group on ribostamycin affords greater activity than the 5’’-

amino derivative **91**, the formamide remains significantly less active than the parent. These observations are not yet well understood and are the subject of further investigation.

3.6. AME Susceptibility

MIC assays were also carried out on clinical isolates of *E. coli* expressing specific isoforms of either APH(3'), AAC(3), or AAC(6'), as shown in Table 3.4, and on engineered *E. coli* strains expressing isoforms of APH(3'), AAC(3), and ribosomal methyltransferases ArmA and RmtB, as shown in Table 3.5. Of the APH(3') isoforms studied here, only members of APH(3')-I phosphorylate both the 3' and 5''-positions.[173]

Table 3.4. MIC assays on isolates of *E. coli* bearing specific resistance determinants

		MIC (μg/mL)					
	Strain	**AG001**	**AG003**	**AG173**	**AG163**	**AG166**	**AG175**
Compound	**5''-Substituent**	**WT**	**AAC(3)-II**	**AAC(3)-IV**	**APH(3')-I**	**APH(3')-II**	**AAC(6')**
Neomycin Series (6 basic amines in parent)							
Neomycin	OH	2	1-2	4-8	64-128	64-128	1-2
83	Erythro	4	2-4	16	>128	>128	2-4
58	H	4	4	16-32	>128	>128	2-4
72	NH_2	4-8	4	8	64-128	64-128	2-4
84	NHCHO	2-4	2-4	2-4	32-64	64	2
85	NHAc	2-4	2	16-32	>128	>128	2-4
Paromomycin Series (5 basic amines in parent)							
Paromomycin	OH	2-4	4	4-8	>128	>128	4
86	Erythro	16	16	128	>128	>128	16-32
87	H	32-64	64	>128	>128	>128	32-64
73	NH_2	8	8	16-32	>64	>64	16
88	NHCHO	4	4	4-8	64	>128	4
89	NHAc	16	32	128	>128	>128	16
Ribostamycin Series (4 basic amines in parent)							
Ribostamycin	OH	4-8	4-8	32	>128	>128	8
90	Erythro	64-128	128	>128	>128	>128	128
91	NH_2	32-64	16	32-64	-	-	-
92	NHCHO	16-32	16-32	>128	>128	>128	32-64
93	NHAc	128	128	>128	>128	>128	>128
Propylamycin Series (5 basic amines in parent)							
Propylamycin	OH	1	2	2	>128	1-2	2
81	NH_2	2	4	4	16	2-4	4
82	NHCHO	1	2	4	4-8	2	2
Apralog Series (5 basic amines in parent)							
17β	OH	4	8	16-32	8-16	4-8	4
21	Erythro	8	8	128	8	8	4-8
27	H	8	8-16	>128	8-16	8-16	8-16
28	NH_2	4-8	4	32	2	8	4
32	NHCHO	8	8	128	16	8-16	8

Table 3.5. MIC assays on engineered strains of *E. coli* expressing specific resistance determinants

		MIC (μg/mL)							
	Strain	**EC026**	**EC118**	**EC189**	**EC191**	**EC125**	**EC141**	**EC102**	**EC103**
Compound	**5''-Substituent**	**WT**	**AAC(3)-IV**	**APH(3')-Ia**	**APH(3')-IIa**	**APH(3')-IIb**	**APH(3')-VI**	**ArmA**	**RmtB**
Neomycin Series (6 basic amines in parent)									
Neomycin	OH	1	1	32-64	16-32	16-32	8-16	1-2	1-2
83	Erythro	1	8	128	≥128	128	64-128	2-4	4
58	H	1	8-16	≥128	>128	128	64-128	4	4-8
72	NH_2	1-2	4	64-128	32	32	16-32	2	2-4
84	NHCHO	1	1-2	8-16	16	8-16	16	1	1-2
85	NHAc	0.5-1	4	≥128	≥128	128	128	2-4	4-8
Paromomycin Series (5 basic amines in parent)									
Paromomycin	OH	1	1-2	>128	32-64	64-128	64	1	1
86	Erythro	4	16-32	>64	>64	>64	>64	16	16-32
87	H	16	64	>128	>128	>128	>128	32-64	32-64
73	NH_2	4	8	16-32	16-32	32	16-32	8	8-16
88	NHCHO	1	1-2	8-16	32	64	32-64	2-4	4
89	NHAc	4-8	32-64	>128	>128	>128	>128	32	64-128
Ribostamycin Series (4 basic amines in parent)									
Ribostamycin	OH	1-2	8-16	>128	>128	>128	>128	2-4	2-4
90	Erythro	16	≥128	>128	>128	>128	>128	16	16-32
91	NH_2	-	-	-	-	-	-	-	-
92	NHCHO	4	>128	>128	>128	>128	>128	8-16	8-16
93	NHAc	16-32	>128	>128	>128	>128	>128	64-128	64-128
Propylamycin Series (5 basic amines in parent)									
Propylamycin	OH	0.25-0.5	1-2	64-128	0.5-1	0.5-1	0.5	0.5	0.5-1
81	NH_2	0.5-1	2-4	2-4	1-2	0.5-1	0.5-1	2	2
82	NHCHO	0.5-1	2	2	0.5-1	0.5	0.25	2	2
Apralog Series (5 basic amines in parent)									
17β	OH	1-2	2-4	1-2	1	1	1	1	1-2
21	Erythro	2	32-64	1-2	1	1	1	1-2	1-2
27	H	2-4	32-64	4-8	2-4	2-4	2-4	2	2-4
28	NH_2	1-2	8-16	1	1	1	1	2	4
32	NHCHO	2-4	32	-	-	-	-	2-4	4

As a whole, trends observed in Table 3.4 with clinical isolates of *E. coli* mirror those observed with the engineered bacterial strains in Table 3.5. In the neomycin, paromomycin, and ribostamycin series, all compounds remained susceptible to each APH(3') isoform. This is because in each derivative the 3'-hydroxyl group is still free for phosphorylation. In the case of propylamycin, whose 4'-*C*-propyl group prevents phosphorylation at the 3'-position, installation of a free amine or a formamido group at 5'' strongly lowers susceptibility to strains of *E. coli* expressing APH(3')-I (strains AG163 and EC189) which act on the 5''-position. Interestingly, 5''-deoxy, erythrosyl, and 5''-acetamido derivatives of neomycin, paromomycin, and ribostamycin induce significant susceptibility to AAC(3)-IV (strains AG173 and EC118), which is not observed in the parent compounds, as evidenced by the sharp increase in MIC values compared to the wild type *E. coli* values. These modifications also induce susceptibility to ArmA and RmtB (strains EC102 and EC103), albeit to a slightly lesser degree than that observed for AAC(3)-IV. At present, this is not understood and will likely be the subject of future study. AAC(6') susceptibility is minimally impacted by the substituents at the 5''-position.

3.7. Conclusions

In light of the disparate reports of the influence of modification at the 5''-position of 4,5-AGAs, systematic modifications of the 5''-position in the neomycin, paromomycin, and ribostamycin series were carried out. Deoxygenation at the 5''-position and cleavage of the hydroxymethyl group generally resulted in diminished antibacterial activity and diminished selectivity for the bacterial ribosome, as did installation of a 5''-acetamido group. Unlike the apralog series, installation of a 5''-amino group in the 4,5-AGAs resulted in decreased activity, possibly due to electrostatic repulsion between N2' and N5''. Also unlike the apralog series,

installation of a 5’’-formamido group in paromomycin, propylamycin, and neomycin resulted in increased antibacterial activity and increased selectivity. Modifications were generally well tolerated in the neomycin series due to the greater number of basic amines in the parent compound, where potential unfavorable interactions were likely outweighed by electrostatic interactions between the positively charged amines and the negatively charged binding site. Interestingly, the presence of a 5’’-acetamido group resulted in sharply increased susceptibility to AAC(3), though the reason for this increase is not yet understood. The causes of the generally contrasting observations between most 4,5-AGAs and the apralog series are as yet not well understood and are still being examined by the Crich group. The lessons learnt in the course of this study will nevertheless be invaluable in the design of future series of compounds in the continuing quest toward next generation AGAs with improved activity, reduced toxicity, and above all activity in the face of the growing resistance problem.

CHAPTER 4

REACTIONS AT THE ANOMERIC CENTER

4.1. Introduction to Glycosylation

Standing at the heart of the glycosciences is the glycosylation reaction, a nucleophilic substitution wherein a glycosidic linkage is formed between a nucleophile termed a glycosyl acceptor and an electrophile termed a glycosyl donor that bears a leaving group at the anomeric position (C1), usually activated by a promoter (Scheme 4.1). The regio- and stereoselectivity arising from glycosylation between a broad range of donors and acceptors in nature gives rise to a tremendous degree of complexity and diversity among natural oligosaccharides and biopolymers, meaning that an in-depth understanding of glycosylation is critical to the design of biologically relevant oligosaccharides and their mimetics, among many other applications.[174]

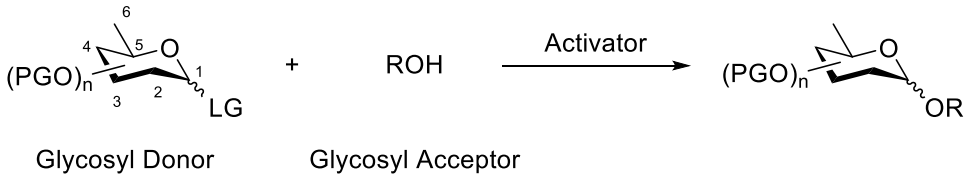

Scheme 4.1. The glycosylation reaction

Nucleophilic substitutions at sp^3-centers are generally viewed from the perspective of two mechanistic extremes: the bimolecular associative S_N2 mechanism, which takes place in a concerted fashion with inversion of configuration, and the unimolecular dissociative S_N1 mechanism, which passes through a discrete carbocation intermediate and proceeds without

memory of stereochemistry. Seminal studies carried out by Winstein and coworkers[175] demonstrated that between these extremes lies a spectrum of ion pair-based mechanisms that has been the ongoing subject of extensive physical organic studies, such as those seeking to identify potential reaction intermediates and determine possible discontinuities in the spectrum that would indicate a shift from S_N1-like character to S_N2-like character.[176, 177]

In 1960, Rhind-Tutt and Vernon applied Winstein's ion-pair mechanism to the glycosylation reaction,[178] with subsequent support and elaboration by Lemieux and Schueurch and their coworkers.[179-182] On addition of a promoter, the activated glycosyl donor undergoes a spectrum of S_N1-like to S_N2-like reactivity, as shown in Scheme 4.2. At the dissociative extreme of the spectrum, a discrete oxocarbenium ion intermediate is generated and stabilized by its counterion (in recent decades most frequently the triflate anion derived from the promoter) as a solvent-separated ion pair (SSIP), resulting in S_N1-like reactivity. In most cases, however, when the mechanism has been studied in detail glycosylation reactions favor the associative, S_N2-like end of the spectrum, generating a covalent intermediate with the counterion (usually a glycosyl triflate) followed by concerted bimolecular displacement to form the new glycosidic linkage. Spanning these two extremes are displacements involving the generation of transient contact ion pairs (CIP), in which an oxocarbenium ion and the corresponding counterion are in close proximity with no solvent molecules between them.[177, 183] In the CIP the position of the counterion blocks one face of the oxocarbenium ion from attack, thereby affording facial selectivity during glycosylation. While initial in depth mechanistic studies on anomeric reactivity have mostly centered on the hydrolysis of glycosidic bonds, there has been a recent surge of studies on the more complex nuances involved in glycosidic bond formation.[184] Despite overwhelming evidence to the contrary (which is discussed in detail below),[185-188] there remains a tendency in the glycoscience

community to oversimplify the glycosylation mechanism to a simple S_N1-like dissociation, presenting naked oxocarbenium ions as intermediates with minimal to no consideration of the role of the counterion.[189]

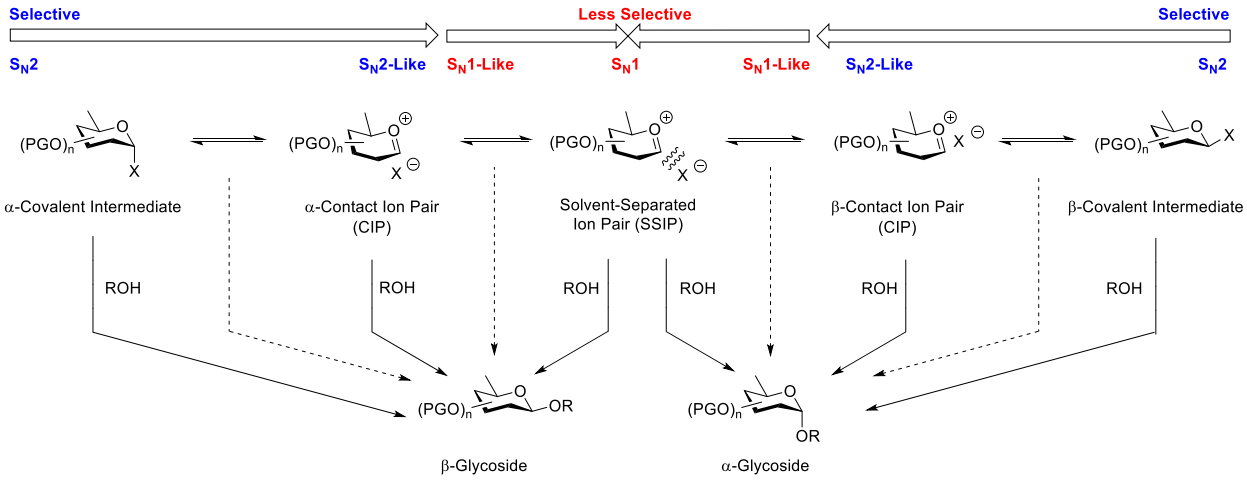

Scheme 4.2. Mechanism of the glycosylation reaction

4.2. Role of Substituents in Glycosylation

The substituents on sugars are known to strongly influence reactivity during glycosylation.[177, 190, 191] In some cases, adjacent functional groups can stabilize the positive charge that develops at the anomeric center through formation of a covalent linkage in a process known as neighboring group participation (NGP), most commonly observed with vicinal ester protecting groups. In cases where the lone pair of the participating group displaces the anomeric leaving group in an S_N2-like fashion as shown in Scheme 4.3, NGP affords an increase in reaction rate known as anchimeric assistance (AA).[192]

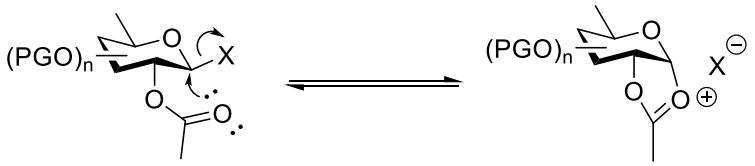

Scheme 4.3. Example of neighboring group participation that affords anchimeric assistance

In cases where AA is not possible, adjacent substituents (as well as more remote substituents) destabilize developing positive charge due to their electron withdrawing potential.[177] This phenomenon is nicely illustrated by kinetic studies from the Lambert and Kirsme groups on the acidic solvolysis of norbornyl sulfonates shown in Figure 4.1.[193, 194] Neither the carbonyl oxygen of the periplanar acetate nor the endocyclic β-oxygen are able to provide anchimeric assistance as they are unable to displace the sulfonate leaving group in an S_N2-like manner. Instead, these electron withdrawing groups destabilize the positive charge that builds up over the course of the reaction, resulting in strongly reduced reactivity.

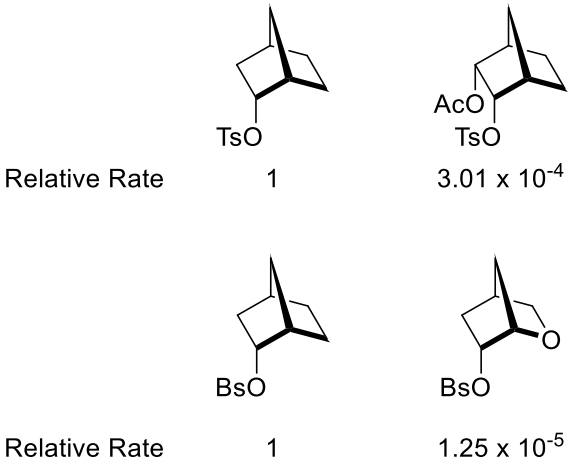

Figure 4.1. Relative rates of solvolysis of norbornyl tosylates in AcOH at 25 °C

Glycosylations with β-phenylthiomethyl glucosides carried out by the Crich group are another prime example of the inductive destabilization of positive charge afforded by adjacent heteroatoms.[195] Activation with *N*-iodosuccinimide (NIS) and triflic acid results in the formation of the trifloxymethyl glycoside shown in Scheme 4.4, which in theory can form either an alkoxymethyl glycoside through displacement of the triflate or a disaccharide through elimination of formaldehyde and triflate. However, as indicated in Scheme 4.4, Crich and coworkers only observed generation of the alkoxymethyl glycosides. This observation can be rationalized by the fact that buildup of positive charge at the anomeric center is disfavored due to the electron withdrawing nature of both the adjacent 2-*O*-benzyl protecting group and the more remote heteroatoms. Given that the exocyclic methylene lacks nearby electron withdrawing groups, reaction at this position is strongly favored.

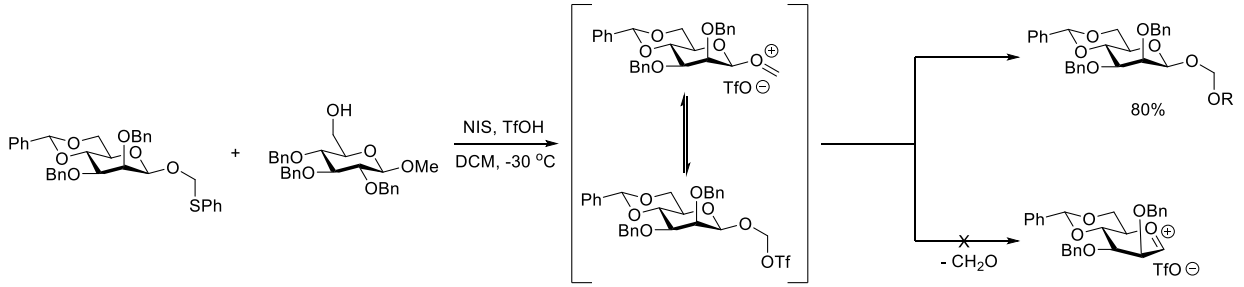

Scheme 4.4. Glycosylation of β-phenylthiomethyl glucosides

These results are further corroborated by the acid hydrolysis of unprotected isoprenyl glycosides, as shown in Scheme 4.5.[196, 197] For each anomer, reactivity is only observed at the isoprene chain while the anomeric C-O bond remains intact, as indicated by the retention of stereochemistry in both cases. As in the above example, the nearby electron withdrawing groups

disfavor buildup of positive charge at the anomeric center relative to at the aglycone, where no such substituents are present.

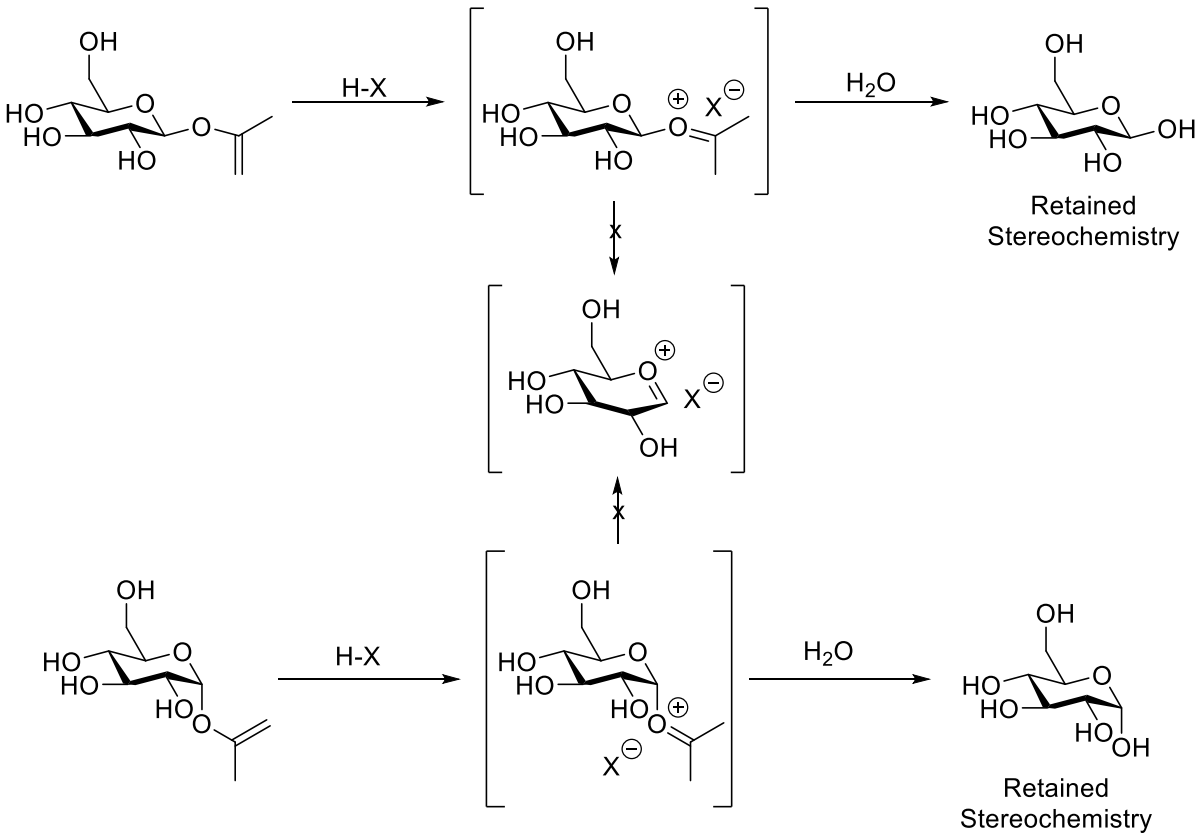

Scheme 4.5. Acidic hydrolysis of unprotected isoprenyl glycosides

Kinetic studies by Sequeira and coworkers on the acidic hydrolysis of several deoxygenated methyl α-glucosides delineate the extent of positive charge destabilization afforded by each endocyclic hydroxyl group (Figure 4.2a).[198] In acidic conditions the 2-deoxy sugar exhibits an over 2000-fold increase in reaction rate compared to the simple methyl glucoside, indicating that the hydroxyl group at the 2-position by far provides the strongest destabilization of the developing positive charge at the anomeric center. Turning to the more remote hydroxyl groups, the difference in rate between the 3-deoxy and 4-deoxy sugars is made readily apparent by the

antiperiplanar relationship between the C4-O4 and C5-O5 bonds. Given that O5 bears a partial positive charge in the glycosylation (and hydrolysis) transition state, the electron-withdrawing O4 will more strongly disfavor reactivity than O3, thus rendering the 4-deoxy sugar more reactive. The above studies were corroborated and extended by the Withers group in their analysis of the spontaneous, pH-independent hydrolysis of α-2,4-dinitrophenyl glycosides first identified by the Sinnott group (Figure 4.2b).[199, 200] In accordance with the above methyl glucosides, the most reactive substrate was the 2-deoxy glycoside, whose rate of hydrolysis was immeasurably fast, followed by the 4-deoxy glycoside. It should be noted that deoxygenations at the 3- and 6-positions resulted in comparable relative rates of hydrolysis.

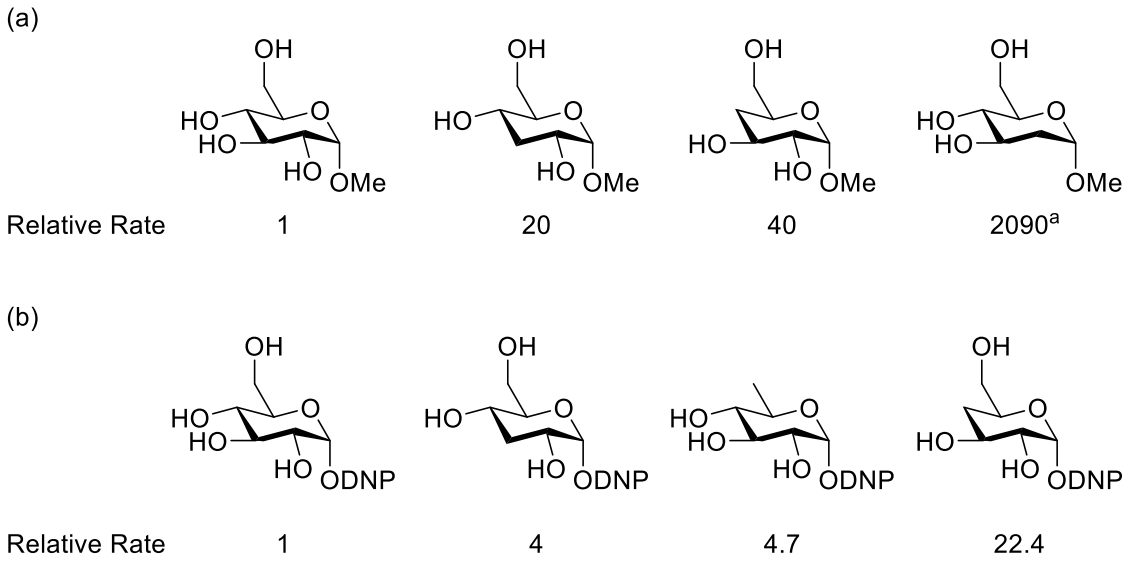

Figure 4.2. Relative rates of (a) acidic hydrolysis of α-methyl glucosides (2 N HCl, 58 °C) and (b) spontaneous hydrolysis of α-2,4-dinitrophenyl glucosides (25 mM sodium phosphate buffer, 0.40 M KCl, 37 °C, pH 6.5)

[a] 0.1 N HCl was used instead of 2 N

The inductive destabilization of positive charge at the anomeric center by the presence of nearby electron withdrawing groups is particularly appreciated in attempts to isolate glycosyl oxocarbenium ions. Since the 1960s, simple oxocarbenium ions lacking β-C-O bonds have been readily characterized by NMR spectroscopy in superacidic media.[201, 202] Subsequently, Yoshida and coworkers developed a method for electrochemical generation of a solution of simple oxocarbenium ions in deuterated dichloromethane that could be characterized by NMR in 2009,[203] but attempts to use this method to generate a solution of glycosyl oxocarbenium ions resulted in undesired reaction with other nucleophiles in the reaction mixture such as disulfides and the tetrafluoroborate anion.[204] It was not until 2016, that Blériot and coworkers successfully characterized a glycosyl oxocarbenium ion by NMR spectroscopy in superacidic media.[205, 206] As illustrated in Scheme 4.6, treatment of peracetylated 2-deoxy-β-D-glucopyranose and 2-bromo-2-deoxy-β-D-glucopyranose, neither of which bears an electron withdrawing group at the 2-position, resulted in generation of glycosyl oxocarbenium ions with all acetate groups protonated. In the case of the 2-bromo derivative, additional stabilization is imparted by the adjacent bromine through formation of a dissymmetric bromonium ion. When the above conditions were replicated with simple per-*O*-acetyl glucopyranose, however, generation of a dioxalenium ion was observed, consistent with neighboring group participation of the acetate at O2. Moreover, treatment of 2-azido-2-deoxy-β-D-glucopyranose resulted only in protonation of the anomeric acetate rather than formation of a glycosyl oxocarbenium ion. Clearly, the electron withdrawing potential of the vicinal azide group is strong enough to disfavor generation of a glycosyl oxocarbenium ion even in superacidic media.

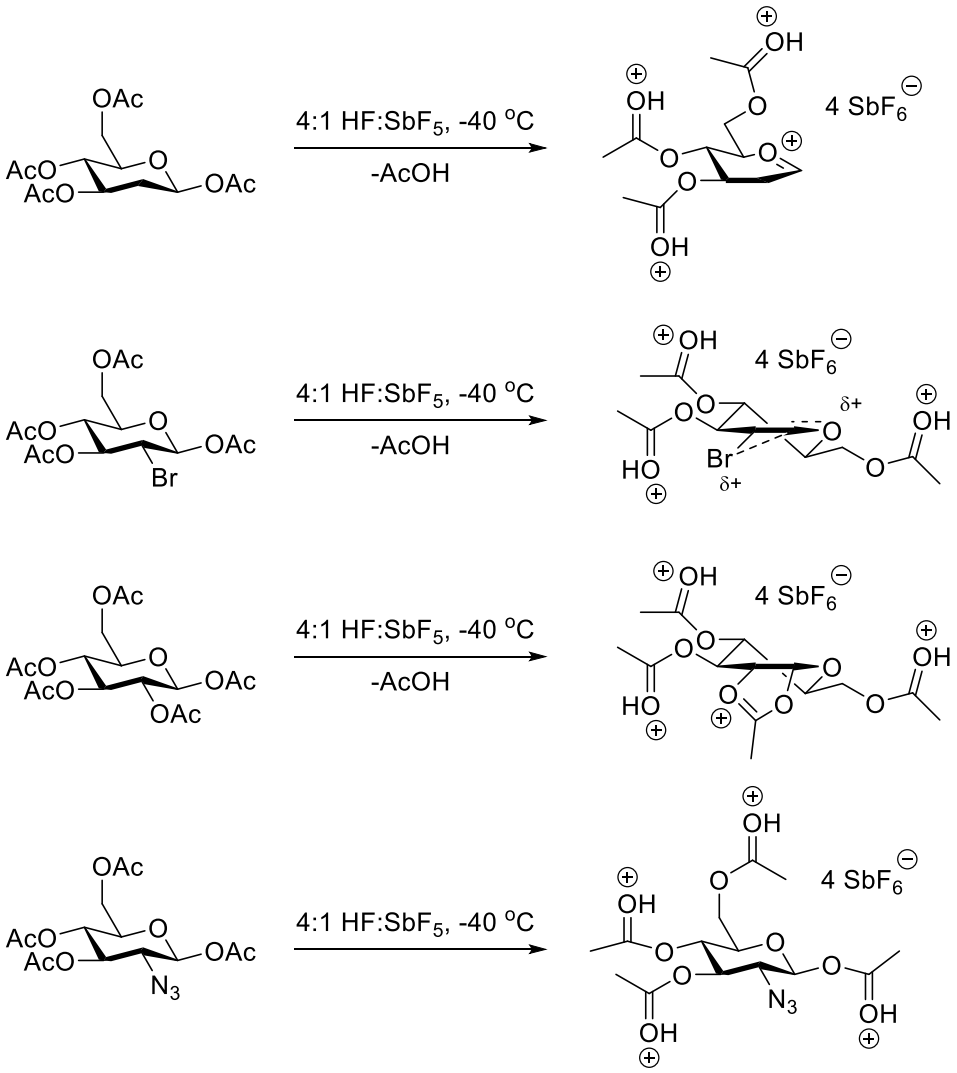

Scheme 4.6. Generation of glycosyl oxocarbenium ions in the presence of superacid

Reactivity at the anomeric center can be modulated through installation of specific protecting groups on the heteroatoms. Owing to their high electron withdrawing potential, ester protecting groups impart additional destabilization to the positive charge that develops at the anomeric center over the course of glycosylation and are thus classed as “disarming”. Likewise, due to their comparatively lower electron withdrawing potential, ether protecting groups result in increased reactivity during glycosylation and are thus considered “arming”. The extent to which

armed glycosyl donors can be selectively activated in the presence of more disarmed donors has been quantified for many systems through the Wong and Ley indeces.[190, 207]

4.3. Influence of Side Chain Conformation on Glycosylation

The conformation of the exocyclic C-O bond is being increasingly recognized as a controlling factor in reactivity during glycosylation.[177] The side chain in pyranosides can take up three possible staggered conformations denoted *gg* (*gauche,gauche*), *gt* (*gauche,trans*), and *tg* (*trans,gauche*), where the first letter represents the relationship between the C6-O6 and C5-O5 bonds and the second designates the relationship between the C6-O6 and C4-C5 bonds (Scheme 4.7). In the *gluco*-series and in 4-deoxysugars, the observed ratio of staggered conformers in solution is roughly 1:1 *gg* to *gt*, with minimal population of the *tg* conformation. In the *galacto*-series where O4 is axial, however, the *gg* conformation is destabilized due to unfavorable steric repulsion between O4 and O6. As a result, the relative abundance of the *gg* conformation is reduced to roughly 15%, with the *gt* and *tg* conformations taking up 55% and 30% abundance respectively in solution.[208-211]

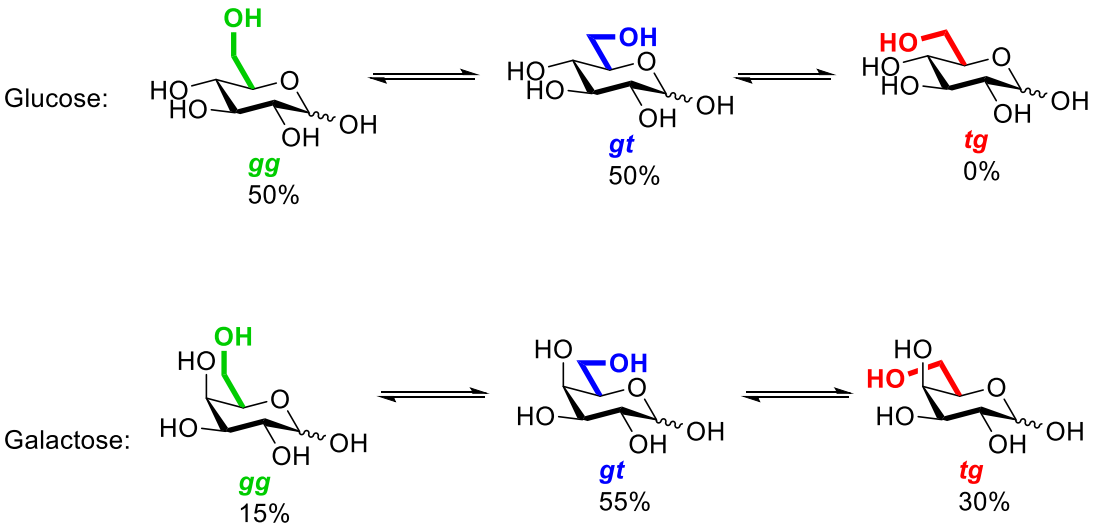

Scheme 4.7. Side chain conformations of glucose and galactose

Seminal studies by Bols and coworkers, wherein glucosyl donors with conformationally locked side chains were subjected to acidic hydrolysis, nicely illustrate that the *gg* conformation affords greater reactivity than the *gt* conformation, which is in turn more reactive than the *tg* conformation (Figure 4.3).[212]

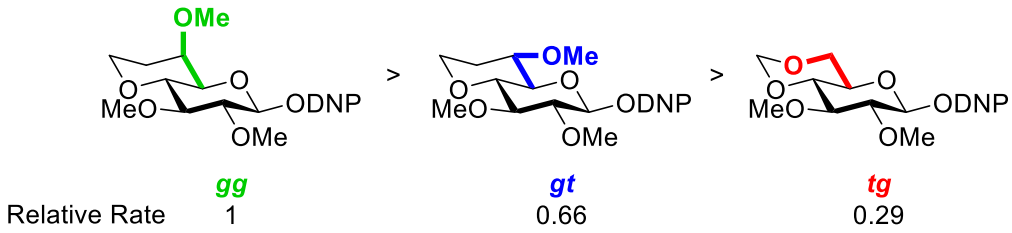

Figure 4.3. Relative rates of hydrolysis of conformationally locked donors

This observation can be rationalized through analysis of the electrostatic interactions between the exocyclic C-O bond of each conformer and the developing positive charge at the anomeric center, with the difference between the *gg* and *tg* conformations being most readily

apparent. In the *gg* case, the side chain hydroxyl group is nicely positioned to electrostatically stabilize the building positive charge, as shown in Figure 4.4. Analogous coulombic stabilization is imparted by the axial O4 of galactose, which accounts for its high reactivity.[213, 214] In the *tg* case, however, the side chain hydroxyl group is antiperiplanar to the anomeric center, meaning that the C6-O6 dipole pulls electron density away from the center of reactivity, thereby destabilizing the developing positive charge; as a result, reactivity is significantly reduced. An analogous effect is observed for the equatorial O4 of glucose, accounting for its reduced reactivity relative to galactose.[215-217] It should be noted that destabilization of positive charge at the anomeric center in the *tg* conformation renders oxocarbenium ion formation in a CIP or SSIP particularly disfavored, meaning that glycosyl donors in the *tg* conformation will shift even further towards the S_N2 side of the mechanistic spectrum of glycosylation reactions. Thus, while enforcement of the *gg* conformation enhances glycosyl donor reactivity, enforcement of the *tg* conformation reduces reactivity and increases selectivity, an observation that has inspired widespread use of bicyclic glycosyl donors in recent years to control reactivity during glycosylation.[218-221]

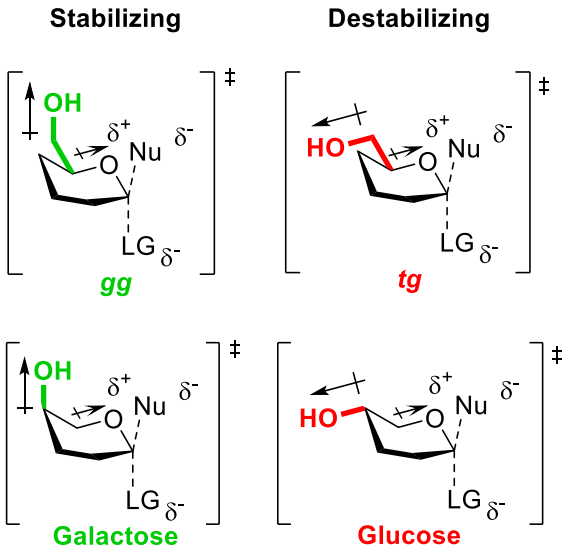

Figure 4.4. Influence of the *gg* and *tg* conformations and of O4 on building positive charge at the anomeric center through an exploded S_N2-like transition state

Interestingly, the electrostatic stabilization imparted by the *gg* and *gt* conformations is phenomenologically equivalent given that both side chain hydroxyl groups are equidistant to the ring oxygen, meaning that other stereoelectronic factors must be responsible for the differential reactivity of these conformers. Thus, when the side chain is in the *gg* conformation, the exocyclic hydroxyl group can donate electron density to the axial *p*-orbital of the ring oxygen, which bears a partial positive charge at the transition state. In the *gt* conformer, however, O6 lies in the nodal plane of this orbital, meaning that it cannot stabilize the partial positive charge in the same manner (Figure 4.5a). Additionally, a lone pair of the side chain hydroxyl group of the *gt* conformer comes in close proximity to the pseudoequatorial sp^2 lone pair of O5, a factor that destabilizes the transition state relative to the *gg* conformer (Figure 4.5b). Interestingly, according to Bock and Duus,[210] the *gg* conformer itself is more stabilized than the *gt* conformer due to hyperconjugation. As shown in Figure 4.5c, the *gg* conformer benefits from both $\sigma_{C5\text{-}H5} \rightarrow \sigma^*_{C6\text{-}O6}$ donation and $\sigma_{C6\text{-}}$

$_{H6R}$ → $\sigma^*_{C5\text{-}O5}$ donation, while the *gt* conformer, on the other hand, only achieves stabilization from $\sigma_{C6\text{-}H6S}$ → $\sigma^*_{C5\text{-}O5}$ donation. Thus, at least three factors potentially contribute to the additional stabilization of the transition state afforded by the *gg* conformation compared to the *gt* conformation, though electrostatic stabilization still renders the *gt* conformer more reactive than the *tg* conformer as discussed above.

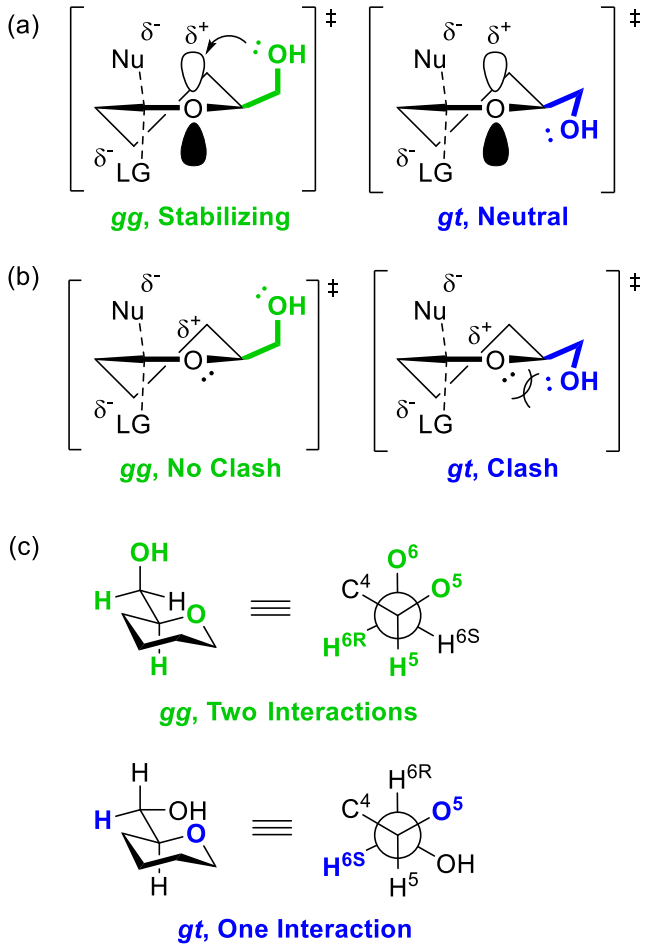

Figure 4.5. Differences in transition state stabilization by the *gg* and *gt* conformations due to (a) electron donation, (b) clash with the pseudoequatorial endocyclic oxygen lone pair, and (c) hyperconjugation

The influence of the side chain C-O bond on glycosylation reactivity is applicable not only to conformationally locked bicyclic donors, but also to monocyclic donors. To this end, the Crich group has done extensive work on the influence of the side chain on reactivity and selectivity in the ulosonic acid series, higher order sugars whose members usually predominantly favor one side chain conformation in solution because of their substitution pattern.[222] The impact of side chain conformation on reactivity is nicely illustrated in a competition experiment between two sialic acid donors: the naturally occurring **112**, which takes up the *gg* conformation in solution, and its synthetic C7-epimer **113**, which takes up the *gt* conformation.[223] When both donors were exposed to standard glycosylation conditions (NIS, TfOH) at -78 °C in the same pot, only compound **112** underwent reaction; epimer **113** was inert until the temperature was raised to -60 °C, at which point glycosylation was observed (Scheme 4.8). Thus, the *gg* conformation clearly imparts greater reactivity than the *gt* conformation.

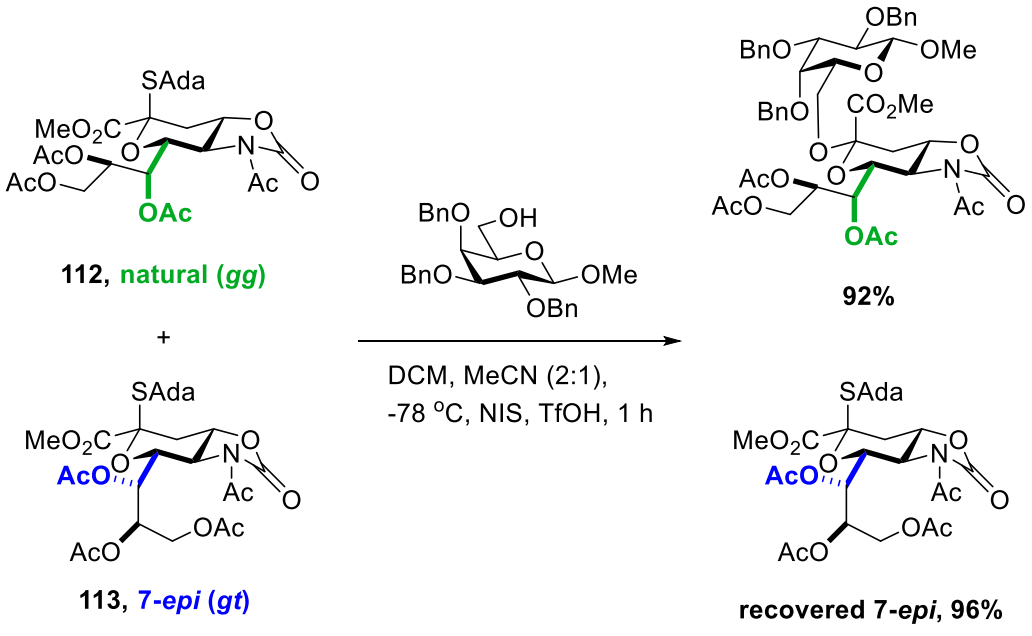

Scheme 4.8. Competition reaction of epimeric sialic acid donors

In an additional demonstration of the role of side chain conformation on glycosylation, Crich and coworkers employed the pseudaminic acid donor **114**, which takes up the *tg* conformation in solution, in a series of selective glycosylation reactions where only the equatorial glycoside was generated, a product previously considered challenging to synthesize (Scheme 4.9).[224] The least reactive *tg* conformation destabilizes building positive charge at the anomeric center, meaning that this conformation increases the S_N2-like character of glycosylation. Thus, glycosylations with donor **114** exhibit the high selectivity associated with an S_N2-like glycosylation mechanism. This is to be contrasted with glycosylations employing legionaminic acid donor **115**,[225] which generally proceeded with only moderate equatorial selectivity, as shown in Scheme 4.10. Thus, glycosylations with a donor whose side chain takes up the *tg* conformation in solution are generally more selective than those involving donors with more reactive side chain conformations that can stabilize building positive charge at the anomeric center.

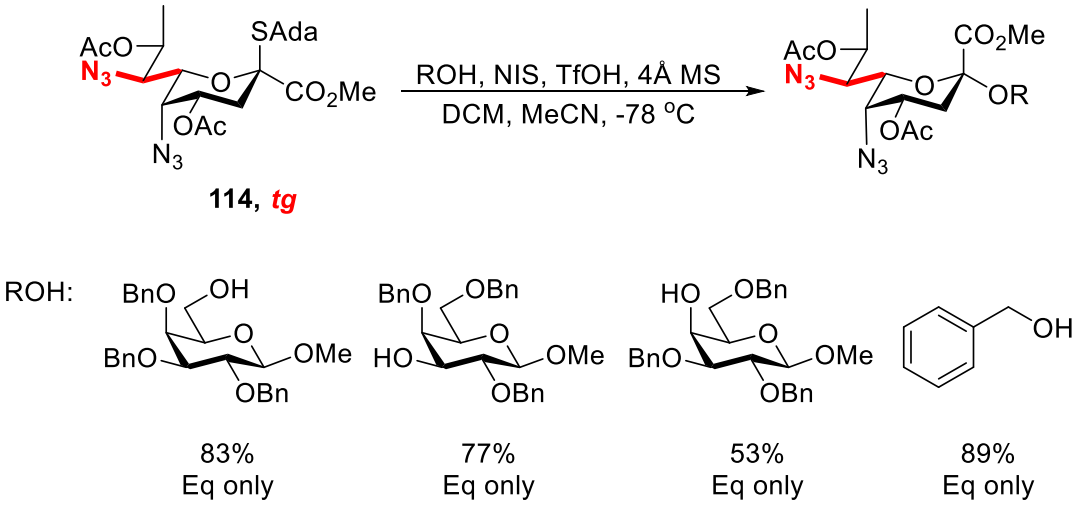

Scheme 4.9. Equatorial selectivity imparted by the *tg* conformation of pseudaminic acid donor **114**

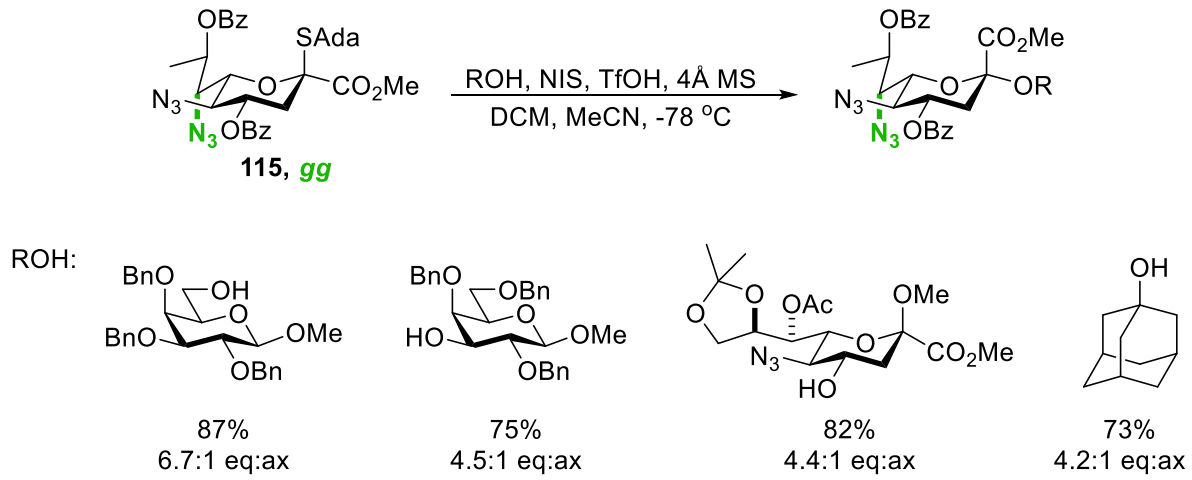

Scheme 4.10. Reduced selectivity imparted by the *gg* conformation of legionaminic acid donor **115**

4.4. Conformational Superarming

In keeping with the above trends in side chain conformation and with the relative reactivity of glucose versus galactose, seminal studies carried out by Bols and coworkers reveal that an increase in the number of axially oriented substituents in a series of methyl glycosides strongly enhances the rate of acidic hydrolysis (Figure 4.6a).[226] Key among the compounds studied is methyl 3,6-anhydro-β-D-glucopyranoside, which is locked in an inverted $^{1}C_{4}$ chair with all substituents in axial orientations, and so capable of providing electrostatic stabilization to positive charge in the transition state. Bols and coworkers later employed this style of conformational restriction in the design of so-called "conformationally superarmed" glycosyl donors whose bulky protecting groups distort the ring into either an inverted $^{1}C_{4}$ chair or a twist boat such that most if not all substituents are held pseudo-axially. These superarmed donors exhibit a roughly 40-fold increase in activity relative to conventionally armed glucosides (Figure 4.6b).[227-233]

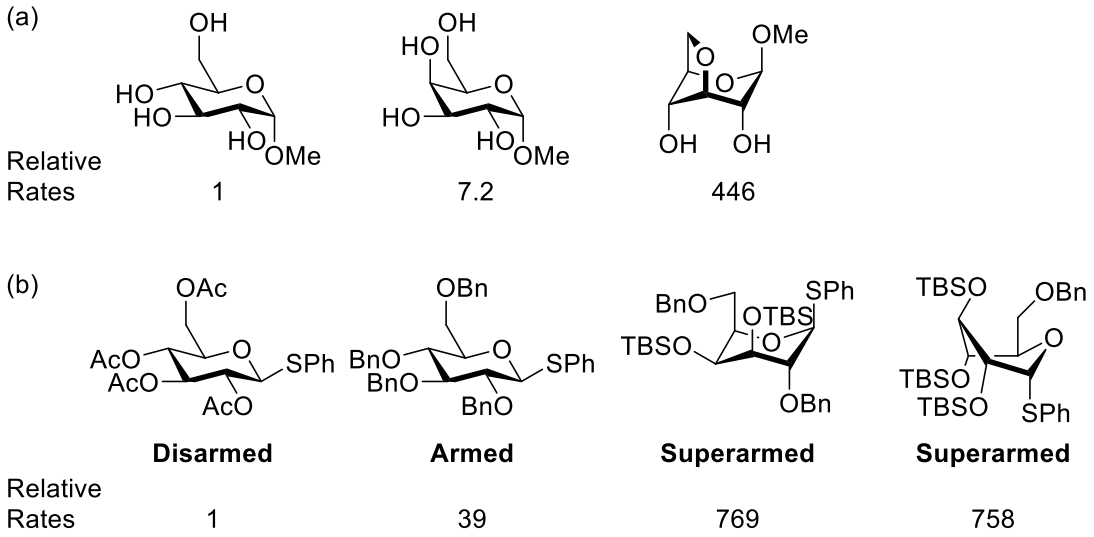

Figure 4.6. (a) Influence of axial character on acidic methyl glycoside hydrolysis (b) Relative activities of glycosylation by disarmed, armed, and superarmed glycosyl donors

4.5. Prevalence of S_N2-Character in Glycosylations

The commonly used 4,6-*O*-benzylidene group locks the substrate side chain in the *tg* conformation in the glucose and mannose series and thereby generally affords predominantly S_N2-like character during glycosylation. The 4,6-*O*-benzylidene-protected mannosyl donors shown in Scheme 4.11, for example, afford exquisite β-selectivity during glycosylation to generate ordinarily elusive products, standing in stark contrast with the minimal selectivity afforded when other protecting groups were used at O4 and O6.[234] Interestingly, deuterium isotope effect studies at the anomeric position gave a secondary deuterium kinetic isotope effect (KIE) of 1.20 at -78 °C (which corresponds to roughly 1.13 at 25 °C).[235] Given that secondary deuterium KIE values for a formal S_N2 reaction are typically much closer to 1.00, at the time Crich and coworkers concluded that the reaction most likely passes through a dissociative mechanism, either forming a discrete oxocarbenium ion as part of a CIP or passing through an exploded S_N2 transition state with significant oxocarbenium ion character (Scheme 4.11).

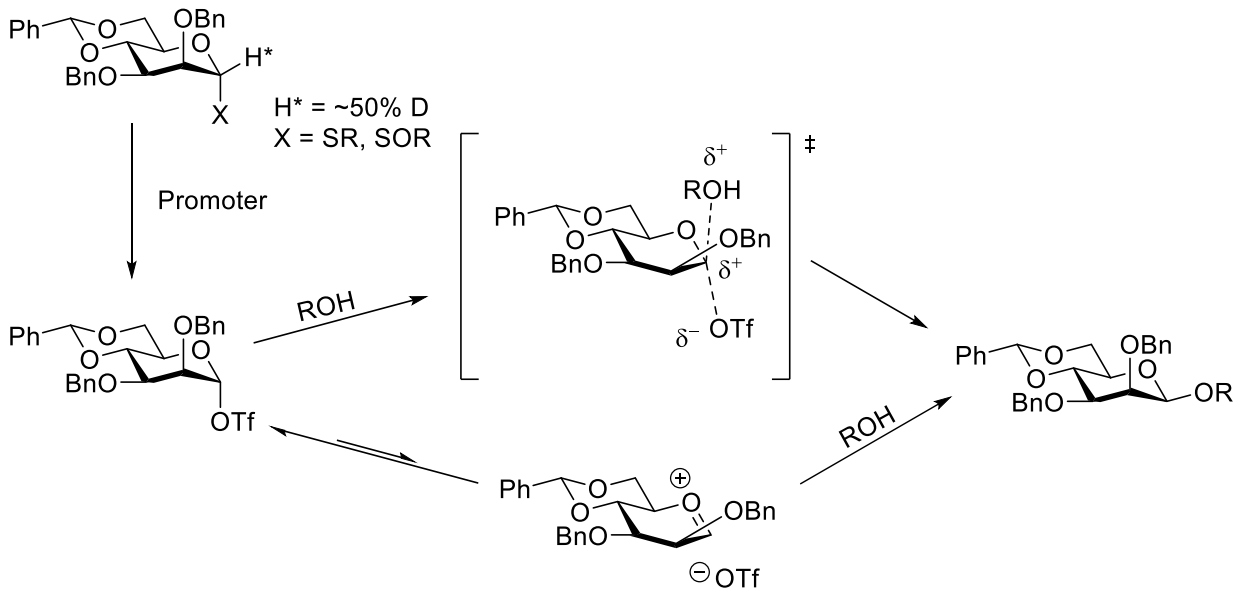

Scheme 4.11. Mechanism of selective β-mannosylation using partially deuterium-enriched starting material

In the *gluco* series, however, installation of a 4,6-*O*-benzylidene group gives rise to high α-selectivity during glycosylation.[236, 237] In light of the differing selectivity between the two sugars, Crich and coworkers synthesized a series of 2- and 3-deoxy sugars as well as their fluorinated analogs and found that a loss of selectivity ensued in all cases.[238, 239] Through these studies they hypothesized that the difference in selectivity between gluco and mannopyranosides could lie primarily in the change in torsional angle between O2 and O3 during the course of the reaction, as illustrated in Scheme 4.12. In the 4,6-*O*-benzylidene protected *manno* series, the shift in equilibrium from the covalent mannosyl triflate to the CIP/SSIP results in either a $^4H_3$ half chair conformation of the oxocarbenium ion, where the O2-C2-C3-O3 torsion angle is reduced from 60° to 45°, or the less likely $B_{2,5}$ boat, where the torsion angle remains unchanged. As a result, there is no torsional driving force to shift the equilibrium from the covalent triflate to the CIP or SSIP. In

the 4,6-*O*-benzylidene protected *gluco* series, however, conversion of the covalent triflate to the CIP/SSIP results in relaxation of the O2-C2-C3-O3 torsion angle in both possible oxocarbenium ring conformations, thereby resulting in sufficient SSIP character to dominate chemistry during glycosylation.[183]

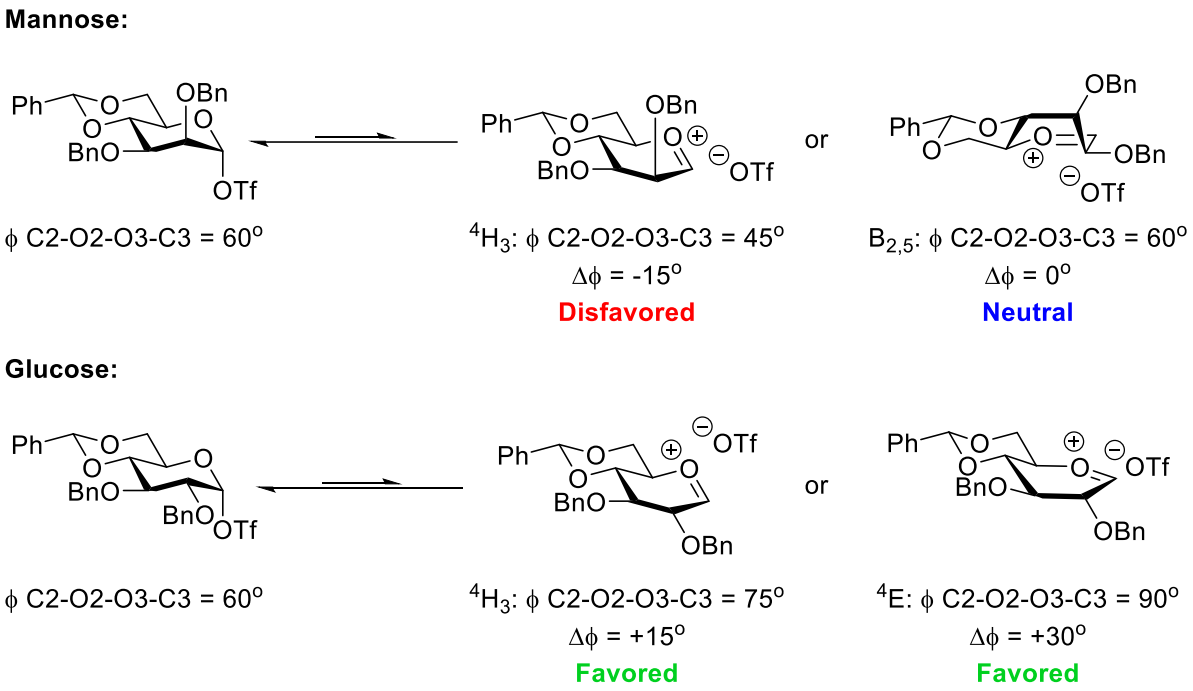

Scheme 4.12. Torsional influence of 4,6-*O*-benzylidene group on mannosyl versus glucosyl donors

More recently, Crich and coworkers described a primary ^{13}C KIE study backed up by computational studies that gives a more detailed picture of the reaction mechanisms in the manno- and gluco series.[240] When mannosyl sulfoxide **116** was activated with Tf_2O and TTBP and subjected to glycosylation with isopropanol, the primary ^{13}C KIE values for formation of the α-mannoside (1.005 ± 0.002) were significantly different than those for the β-product (1.023 ± 0.003). Given that ^{13}C KIE values of 1.03-1.08 are typical for S_N2 reactions while values of 1.00-

1.01 are typical for S_N1 reactions, the mechanism for α-mannoside formation clearly proceeds with significant S_N1 character, while β-mannoside formation proceeds with significant S_N2 character. The secondary deuterium KIE measured earlier is also consistent with the exploded S_N2-like transition state for β-mannoside formation as revealed by the DFT calculations reported in this paper. In the case of glucosyl sulfoxide **117**, however, the KIE values for both the α- and β-glucosides (1.023 ± 0.006 and 1.019 ± 0.001) are indicative of S_N2-like character. In the α-glucoside case, the reaction likely proceeds from a small amount of β-triflate in solution as a result of rapid interconversion between the α- and β-triflates, as further evidenced by recent studies from the Asensio and Jiménez-Barbero groups.[241] The proposed mechanism for formation of each product is summarized in Scheme 4.13.

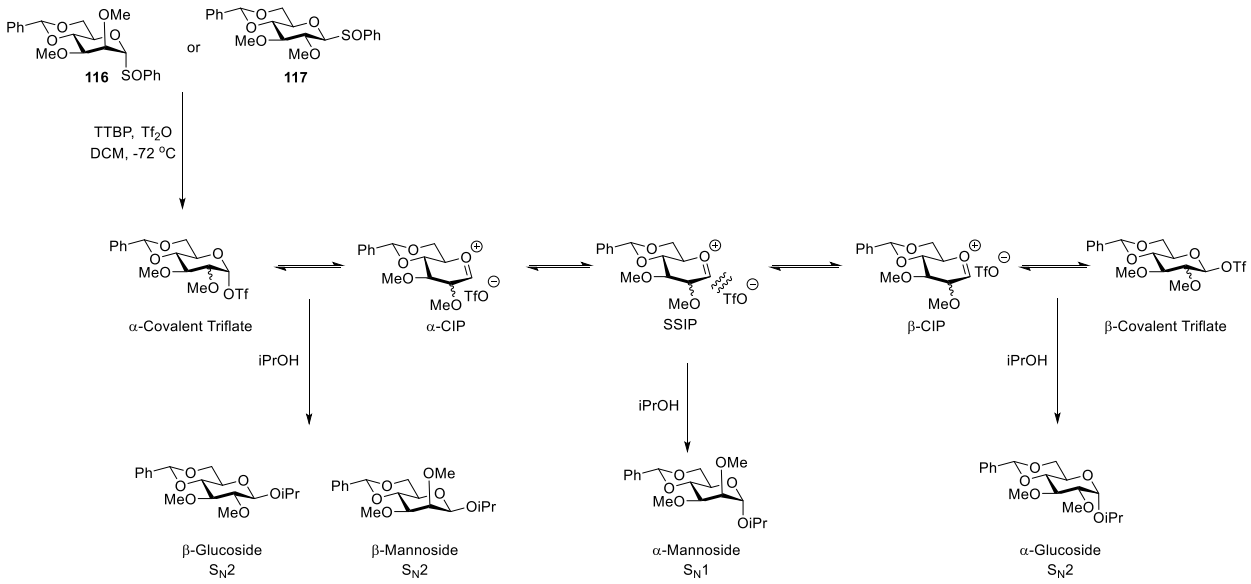

Scheme 4.13. Mechanistic differences between α- and β-glucosides and mannosides bearing a 4,6-benzylidene protecting group

Crich and coworkers employed DFT calculations to model bimolecular transition states for formation of each of the four above glycosides along with corresponding calculated $\Delta G^{\ddagger}$ and primary ^{13}C KIE values, summarized in Figure 4.5. For β-mannoside, β-glucoside, and α-glucoside formation, the observed ^{13}C KIE values strongly match those calculated for the predicted model (as shown in Figure 4.7), supporting formation of each of these glycosides through an associative S_N2-like mechanism. Turning to α-mannoside formation and as discussed above, the observed ^{13}C KIE value (1.005 ± 0.002) strongly differs from the calculated primary ^{13}C KIE for a bimolecular mechanism (1.023), indicating that its formation likely passes through an S_N1-like mechanism. It should be noted that the transition state for the dissociative S_N1-like pathway was not calculated due to errors in calculation resulting from spontaneous collapse of the ion pair in the model.[177]

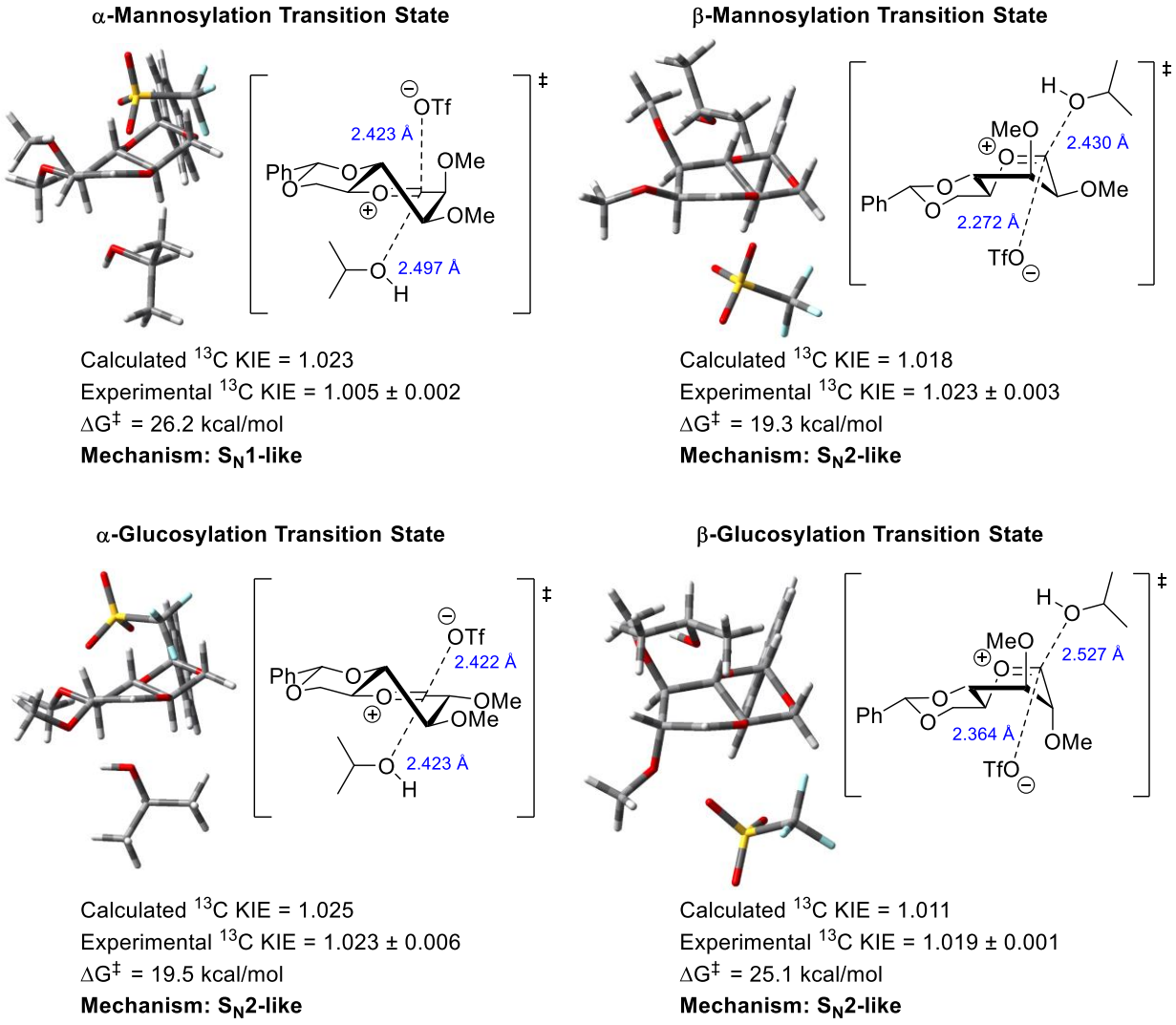

Figure 4.7. Transition states of glucoside and mannoside formation

The results of the above KIE studies are supported by subsequent competition kinetic experiments from the Crich group using a specially devised cation clock reaction,[242] inspired by the Jencks azide clock reaction used to estimate glycosyl oxocarbenium ion lifetimes in aqueous media[243, 244] and by radical clocks for intermolecular reactions.[245] As shown in Schemes 4.14a and 4.14b, Crich and coworkers ran competition reactions with either mannosyl donor **118** or glucosyl donor **121** and varying concentrations of an external nucleophile, either isopropanol or

methylallyltrimethylsilane. After quenching the reaction, the ratio of the glycosylation product to the intramolecular cyclization products was determined at each concentration of the nucleophile. Glycosylations that proceed in an S_N1-like dissociative fashion will show minimal change in the ratio of glycosylation to cyclization, as the rate of reaction will only be minimally dependent on acceptor concentration. Glycosylations passing through an S_N2-like associative pathway, on the other hand, will show clear increases in the glycosylation to cyclization ratio as acceptor concentration increases, as the rate of S_N2-reactions is dependent on concentration of both the nucleophile and the electrophile. It should be noted that, when methylallyltrimethylsilane was used as a nucleophile, only the β-mannoside and α-glucoside were generated, consistent with the selectivities discussed above and with previous studies on *C*-glycoside formation with 4,6-*O*-benzylidene-protected donors.[246]

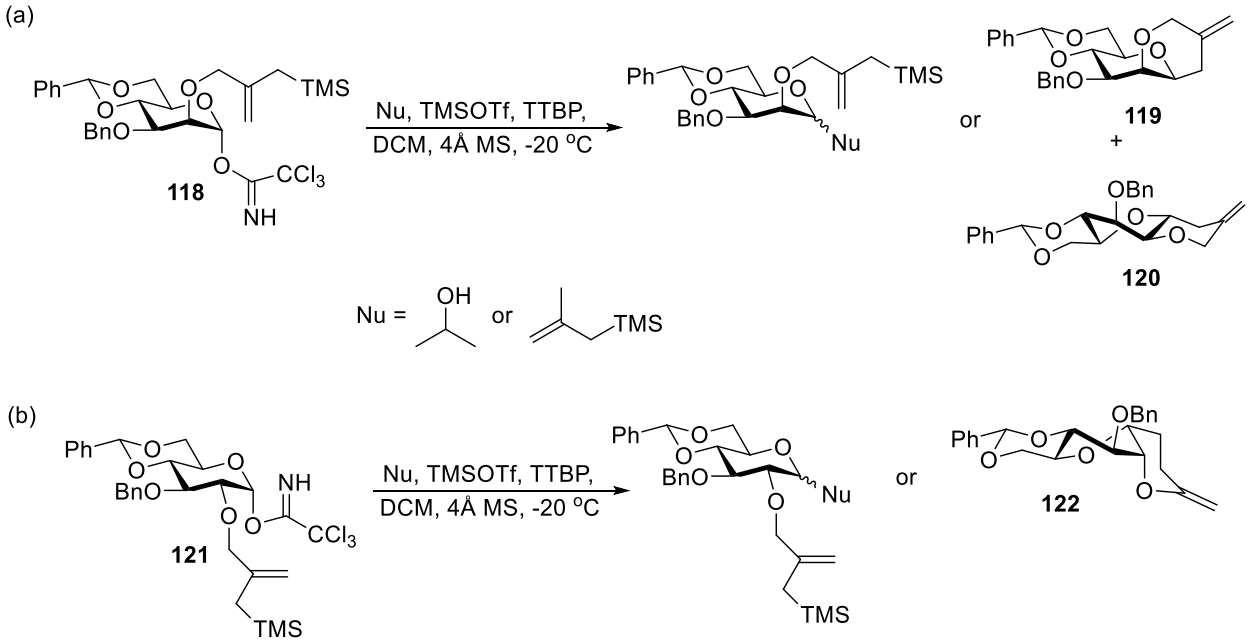

Scheme 4.14. Competition reactions for (a) mannosyl donor **118** and (b) glucosyl donor **121**

Figures 4.8a and 4.8b show the plots of the ratio of glycosylation product to intramolecular cyclization product as a function of nucleophile concentration for the α- and β-mannosides and glucosides. In accordance with the above ^{13}C KIE studies, β-*O*-mannoside formation exhibits a very clear dependence on nucleophile, consistent with an S_N2-like mechanism, while α-*O*-mannoside formation shows a much lower dependence on nucleophile concentration, consistent with a more S_N1-like mechanism. Even more pronounced is the lack of nucleophile concentration dependence in formation of the β-*C*-mannoside, suggesting an S_N1 mechanism with only loose association of the counterion that is consistent with the weak nucleophilicity of methylallyltrimethylsilane. Also consistent with the above ^{13}C KIE studies are the significant dependences on rate concentration observed in both α- and β-*O*-glucoside formation, indicating both reactions pass through an S_N2-like mechanism. The rate of *C*-glucoside formation, on the other hand, exhibits a minimal dependence on nucleophile concentration, suggesting an S_N1-like mechanism.

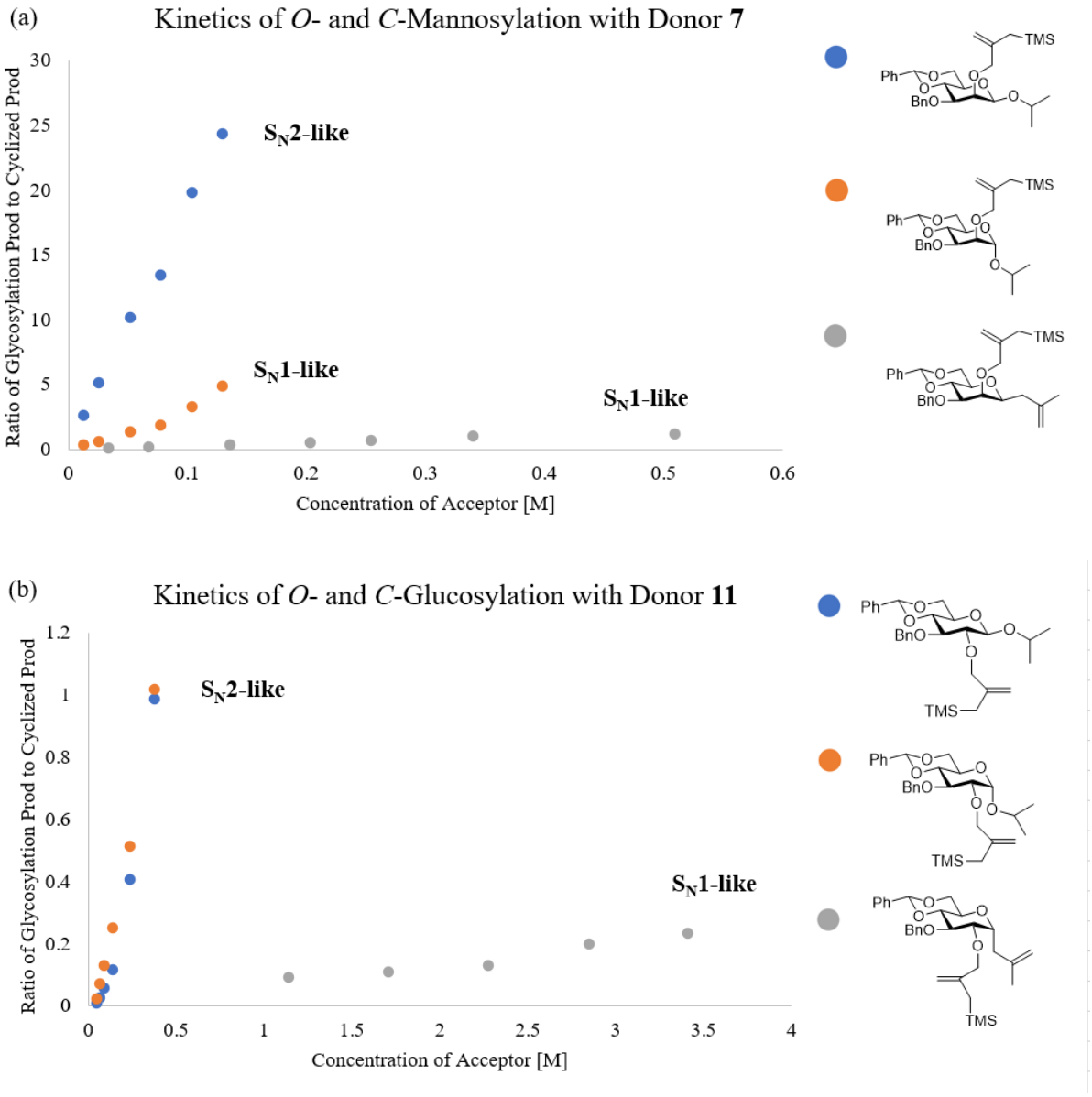

Figure 4.8. Results of clock reactions for (a) mannosylation and (b) glucosylation

Subsequent KIE and kinetic work from numerous groups supports the role of S_N2-like mechanisms in a diverse set of glycosylation reactions. Using a mannosyl iodide donor partially enriched with deuterium at the anomeric position, Gervay-Hague and coworkers observed secondary α-deuterium KIE values of 1.16 and 1.19 for the respective formation of α- and β-mannosides in glycosylation with oxetane (Scheme 4.15a), both of which consistent with

mechanisms passing through exploded S_N2-like transition states.[247] On a similar vein, the Bennet group determined through ^{19}F NMR-derived KIE studies at varied positions that nucleophilic substitution between α-glucopyranosyl fluoride and azide proceeds through an exploded S_N2-like transition state (Scheme 4.15b).[248]

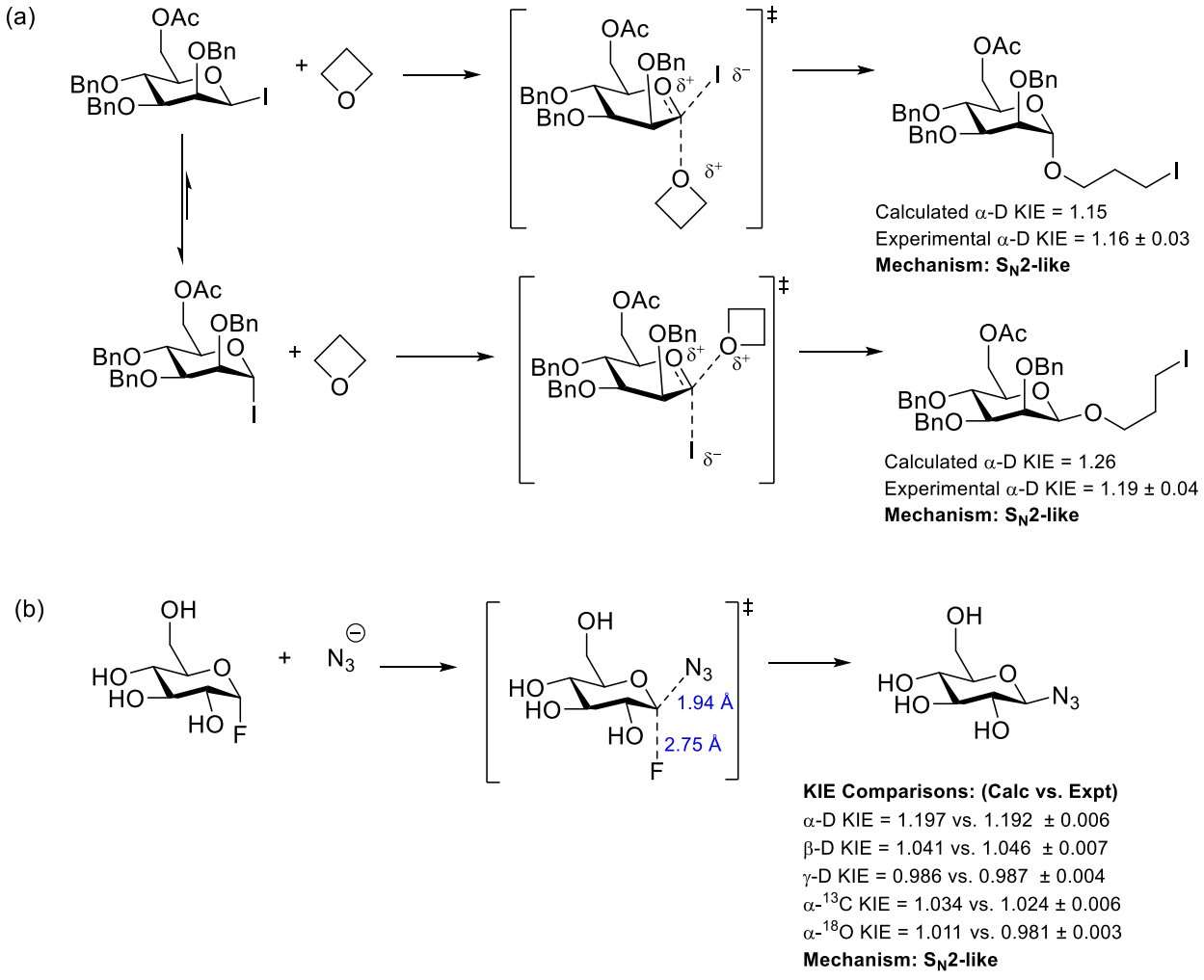

Scheme 4.15. Kinetic studies on (a) oxetane mannoside formation and (b) glucosyl azide formation

In their studies on thiourea-catalyzed glycosylations, Jacobsen and coworkers calculated ^{13}C KIE values from several positions for glycosylation of 2,3,4,6-tetra-*O*-methyl-α-D-galactopyranosyl chloride and benzyl alcohol that were consistent with a loose S_N2-like transition state bearing a high degree of oxocarbenium character (Scheme 4.16a).[249] Secondary deuterium KIE values indicate that formation of the corresponding β-mannoside (α-D KIE 1.15) passes through a loose associative mechanism, while formation of the corresponding α-mannoside (α-D KIE 1.25) passes through a dissociative S_N1-like mechanism (Scheme 4.16b).[250]

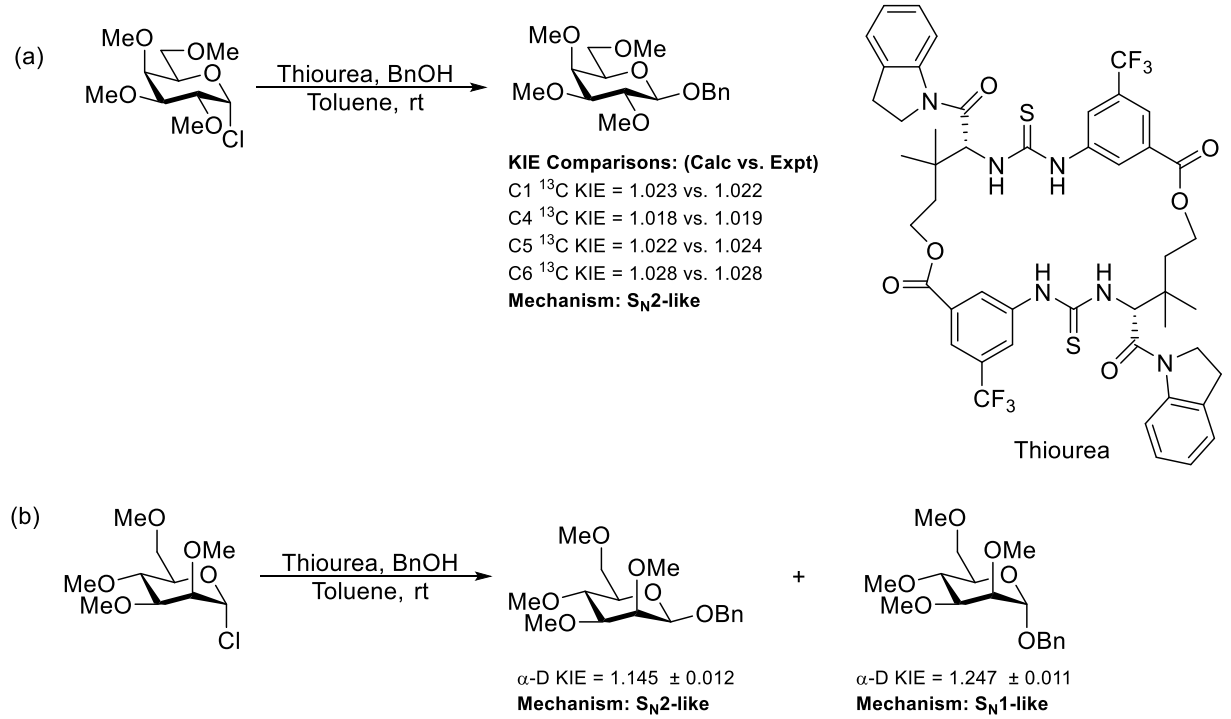

Scheme 4.16. Kinetic studies on (a) thiourea-catalyzed benzyl galactoside formation and (b) thiourea-catalyzed mannosylation

In initial kinetic studies of diarylborinic acid-catalyzed glycosylations summarized in Scheme 4.17a, Taylor and coworkers determined that glycosylation is first order with respect to

the acceptor, catalyst, and donor, indicating that the reaction proceeds through an associative S_N2-like mechanism.[251] Turning to their subsequent studies on glycosyl mesylates, Taylor and coworkers observed that, in the presence of the borinic acid catalyst shown in Scheme 4.17b, glycosylation occurs with excellent β-selectivity (1:10 α:β) and is first order with respect to donor, first order with respect to the catalyst, and zero order with respect to the acceptor. These results indicate that the catalyst rapidly chelates O2 and O3 of the acceptor prior to the rate determining step, and that the reaction proceeds in an S_N2-like fashion. In the absence of the borinic acid, however, Taylor and coworkers observed 2:1 selectivity favoring the α-anomer, along with first order kinetics with respect to both the donor and the acceptor. Thus, the uncatalyzed pathway must also proceed in an S_N2-like displacement. Though the α-mesylate is clearly more reactive in the catalyzed reaction and less reactive in the absence of catalyst, further kinetic studies are needed to fully rationalize the differing product ratios.

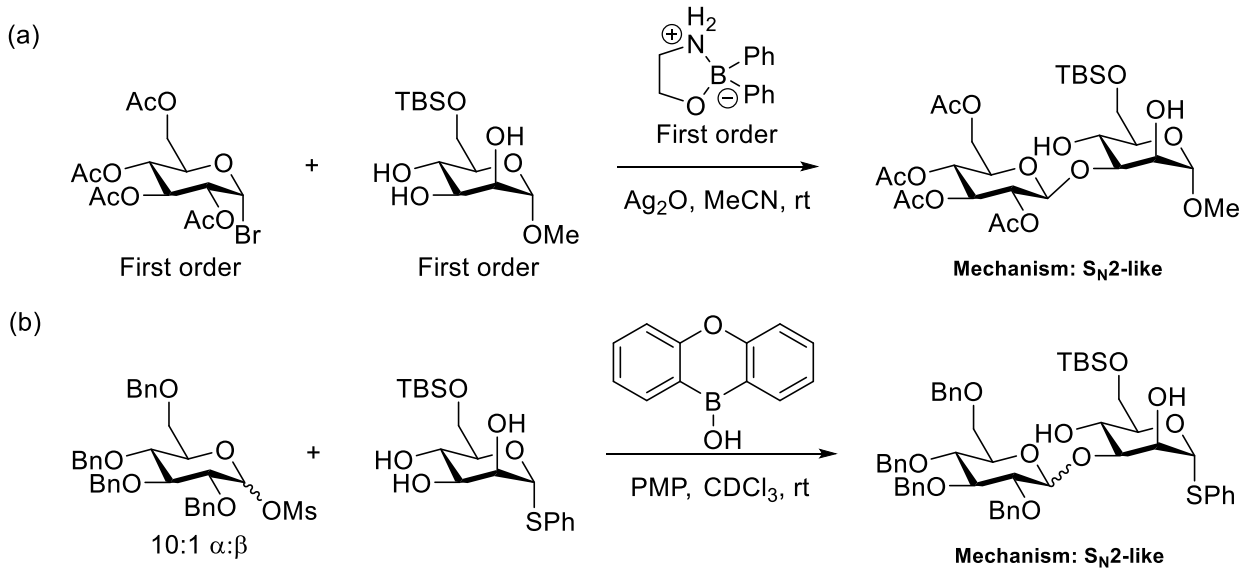

Component	Catalyzed	Uncatalyzed
Donor	First Order	First Order
Acceptor	Zero Order	First Order
Catalyst	First Order	-
Prod. Ratio	1:10 β:α	2:1 α:β

Scheme 4.17. Borinic acid-catalyzed glycosylations of (a) glycosyl bromide donors and (b) glycosyl mesylate donors, with direct kinetic measurements

Over the past few years, the Bennett group has developed a series of β-selective glycosylations using glycosyl sulfonate donors.[252] In 2019 Bennett and coworkers reported an inverse correlation between donor reactivity, determined by Wong's RRV indices, and electrophilicity of the sulfonate; a more reactive donor requires a less electron-deficient sulfonate to maximize selectivity, while less reactive donors require very active sulfonates.[253] This difference is illustrated in Scheme 4.18a-b, where per-*O*-benzylated glucose requires the electron-deficient 3,5-bis(trifluoromethyl)benzenesulfonyl chloride for optimal reactivity, while its 2-deoxy analog warrants use of the much more electron-rich tosylate.[254] To determine the degree of

oxocarbenium ion-character in the transition state of these reactions, Bennett and coworkers ran a series of KIE studies at various positions of per-*O*-benzylated glucose (Scheme 4.18b), each of which was consistent with significant associative character. A similar protocol was subsequently applied to the generation of *C*-glycosides, which exhibited a primary ^{13}C KIE value of 1.029 consistent with an S_N2-like mechanism (Scheme 4.18c).[255]

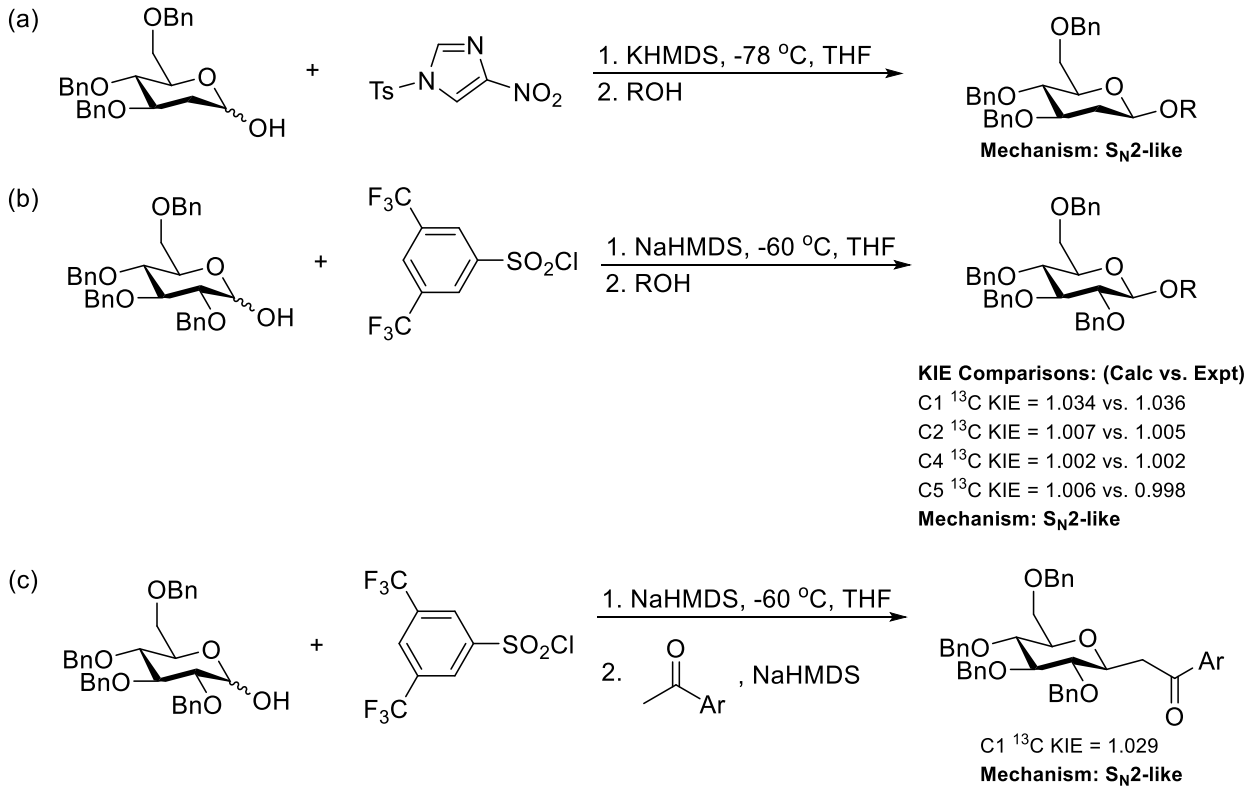

Scheme 4.18. Kinetic studies on (a) glycosylation with glycosyl tosylate donors and generation of (b) *O*-glycosides and (c) *C*-glycosides from glycosyl sulfonates

4.7. Glycoside Hydrolysis and Synthesis in Nature

In Nature, carbohydrate processing enzymes control the regio- and stereoselective formation and cleavage of glycosidic linkages in biomolecules and thus play a critical role in

ensuring proper function of biological systems.[256-261] Several classes of carbohydrate processing enzymes, which are presented below, generally proceed through an exploded oxocarbenium ion-like transition state in their mechanisms. The glycoside hydrolases (GHs) or glycosidases, catalyze the hydrolysis of glycosidic linkages with either inversion or retention of stereochemistry. Inverting GHs employ water as the nucleophile to directly displace the leaving group in an S_N2 fashion (Scheme 4.19a). The retaining GHs, on the other hand, proceed through a classical Koshland double displacement mechanism, where a catalytic aspartate or glutamate residue displaces the leaving group to form a covalent complex with the sugar that is subsequently displaced in an S_N2-like fashion by water (Scheme 4.19b).[262]

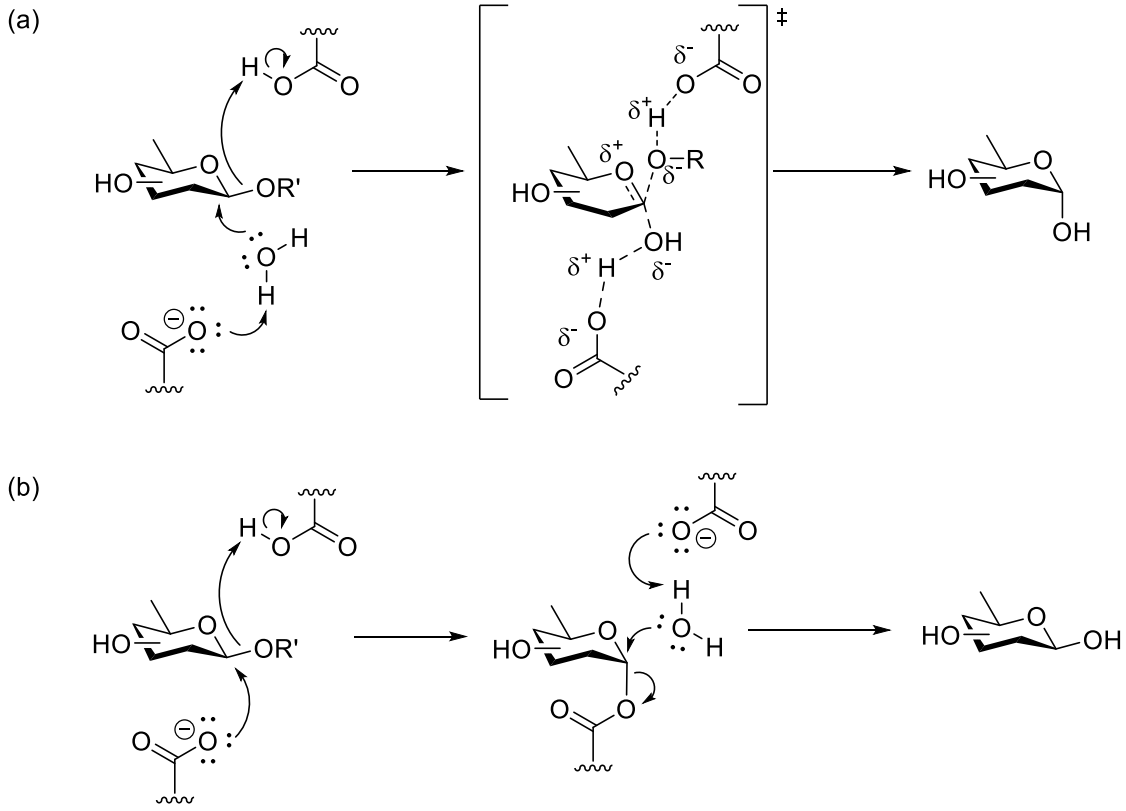

Scheme 4.19. General mechanism of (a) inverting and (b) retaining glycosidases

These enzymes are subdivided according to their amino acid sequences into approximately 170 families.[263] While the above mechanistic outline holds true for almost all GHs, a handful of families proceed through alternative mechanisms that do not involve an oxocarbenium ion-like transition state. For example, GHs 4 and 109, which act on a range of gluco- and galactopyranosides, pass through an NAD-mediated oxidation of C3 followed by a series of eliminations and rearrangements to generate the hydrolyzed product (Scheme 4.20).[264-266]

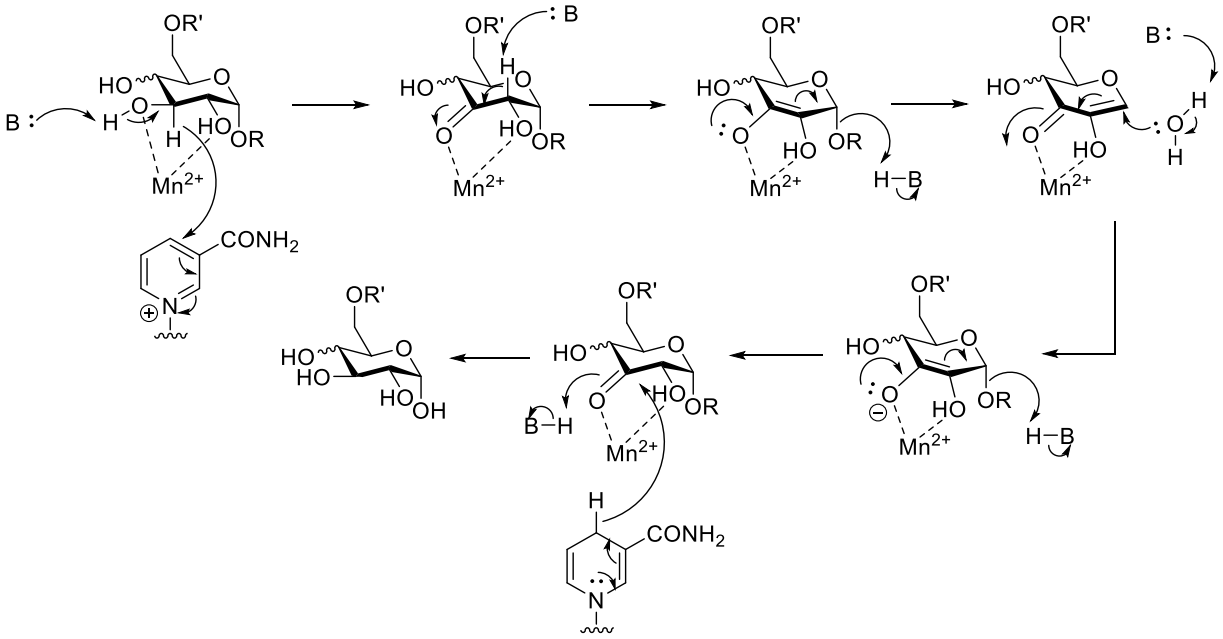

Scheme 4.20. Mechanism of GHs 4 and 109

The glycosyltransferases (GTs) are a class of carbohydrate processing enzyme that synthesize glycosidic linkages. Like the inverting GHs, inverting GTs proceed through an S_N2-like displacement, as shown in Scheme 4.21a. The retaining GTs, on the other hand, differ from their GH counterparts in that they predominantly lack an appropriately positioned aspartate or glutamate to form the covalent intermediate observed in the classical Koshland double

displacement. While there have been a handful of covalent intermediates proposed in computational and mass spectrometric studies,[267, 268] the retaining GTs are generally thought to undergo a concerted S_Ni mechanism presented in Scheme 4.21b, though there remains a significant degree of debate.[269, 270]

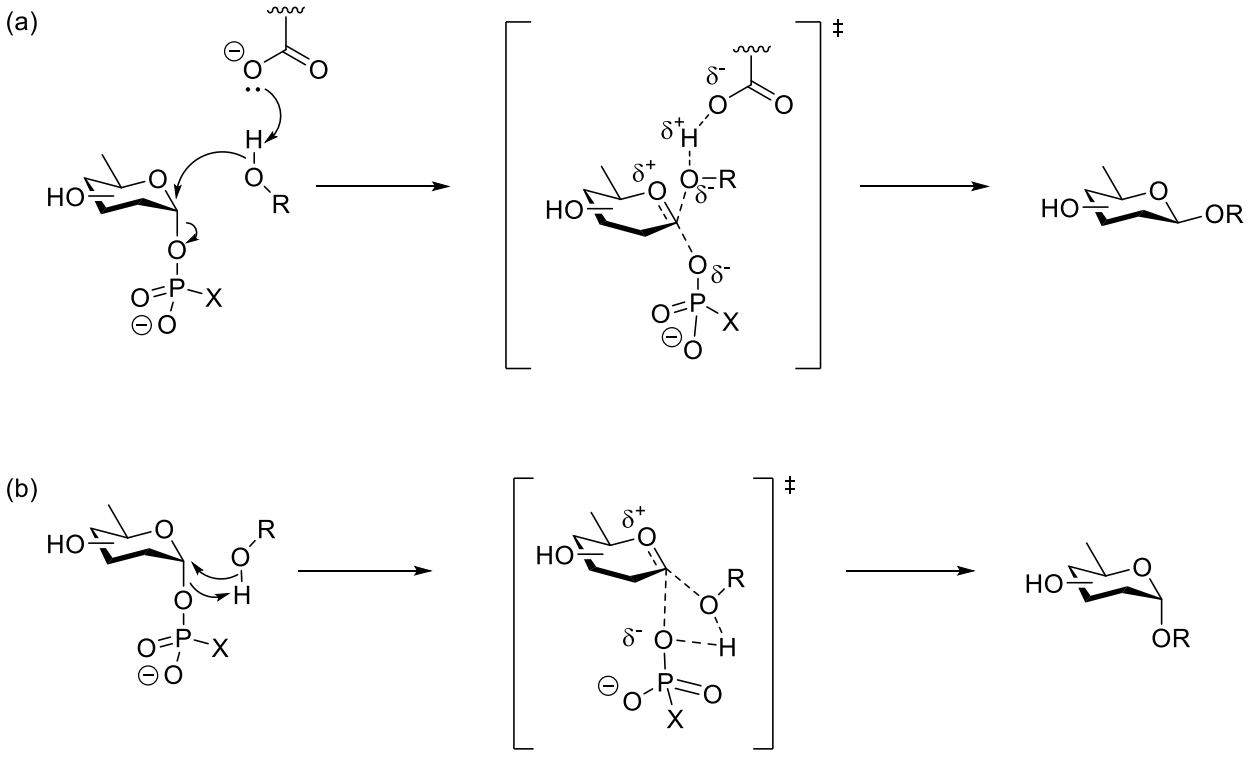

Scheme 4.21. Mechanism of (a) inverting and (b) retaining glycosyltransferases

In addition to classification by mechanism, the GTs are also subdivided by their leaving groups. As shown in Scheme 4.22, Leloir GTs bear an anomeric nucleotidyl diphosphate group, usually UDP, whereas non-Leloir GTs bear an anomeric phospholipid.[271]

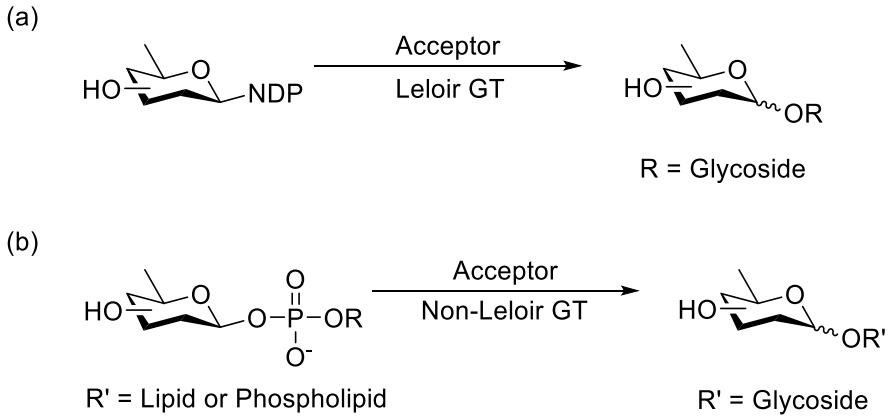

Scheme 4.22. Reactions catalyzed by (a) Leloir and (b) non-Leloir GTs

Transglycosidases are a second class of enzymes responsible for the synthesis of glycosidic linkages, which bear several key mechanistic distinctions from the GTs. In addition to being exclusively retaining enzymes, the transglycosidases pass through a classic Koshland double displacement mechanism shown in Scheme 4.23, just as is observed with the retaining GHs. Despite their role in the synthesis of glycosidic linkages, the transglycosidases are classified under GH families as a result of similarities in their amino acid sequences.[272]

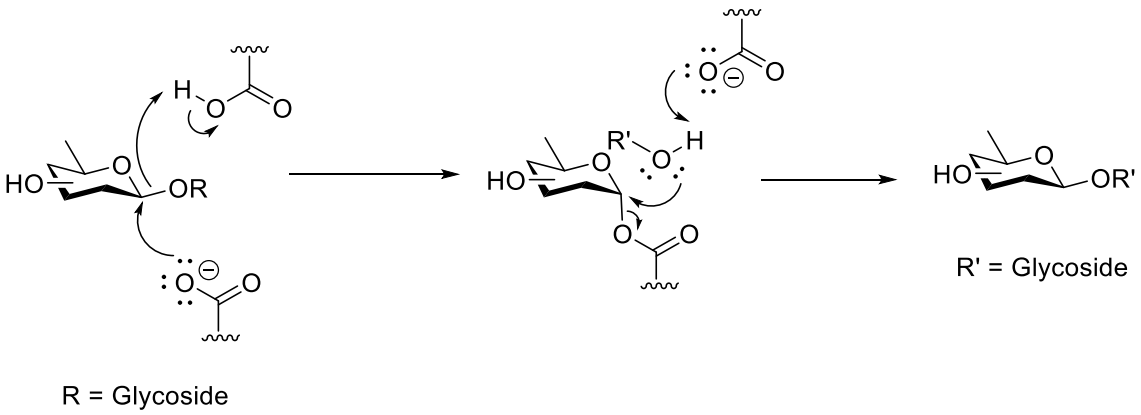

Scheme 4.23. General mechanism of transglycosidases

Glycoside phosphorylases catalyze the reversible formation of an anomeric phosphate through cleavage of a glycosidic bond (Scheme 4.24). In accordance with their amino acid sequences, the phosphorylases are divided into either GH families, as is the case with maltose and starch phosphorylases, or GT families, as observed with glycogen and starch phosphorylases.[258, 273]

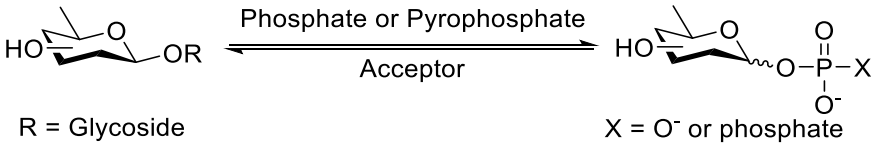

Scheme 4.24. Reactions of phosphorylases

4.7. Mechanistic Studies on Enzymatic Glycoside Hydrolysis and Synthesis

Long before their application in analysis of chemical glycosylation, kinetic isotope studies were extensively employed in mechanistic analysis of the GHs and GTs beginning in the 1960s with the Raftery group's work on the retaining hen egg white lysozyme (HEWL).[274-276] Raftery and coworkers observed a secondary α-D KIE value of 1.11 in the hydrolysis of aryl chitobiose by HEWL (Scheme 4.25a), which is consistent with an exploded transition state bearing a significant degree of oxocarbenium character rather than with a purely associative mechanism. Similar observations were made by Withers and coworkers in their kinetic experiments on *Agrobacterium faecalis* β-glucosidase, where the rates of hydrolysis of several isotopically labeled aryl glycosides were studied.[277] For substrates bearing relatively acidic leaving groups (conjugate acid $pK_a < 8$), the rate-limiting step was determined to be hydrolysis of the covalent enzyme-substrate intermediate, for which secondary α-D KIEs of 1.11 ± 0.03 were measured. For substrates with less acidic leaving groups, however, the rate-limiting step was determined to be generation of the

covalent intermediate, with secondary α-D KIEs of 1.06 ± 0.03, as shown in Scheme 4.25b. Thus, Withers and coworkers concluded that both formation and cleavage of the covalent intermediate pass through transitions states containing significant oxocarbenium character, though the first step of double displacement takes place with slightly more associative character.[278] Consistent with the above results, Hehre and coworkers carried out a series of KIE studies on hydrolysis of isotopically labelled α-D-glucosyl fluoride by both the retaining sugar beet seed α-glucosidase and the inverting *Rhizopus niveus* α-glucosidase, and determined that the processes catalyzed by both enzymes proceed with a significant degree of dissociative character (Schemes 4.25c-d).[279]

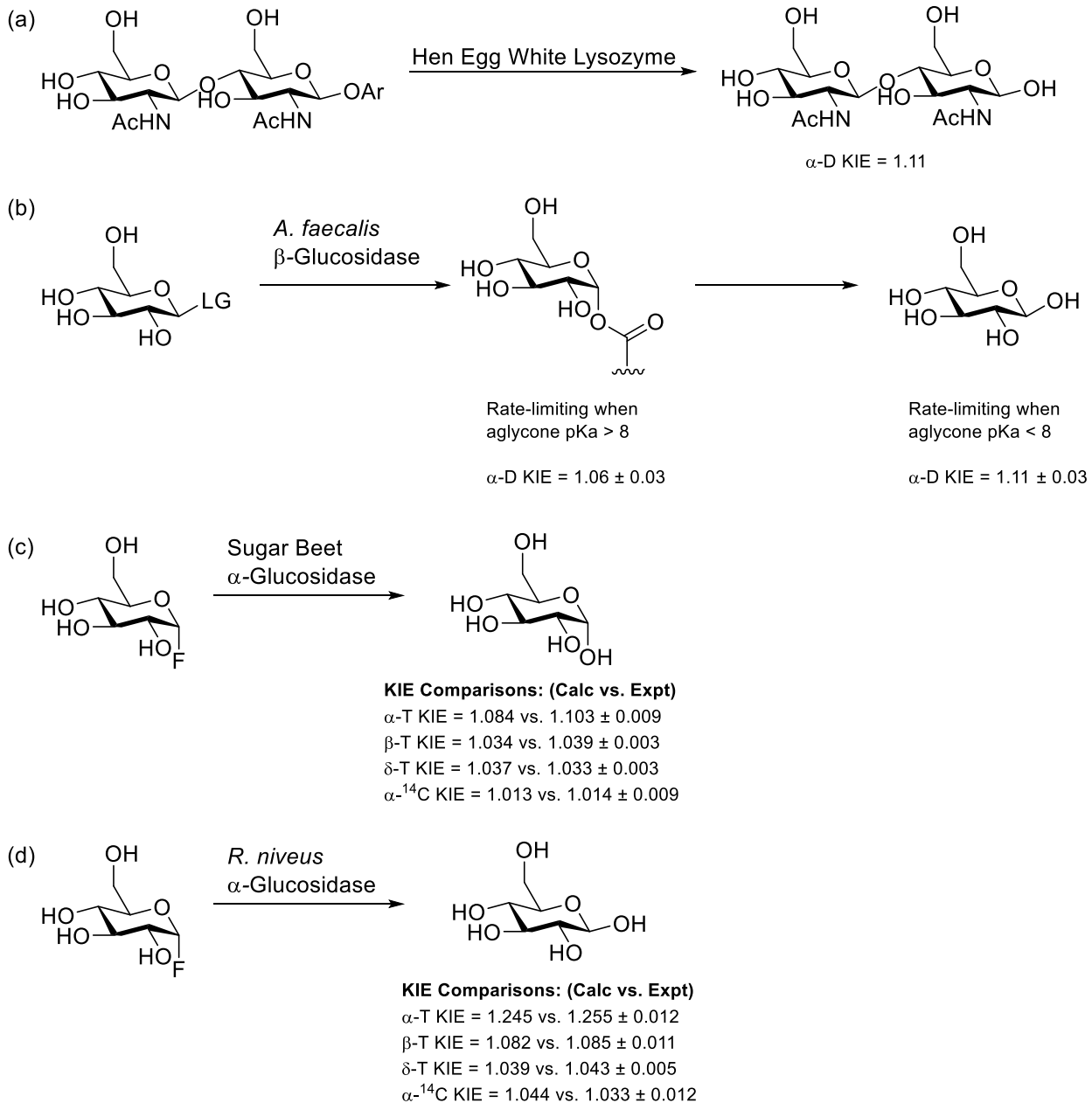

Scheme 4.25. Kinetic studies on (a) hen egg white lysozyme, (b) *Agrobacterium faecalis* β-glucosidase, (c) sugar beet seed α-glucosidase, and (d) *Rhizopus niveus* α-glucosidase

Turning to the glycosyltransferases, Wong and coworkers concluded that the mechanism of the inverting human α-1,3-fucosyltransferase V (FucT V) proceeds in a primarily dissociative pathway, as evidenced by a secondary α-D KIE of 1.27 ± 0.07 (Scheme 4.26a).[280] In 2011, the

Davies and Davis groups ran extensive kinetic studies on *Escherichia coli* trehalose-6-phosphate (T6P) synthase, concluding that glycosyltransfer most likely proceeds in an S_Ni fashion with significant dissociative character rather than through a Koshland double displacement observed in the retaining GHs and the transglycosidases (Scheme 4.26b). Of particular note is the observed primary ^{18}O KIE value of 1.024 ± 0.002, which is in the range of typical values corresponding to partial protonation of the leaving group at the transition state level. At the same time, the Davies and Davis groups determined that reaction rate increases with basicity of the acceptor, meaning that the acceptor is also involved in the rate-determining step. Given that both the partially protonated leaving group and the acceptor are involved in the rate determining step, the reaction most likely proceeds intermolecular hydrogen-bonding between the donor and the acceptor, as shown in Scheme 4.26b.

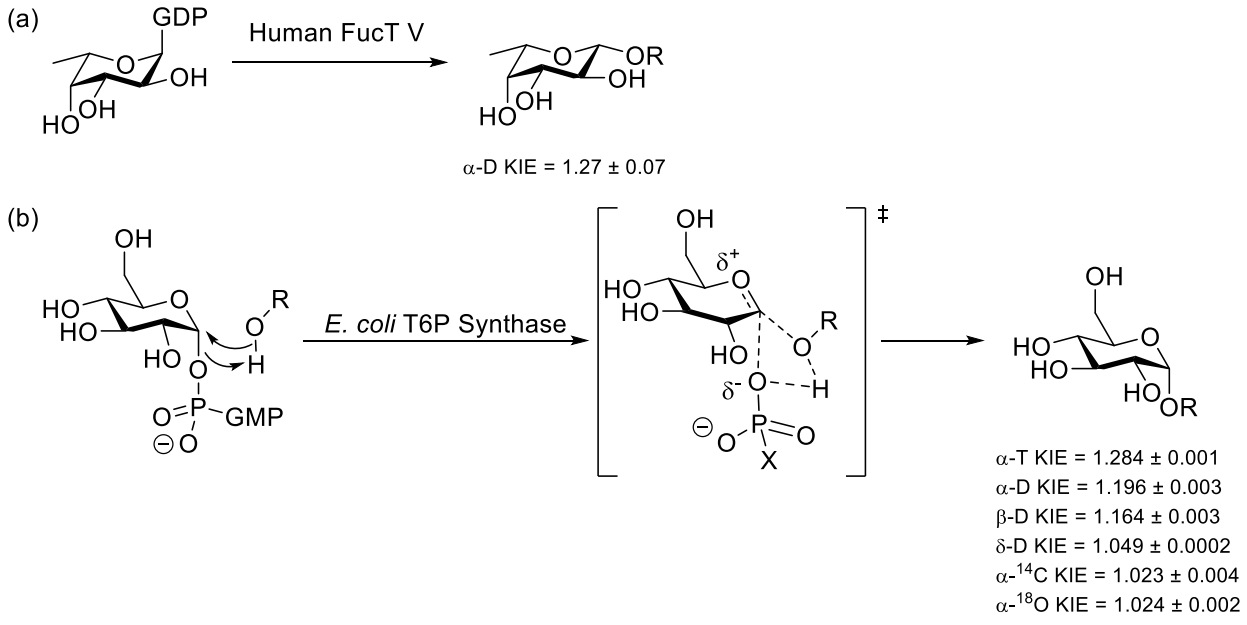

Scheme 4.26. Kinetic studies on (a) human α-1,3-fucosyltransferase V and (b) *Escherichia coli* trehalose-6-phosphate synthase

More recently, mechanistic understanding of the GHs and GTs has been bolstered by crystallographic snapshot studies, which allow for the visualization of the conformational itinerary taken up by the substrate over the course of the reaction. An example of this type of study is the snapshot study of *Caulobacter sp.* GH47 α-mannosidase carried out by the Davies group.[281, 282] Through crystallization of the mannosidase with a non-hydrolyzable starting material analog, a mannoimidazole that mimics the transition state, and a competitive inhibitor that mimics the binding of the hydrolysis product, Davies and coworkers were able to readily visualize the conformations taken up at each stage of the reaction, as shown in Figure 4.9: the substrate binds in a $^{3}S_{1}$ skew boat and passes through a $^{3}H_{4}$ half chair until it is released as an inverted $^{1}C_{4}$ chair. These studies are elaborated upon in Chapter 5.

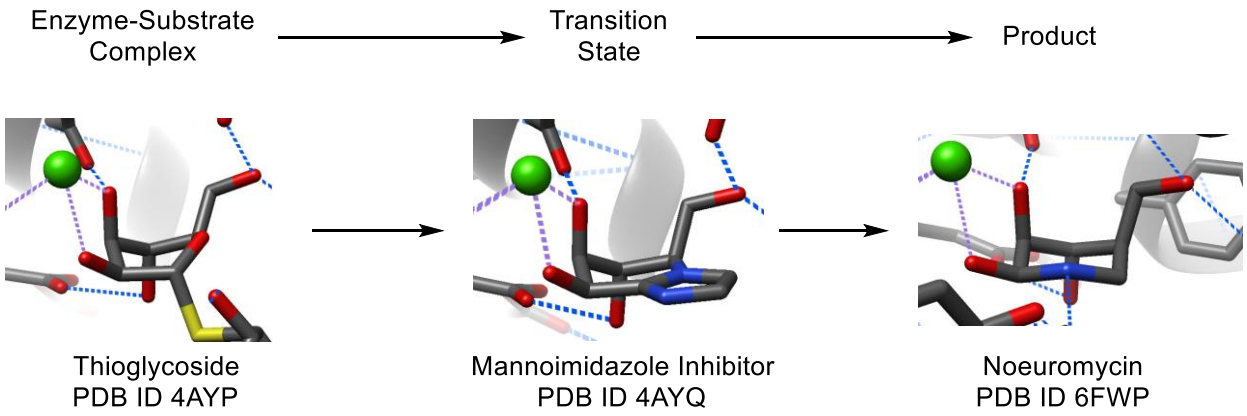

Figure 4.9. Crystallographic snapshot of *Caulobacter sp.* GH47 α-mannosidase

Overall, physical organic studies have revealed that both chemical and enzymatic glycosylation reactions take place through analogous pathways with loose or exploded S_N2-like, or loose S_Ni-like transition states with significant oxocarbenium ion character.

4.8. Overall Goals

In light of the well-established influence of side chain conformation on glycosylation reactivity, the original goal inspiring the crystallographic analysis presented in Chapter 5 was to determine the degree to which the GHs, GTs, transglycosidases, and phosphorylases have evolved to restrict their substrate side chains to the most reactive *gg* conformation. Given that these enzymes invoke oxocarbenium ion-like transition states in their reaction mechanisms, enforcement of the *gg* conformation would increase reactivity during hydrolysis or glycosylation, thereby increasing catalytic efficiency.

CHAPTER 5

TRANSITION STATE STABILIZATION BY CARBOHYDRATE PROCESSING ENZYMES

5.1. Introduction

Given their involvement in a wide range of physiological processes, the GHs and GTs have garnered significant attention as drug targets.[260, 261, 283-287] To this end, their inhibitors have seen use against disease states such as cancer, diabetes, and autoimmune disorders, and exhibit antiviral, antifungal, antibacterial, and pesticidal activity. Examples of commercial GH inhibitors include the α-glucosidase inhibitors miglitol **123**, which is used for treatment of diabetes, and the neuraminidase inhibitor zanamivir **124**, which is used as an antiviral agent.

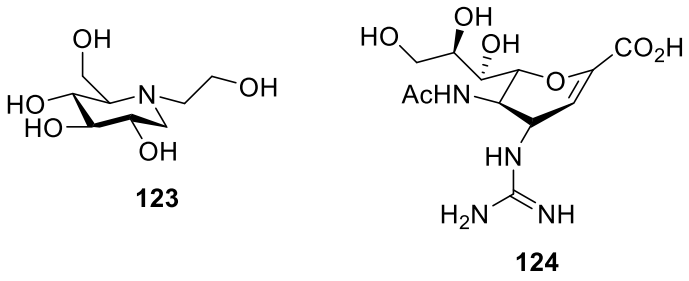

Figure 5.1. Structures of miglitol **123** and zanamivir **124**

In order to design more active and/or selective inhibitors, it is crucial to have a thorough understanding of how the GHs and GTs bind their substrates and of the reactions that they catalyze. To this end, and in light of the well-established influence of side chain conformation on reactivity in chemical glycosylation, an in-depth analysis of crystal structures from the Protein Data Bank

(PDB) was carried out to determine whether or not carbohydrate processing enzymes that pass through oxocarbenium ion-like transition states have evolved to restrict their substrate side chains to maximize reactivity.

5.2. Data Collection

Using the Carbohydrate Active Enzymes database (CAZy, http://www.cazy.org),[288] all available crystal structures of GHs, GTs, phosphorylases, and transglycosidases with hexopyranoses or corresponding analogs bearing a hydroxymethyl side chain bound to the active site (-1 site in GHs and transglycosidases)[289] were compiled, as summarized in Tables 5.1 and 5.2.[290, 291] Also recorded in Tables 5.1 and 5.2 is the number of structures exhibiting hydrogen bonding between the side chain and the active site. Crystal structures belonging to GH families 4 and 109 which pass through an alternate mechanism discussed in Chapter 4 were not included in this study.[264-266, 292]

In addition to manual inspection of each crystal structure to prevent such errors as incorrect active site identification, each structure was validated using the Privateer software,[293] using 0.8 as the minimum allowable real space correlation coefficient (RSCC) value.[294] Likewise, a ≤2.00 Å cutoff[295] was imposed on the GH data set to minimize inclusion of potential errors in crystallography.[296] For the GTs, phosphorylases, and transglycosidases, a more relaxed cutoff of ≤2.50 Å was used due to the limited number of available structures, though trends collected using this relaxed cutoff showed no significant difference to those using a ≤2.00 Å cutoff.[291] Of note, only Leloir GTs are represented due to the lack of available sufficiently high resolution crystal structures of non-Leloir GTs. Crystal structures bearing multiple copies of the active site were listed as one entry in the tables below if the side chain of the ligand bound in each copy was held

in the same conformation; cases where differences in the ligand side chain conformation were observed were classed as ambiguous and accounted for in the total number of structures without further discussion.

5.3. Glucoside, Mannoside, and Ulosonide Processing Enzymes

Table 5.1. Side chain populations of ligands bound to glucoside, mannoside, and ulosonide processing enzymes

Enzyme Class	*gg*	*gt*	*tg*	Eclipse	Total	H-bonds to O6
α-Glucosidase	77	1	-	-	78	74
α-*N*-Acetyl Glucosaminidase	9	-	-	-	9	9
α-Glucosyltransferase	30	3	1	3	39	37
α-*N*-Acetyl Glucosaminyltransferase	4	1	1	1	7	6
α-Glucoside Phosphorylase	126	-	-	-	126	126
α-Glucoside Transglycosidase	29	4	-	2	41	29
β-Glucosidase	131	19	-	-	156	139
β-*N*-Acetyl Glucosaminidase	54	16	-	-	72	72
β-Glucosyltransferase	10	1	1	-	12	12
β-*N*-Acetyl Glucosaminyltransferase	10	4	-	2	16	14
β-Glucoside Phosphorylase	3	-	-	-	4	4
β-Glucoside Transglycosidase	7	1	-	1	9	6
α-Mannosyltransferase	-	-	1	-	1	1
α-Mannosidase	25	28	-	1	54	54
α-Mannoside Phosphorylase	6	-	-	-	6	6
β-Mannosidase	21	-	-	-	21	15
β-Mannosyltransferase	2	-	-	-	2	2
Neuraminidase	38	-	-	-	38	14
α-Sialyltransferase	9	-	1	1	11	7
Trans-Sialidase	4	-	-	-	4	2
Total	595	78	5	11	706	629

Table 5.1 illustrates that, with the exception of the α-mannosidases and the β-*N*-Acetyl glucosaminyltransferases, most glucoside, mannoside, and ulosonide acid processing enzymes bind their substrates in the most reactive *gg* conformation with enforcement through H-bonding. As a whole, relatively similar trends are observed between the hydrolases of a given substrate and the corresponding transferases, phosphorylases, and transglycosidases. For example, 84% of β-glucosidases and 83% of β-glucosyltransferases restrict the bound side chain to the *gg* conformation. Similar selectivity is observed among the α-glucosyltransferases and α-transglycosidases, 77% and 71% of which respectively favor the *gg* conformation. Some classes of enzyme exclusively bind their substrates in the *gg* conformation, as is the case with the β-mannosidases and α-glucoside phosphorylases, or almost exclusively as is observed with α-glucosidases. In some cases, such as the β-mannosyltransferases and the α-*N*-acetyl glucosaminyltransferases, the paucity of crystal structures prevents proper conclusions from being drawn. The high percentage of H-bonding between the ligand side chains and the enzyme active site indicates that the side chain is actively restricted by the enzyme to the observed conformation rather than freely rotating in the active site.

The above trends stand in stark contrast with the side chain distributions observed both in free solution, which for simple glucosides and mannosides is roughly 1:1 *gg* to *gt*, and when bound to lectins or alternate binding sites of the above enzymes, which approximate the free solution populations.[290, 291] Thus, preferential restriction of the side chain to the most reactive conformation is only observed in sites where glycosylation or hydrolysis takes place. This conformational restriction is best appreciated through comparison of bound and free solution side chain populations of specific ligands. Scheme 5.1, for example, shows that of the 14 crystal structures of glucosidases with β-glucopyranose **125** bound in the -1 site, 13 hold the side chain in the *gg*

conformation. Likewise, seven out of nine glucosyltransferases bound to UDP-2-deoxy-2-fluoro-α-glucose **126** enforce the *gg* conformation, as shown in Scheme 5.2.

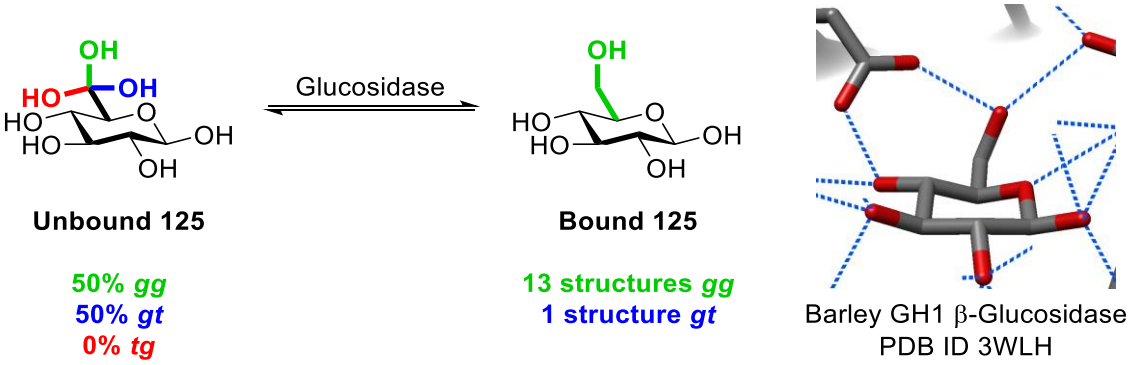

Scheme 5.1. Side chain restriction of β-glucopyranose **125** by glucosidases

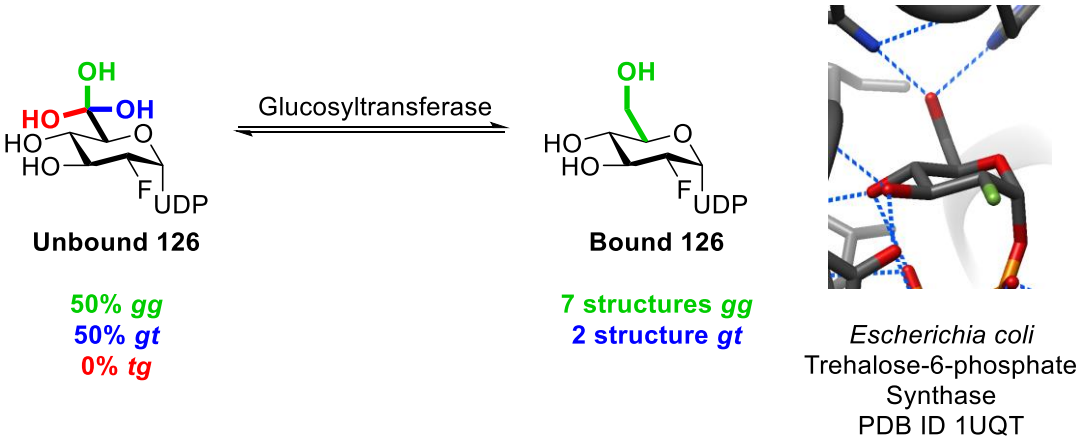

Scheme 5.2. Side chain restriction of UDP-2-deoxy-2-fluoro-α-glucose **126** by glucosyltransferases

For some ligands such as GH transition state analog inhibitors, whose structures generally mimic the glycosyl oxocarbenium ion in both hybridization and charge,[262] it is insufficient to assume similar side chain populations to those of a simple glycoside. Such cases necessitate estimation of the free solution conformer distribution through ^{1}H NMR analysis. Given the low

barrier to rotation of the exocyclic C5-C6 bond, it is not possible to see the individual *gg*, *gt*, and *tg* conformers as separate sets of signals during NMR analysis; instead, the NMR spectrum of a given sugar is a time-weighted average of the different side chain populations. However, the ratio of the three staggered conformers in solution can be derived from the observed H5-H6 coupling constants using the three equations in Figure 5.2. The labels H6*R* and H6*S* denote the pro-*R* and pro-*S* protons of the exocyclic methylene group, while $^{3}J_{H5,H6R}$ and $^{3}J_{H5,H6S}$ in equations 1 and 2 represent the observed coupling constants. The term f_{xx} denotes the fraction of the specified conformer in solution, and the constant preceding each of these fractions in equations 1 and 2 is a representative "ideal" coupling constant for the specified conformation known as a limiting coupling constant as shown in Figure 5.2. Using equations 1 and 2, limiting coupling constants are used to calculate the degree of contribution offered by each conformation to the observed coupling constants, while equation 3 ensures that the fractions of all conformers add to unity. Recently, the Crich group experimentally determined an updated, and reliable set of limiting coupling constants,[297] which are identified in Figure 5.2 and which were used in determination of the side chain populations discussed below.

(1) $^3J_{H5,H6R} = {}^3J_{R,gg}f_{gg} + {}^3J_{R,gt}f_{gt} + {}^3J_{R,tg}f_{tg}$

(2) $^3J_{H5,H6S} = {}^3J_{S,gg}f_{gg} + {}^3J_{S,gt}f_{gt} + {}^3J_{S,tg}f_{tg}$

(3) $1 = f_{gg} + f_{gt} + f_{tg}$

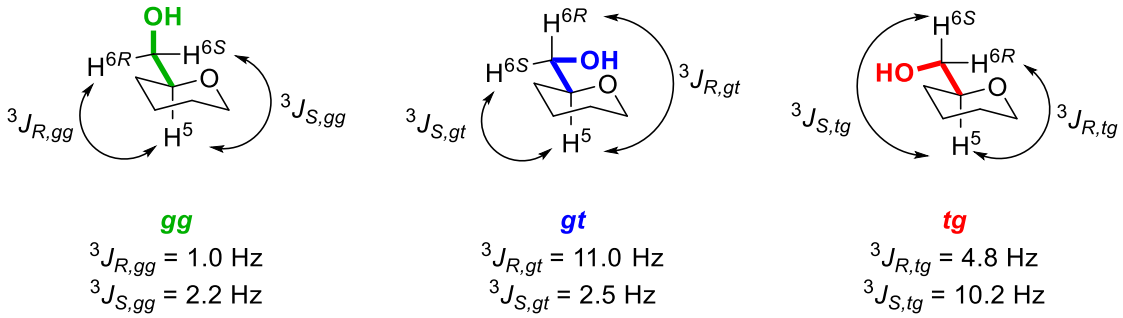

gg
$^3J_{R,gg}$ = 1.0 Hz
$^3J_{S,gg}$ = 2.2 Hz

gt
$^3J_{R,gt}$ = 11.0 Hz
$^3J_{S,gt}$ = 2.5 Hz

tg
$^3J_{R,tg}$ = 4.8 Hz
$^3J_{S,tg}$ = 10.2 Hz

Figure 5.2. Equations to determine side chain populations in free solution and the corresponding limiting coupling constants

It should be noted that in most NMR assignments, H6*R* and H6*S* are not distinguished from one another. In these cases, each observed $^3J_{H5,H6}$ coupling constant is plugged into equations 1-3 twice: once assuming H6 is the pro-*R* proton and once assuming it is the pro-*S* proton. Thus, two possible populations are determined and reported for a single compound (or two sets of populations if analyzing a series of compounds), as is observed below.

While lactam **127** is calculated to be only 11 or 14% *gg* in solution using the above equations, its side chain is held in the *gg* conformation when bound to GH1 glycosidases as shown in Scheme 5.3. This is especially noteworthy given that, in the *galacto* series, the *gg* conformation is destabilized due to the unfavorable interactions between O4 and O6, a discussion point which is elaborated upon below.

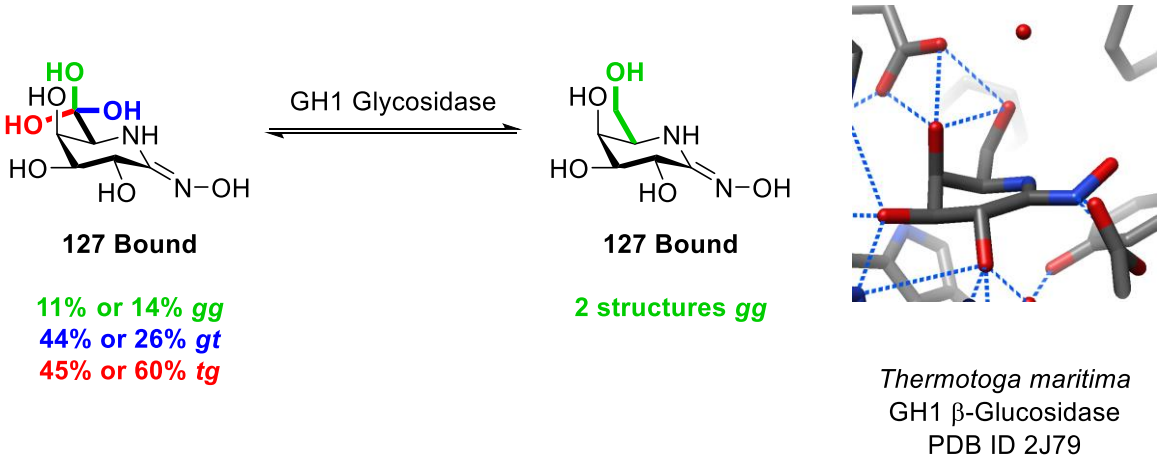

Scheme 5.3. Side chain restriction of galactohydroximinolactam **127** by GH1 glycosidases

Similarly, members of the isofagomine series, which are roughly 37-47% *gg* in free solution, are held in the *gg* conformation when bound to various glycosidases in 14 out of 15 structures (Scheme 5.4). Thus, the preference for the *gg* conformation across the above enzymes is clearly distinct from the side chain populations observed in solution.

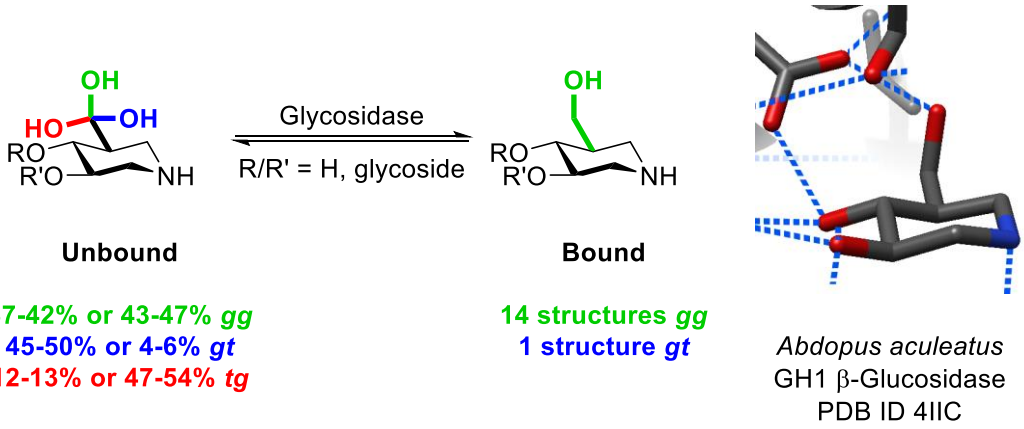

Scheme 5.4. Side chain restriction of the isofagomine series by glycosidases

Though Table 5.1 indicates that the α-mannosidases and the β-*N*-acetyl glucosaminyltransferases exhibit minimal preference between the *gg* and *gt* conformations, subdivision of these enzymes into their corresponding families reveals much higher selectivity at the family level. In the case of the α-mannosidases, while Table 5.1 shows a roughly 1:1 ratio of *gg* to *gt* conformers overall, further analysis reveals that families 38 and 47 only bind their substrates in the second-most reactive *gt* conformation, while all *gg*-enforcing structures were observed with members of families 63, 92, 99, and 125. These preferences are nicely illustrated through the differential restriction of the side chain of mannoimidazole **128** in Scheme 5.5 (though no structures of family 63 or 99 mannosidases bound to **128** were located), whose free solution side chain populations were determined through NMR analysis as discussed above (only one set of solution phase conformers is listed because both coupling constants used for analysis were identical).

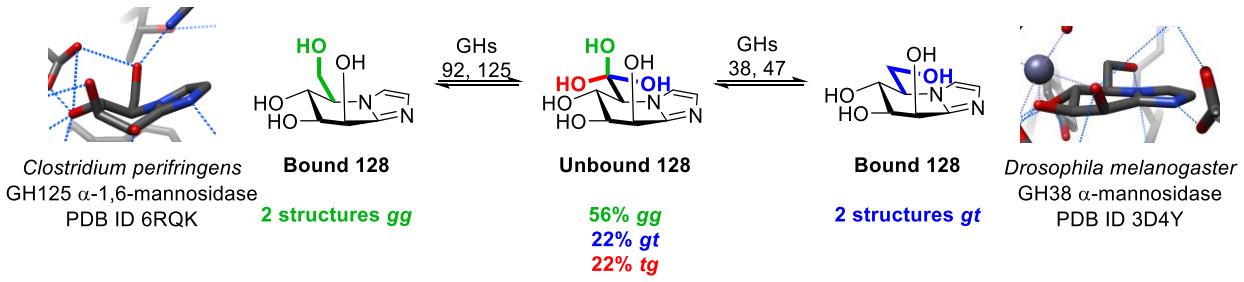

Scheme 5.5. Differing side chain preferences observed with mannoimidazole **128** among α-mannosidase families

Similarly, dividing the β-*N*-acetyl glucosaminyltransferases into their corresponding families reveals that GT families 2 and 41 preferentially bind their substrates in the *gg* conformation while GT family 13 members favor the *gt* conformation, as illustrated through

comparison of crystal structures with bound UDP-α-*N*-acetylglucosamine **129** (Scheme 5.6). Notably, the catalytic aspartate lying directly above the pyranoside ring in GT13 enzymes sterically prevents the substrate from taking up the *gg* conformation, thereby enforcing the *gt* conformation.

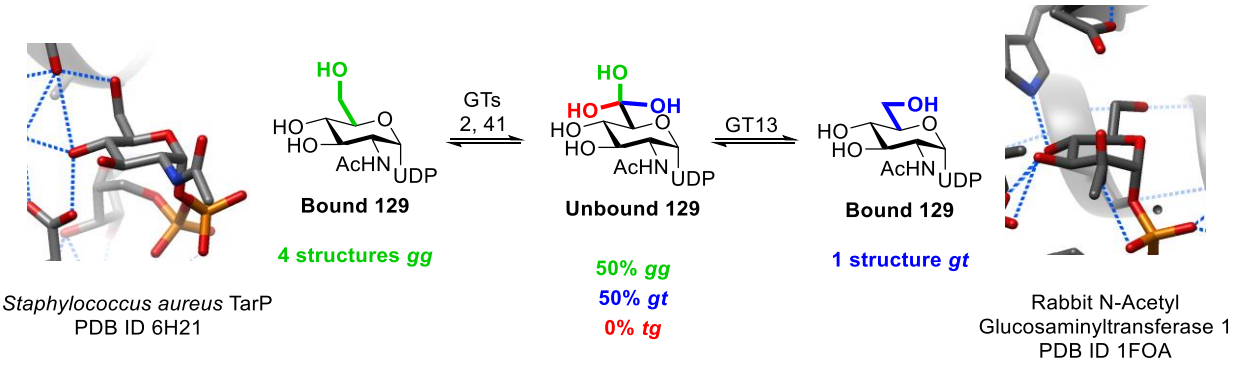

Scheme 5.6. Differing side chain preferences for UDP-α-*N*-acetylglucosamine **129** among β-*N*-acetyl glucosaminyltransferases

Recently the Davies and Rovira groups carried out crystallographic snapshot studies on *Bacteroides xylanisolvens* GH99 endo-α-mannanase,[298] wherein a substrate analog, a mimic of a reaction intermediate, and a hydrolysis product are each crystallized in the enzyme active site to probe the conformational itinerary of the pyranose ring during reaction. Analysis of each of these crystal structures reveals that the side chain is restricted to the *gg* conformation on initial substrate binding and remains held as such over the course of the reaction up until release of the product (Figure 5.3a). Similar studies were carried out by Wang and coworkers on termite GH1 β-glucosidase,[282] where despite changes in the ring conformation, the side chain appears to be preorganized in the *gg* conformation and is maintained as such over the course of the entire reaction through product release (Figure 5.3b). Moreover, crystallographic studies from Dijkstra and

coworkers on the retaining transglycosidsae *Bacillus circulans* cyclodextrin glycosyltransferase (CGTase) show that the side chains of the starting material γ-cyclodextrin,[299] an acarbose derivative,[300] and the covalently bound 4-deoxymaltotriose[301] are all held in the *gg* conformation (Figure 5.3c). It should be noted that the while the inhibitors in each study mimic aspects of the transition state, they cannot be formally classed as true transition state analog inhibitors, whose hybridization and charge must both resemble that of the transition state.[262]

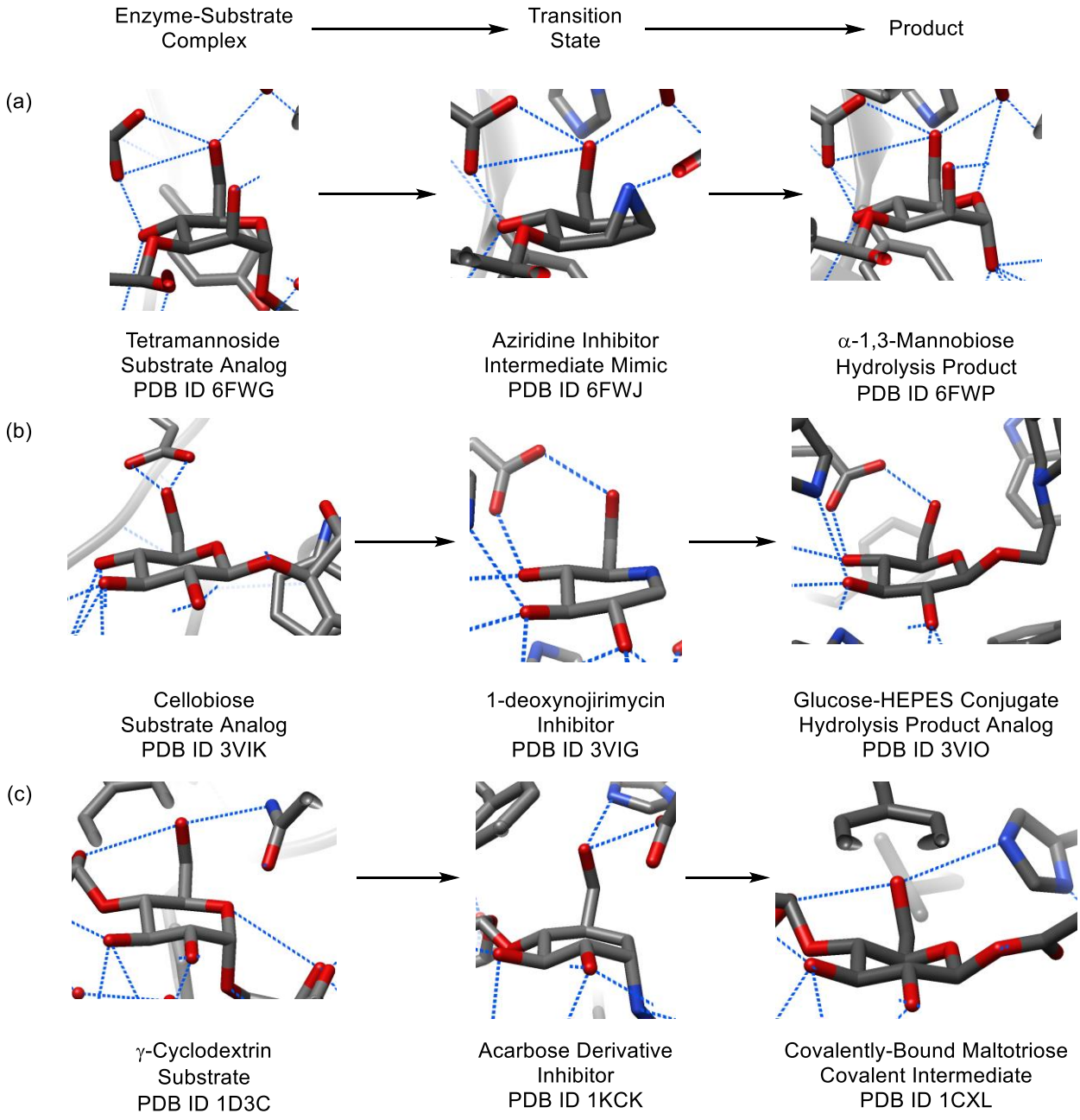

Figure 5.3. Reaction coordinates and partial X-ray crystal structures of (a) *Bacteroides xylanisolvens* GH99 endo-α-mannanase, (b) termite GH1 β-glucosidase, and (c) *Bacillus circulans* CGTase

Given the difficulty in mimicking the transition states of glycosyltransferases,[261, 302, 303] similar snapshot studies cannot be conducted to the same extent for GTs. While the transition states of some GTs have been computationally modeled, these calculations often neglect both side chain conformation and potential hydrogen bonding between the side chain and the active site. However, as evidenced by crystallographic studies carried out by the Vocadlo and Walker groups on human *O*-GlcNAc transferase,[304] preorganization of the side chain is supported given that the *gg* conformation is observed in both the enzyme-substrate complex and the product of glycosyl transfer (Figure 5.4).

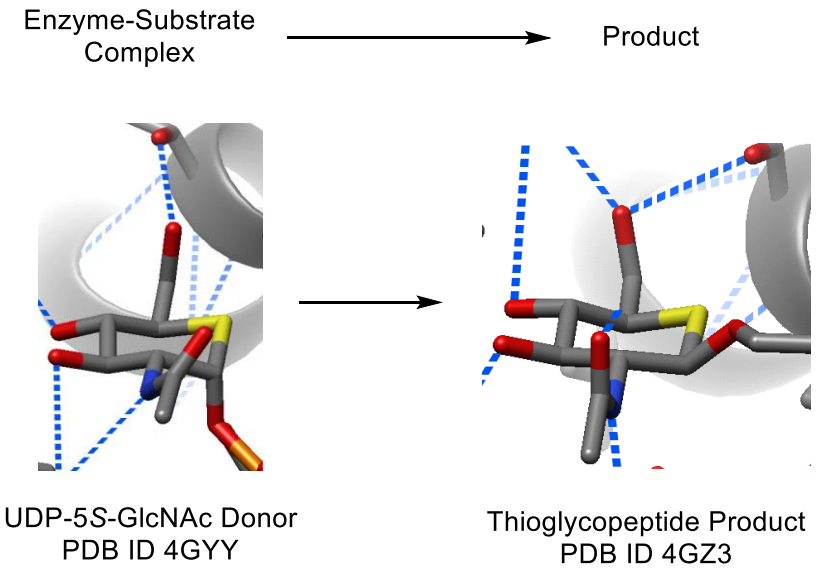

Figure 5.4. Partial crystal structures of starting material and product analogs for human *O*-GlcNAc transferase

Preorganization of the side chain at the level of the enzyme-substrate complex is in accordance with kinetic studies carried out by Namchuk and Withers on *Agrobacterium faecalis* β-glucosidase, which determined that while interactions at O3 and O4 predominantly influence the

transition state, H-bonds between O6 and the active site afford significant ground state stabilization in addition to transition state stabilization (Figure 5.5a).[305] Thus, by preorganizing the side chain into the most reactive *gg* conformation, the GTs, GHs, phosphorylases, and transglycosidases benefit from both ground state stabilization and reactivity enhancement through transition state stabilization. The above results are also consistent with proposals by Wolfenden that the rate enhancement afforded by enzymes is primarily enthalpic.[306] In their kinetic studies on cytidine deaminase,[307] Wolfenden and coworkers determined that the entropic contribution to activation energy is approximately 15-fold lower than the enthalpic contribution. Moreover, binding of the substrate to the enzyme active site results in a release of enthalpy that is close in magnitude to the activation energy and that strongly outweighs the reduction in entropy resulting from restraining the substrate (Figure 5.5b). Thus, the entropic penalty due to side chain preorganization by the GHs and GTs is strongly outweighed by the enthalpic stabilization provided to both the Michaelis complex and the transition state. This form of side chain restriction should not be confused with the frequently observed preorganization of reactive groups achieved by ground state destabilization.[257, 308-310] In the latter case, rather than stabilizing the ground state, the enzyme distorts the substrate into a higher energy ring conformation closer in structure to the transition state, thereby reducing the activation energy of the reaction.

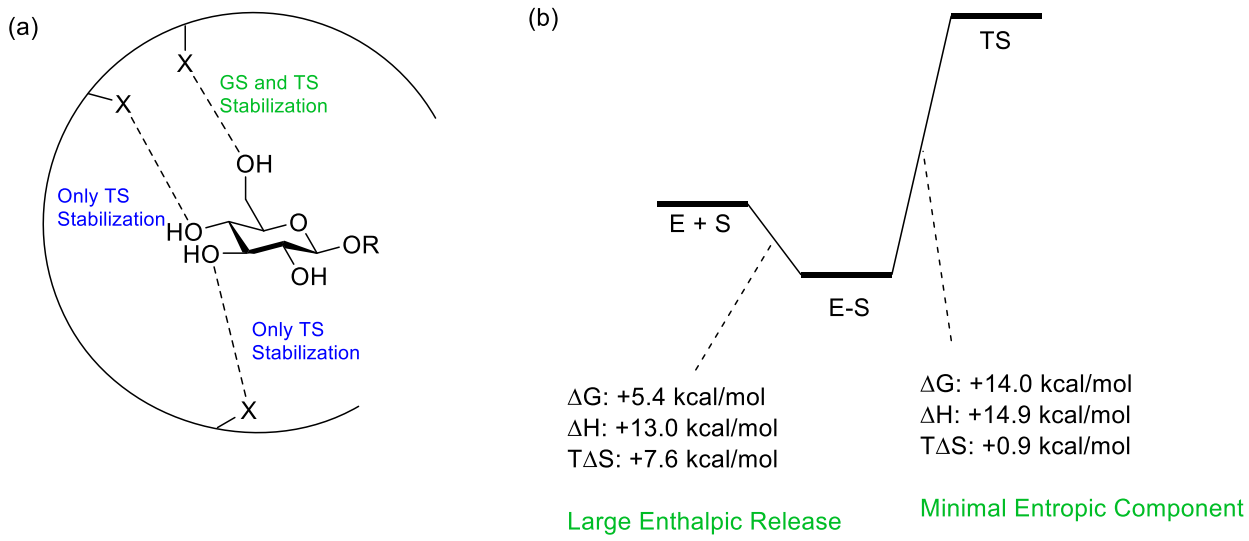

Figure 5.5. (a) Summary of stabilization offered by H-bonding between O3, O4, and O6 of a pyranoside and an enzyme active site (b) Energy profile of *Escherichia coli* cytidine deaminase outlining enthalpic and entropic contributions to substrate binding and to activation energy

Turning to the ulosonic acid processing enzymes, though the neuraminidases, sialyltransferases, and trans-sialidases all show extremely high selectivity for the *gg* conformation, their natural substrates, which are derivatives of neuraminic acid **130**, predominantly take up the *gg* conformation in solution.[223] Thus, it is unclear whether these enzymes have evolved to maximize transition state stabilization or whether they have evolved to simply bind the substrate in its ground state conformation. To this end, it is possible that these enzymes are analogous to lectins of higher order sugars, which are known to bind their ligands in their ground state conformations.[221, 295] Notably, while other ulosonic acids such as pseudaminic acid **131** and Kdo **132** take up the least reactive *tg* conformation in solution (Figure 5.6),[311, 312] there are no crystal structures of their hydrolases or transferases with bound ligands, meaning that the side chain conformation enforced on these substrates remains unknown. Interestingly, docking studies of CMP-Kdo bound to the Kdo GT domain of the WbbB protein predict binding of the ligand side

chain in the more reactive *gt* conformation rather than in the ground state *tg* conformation,[313] meaning that further study could potentially reveal similar side chain restriction by Kdo or pseudaminic acid processing enzymes to increase transition state stabilization.

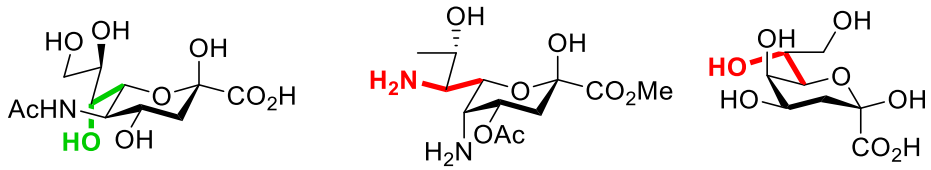

N-Acetylneuraminic Acid, 130 ***gg***

Pseudaminic Acid, 131 ***tg***

Kdo, 132 ***tg***

Figure 5.6. Ground state side chain conformations of several ulosonic acids

5.4. Galactoside Processing Enzymes

Table 5.2. Side chain restriction by galactoside processing enzymes

Enzyme Class	*gg*	*gt*	*tg*	Eclipsed[a]	Total	H-bonds to O6
α-Galactosidase	-	12	-	4	16	16
α-*N*-Acetyl Galactosaminidase	-	5	-	-	5	5
α-Galactosyltransferase	-	6	2	-	8	8
α-*N*-Acetyl Galactosaminyltransferase	1	2	5	-	8	8
β-Galactosidase	5	11	26	-	43	42
β-*N*-Acetyl Galactosaminidase	-	1	-	-	1	1
β-Galactosyltransferase	-	-	8	-	8	8
Total	6	37	41	4	89	88

[a]These structures of cyclohexene derivatives hold the side chain eclipsed with the C=C π-bond

The galactoside processing enzymes present a prominent set of exceptions to the trends established in Table 5.1. Table 5.2 shows that the α-galactosidases and α-galactosyltransferases

demonstrate a very strong preference for the second-most reactive *gt* conformation, which is expected given that the *gg* conformation is destabilized in free solution in the galactose series due to unfavorable interactions between the side chain C6-O6 bond and the axial C4-O4 bond. These values stand in sharp contrast with the 55% *gt* abundance observed in free solution. Interestingly, the four eclipsed structures found for the α-galactosidases when bound to cyclohexene derivatives are formally analogous to the *gt* conformation, given that the side chain is held trans to the C4-C5 bond (Figure 5.7). Despite the significant ensuing allylic strain, the α-galactosidases still place the side chain such that it eclipses the C-C π-bond, indicating that the preference for the *gt* conformation is strong.

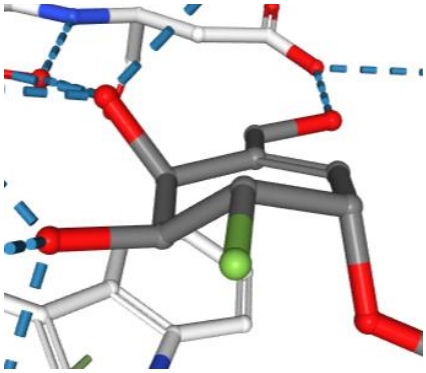

Figure 5.7. Eclipsing interactions of a cyclohexene-derived inhibitor bound to *Thermotoga maritima* α-galactosidase (PDB ID 6GWF)

Further details on side chain restriction by GTs are nicely illustrated in studies by Lowary and coworkers on human α-(1→3)-*N*-acetyl galactosaminyltransferase (GTA) and human α-(1→3)-galactosyltransferase (GTB).[314] Crystal structures of several UDP sugars in the active site show that in each case the donor binds in a stepwise fashion, wherein UDP is anchored on initial binding and the pyranoside is subsequently rotated until it is placed directly above the

pyrophosphate group; only in this conformation, denoted the "tucked under" conformation, will catalytic activity be observed (Figure 5.8).

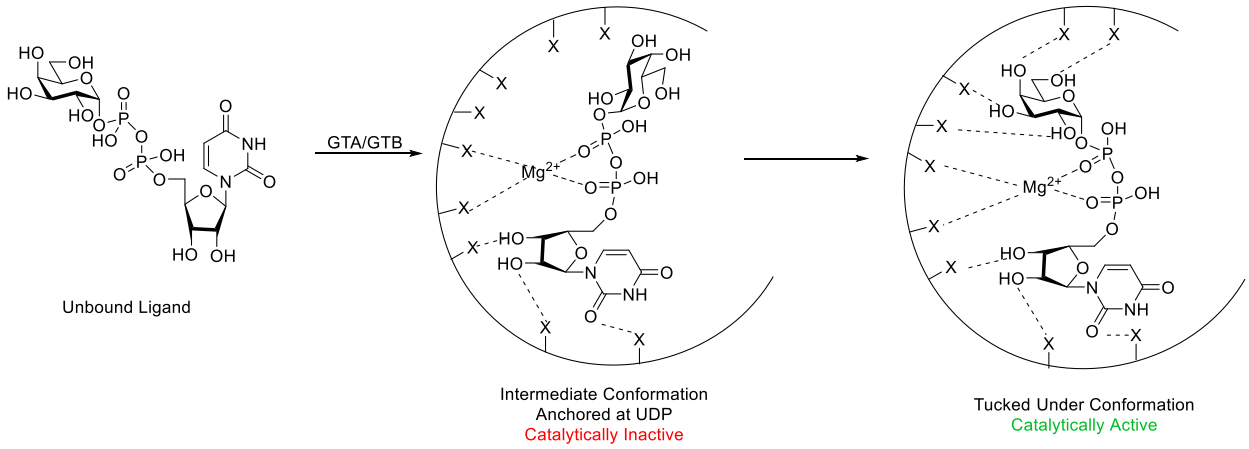

Figure 5.8. Outline of stepwise binding of UDP-galactose to human GTA/GTB

While crystal structures with the natural donor UDP-α-galactopyranose reveal that the side chain takes up the *gt* conformation throughout the binding process, H-bonding between the side chain and the enzyme is only observed in the catalytically active tucked under conformation. Likewise, in all crystal structures with bound UDP-α-*C*-galactopyranose, all of which exhibit the *gt* conformation, the pyranose ring is unable to take up the catalytically active tucked under conformation due to the differences between the bond angle of the *C*-glycoside and that of the natural donor, and consequently no H-bonding between the side chain and the enzyme is observed. Interestingly, while most crystal structures with bound UDP-α-glucopyranose show the sugar positioned in an alternate, catalytically inactive orientation in the active site bearing the *gg* conformation, one structure holds the sugar in the tucked under conformation and shows H-bonding mediated restriction of the side chain to the *gt* conformation (Figure 5.9). Thus, it is

apparent that GTA and GTB only restrict the side chain conformation when the substrate is primed for catalysis.

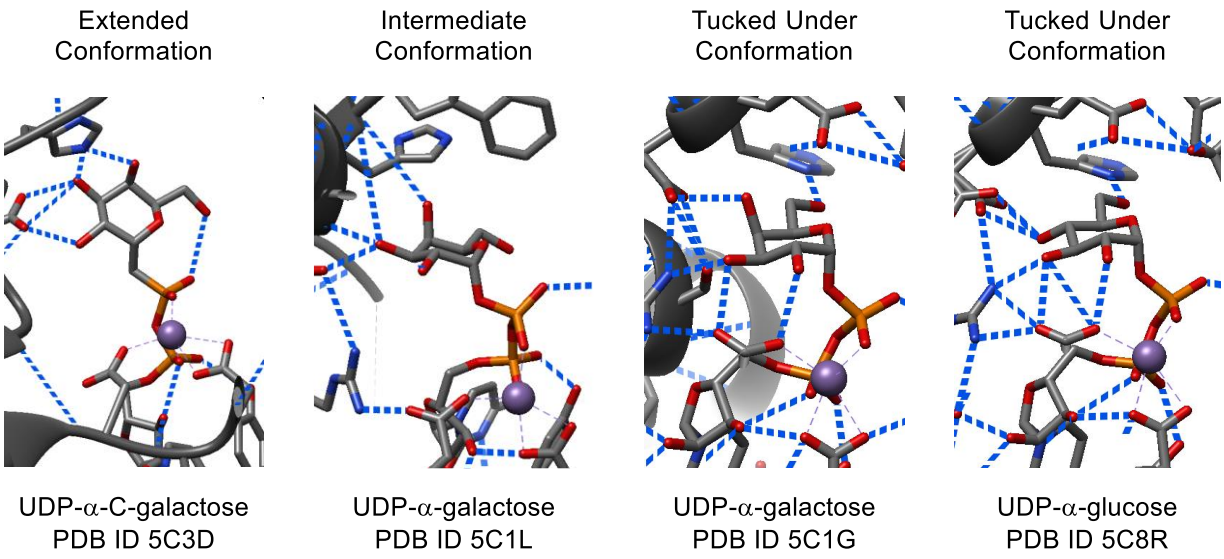

Figure 5.9. Partial crystal structures of human GTA/GTB with bound UDP-sugars in various conformations

Unlike the α-galactose series, β-galactoside processing enzymes show generally strong selectivity for binding their substrates in the least reactive *tg* conformation. Dividing the β-galactosidases into their corresponding families reveals that *gg*-selective members belong to families 16 and 45 and the *gt*-selective members belong to families 42, 59, and 98, while the majority of the structures, which favor the *tg* conformation, are members of families 2, 35, and 86. Likewise, all eight structures of β-galactosyltransferases belong to GT family 7. The difference in side chain restriction between the α- and β-galactosyltransferases is nicely illustrated by comparison of crystal structures with bound UDP-α-galactose **133** (Scheme 5.7). Though the evolutionary reason for enforcement of the *tg* conformation is yet unknown, it is certainly possible

that these β-galactoside processing enzymes have evolved to control reaction rate rather than maximize it given the high reactivity of galactosyl donors, consequently increasing substrate selectivity.

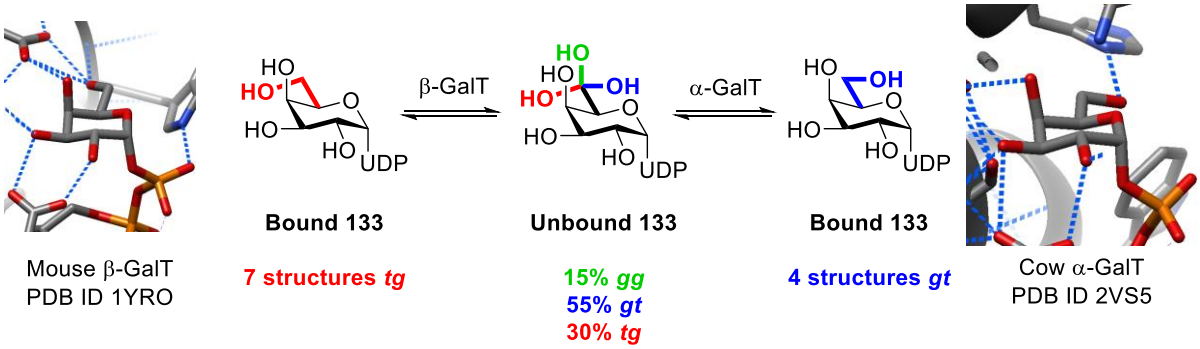

Scheme 5.7. Side chain restriction of **133** in α- and β-galactosyltransferases (GalTs)

5.5. α-Mannosidases

The differential selectivity of GH families 38 and 47 for the *gt* conformation, two exceptions to the well-established preference for the *gg* conformation illustrated above, inspired further examination of the α-mannosidases.[315] Among all 170+ known GH families, only the retaining GH38 and the inverting GHs 47 and 92 (the latter of which favors the *gg* conformation) bear a divalent metal cation chelating O2 and O3: Zn^{2+} in GH38 and Ca^{2+} in GHs 47 and 92. For the GH38 and 92 enzymes, this chelation stabilizes the distortion of the natural substrate to an $^{O}S_2$ skew boat closer in character to the $B_{2,5}$ transition state, as illustrated in their shared conformational itinerary in Scheme 5.8.[316, 317] In addition to this ground state destabilization, Zn^{2+} also acidifies all coordinated hydroxyl groups, as is consistent with previous reports of pKa reduction of coordinated water to 9 in free solution and to 6 in the active site of carboxypeptidases.[318, 319] The ensuing acidification of O2 and O3 reduces the electron withdrawing nature of these groups,

allowing for additional transition state stabilization. Likewise, coordination with the catalytic aspartate (Figure 5.10a) allows for more facile cleavage of the covalent intermediate, thereby aiding in hydrolysis.

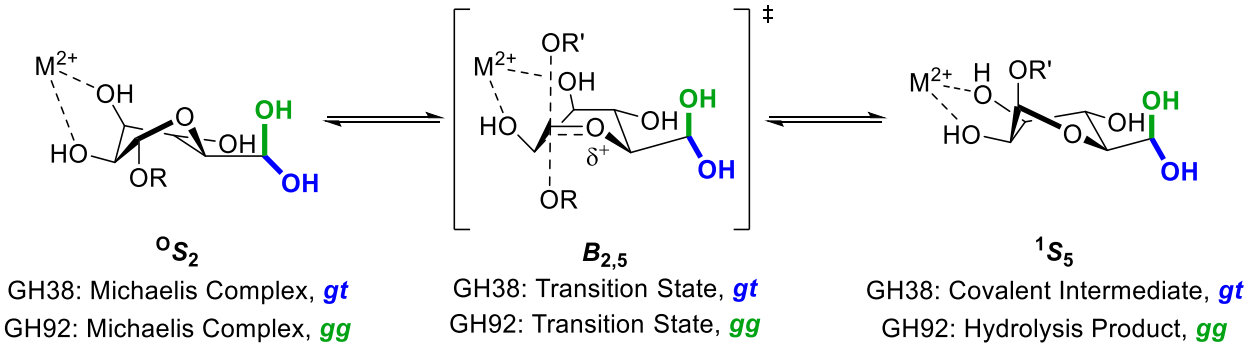

Scheme 5.8. Conformational itinerary of GH38 and GH92 mannosidases

Ca^{2+}, on the other hand, is less acidifying compared to Zn^{2+}, as evidenced by the lowered pKa reduction of coordinated water to 12.6, meaning that there is no significant transition state stabilization through acidification of O2 and O3 as is observed in the GH38 series.[320, 321] Instead, its primary roles lie in ligand binding, as has been observed in lectins, and in orientation of the nucleophilic water, thereby aiding hydrolysis.[322, 323] In *B. thetaiotaomicron* GH92 enzymes, Ca^{2+} also coordinates to the catalytic base (Figure 5.10b), which in accordance with studies carried out on GH97 glucosidases provides a slight increase in reactivity.[324] As such, enforcement of the *gg* conformation compensates for the lack of additional transition state stabilization afforded by Ca^{2+} in the GH92 series. GH47 enzymes, on the other hand, are held in the *gt* conformation and do not benefit from the slight activation of their catalytic residues by Ca^{2+}; indeed, analysis of the cation coordination sphere reveals that the metal coordinates only to O2 and O3 of the ligand and to a threonine residue that holds the cation in the active site (Figure 5.10c).

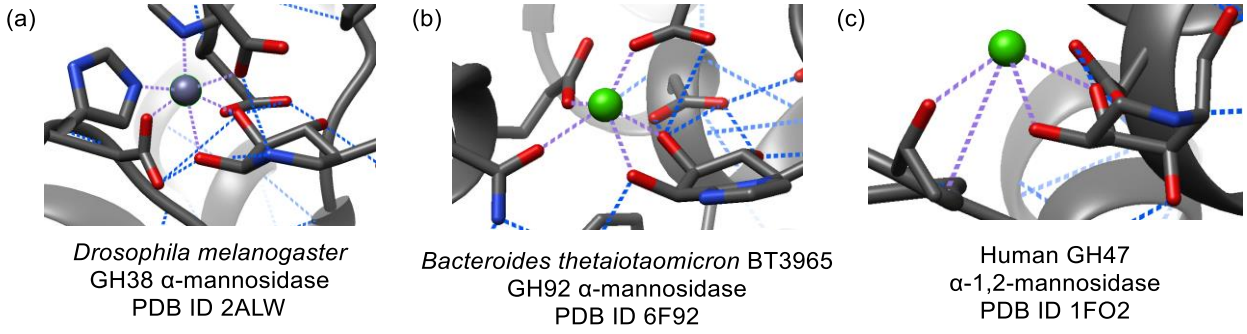

Figure 5.10. Coordination environments of (a) Zn^{2+} in *Drosophila melanogaster* GH38 α-mannosidase, (b) Ca^{2+} in *Bacteriodes thetaiotaomicron* BT3965 GH92 α-mannosidase, and (c) Ca^{2+} in human GH47 α-1,2-mannosidase

The conformational itinerary of GH47 mannosidases is distinct from that of the GH38/92 enzymes. Initially binding in a $^{3}S_{1}$ skew boat, the pyranoside distorts into a $^{3}H_{4}$ half chair transition state and is eventually released as a $^{1}C_{4}$ inverted chair as indicated in Scheme 5.9.[317] In each case, the majority of the substituents are held in (pseudo)axial positions as opposed to the (pseudo)equatorial orientations observed throughout the GH38 reaction coordinate. The difference in substituent orientation between GH38 and GH47 mannosidases is best appreciated through comparison of ligand binding in crystal structures of *Drosophila melanogaster* GH38 Golgi α-mannosidase and *Caulobacter sp.* K31 GH47 α-1,2-mannosidase, as shown in Figure 5.11.

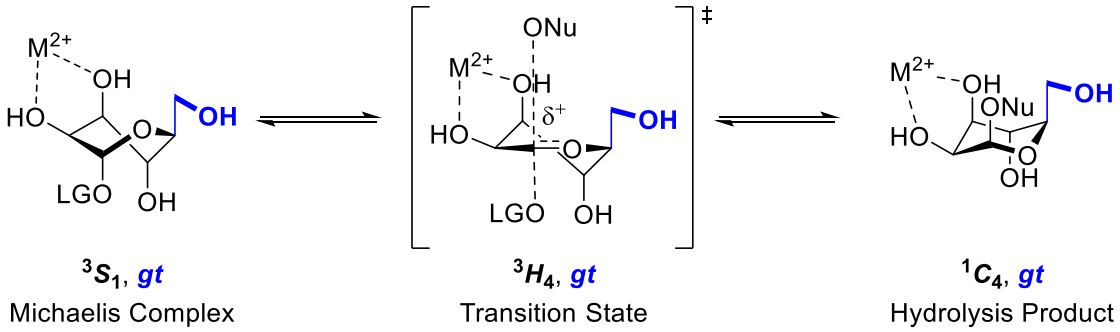

Scheme 5.9. Conformational itinerary of GH47 mannosidases

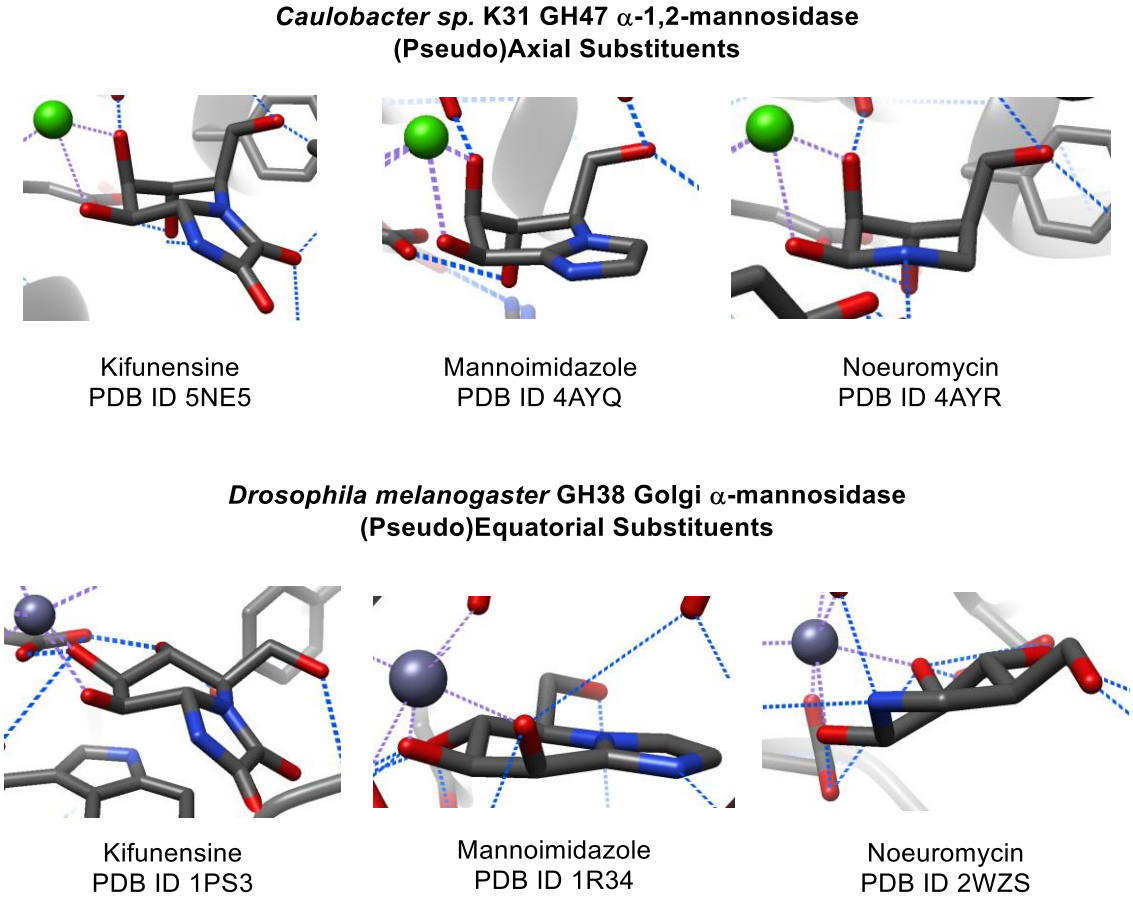

Figure 5.11. Contrasting binding preferences of *Caulobacter sp.* K31 GH47 α-1,2-mannosidase and *Drosophila melanogaster* GH38 Golgi α-mannosidase

Coinciding with the unusual conformational itinerary of the GH47 mannosidases is the naturally occurring inhibitor kifunensine **134**, whose structure in solution strongly favors the $^{1}C_{4}$ inverted chair over the standard $^{4}C_{1}$ chair (Scheme 5.10), as is clear from NMR coupling constant analysis.[325, 326] When in the inverted $^{1}C_{4}$ chair, the *gg* conformation is strongly destabilized, as the side chain would be placed directly above the plane of the ring. As such, the side chain distribution of kifunensine is roughly 3:1 *gt* to *tg* (as determined using equations 1-3 in Figure 5.2), thereby approaching the *gt* selectivity of the GH47 enzymes. Due to its unusual structure, kifunensine is both strongly selective for and highly active against the GH47 mannosidases, binding much more weakly to other mannosidase families; as observed in Figure 5.11, kifunensine is highly distorted from its ground state conformation when bound to GH38 mannosidases, for which it is a weak inhibitor.[327]

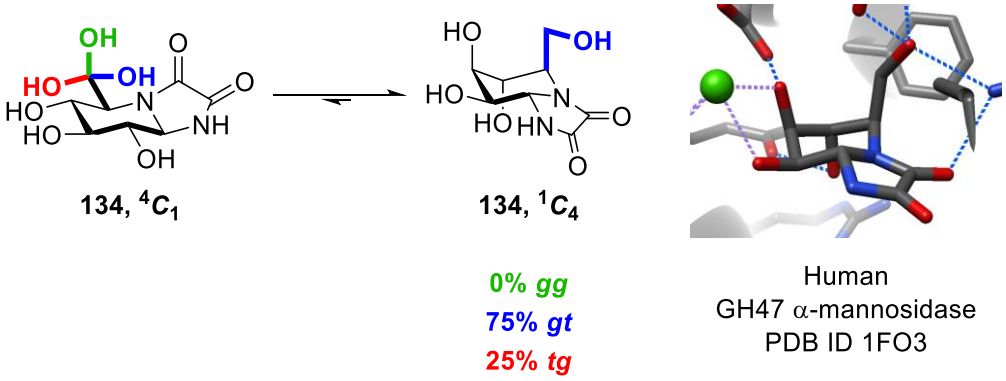

Scheme 5.10. Solution phase equilibrium of kifunensine **134**

Analysis of the GH47 active site reveals a key phenyl group (F659 in human ER α-mannosidase) that lies parallel and in close proximity to the C4-C5-C6 plane of the bound ligand (Figure 5.12). In addition to stabilization of the partial positive charge that develops at the transition state through CH-π interactions,[294] the aryl moiety forces the substrate to take up a

conformation bearing an axial or pseudoaxial C5-C6 bond, as the equatorial C5-C6 bond of a relaxed $^4C_1$ chair (or an analogous conformation) would sterically clash with the phenyl ring. Mutagenesis studies carried out by the Moremen group on human ER α-mannosidase reveal that the F659A mutation causes both a 60-fold reduction in binding affinity for kifunensine, whose binding to the wild type enzyme is near irreversible, and an over 140-fold reduction in k_{cat}/K_M compared to the wild type enzyme.[328] The reduced affinity for kifunensine indicates that the $^1C_4$ conformation taken up by the inhibitor in solution is likely no longer favored by the mutant enzyme; when the steric bulk of the phenyl ring of F659 is removed in the F659A mutant, there is no driving force for the C5-C6 bond to be held in a pseudoaxial position, meaning that the substrate is free to take up a more relaxed conformation such as the $^4C_1$ chair. The 140-fold drop in reactivity of the F659A mutant is also consistent with substrate binding in a more relaxed conformer such as the $^4C_1$ chair.

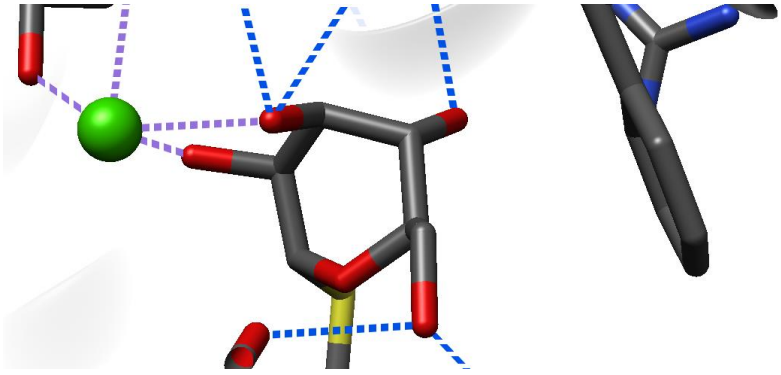

Figure 5.12. Partial crystal structure of human GH47 α-1,2-mannosidase bound to thiomannobiose, (PDB ID 1X9D) with F659 lying parallel to the C4-C5-C6 plane

When the C5-C6 bond is forced into a pseudoaxial position as is observed in the wild type enzyme, the C3-O3 and C4-O4 bonds also take up a pseudoaxial orientation, as observed in the GH47

conformational itinerary in Scheme 5.9. As the reaction progresses, these pseudoaxial C-O bonds strongly stabilize the positive charge that builds up at the anomeric center, thereby significantly increasing reactivity as discussed in Chapter 4 (Figure 5.13); in effect, the GH47 substrates are conformationally superarmed in an analogous fashion to the donors designed by Bols and coworkers.[230] With a more relaxed conformer such as the $^4C_1$ chair that is likely enabled by the F659A mutant, however, the equatorial (or pseudoequatorial) hydroxyl groups cannot offer the same degree of transition state stabilization, which would account for the observed sharp decrease in activity.

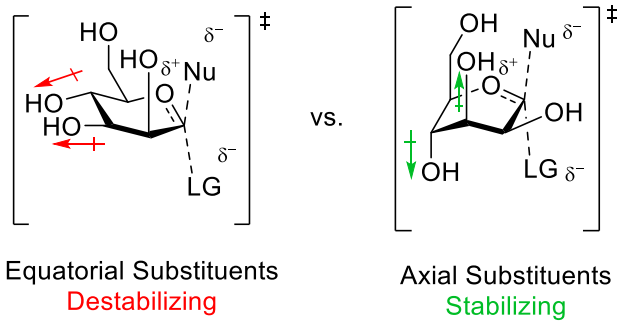

Figure 5.13. Stabilization of building positive charge at the anomeric center by axially-oriented substituents

5.6. Superarming in Other GH Families

GH6 cellulases exhibit a similar superarming effect to that observed in GH47. In analogy to the active site phenyl ring of the GH47 mannosidases, these cellulases bear a tyrosine ring in the active site whose phenolic hydroxyl group sterically prevents the substrate C6-C5 bond from taking up a standard equatorial position observed in the $^4C_1$ conformation. As a result, the wild type substrate binds in either an E_2 envelope or a ^2S_O skew boat, such that the substituents at C4 and C5 are held pseudoaxially. According to mutagenesis studies by Larsson and coworkers on

Thermobifida fusca Cel6A, the Y73F and Y73S mutations result in a 10-fold and 500-fold drop in activity respectively.[329] In the former case, the mutated amino acid still bears some steric bulk at the required position, accounting for the relatively small drop in activity. In the latter case, however, the mutated serine residue lacks the steric bulk needed to induce superarming, thereby strongly reducing activity. Crystallographic studies of the Y73S mutant bound to cellotetraose show that, unlike in the wild type enzyme, the substrate in the -1 site takes up the relaxed $^4C_1$ chair conformation (Figure 5.14). It should also be noted that the side chain in the wild type GH6 enzymes is held in the most reactive *gg* conformation, despite the destabilization afforded by placing the side chain directly above the pyranose ring.

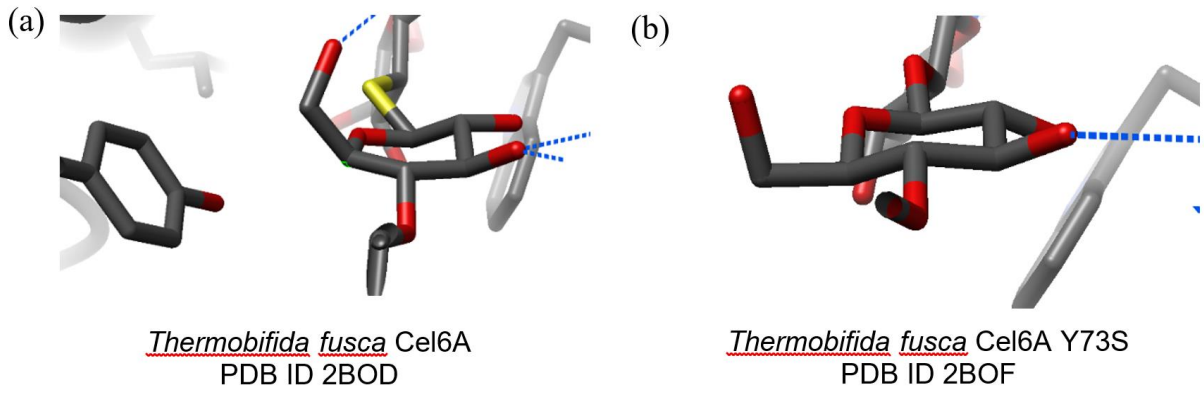

Figure 5.14. Partial crystal structures of (a) Wild type *Thermobifida fusca* Cel6A bound to thiocellotetraose and (b) Y73S *T. fusca* Cel6A bound to cellotetraose

Some families such as the GH134 β-mannosidases and the GH45 and 81 endoglucanases enforce a superarmed conformation across all members through H-bonding rather than through steric influence (Figure 5.15a-c). Of these families, GHs 134 and 45 both hold their side chains in the destabilized *gg* conformation, while the GH81 endoglucanases enforce the *gt* conformation among their substrates; the latter constitute a primary exception to the general preference for the

gg conformation among β-glucosidases. Other families contain only one or two members that enforce a superarmed conformation, as is the case with *Bacillus pumilus* GH48 endoglucanase (Figure 5.15d). Likewise, a crystal structure *Meretrix lusoria* GH22 lysozyme with an unsaturated inhibitor holds C4 and C5 in pseudoaxial positions (Figure 5.15e), meaning that there is potential superarming of the natural substrate (though further crystallographic studies with a standard pyranoside are required to confirm this hypothesis). Of note, while the unsaturated lactone is bound to the active site in a ^{5}E conformation as shown in Figure 5.15e, coupling constant analysis of the lactone in free solution reveals that the ring takes up the flipped E_5 conformation in solution,[330] indicating that the enzyme is actively distorting the inhibitor and thus potentially enforces superarming in its substrates.

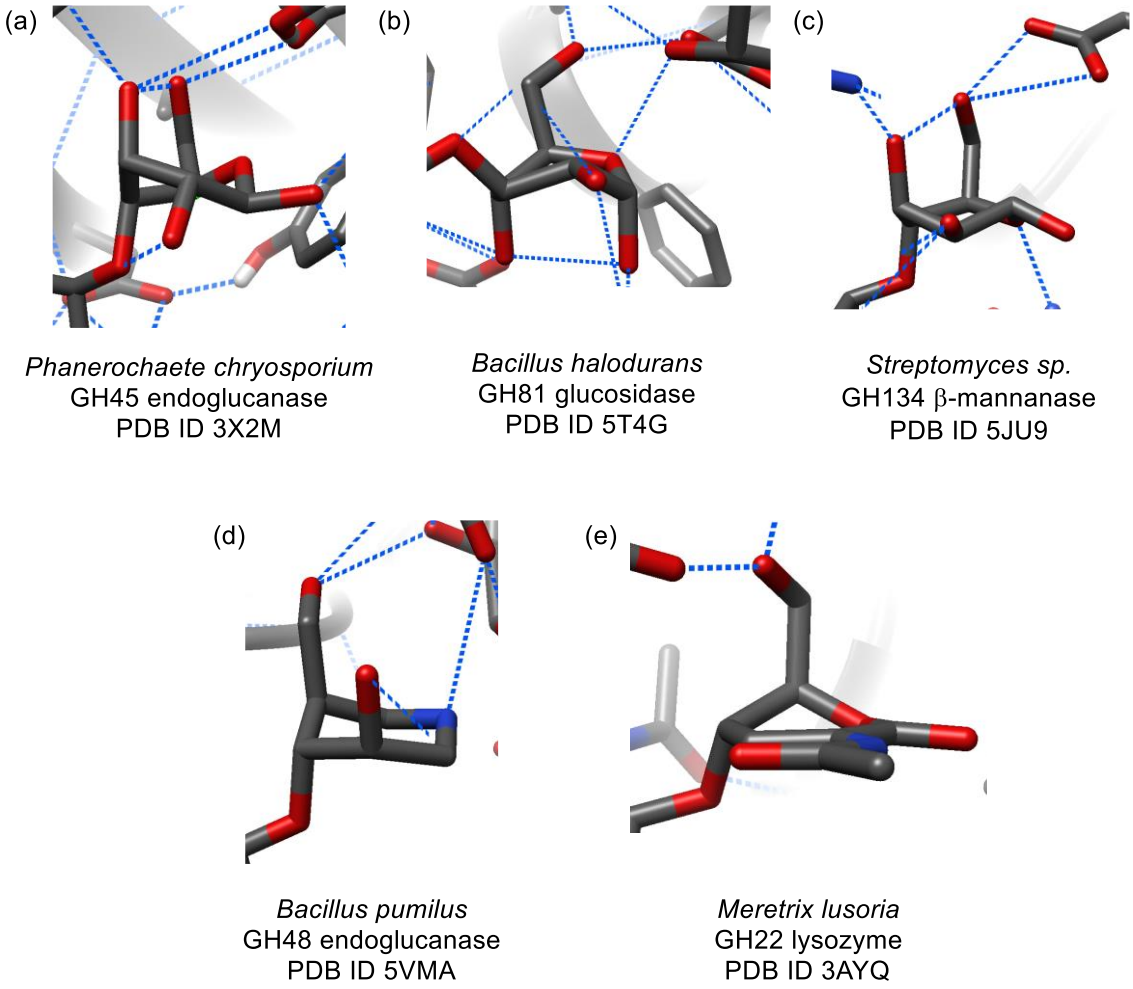

Figure 5.15. Partial crystal structures of (a) *Phanerochaete chryosporium* GH45 endoglucanase bound to cellopentaose, (b) *Bacillus halodurans* GH81 glucosidase bound to laminarin, (c) *Streptomyces sp.* GH134 β-mannanase bound to mannotriose, (d) *Bacillus pumilus* GH48 endoglucanase bound to cellobiose-derived isofagomine, and (e) *Meretrix lusoria* GH22 lysozyme bound to a tetrasaccharide inhibitor

5.7. Further Directions: Design of Conformationally Locked Inhibitors

With the above trends established, the intuitive next step is the design of inhibitors whose side chains are locked in the conformation matching the preference of the target enzyme to achieve greater binding affinity and/or selectivity. Kinetic studies on the *E. coli* heptosyltransferase WaaC

reveal that the natural substrate ADP-L-*glycero*-β-D-*manno*-heptose **135**, whose side chain is predicted to take up the *gg* conformation in solution, exhibits 10-fold greater activity than its isomer ADP-L-*glycero*-β-D-*manno*-heptose **136**, which is predicted to take up the *gt* side chain conformation in solution.[211, 331, 332] A crystal structure of *Escherichia coli* WaaC bound to the 2-deoxy-2-fluoro derivative of **136** shows that the side chain is indeed held in the *gg* conformation through H-bonding with Lys192 (Figure 5.16).[333] Notably, binding of the less active donor **136** to the active site of WaaC would result in steric clash of the hydroxymethyl substituent with the lysine above the plane of the ring if the *gt* conformation were enforced, while rotation of the C5-C6 bond to enforce of the *gg* conformation would result in destabilization both through the ensuing 1,5-*syn* relationship with the C4-O4 bond and through steric interaction with a nearby aspartate residue.

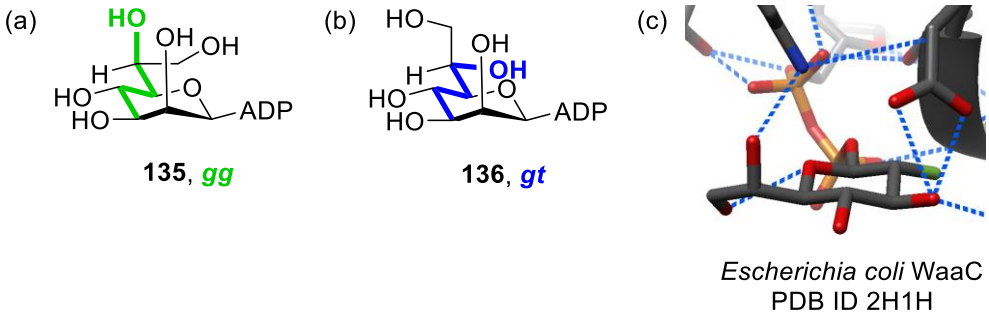

Figure 5.16. Free solution side chain conformations of (a) ADP-L-*glycero*-β-D-*manno*-heptose **135** and (b) ADP-L-*glycero*-β-D-*manno*-heptose **136** (c) Partial crystal structure of ADP-2-deoxy-2-fluoro-L-*glycero*-β-D-*manno*-heptose bound to *Escherichia coli* WaaC

Enzyme inhibition studies carried out by the Davies group on *Thermotoga maritima* GH1 β-glucosidase using the naturally occurring glycosidase inhibitors 1-deoxynojirimycin **137**, whose side chain is freely rotating, and castanospermine **138**, whose side chain is locked in the *gg*

conformation through an ethylene bridge, reveal that the latter exhibits fourfold greater binding affinity than the former (Figure 5.167).[334, 335] This increase in affinity can only be attributed to the conformationally restricted side chain. Thus, Nature has paved the way for the design of a next generation of conformationally locked inhibitors, whether through a bridging alkyl group as observed in **138** or through installation of a methyl or hydroxymethyl group at C6 as observed in **135**.

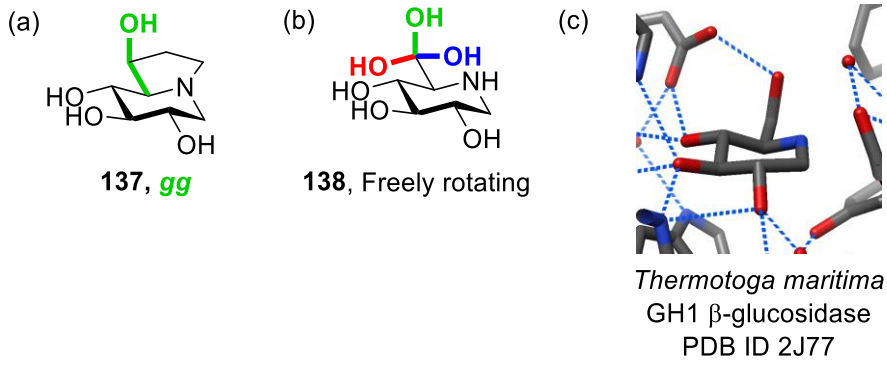

Figure 5.17. Free solution side chain conformations of (a) 1-deoxynojirimycin **137** and (b) castanospermine **138** (c) Partial crystal structure of *Thermotoga maritima* GH1 β-glucosidase with bound 1-deoxynojirimycin

5.8. Conclusions

The above analyses illustrate that the GHs, GTs, transglycosidases, and phosphorylases have evolved to take advantage of the reactivity-enhancing influence of side chain conformation in glycosylation and hydrolysis. Glucoside, β-mannoside, and ulosonic acid processing enzymes show strong selectivity for binding their substrates in the *gg* conformation, thereby increasing transition state stabilization. GHs and GTs acting on α-galactosides preferentially bind their substrates in the second-most reactive *gt* conformation, thereby avoiding the energetic penalty of

enforcing the *gg* conformation, while most β-galactoside processing enzymes favor the least reactive *tg* conformation. Examination of the α-mannosidases reveals that most families preferentially bind their substrates in the *gg* conformation while a handful of exceptions favor the *gt* conformation. Likewise, some GH families have evolved to increase reactivity through enforcement of the superarmed conformation of its substrates in certain GH families, whether through steric clashes such as in GHs 47 and 6 or through H-bonding as observed in GHs 134, 81, and 45. The information gleaned in this study should aid in the design of new and improved GH and GT inhibitors with conformationally locked side chains that match the preferences of the target enzyme and thus increase selectivity and/or affinity of the drug, and such studies are ongoing in the Crich laboratory.

CHAPTER 6

OVERALL CONCLUSIONS

Installation of a β-D-furanosyl ring onto O5 of apramycin afforded compounds with promising antibacterial activity and ribosomal selectivity while successfully overcoming susceptibility to AAC(3)-IV. Apralogs bearing a simple ribofuranosyl group at O5 exhibited comparable antibacterial activity to the parent and increased selectivity at the cost of heightened susceptibility to APH(3',5''). This susceptibility was avoided in the erythrosyl and 5-amino-5-deoxyribosyl apralogs, which exhibited greater activity than the parent against most of the ESKAPE pathogens. The most promising of the apralogs is 5-*O*-[5-amino-3-*O*-(2-aminoethyl)-5-deoxy-β-D-ribofuranosyl]apramycin **31**, which displayed a 2.5-fold reduction in ototoxicity compared to apramycin in cochlear explant studies and a twofold increase in antibacterial activity compared to the parent in in vivo efficacy studies. Moreover, compound **31** can be synthesized from the parent in only six linear steps, making it a prime candidate for large scale synthesis.

Though installation of a 5-deoxy-5-amino-β-D-ribofuranosyl group on apramycin resulted in significantly increased antibacterial activity, the analogous modification in neomycin, paromomycin, ribostamycin, and propylamycin proved to be significantly less promising, with general reduction in activity. Likewise, the 5''-deoxy, erythrosyl, and 5''-acetamido derivatives afforded reduced activity and/or selectivity for the above AGAs, though most modifications were better tolerated in neomycin due to the large number of basic amines. In contrast with the apralog series, installation of a 5''-formamido group onto neomycin, paromomycin, and propylamycin

afforded the most promising results, with significantly increased activity and significantly reduced toxicity with respect to the parent. The contrasting trends between the apralogs and the 4,5-AGAs are not yet fully understood and remain the subject of further investigation. Nevertheless, the knowledge gained from these studies should aid in the design of next-generation AGAs in the fight against antibiotic resistance.

Turning to the carbohydrate processing enzymes, GHs, GTs, transglycosidases, and phosphorylases have for the most part evolved to enhance reactivity of their substrates through side chain restriction. Glucoside, β-mannoside, and ulosonide processing enzymes predominantly bind their substrates in the most reactive *gg* conformation, which most strongly stabilizes the transition state. The α-galactoside processing enzymes restrict their substrate side chains to the second-most reactive *gt* conformation, which circumvents the unfavorable energetic penalty of imposing the *gg* conformation on galactose. The β-galactosidases and galactosyltransferases, on the other hand, selectively enforce the least reactive *tg* conformation on their substrates. Some families of GHs enhance reactivity by binding their substrates in a superarmed conformation where most substituents are held axially or pseudoaxially, thereby providing significant electrostatic stabilization to the transition state. This information will be useful in the design of next generation conformationally locked inhibitors, whose side chains are trapped in a conformation favored by the target enzyme and which are expected to exhibit greater activity and/or selectivity.

CHAPTER 7

EXPERIMENTAL SECTION

General experimental: All experiments were carried out under a dry argon atmosphere unless otherwise specified. All reagents and solvents were purchased from commercial suppliers and were used without further purification unless otherwise specified. Chromatographic purifications were carried over silica gel (230-400 mesh). Thin layer chromatography was performed with precoated glass backed plates (w/UV 254). TLC were visualized by UV irradiation (254 nm) and by charring with sulfuric acid in ethanol (20:80, v/v) or with ceric ammonium molybdate solution [$Ce(SO_4)_2$: 4 g, $(NH_4)_6Mo_7O_{24}$: 10 g, H_2SO_4: 40 mL, H_2O: 360 mL]. Optical rotations were measured at 589 nm and 21 ºC on a digital polarimeter with a path length of 10 cm. ^1H and ^{13}C NMR spectra of all compounds were recorded using 600 MHz instrument unless otherwise specified and assignments made with the help of COSY, HMBC, and HSQC spectra. ESIHRMS were recorded using a time-of-flight mass spectrometer fitted with an electrospray source.

1,3,2′,4′′-Tetraazido-6,2′′,3′′,6′′-tetra-*O*-benzoyl-6′,7′-oxazolidino-apramycin (35). To a stirred solution of **34** (500 mg, 0.75 mmol) in pyridine (4.4 mL, 52.3 mmol) at 0ºC was added benzoyl chloride (0.44 mL, 3.73 mmol) dropwise over 10 minutes. After 2h, the reaction was quenched with methanol, diluted with EtOAc, washed with 1N HCl, saturated aqueous $NaHCO_3$, and brine, and dried over Na_2SO_4. The organic layer was concentrated to dryness and the residue was purified via silica gel chromatography, eluting with 50% EtOAc in hexanes (*Rf* = 0.4) to give

35 as an off-white foam (691 mg, 85%). $[\alpha]_D^{23}$= +45.3 (c = 1.0, chloroform). ^{1}H NMR (600 MHz, Chloroform-*d*) δ 8.10 – 8.04 (m, 6H, Ar), 7.97 – 7.93 (m, 2H, Ar), 7.60 – 7.56 (m, 3H, Ar), 7.51 – 7.47 (m, 3H, Ar), 7.44 (td, *J* = 7.9, 2.5 Hz, 4H, Ar), 7.37 (t, *J* = 7.7 Hz, 2H, Ar), 5.92 (t, *J* = 10.1 Hz, 1H, H3’’), 5.69 (d, *J* = 3.7 Hz, 1H, H1’’), 5.22 (t, *J* = 9.9 Hz, 1H, H6), 5.14 (dd, *J* = 10.5, 3.6 Hz, 1H, H2’’), 5.04 (d, *J* = 3.5 Hz, 1H, H1’), 4.91 (d, *J* = 3.4 Hz, 1H, H8’), 4.81 (dd, *J* = 8.3, 3.3 Hz, 1H, H6’), 4.68 (dd, *J* = 12.3, 2.4 Hz, 1H, H6’’$_a$), 4.64 (dd, *J* = 12.2, 5.3 Hz, 1H, H6’’$_b$), 4.40 (dd, *J* = 10.5, 3.3 Hz, 1H, H5’), 4.07 (ddd, *J* = 10.6, 5.3, 2.5 Hz, 1H, H5’’), 3.92 (t, *J* = 10.1 Hz, 1H, H4’), 3.87 – 3.74 (m, 4H, H5, H7’, H1, H3), 3.63 (td, *J* = 11.0, 4.4 Hz, 1H, H4’), 3.47 (t, *J* = 9.4 Hz, 1H, H4), 3.38 (dt, *J* = 12.6, 4.1 Hz, 1H, H2’), 2.79 (s, 3H, NCH_3), 2.49 (dt, *J* = 13.2, 4.6 Hz, 1H, H3’$_{eq}$), 1.79 – 1.63 (m, 2H, H2$_{eq}$, H3’$_{ax}$), 1.37 (q, *J* = 11.8 Hz, 1H, H2$_{ax}$). ^{13}C NMR (151 MHz, Chloroform-*d*) δ 166.09, 165.97, 165.83, 156.98 (oxazolidinone), 133.98, 133.85, 133.66, 133.52, 133.47, 130.11, 129.92, 129.88, 129.73, 129.67, 129.39, 129.33, 128.82, 128.78, 128.69, 128.60, 128.52, 128.44, 98.85 (C1’), 97.56 (C8’), 96.08 (C1’’), 84.33 (C4), 75.43 (C6), 74.42 (C5), 71.78 (C2’’), 70.67 (C3’’), 70.09 (C6’), 69.52 (C5’’), 65.77 (C5’), 64.99 (C4’), 63.35 (C6’’), 60.89 (C4’’), 60.14 (C7’), 59.01 (C3), 58.57 (C1), 57.45 (C2’), 32.20 (C3’), 29.75 (NCH_3), 29.49 (C2). ESI-HRMS: m/z calcd for $C_{50}H_{47}N_{13}O_{16}Na$ $[M+Na]^+$ 1108.3161, found 1108.3125.

3-*O*-Allyl-1,2-di-*O*-isopropylidine-β-D-erythrose (37). To a stirred solution of **36** (850 mg, 5.3 mmol) at 0ºC in DMF (12 mL) was added NaH (335 mg, 8.3 mmol). After 5 min of stirring, the reaction mixture was warmed to rt, the flask was covered in aluminum foil, and allyl iodide (0.68 mL, 8.3 mmol) was added. After 1 h, the reaction was quenched with saturated aqueous NH_4Cl, diluted with EtOAc, and washed with saturated aqueous NH_4Cl and brine. The organic layer was concentrated to dryness after drying over Na_2SO_4 and purified via silica gel chromatography, eluting with 20% EtOAc in hexanes (*Rf* = 0.4) to give **37** as a colorless oil (774

mg, 70%). $[\alpha]_D^{23}$ = +40.2 (c = 0.46, chloroform). ^{1}H NMR (400 MHz, $CDCl_3$) δ 5.94 (ddt, *J* = 16.8, 10.5, 6.0 Hz, 1H, $H_2CC\mathit{H}$), 5.75 (d, *J* = 3.6 Hz, 1H, H1), 5.36 – 5.20 (m, 2H, H_2CCH), 4.58 (t, *J* = 3.9 Hz, 1H, H2), 4.20 – 4.13 (m, 1H, OCH_2), 4.11 – 4.04 (m, 1H, OCH_2), 4.00 – 3.94 (m, 1H, $H4_a$), 3.90 (ddd, *J* = 10.3, 6.2, 4.1 Hz, 1H, H3), 3.81 (dd, *J* = 9.4, 7.1 Hz, 1H, $H4_b$), 1.58 (s, 3H, CH_3), 1.35 (s, 3H, CH_3). ^{13}C NMR (101 MHz, $CDCl_3$) δ 134.43 ($H_2C\mathit{C}H$), 118.21 ($\mathit{C}(CH_3)_2$), 113.06 ($H_2\mathit{C}CH$), 104.97 (C1), 77.62 (C2), 77.44 (C3), 71.87 (CH_2O), 67.15 (C4), 26.64 (CH_3), 26.43 (CH_3). ESI-HRMS: m/z calcd for $C_{10}H_{16}O_4Na$ $[M+Na]^+$ 223.0946, found 223.0950.

3-*O*-Allyl-1,2-di-*O*-acetyl-D-erythrose (38). To a stirred solution of **37** (322 mg, 1.61 mmol) with a reflux condenser was added 80% aqueous acetic acid (10 mL) and the reaction mixture was heated to 80ºC. After 2h, the reaction was cooled down and the solvent was evaporated. The crude product was coevaporated with pyridine twice, purged with Ar, and dissolved in anhydrous DCM (16 mL). Pyridine (0.78 mL, 9.67 mmol), acetic anhydride (0.46 mL, 4.84 mmol), and DMAP (41.2 mg, 0.34 mmol) were added. After 2h, the reaction was quenched with MeOH, diluted with EtOAc, washed with 1N HCl, saturated aqueous $NaHCO_3$, and brine, and dried over Na_2SO_4. The organic layer was concentrated to dryness and the residue was purified via silica gel chromatography, eluting with 20% EtOAc in hexanes (*Rf* = 0.35) to give a mixture of anomers **38α** and **38β** (164.1 mg, 42% over 2 steps). α anomer: $[\alpha]_D^{23}$ = -84.3 (c = 1.0, chloroform). ^{1}H NMR (600 MHz, $CDCl_3$) δ 6.31 (d, *J* = 4.7 Hz, 1H, H1), 5.85 (ddt, *J* = 17.1, 10.2, 5.6 Hz, 1H, $H_2CC\mathit{H}$), 5.27 (dq, *J* = 17.2, 1.6 Hz, 1H, H_2CCH), 5.19 (dq, *J* = 10.4, 1.4 Hz, 1H, H_2CCH), 5.05 (dd, *J* = 6.2, 4.7 Hz, 1H, H2), 4.18 (td, *J* = 6.0, 4.0 Hz, 1H, H3), 4.14 (dd, *J* = 9.5, 5.9 Hz, 1H, $H4_a$), 4.10 – 3.97 (m, 3H, H4b, $OC\mathit{H}_2$), 2.13 (s, 3H, H_3CCO), 2.11 (s, 3H, H_3CCO). ^{13}C NMR (151 MHz, $CDCl_3$) δ 170.10 ($H_3C\mathit{C}O$), 170.05 ($H_3C\mathit{C}O$), 134.19 ($H_2C\mathit{C}H$), 117.57 ($H_2\mathit{C}CH$), 93.94 (C1), 73.70 (C3), 72.13 (C4), 71.95 (OCH_2), 71.45 (C2), 21.16 ($H_3\mathit{C}CO$), 20.58

(H_3CCO). ESI-HRMS: m/z calcd for $C_{11}H_{16}O_6Na$ $[M+Na]^+$ 267.0845, found 267.0844. β anomer: $[\alpha]_D^{23}$= +30.3 (c = 1.0, chloroform). ^{1}H NMR (600 MHz, Chloroform-*d*) δ 6.16 (d, *J* = 1.1 Hz, 1H, H1), 5.84 (ddt, *J* = 17.2, 10.4, 5.6 Hz, 1H, H_2CCH), 5.27 (dq, *J* = 17.3, 1.7 Hz, 1H, H_2CCH), 5.21 – 5.17 (m, 2H, H_2CCH, H2), 4.33 (td, *J* = 6.4, 4.7 Hz, 1H, H3), 4.19 (dd, *J* = 9.1, 6.6 Hz, 1H, $H4_a$), 4.03 (ddt, *J* = 12.7, 5.5, 1.5 Hz, 1H, OCH_2), 3.98 (ddt, *J* = 12.6, 5.8, 1.4 Hz, 1H, OCH_2), 3.90 (dd, *J* = 9.1, 6.2 Hz, 1H, $H4_b$), 2.13 (s, 3H, H_3CCO), 2.06 (s, 3H, H_3CCO). ^{13}C NMR (151 MHz, Chloroform-*d*) δ 169.94 (H_3CCO), 169.36 (H_3CCO), 133.88 (H_2CCH), 117.66 (H_2CCH), 99.35 (C1), 75.82 (C3), 74.38 (C2), 71.83 (OCH_2), 70.63 (C4), 21.04 (H_3CCO), 20.67 (H_3CCO). ESI-HRMS: m/z calcd for $C_{11}H_{16}O_6Na$ $[M+Na]^+$ 267.0845, found 267.0853.

5-*O*-[(2′′′-*O*-Acetyl-3′′′-*O*-allyl)-*β*-D-erythrofuranosyl]-1,3,2′,4′′-tetraazido-6,2′′,3′′,6′′-tetra-*O*-benzoyl-1,3,2′,4′′-tetra(desamino)-6′,7′-oxazolidino-apramycin (39): To a stirred solution of **37** (222 mg, 0.91 mmol) and **35** (508 mg, 0.47 mmol) in anhydrous dichloromethane (9 mL) at 0 °C with oven-dried 4Å molecular sieves was added $BF_3{\cdot}OEt_2$ (0.34 mL, 2.73 mmol). After 2 h, the reaction was quenched with excess triethylamine and left to stir at 0 °C for 20 mins. The crude product was then diluted with ethyl acetate, washed with saturated aqueous sodium bicarbonate and brine, and dried over Na_2SO_4. The organic layer was concentrated to dryness and the product was dissolved in anhydrous acetonitrile (4.6 mL). Hexamethyldisilazane (0.3 mL, 1.37 mmol) and TMSOTf (2 drops) were added to protect any unreacted **33**, and after 1 h the reaction was concentrated to dryness. The residue was purified via silica gel chromatography, eluting with a gradient of 6-10% ethyl acetate in dichloromethane (R_f = 0.3 in 2% methanol in dichloromethane) to give **39** as a white solid (205 mg, 34 %). $[\alpha]_D^{21}$= +104.3 (*c* = 1.0, $CHCl_3$). ^{1}H NMR (600 MHz, $CDCl_3$) δ 8.11 – 8.05 (m, 4H, Ar), 8.03 – 8.00 (m, 2H, Ar), 7.98 – 7.95 (m, 2H, Ar), 7.60 (dt, J = 13.4, 7.5 Hz, 2H, Ar), 7.51 (tq, *J* = 23.8, 7.7 Hz,

6H, Ar), 7.41 (dt, *J* = 10.0, 7.8 Hz, 4H, Ar), 6.00 (t, *J* = 10.1 Hz, 1H, H3″), 5.69 (d, *J* = 3.8 Hz, 1H, H1″), 5.64 (ddt, *J* = 16.2, 10.7, 5.9 Hz, 1H, $H_2CC\mathit{H}$), 5.43 (d, *J* = 3.7 Hz, 1H, H1′), 5.30 (d, *J* = 1.6 Hz, 1H, H1‴), 5.19 (t, *J* = 9.9 Hz, 1H, H6), 5.14 (dd, *J* = 10.4, 3.7 Hz, 1H, H2″), 5.10 – 5.04 (m, 2H, H_2CCH), 4.82 (dd, *J* = 4.6, 1.5 Hz, 1H, H2‴), 4.76 (d, *J* = 5.7 Hz, 1H, H8′), 4.71 (dd, *J* = 6.9, 3.6 Hz, 1H, H6′), 4.66 (dd, *J* = 12.2, 2.4 Hz, 1H, H6″a), 4.61 (dd, *J* = 12.1, 5.3 Hz, 1H, H6″b), 4.13 (dd, *J* = 10.3, 3.7 Hz, 1H, H5′), 4.11 – 4.03 (m, 2H, H5′, H4‴a), 4.01 (td, *J* = 6.2, 4.6 Hz, 1H, H3‴), 3.91 (t, *J* = 9.3 Hz, 1H, H5), 3.87 (t, *J* = 10.1 Hz, 1H, H4″), 3.74 – 3.66 (m, 5H, H7′, H4‴a, H4, OCH_2), 3.55 (ddd, *J* = 12.5, 10.3, 5.2 Hz, 1H, H1), 3.45 (td, *J* = 10.9, 4.5 Hz, 1H, H4′), 3.37 (ddd, *J* = 12.1, 9.9, 4.8 Hz, 1H, H3), 2.94 (s, 3H, NCH_3), 2.89 (dt, *J* = 13.1, 4.0 Hz, 1H, H2′), 2.43 (dt, *J* = 13.2, 4.6 Hz, 1H, H3′eq), 1.76 – 1.60 (m, 2H, H2eq, H3′eqx), 1.57 (s, 3H, H_3CCO) 1.30 (q, *J* = 11.9 Hz, 1H, H2ax). ^{13}C NMR (150 MHz, $CDCl_3$) δ 169.3, 166.1, 165.9, 165.6, 164.8 (C=O), 156.9 (NC=O), 133.8 ($H_2C\mathit{C}H$), 133.7, 133.64, 133.60, 130.1, 130.0, 129.8, 129.7, 129.3, 128.9, 128.8, 128.68, 128.67, 128.62, 128.5, 128.4, 117.2 ($H_2\mathit{C}CH$), 107.1 (C1‴), 100.7 (C8′), 97.0 (C1′), 95.6 (C1″), 79.9 (C5), 76.3 (C4), 75.9 (C3‴), 75.5 (C6), 74.9 (C2‴), 71.8 (C6′), 71.5 (OCH_2), 71.2 (C2″), 70.4 (C3″), 70.2 (C4‴), 69.9 (C5″), 66.5 (C5′), 65.9 (C4′), 63.3 (C6″), 60.9 (C4″), 60.2 (C7′), 59.1 (C3), 58.1 (C1), 55.5 (C2′), 31.6 (C3′), 30.3 (NCH_3), 28.1 (C2), 19.9 ($H_3\mathit{C}CO$). ESI-HRMS: m/z calcd for $C_{59}H_{59}N_{13}O_{20}Na$ $[M+Na]^+$ 1292.3849, found 1292.3897.

5-*O*-[(2‴-Acetyl-3‴-*O*-ethylformyl)-*β*-D-erythrofuranosyl]-1,3,2′,4″-tetraazido-6,2″,3″,6″-tetra-*O*-benzoyl-1,3,2′,4″-tetra(desamino)-6′,7′-oxazolidino-apramycin (40): To a stirred solution of **39** (193.4 mg, 0.152 mmol) in acetone/water/*t*-butanol (3:1:1, 5 mL) was added NMO (28 mg, 0.24 mmol) and OsO_4 (2.5% in *t*-butanol, 5 drops). After 22 h, the reaction was quenched with sat. $NaHSO_3$, diluted with ethyl acetate, washed with saturated $NaHSO_3$ and brine, and dried over Na_2SO_4. The organic layer was concentrated to dryness to give an off white mixture

of diastereomers (192 mg, 0.147 mmol). A portion of the solid (64 mg, 0.049 mmol) was dissolved in dichloromethane (1.5 mL) and $NaIO_4$ (20% on silica gel, 261 mg, 0.244 mmol) was added. After 2 h the reaction was filtered through Celite® to generate **40** as a white solid (63 mg, 97% over two steps, R_f = 0.3 in 2% methanol in dichloromethane). $[\alpha]_D^{21}$ = +78.7 (*c* = 0.71, chloroform). ^{1}H NMR (500 MHz, $CDCl_3$) δ 9.38 (s, 1H, HCO), 8.08 (td, *J* = 8.4, 1.4 Hz, 4H, Ar), 8.04 – 8.01 (m, 2H, Ar), 7.98 – 7.96 (m, 2H, Ar), 7.64 – 7.60 (m, 2H, Ar), 7.58 – 7.46 (m, 7H, Ar), 7.41 (q, *J* = 8.1 Hz, 4H, Ar), 6.00 (t, *J* = 10.1 Hz, 1H, H3″), 5.70 (d, *J* = 3.7 Hz, 1H, H1″), 5.41 (d, *J* = 3.6 Hz, 1H, H1′), 5.33 (d, *J* = 1.6 Hz, 1H, H1‴), 5.20 (t, *J* = 9.9 Hz, 1H, H6), 5.15 (dd, *J* = 10.4, 3.7 Hz, 1H, H2″), 4.80 (dd, *J* = 4.4, 1.6 Hz, 1H, H2‴), 4.77 (d, *J* = 5.8 Hz, 1H, H8′), 4.72 (dd, *J* = 6.8, 3.6 Hz, 1H, H6″), 4.67 (dd, *J* = 12.2, 2.5 Hz, 1H, H6″a), 4.62 (dd, *J* = 12.2, 5.3 Hz, 1H, H6″b), 4.18 – 4.11 (m, 2H, H4‴a, H5′), 4.08 (ddd, *J* = 10.4, 5.3, 2.4 Hz, 1H, H5″), 4.03 (td, *J* = 6.3, 4.5 Hz, 1H, H3‴), 3.94 – 3.85 (m, 2H, H5, H4″), 3.84 (d, *J* = 2.8 Hz, 2H, OCH_2), 3.79 (dd, *J* = 9.4, 6.0 Hz, 1H, H4‴b), 3.76 – 3.67 (m, 2H, H7′, H4), 3.57 (ddd, *J* = 12.4, 10.3, 4.5 Hz, 1H, H1), 3.46 (td, *J* = 10.8, 4.4 Hz, 1H, H4′), 3.39 (ddd, *J* = 12.3, 9.8, 4.7 Hz, 1H, H3), 2.94 (m, 4H, NCH_3, H2′), 2.44 (dt, *J* = 13.2, 4.6 Hz, 1H, H3′eq), 1.77 – 1.63 (m, 2H, H2eq, H3′eqx), 1.60 (s, 3H, CH_3CO), 1.30 (q, *J* = 11.8 Hz, 1H, H2ax). ^{13}C NMR (125 MHz, $CDCl_3$) δ 198.6 (CHO), 169.7 (CH_3CO), 166.3, 166.1, 165.8, 164.9, 157.1 (oxazolidinone), 134.0, 133.9, 133.8, 130.23, 130.17, 129.9, 129.8, 129.4, 129.1, 128.9, 128.89, 128.86, 128.82, 128.7, 128.6, 106.99 (C1‴), 100.9 (C8′), 97.2 (C1′), 95.8 (C1″), 80.2 (C5), 77.8 (C3‴), 76.5 (C4), 76.0 (OCH_2), 75.7 (C6), 74.9 (C2‴), 71.9 (C6′), 71.4 (C2″), 70.6 (C3″), 70.07 (C4‴), 70.05 (C5″), 66.7 (C5′), 66.1 (C4′), 63.5 (C6″), 61.1 (C4″), 60.4 (C7′), 59.3 (C3), 58.2 (C1), 55.6 (C2′), 31.8 (C3′), 30.5 (NCH_3), 28.3 (C2), 20.1 (H_3CCO). ESI-HRMS: m/z calcd for $C_{59}H_{61}N_{13}O_{22}Na$ $[M+methanol+Na]^+$ 1326.3952, found 1326.3975.

5-*O*-[(3‴-*O*-2-Aminoethyl)-*β*-D-erythrofuranosyl]-apramycin hexaacetate salt (22): To a stirred solution of **40** (130 mg, 0.102 mmol) in anhydrous dichloromethane/methanol (4:1, 1 mL) at 0 °C was added benzylamine (0.08 mL, 0.71 mmol) and glacial acetic acid (2 drops). After 1.5 h, the reaction was warmed to room temperature and $NaBH_3CN$ (49 mg, 0.76 mmol) was added. Anhydrous methanol (1 mL) was added over the course of the reaction to dissolve solid that was forming. After 20 h, the reaction was diluted in ethyl acetate, washed with brine, and dried over Na_2SO_4. The organic layer was concentrated to dryness and the crude residue was passed through silica gel, eluting with a gradient of 1-5% ammoniacal methanol in dichloromethane. The product was then dissolved in dioxane/1N NaOH (1:1, 6 mL) and stirred at 80 °C. After 3 h, the reaction neutralized with glacial acetic acid and concentrated to dryness, and the resulting residue was passed through silica gel, eluting with a gradient of 10-12% ammoniacal methanol in dichloromethane to give an off-white solid (43.6 mg). A portion of the resulting residue (14.7 mg) was taken up in dioxane/deionized water (1:1, 0.6 mL) and $Pd(OH)_2$ on carbon (29.8 mg) was added. After stirring at 50 psi under H_2 for 4 h, the reaction was filtered through Celite® and the solution was concentrated to dryness. The crude product was passed through a CM Sephadex C25 column, loading in 10% aqueous acetic acid and eluting with a gradient of 0.2-1.2% ammonium hydroxide in deionized water. The product-containing fractions were lyophilized in vacuo with glacial acetic acid to generate the peracetate salt of **22** (6.4 mg, 18% over 4 steps). $[\alpha]_D^{21}$= +58.0 (*c* = 0.75, water). ^{1}H NMR (600 MHz, D_2O) δ 5.57 (d, *J* = 4.0 Hz, 1H, H1′), 5.32 (d, *J* = 4.0 Hz, 1H, H1″), 5.24 (d, *J* = 3.7 Hz, 1H, H1‴), 5.03 (d, *J* = 8.5 Hz, 1H, H8′), 4.40 (t, *J* = 2.8 Hz, 1H, H6′), 4.17 (dd, *J* = 5.3, 3.0 Hz, 1H, H2‴), 4.13 – 4.05 (m, 2H, H4‴a, H3‴), 3.83 – 3.59 (m, 10H, H4‴b, H4′, H5″, H3″, H6″a, H4, H5, OC*H*$_2$CH$_2$NH$_2$, H6″b), 3.57 (dd, *J* = 10.0, 2.6 Hz, 1H, H5′), 3.55 – 3.45 (m, 3H, H2″, H2′, H6), 3.19 – 3.16 (m, 1H, H7′), δ 3.12 (ddd, *J* = 12.5, 10.4, 4.3 Hz,

2H, H3, H1), 3.09 – 3.01 (m, 3H, $OCH_2CH_2NH_2$, H4″), 2.60 (s, 3H, NCH_3), 2.20 (ddt, *J* = 20.0, 12.7, 4.4 Hz, 2H, H3′eq, H2eq), 1.90 – 1.81 (m, 1H, H3′eqx), 1.53 (q, *J* = 12.6 Hz, 1H, H2ax). ^{13}C NMR (150 MHz, D_2O) δ 110.2 (C1‴), 94.5 (C1′), 94.4 (C1″), 92.97 (C8′), 84.6 (C5), 78.1 (C4), 77.6 (C3‴), 74.4 (C2‴), 72.9 (C6), 70.24 (C2″), 70.16 (C5″), 69.6 (C5′), 69.1 (C4‴), 68.98 (C3″), 65.9 (C4′), 65.7 ($OCH_2CH_2NH_2$), 62.8 (C6′), 60.3 (C6″), 59.5 (C7′), 51.99 (C4″), 49.9 (C1), 48.7 (C3), 47.8 (C2′), 39.2 ($OCH_2CH_2NH_2$), 30.1 (NCH_3), 29.8 (C2), 27.1 (C3′). ESI-HRMS: m/z calcd for $C_{27}H_{53}N_6O_{14}$ $[M+H]^+$ 685.3620, found 685.3624.

5-*O*-[3‴-*O*-((*N*-2-Hydroxyethyl)-2-aminoethyl)-*β*-D-erythrofuranosyl]-apramycin hexaacetate salt (23): To a stirred solution of **40** (115 mg, 0.090 mmol) in anhydrous dichloromethane (1 mL) at 0 °C was added aminoethanol (0.12 mL, 1.98 mmol) and glacial acetic acid (2 drops). After 2 h, the reaction was warmed to room temperature and $NaBH_3CN$ (41 mg, 0.67 mmol) was added. After 16 h, the solvent was evaporated to dryness and the crude product was taken up in ethyl acetate, washed with brine, and dried over Na_2SO_4. The organic solvent was evaporated to dryness and the residue was dissolved in dioxane/1N NaOH (1:1, 6 mL) and stirred at 80 °C. After 3 h, the reaction was neutralized with glacial acetic acid and concentrated to dryness, and the resulting residue was passed through silica, eluting with 30% ammoniacal methanol in dichloromethane to give a yellow-brown solid (47.7 mg). A portion of the resulting residue (22.7 mg) was taken up in dioxane/deionized water (1:1, 0.6 mL) and $Pd(OH)_2$ on carbon (43.5 mg) was added. After stirring at 50 psi under H_2 for 3 h, the reaction was filtered through Celite® and the solution was concentrated to dryness. The crude product was passed through a CM Sephadex C25 column, loading in 10% aqueous acetic acid and eluting with a gradient of 0.1-1.2% ammonium hydroxide in deionized water. The product-containing fractions were lyophilized in vacuo with glacial acetic acid to generate the peracetate salt of **23** (2.5 mg, 3% over 4 steps).

$[\alpha]_D^{21}$= +63.8 (*c* = 0.16, water). ^{1}H NMR (600 MHz, D_2O) δ 5.61 (d, *J* = 4.0 Hz, 1H, H1′), 5.37 (d, *J* = 4.0 Hz, 1H, H1″), 5.29 (d, *J* = 3.8 Hz, 1H, H1‴), 5.08 (d, *J* = 8.5 Hz, 1H, H8′), 4.44 (t, *J* = 2.7 Hz, 1H, H6′), 4.22 (t, *J* = 4.2 Hz, 1H, H2‴), 4.16 – 4.09 (m, 2H, H4‴a, H3‴), 3.89 – 3.84 (m, 1H, H4‴b), 3.84 – 3.50 (m, 15H, H5″, H4′, OC*H*$_2$CH$_2$NH, H3″, H6″a, OC*H*$_2$CH$_2$NH, HNCH$_2$C*H*$_2$OH, H5, H4, H6″b, H5′, H2″, H2′, H6), 3.27 – 3.06 (m, 8H, H7′, HNC*H*$_2$CH$_2$OH, H3, H1, OCH$_2$C*H*$_2$NH, H4″), 2.64 (s, 3H, NCH_3), 2.31 – 2.19 (m, 2H, H3′eq, H2eq), 1.93 – 1.84 (m, 1H, H3ax), 1.56 (q, *J* = 12.6 Hz, 1H, H2ax). ^{13}C NMR (150 MHz, D_2O) δ 110.2 (C1‴), 94.52 (C1′), 94.46 (C1″), 93.0 (C8′), 84.7 (C5), 78.4 (C4), 77.7 (C3‴), 74.5 (C2‴), 72.9 (C6), 70.2 (C2″), 70.1 (C5″), 69.7 (C5′), 69.2 (C4‴), 68.9 (C3″), 65.9 (C4′), 64.6 (O*C*H$_2$CH$_2$OH), 62.8 (C6′), 60.3 (C6″), 59.5 (C7′), 56.4 (HNCH$_2$*C*H$_2$OH), 52.0 (C4″), 49.9 (C1), 48.9 (C3), 48.8 (OCH$_2$*C*H$_2$NH), 47.8 (C2′), 46.8 (HN*C*H$_2$CH$_2$OH), 30.2 (NCH_3), 29.9 (C2), 27.1 (C3′). ESI-HRMS: m/z calcd for $C_{29}H_{57}N_6O_{15}$ $[M+H]^+$ 729.3882, found 729.3868.

5-*O*-[3‴-*O*-((*N*-2-Aminoethyl)-2-aminoethyl)-*β*-D-erythrofuranosyl]-apramycin heptaacetate salt (24): To a stirred solution of **40** (477 mg, 0.38 mmol) in anhydrous dichloromethane/methanol (1:1 7.5 mL) at 0 °C was added ethylene diamine (1 mL, 15 mmol), and glacial acetic acid was added to acidify the reaction to pH 6. After 1 h, the reaction was warmed to room temperature and $NaBH_3CN$ (257 mg, 4.09 mmol) was added. After 4 h, the reaction was evaporated to dryness and the residue was passed through silica gel, eluting with 12% ammoniacal methanol in dichloromethane. The resulting solid was taken in dioxane/1N NaOH (6 mL) and stirred at 80 °C. After 16 h, the reaction was neutralized with glacial acetic acid and the solvent was evaporated to dryness. The residue was purified via silica gel chromatography, eluting with 20% ammoniacal methanol in dichloromethane, giving a mixture of desired compound and acetate migration byproduct in trace amounts. The mixture was taken up in dioxane/deionized water (1:1,

1 mL) and $Pd(OH)_2$ on carbon (131.8 mg) was added. After stirring at 50 psi under H_2 for 17 h, the reaction was filtered through Celite® and the solution was concentrated to dryness. The crude product passed through a CM Sephadex C25 column, loading in 10% aqueous acetic acid and eluting with a gradient of 0.1-1.3% ammonium hydroxide in deionized water. The product-containing fractions were lyophilized in vacuo with glacial acetic acid to generate the peracetate salt of **24** (18.5 mg, 18% over 4 steps). $[\alpha]_D^{21}$= +26.8 (*c* = 0.33, water). ^{1}H NMR (600 MHz, D_2O) δ 5.63 (d, *J* = 4.0 Hz, 1H, H1′), 5.36 (d, *J* = 3.9 Hz, 1H, H1″), 5.27 (d, *J* = 3.7 Hz, 1H, H1‴), 5.07 (d, *J* = 8.5 Hz, 1H, H8′), 4.44 (t, *J* = 2.7 Hz, 1H, H6′), 4.22 – 4.19 (m, 1H, H2‴), 4.14 – 4.09 (m, 2H, H4‴a, H3‴), 3.85 – 3.67 (m, 9H, H4‴b, H5″, H4′, H3″, H4, H6″a, OC*H*$_2$CH$_2$NH, H5), 3.65 (dd, *J* = 12.5, 4.7 Hz, 1H, H6″b), 3.60 – 3.54 (m, 3H, H5′, H2″, H2′), 3.52 (dd, *J* = 10.6, 9.0 Hz, 1H, H6), 3.25 – 3.12 (m, 9H, H7′, H3, NHC*H*$_2$CH$_2$NH$_2$, NHCH$_2$C*H*$_2$NH$_2$, OCH$_2$C*H*$_2$NH, H1), 3.10 (t, *J* = 10.3 Hz, 1H, H4″), 2.64 (s, 3H, NCH_3), 2.24 (dt, *J* = 9.4, 4.0 Hz, 2H, H2eq, H3′eq), 1.93 – 1.84 (m, 1H, H3′eqx), 1.60 (q, *J* = 12.6 Hz, 1H, H2′ax). ^{13}C NMR (150 MHz, D_2O) δ 110.3 (C1‴), 94.4 (C1″), 94.3 (C1′), 92.9 (C8′), 84.6 (C5), 77.6 (C3‴), 77.4 (C4), 74.3 (C2‴), 72.8 (C6), 70.2 (C2″), 69.9 (C5″), 69.7 (C5′), 69.1 (C4‴), 68.7 (C3″), 65.9 (C4′), 65.3 (O*C*H$_2$CH$_2$NH), 62.7 (C6′), 60.3 (C6″), 59.5 (C7′), 52.0 (C4″), 49.8 (C1), 48.7 (C3), 47.7 (C2′), 47.6 (OCH$_2$*C*H$_2$NH), 44.3 (HN*C*H$_2$CH$_2$NH$_2$), 35.8 (HNCH$_2$*C*H$_2$NH$_2$), 30.1 (NCH_3), 29.3 (C2), 27.1 (C3′). ESI-HRMS: m/z calcd for $C_{29}H_{58}N_7O_{14}$ $[M+H]^+$ 728.4042, found 728.4013.

5-*O*-[3‴-*O*-((*N*-3-Aminopropyl)-2-aminoethyl)-*β*-D-erythrofuranosyl]-apramycin heptaacetate salt (25): To a stirred solution of **40** (127 mg, 0.10 mmol) in anhydrous methanol (2.5 mL) at 0 °C was added benzyl-(3-aminopropyl)carbamate[15] (215 mg, 1.03 mmol). Glacial acetic acid was added to acidify the solution to pH 5. After 1 h, the solution was warmed to room temperature and $NaBH_3CN$ (55.6 mg, 0.88 mmol) was added. After 12 h, the reaction was diluted

with ethyl acetate, washed with brine, and dried over Na_2SO_4. The organic layer was evaporated to dryness and the crude product was taken up in dioxane/1N NaOH (1:1, 4 mL) and stirred at 50 °C. After 1.5 h, the reaction temperature was lowered to 45 °C to prevent potential decomposition. After 3.5 h, the reaction was neutralized with glacial acetic acid, the solvent was evaporated to dryness, and the crude product was passed through silica gel, with stepwise elution using 10-22% ammoniacal methanol in dichloromethane to yield a mixture of two compounds. The crude mixture was then taken up in dioxane/deionized water (1:1, 0.6 mL) and $Pd(OH)_2$ on carbon (32.8 mg) was added. After stirring at 50 psi under H_2 for 17 h, the reaction was filtered through Celite® and the solution was concentrated to dryness. The crude product was passed through a CM Sephadex C25 column, loading in 10% aqueous acetic acid and eluting with a gradient of 0.1-1.8% ammonium hydroxide in deionized water. The product-containing fractions were lyophilized in vacuo with glacial acetic acid to generate the peracetate salt of **25** (3.5 mg, 3% over 4 steps). $[\alpha]_D^{21}$= +102.0 (*c* = 0.05, water). ^{1}H NMR (600 MHz, D_2O) δ 5.50 (d, *J* = 3.9 Hz, 1H, H1′), 5.34 (d, *J* = 4.0 Hz, 1H, H1″), 5.27 (d, *J* = 3.7 Hz, 1H, H1‴), 5.03 (d, *J* = 8.5 Hz, 1H, H8′), 4.40 (t, *J* = 2.7 Hz, 1H, H6′), 4.21 (t, *J* = 4.0 Hz, 1H, H2‴), 4.16 – 4.09 (m, 2H, H4‴a, H3‴), 3.84 (q, *J* = 6.1 Hz, 1H, H4‴b), 3.79 (td, *J* = 10.9, 4.5 Hz, 1H, H4′), 3.76 – 3.62 (m, 8H, OC*H*$_2$CH$_2$NH, H6″a, H5″, OC*H*$_2$CH$_2$NH, H3″, H5, H6″b, H5′), 3.58 – 3.54 (m, 2H, H2″, H4), 3.49 (m, 2H, H2′, H6), 3.22 – 3.08 (m, 4H, OCH$_2$C*H*$_2$NH, H7′, H1), 3.07 – 2.99 (m, 3H, NHCH$_2$CH$_2$C*H*$_2$NH$_2$, H3), 2.96 (m, 3H, NHC*H*$_2$CH$_2$CH$_2$NH$_2$, H4″), 2.59 (s, 3H, NCH$_3$), 2.27 – 2.20 (m, 1H, H3′eq), 2.18 – 2.10 (m, 1H, H2eq), 1.96 (p, *J* = 8.0 Hz, 2H, NHCH$_2$C*H*$_2$CH$_2$NH$_2$), 1.84 (q, *J* = 11.9 Hz, 1H, H3′eqx), 1.45 (q, *J* = 12.5 Hz, 1H, H2ax). ^{13}C NMR (150 MHz, D_2O) δ 110.2 (C1‴), 95.1 (C1′), 94.5 (C1″), 93.3 (C8′), 84.7 (C5), 80.1 (C4), 77.7 (C3‴), 74.3 (C2‴), 73.3 (C6), 71.1 (C5″), 70.3 (C2″), 69.8 (C3″), 69.7 (C5′), 69.0 (C4‴), 66.0 (C4′), 64.8 (OH*C*H$_2$CH$_2$NH), 63.1 (C6′), 60.5 (C6″), 59.8 (C7′), 52.1

(C4″), 50.1 (C1), 49.0 (C3), 48.0 (C2′), 47.3 (OHCH$_2$*C*H$_2$NH), 44.4 (NHCH$_2$CH$_2$*C*H$_2$NH$_2$), 36.5 (NH*C*H$_2$CH$_2$CH$_2$NH$_2$), 30.99 (C2), 30.3 (NCH$_3$), 27.6 (C3′), 23.6 (NHCH$_2$*C*H$_2$CH$_2$NH$_2$), 23.1. ESI-HRMS: m/z calcd for $C_{30}H_{60}N_7O_{14}$ $[M+H]^+$ 742.4198, found 742.4221.

5-*O*-[3‴-*O*-((*N*-3-*N*′,*N*′-Dimethylaminopropyl)-2-aminoethyl)-*β*-D-erythrofuranosyl]-apramycin heptaacetate salt (26): To a stirred solution of **40** (149 mg, 0.12 mmol) in anhydrous dichloromethane (1.2 mL) at room temperature was added 3-dimethylaminopropylamine (0.1 mL, 0.82 mmol) and glacial acetic acid (2 drops). After 1 h, $NaBH_3CN$ (75.9 mg, 1.21 mmol) and anhydrous methanol (1 mL) were added. After 14 h, the reaction was diluted with ethyl acetate, washed with brine, and dried over Na_2SO_4. The organic layer was evaporated to dryness and the crude product was taken up in dioxane/1N NaOH (1:1, 6 mL) and stirred at 80 °C. After 4 h, the reaction was neutralized with glacial acetic acid, the solvent was evaporated to dryness, and the crude product was passed through silica gel, eluting with a gradient of 8-20% ammoniacal methanol in dichloromethane to give an off-white solid (65.5 mg). A portion of the resulting residue (28.4 mg) was taken up in dioxane/deionized water (1:1, 1 mL) and $Pd(OH)_2$ on carbon (62 mg) was added. After stirring at 50 psi under H_2 for 2.5 h, the reaction was filtered through Celite® and the solution was concentrated to dryness. The crude product was passed through a CM Sephadex C25 column, loading in 10% aqueous acetic acid and eluting with a gradient of 0.2-1.5% ammonium hydroxide in deionized water. The product-containing fractions were lyophilized in vacuo with glacial acetic acid to generate the peracetate salt of **26** (4.5 mg, 8% over 4 steps). $[\alpha]_D^{21}$= +56.4 (*c* = 0.14, water). ^{1}H NMR (600 MHz, D_2O) δ 5.58 (d, *J* = 3.9 Hz, 1H, H1′), 5.36 (d, *J* = 4.0 Hz, 1H, H1″), 5.28 (d, *J* = 3.7 Hz, 1H, H1‴), 5.07 (d, *J* = 8.5 Hz, 1H, H8′), 4.43 (t, *J* = 2.7 Hz, 1H, H6′), 4.22 (t, *J* = 4.0 Hz, 1H, H2‴), 4.15 – 4.09 (m, 2H, H4‴a, H3‴), 3.84 (q, *J* = 6.0 Hz, 1H, H4‴b), 3.82 – 3.49 (m, 15H, H4′, H5″, H6″a, OC*H*$_2$CH$_2$NH, H3″,

OC*H*$_2$CH$_2$NH, H5, H4, H6″b, H5′, H2″, H2′, H6), 3.23 – 3.00 (m, 10H, H7′, OCH$_2$C*H*$_2$NH, H1, H3, NHCH$_2$CH$_2$C*H*$_2$N(CH$_3$)$_2$, H4″, NHC*H*$_2$CH$_2$CH$_2$N(CH$_3$)$_2$), 2.77 (s, 6H, N(CH$_3$)$_2$), 2.63 (s, 3H, NCH$_3$), 2.25 (dt, *J* = 11.1, 4.6 Hz, 1H, H3′eq), 2.20 (dt, *J* = 12.8, 4.3 Hz, 1H, H2eq), 2.06 – 1.99 (m, 2H, NHCH$_2$C*H*$_2$CH$_2$N(CH$_3$)$_2$), 1.88 (q, *J* = 12.1 Hz, 1H, H3′eq), 1.54 (q, *J* = 12.6 Hz, 1H, H2ax). ^{13}C NMR (150 MHz, D$_2$O) δ 110.3 (C1‴), 94.6 (C1′), 94.5 (C1″), 93.1 (C8′), 84.7 (C5), 78.6 (C4), 77.7 (C3‴), 74.3 (C2‴), 73.0 (C6), 70.3 (C5″, C2″), 69.7 (C5′), 69.1 (C3″), 69.0 (C4‴), 65.9 (C4′), 64.7 (O*C*H$_2$CH$_2$NH), 62.9 (C6′), 60.4 (C6″), 59.6 (C7′), 54.2 (NHCH$_2$CH$_2$*C*H$_2$N(CH$_3$)$_2$), 52.1 (C4″), 49.9 (C1), 48.8 (C3), 47.8 (C2′), 47.3 (OCH$_2$*C*H$_2$NH), 44.2 (NH*C*H$_2$CH$_2$CH$_2$N(CH$_3$)$_2$), 42.7 (N(CH$_3$)$_2$), 30.2 (C2), 30.1 (NCH$_3$), 27.3 (C3′), 21.1 (NHCH$_2$*C*H$_2$CH$_2$N(CH$_3$)$_2$). ESI-HRMS: m/z calcd for C$_{32}$H$_{64}$N$_7$O$_{14}$ [M+H]$^+$ 770.4511, found 770.4536.

5-*O*-[(2,3-Di-*O*-acetyl-5-deoxy)-β-D-ribofuranosyl]-1,3,2′,4″-tetraazido-6,2″,3″,6″-tetra-*O*-benzoyl-1,3,2′,4″-tetradesamino-6′,7′-oxazolidino-apramycin (42). To a stirred solution of **41** (244 mg, 0.94 mmol) and **35** (480 mg, 0.44 mmol) in DCM (4.6 mL) at 0 °C with oven-dried 4Å molecular sieves was added BF$_3$·OEt$_2$ (0.35 mL, 2.66 mmol). Additional BF$_3$·OEt$_2$ (0.1 mL, 0.76 mmol) was added as progress slowed. After 1.5 h, the reaction was quenched with excess triethylamine and left to stir at 0 °C for 10 mins. The reaction mixture was then diluted with EtOAc, washed with saturated aqueous NaHCO$_3$ and brine, and dried over Na$_2$SO$_4$. The crude product was purified via silica gel chromatography (0.3-0.8% MeOH in DCM, R$_f$ = 0.55 in 2% MeOH in DCM) to give **42** (154 mg, 27%) as a white solid. [α]$_D^{23}$ = +108.6 (*c* = 1.0, EtOAc); ^{1}H NMR (600 MHz, CDCl$_3$) δ 8.11 (dd, *J* = 12.1, 7.9 Hz, 4H, Ar), 8.05 (d, *J* = 7.8 Hz, 2H, Ar), 8.00 (d, *J* = 7.8 Hz, 2H, Ar), 7.63 (dt, *J* = 12.7, 7.5 Hz, 2H, Ar), 7.55 (dt, *J* = 15.8, 7.3 Hz, 4H, Ar), 7.50 (t, *J* = 7.6 Hz, 2H, Ar), 7.44 (q, *J* = 7.4 Hz, 4H, Ar), 6.03 (t, *J* = 10.1 Hz, 1H, H3’’), 5.72 (d, *J* =

3.7 Hz, 1H, H1’’), 5.69 (d, *J* = 3.5 Hz, 1H, H1’), 5.33 (d, *J* = 3.3 Hz, 1H, H1’’’), 5.23 (t, *J* = 9.9 Hz, 1H, H6), 5.19 (dd, *J* = 10.6, 3.8 Hz, 1H, H2’’), 4.93 (t, *J* = 4.0 Hz, 1H, H2’’’), 4.86 (t, *J* = 5.0 Hz, 1H, H3’’’), 4.80 (d, *J* = 5.7 Hz, 1H, H8’), 4.76 (dd, *J* = 7.0, 3.6 Hz, 1H, H6’), 4.72 – 4.62 (m, 2H, H6’’), 4.15 (dd, *J* = 10.4, 3.5 Hz, 1H, H5’), 4.14 – 4.09 (m, 1H, H5’’), 4.03 (m, 2H, H4, H4’’’), 3.91 (t, *J* = 10.1 Hz, 1H, H4’’), 3.81 (t, *J* = 9.3 Hz, 1H, H5), 3.76 (t, *J* = 6.3 Hz, 1H, H7’), 3.59 – 3.52 (m, 1H H1), 3.49 (td, *J* = 10.7, 4.2 Hz, 1H, H4’), 3.46 – 3.39 (m, 1H, H3), 2.98 – 2.91 (m, 4H, NCH_3, H2’), 2.45 (dt, *J* = 13.2, 4.6 Hz, 1H, H2eq), 1.80 (s, 3H, CH_3CO), 1.73 (dd, *J* = 24.9, 12.4 Hz, 2H, H3’eq, H2ax), 1.66 (s, 3H, CH_3CO), 1.36 (q, *J* = 12.0 Hz, 1H, H3’ax), 1.28 (d, *J* = 6.6 Hz, 3H, H5’’); ^{13}C NMR (151 MHz, $CDCl_3$) δ 169.3 (CH_3*C*O), 169.2 (CH_3*C*O), 166.1 (ArCO), 165.9 (ArCO), 165.6 (ArCO), 164.8 (ArCO), 157.0 (Oxazolidinone), 133.7 (Ar), 133.6 (Ar), 133.6 (Ar), 130.1 (Ar), 130.0 (Ar), 129.8 (Ar), 129.7 (Ar), 129.3 (Ar), 129.0 (Ar), 129.0 (Ar), 128.8 (Ar), 128.7 (Ar), 128.6 (Ar), 128.5 (Ar), 128.5 (Ar), 105.5 (C1’’’), 100.6 (C1’), 96.6 (C8’), 95.6 (C1’’), 80.7 (C4), 77.4 (C4’’’), 76.4 (C5), 75.5 (C6), 74.6 (C2’’’), 74.4 (C3’’’), 71.8 (C6’), 71.3 (C2’’), 70.5 (C3’’), 69.9 (C5’’), 66.5 (C5’), 65.9 (C4’), 63.4 (C6’’), 60.9 (C4’’), 60.3 (C7’), 59.3 (C3), 58.3 (C1), 55.5 (C2’), 31.4 (C2), 30.3 (NCH_3), 28.4 (C3’), 20.3 (CH_3CO), 19.9 (CH_3CO), 19.4 (C5’’’); ESI-HRMS: *m/z* calc for $C_{59}H_{59}N_{13}O_{21}Na$ $[M+Na]^+$ 1308.38407, found 1308.3816. Although not isolated pure, the minor α-anomer was identified in the crude reaction mixture by the following diagnostic signals: δ 5.86 (d, *J* = 10.1 Hz, 1H), 2.74 (s, 3H), 2.42 (dt, *J* = 13.1, 4.6 Hz, 1H).

5-*O*-[5-deoxy-β-D-ribofuranosyl]-apramycin pentaacetate salt (27). To a stirred solution of **42** (51 mg, 0.040 mmol) in dioxane (1.5 mL) was added aqueous NaOH (1.5 mL, 3 N) and the reaction was heated to reflux. After 4 h, the temperature was reduced to 60 °C and PMe_3 solution (0.35 mL, 1.0 M in THF). After 2.5 h, the reaction was neutralized with AcOH and

concentrated to dryness. The crude product was passed through a CM Sephadex C25 column, loading in 10% aqueous acetic acid and eluting with a gradient of 0.1-1.2% ammonium hydroxide in deionized water. The product-containing fractions were lyophilized in vacuo with glacial acetic acid to generate the peracetate salt of **27** (22 mg, 57% over 3 steps) $[\alpha]_D^{23}$ = +25.0 (*c* = 0.08, H_2O); ^{1}H NMR (900 MHz, D_2O) δ 5.79 (d, *J* = 4.1 Hz, 1H, H1'), 5.42 (d, *J* = 4.0 Hz, 1H, H1''), 5.19 (d, *J* = 2.2 Hz, 1H, H1'''), 5.13 (d, *J* = 8.6 Hz, 1H, H8'), 4.50 (t, *J* = 2.9 Hz, 1H, H6'), 4.13 (dd, *J* = 4.9, 2.1 Hz, 1H, H2'''), 3.98 (p, *J* = 6.5 Hz, 1H, H4'''), 3.86 (ddd, *J* = 11.4, 9.4, 4.7 Hz, 4H, H3''', H5, H4', H5''), 3.82 (t, *J* = 9.7 Hz, 1H, H3''), 3.78 (dd, *J* = 12.4, 3.3 Hz, 1H, H6''a), 3.76 (t, *J* = 9.1 Hz, 1H, H4), 3.71 (dd, *J* = 12.4, 4.7 Hz, 1H, H6''b), 3.66 – 3.63 (m, 2H, H2'', H5'), 3.60 (dt, *J* = 12.8, 4.4 Hz, 1H, H2'), 3.56 (dd, *J* = 10.5, 9.1 Hz, 1H, H6), 3.33 – 3.27 (m, 2H, H7', H3), 3.23 (ddd, *J* = 12.4, 10.4, 4.3 Hz, 1H, H1), 3.16 (t, *J* = 10.3 Hz, 1H, H4''), 2.70 (s, 3H, NCH_3), 2.31 (m, 2H, H3'eq, H2eq), 1.96 (q, *J* = 11.9 Hz, 1H, H3'ax), 1.83 (s, 15H, CH_3CO), 1.68 (q, *J* = 12.6 Hz, 1H, H2ax), 1.28 (d, *J* = 6.3 Hz, 3H, H5'''); ^{13}C NMR (226 MHz, D_2O) δ 181.1 ($CH_3\mathit{C}O$), 110.6 (C1'''), 94.5 (C1''), 94.3 (C1'), 93.0 (C8'), 85.3 (C5), 78.6 (C4'''), 77.2 (C4), 75.1 (C2'''), 74.4 (C3'''), 72.8 (C6), 70.3 (C2''), 69.9 (C5''), 69.7 (C5'), 68.8 (C3''), 65.9 (C4'), 62.8 (C6'), 60.4 (C6''), 59.5 (C7'), 52.1 (C4''), 49.9 (C1), 48.6 (C3), 47.7 (C2'), 30.2 (NCH_3), 29.3 (C2), 27.1 (3'), 23.0 ($\mathit{C}H_3CO$), 18.3 (C5'''); ESI-HRMS: *m/z* calc for $C_{26}H_{49}N_5O_{14}Na$ $[M+Na]^+$ 678.31682, found 678.3181.

5-Azido-3-*O*-(2-azidoethyl)-5-deoxy-1,2-*O*-isopropylidene-α-D-ribofuranose (44): To a stirred solution of **43** (1.31 g, 6.07 mmol) in tetrahydrofuran (12 mL) at 0 °C was added NaH (1.02 g, 25.4 mmol, 60% dispersion in mineral oil). After 10 mins, a solution of 2-azidoethyltosylate (6.13 g, 25.4 mmol) in tetrahydrofuran (11 mL) was added and the reaction mixture was warmed to room temperature. After 17 h, the reaction was quenched with saturated

ammonium chloride and diluted with ethyl acetate. The organic layer was washed with 1N HCl and brine, dried over Na_2SO_4, and concentrated to dryness. The residue was purified via silica gel chromatography, eluting with a gradient of 5%-50% ethyl acetate in hexanes (Rf = 0.3 in 20% ethyl acetate/hexanes) to give the desired compound **44** as a colorless oil (796 mg, 46%). $[\alpha]_D^{21}$ = +73.4 (*c* 0.4, $CHCl_3$); ^{1}H NMR (600 MHz, $CDCl_3$) δ 5.84 (d, *J* = 3.7 Hz, 1H, H1), 4.68 (t, *J* = 4.0 Hz, 1H, H2), 4.18 (ddd, *J* = 8.9, 3.8, 2.7 Hz, 1H, H4), 3.93 (ddd, *J* = 10.2, 5.6, 3.4 Hz, 1H, CH_2O), 3.81 (dd, *J* = 8.9, 4.4 Hz, 1H, H3), 3.75 (dd, *J* = 13.6, 2.7 Hz, 1H, H5), 3.70 (ddd, *J* = 10.2, 7.6, 3.3 Hz, 1H, CH_2O), 3.52 (ddd, *J* = 13.4, 7.6, 3.4 Hz, 1H, C*H*$_2$CH$_2$O), 3.41 – 3.32 (m, 2H, H5, C*H*$_2$CH$_2$O), 1.60 (s, 3H, CH_3), 1.39 (s, 3H, CH_3); ^{13}C NMR (150 MHz, $CDCl_3$) δ 113.4 (*C*$(CH_3)_2$), 104.2 (C1), 79.3 (C3), 77.4 (C2), 77.1 (C4), 69.4 (CH_2O), 50.6 (*C*H$_2$CH$_2$O), 50.4 (C5), 26.7 (CH_3), 26.59 (CH_3); ESI-HRMS: m/z calcd. for $C_{10}H_{16}N_6O_4Na$ $[M+Na]^+$ 307.1125; found, 307.1112.

1,2-Di-*O*-acetyl-5-azido-3-*O*-(2-azidoethyl)-5-deoxy-D-ribofuranose (45): Compound **44** (360 mg, 1.3 mmol) was dissolved in aqueous acetic acid (80%, 5 mL) and heated to reflux. After 3.5 h, the reaction mixture was concentrated to dryness and co-evaporated thrice with pyridine. The crude mixture was dissolved in acetic anhydride (1.3 mL) and pyridine (1.3 mL) followed by addition of DMAP (52 mg, 0.43 mmol). After 2 h, the reaction mixture was quenched with methanol and diluted in ethyl acetate. The organic layer was washed with 1N HCl, saturated aqueous $NaHCO_3$, and brine, dried over Na_2SO_4, and concentrated to dryness. The residue was purified via silica gel chromatography, eluting with a gradient of 0%-50% ethyl acetate in hexanes (Rf = 0.35 in 20% ethyl acetate/hexanes) to give a mixture of anomers **45** (0.25:1 α:β, 348 mg, 82% over 2 steps) as a yellow oil that was used without further purification. ESI-HRMS: m/z calcd. for $C_{11}H_{16}N_6O_6Na$ $[M+Na]^+$ 351.1024; found, 351.1008. α: ^{1}H NMR (600 MHz, $CDCl_3$) δ 6.43 (d, *J* = 4.5 Hz, 1H, H1), 5.17 (dd, *J* = 6.5, 4.5 Hz, 1H, H2), 4.36 (d, *J* = 4.2 Hz, 1H, H4), 4.03 (dd,

J = 6.5, 4.7 Hz, 1H, H3), 3.79 – 3.73 (m, 1H, CH_2O), 3.70 – 3.62 (m, 2H, CH_2O, H5), 3.48 (d, *J* = 3.8 Hz, 1H, H5), 3.39 – 3.32 (m, 2H, C*H*$_2$$CH_2O$), 2.18 (s, 3H, CH_3CO), 2.14 (s, 3H, CH_3CO); ^{13}C NMR (150 MHz, $CDCl_3$) δ 170.0 (CH_3*C*O), 169.8 (CH_3*C*O), 94.5 (C1), 82.3 (C4), 77.1 (C3), 71.0 (C2), 70.7 (CH_2O), 51.9 (C5), 50.8 (*C*H_2CH_2O), 21.00 (*C*H_3CO), 20.5 (*C*H_3CO); β: ^{1}H NMR (600 MHz, $CDCl_3$) δ 6.18 (s, 1H, H1), 5.34 (d, *J* = 4.1 Hz, 1H, H2), 4.26 (dd, *J* = 8.3, 4.2 Hz, 1H, H3), 4.22 (dt, *J* = 8.3, 3.1 Hz, 1H, H4), 3.84 – 3.79 (m, 1H, CH_2O), 3.79 – 3.73 (m, 1H, H5), 3.70 – 3.62 (m, 1H, CH_2O), 3.39 – 3.32 (m, 2H, C*H*$_2$$CH_2O$), 3.28 (dd, *J* = 13.7, 3.1 Hz, 1H, H5), 2.20 (s, 3H, CH_3CO), 2.14 (s, 3H, CH_3CO). ^{13}C NMR (150 MHz, $CDCl_3$) δ 169.8 (CH_3*C*O), 169.0 (CH_3*C*O), 98.1 (C1), 80.5 (C4), 77.2 (C3), 73.3 (C2), 70.4 (CH_2O), 50.72 (*C*H_2CH_2O), 50.68 (C5), 21.03 (*C*H_3CO), 20.7 (*C*H_3CO).

5-*O*-[2‴-*O*-Acetyl-5‴-azido-3‴-*O*-(2-azidoethyl)-5’’’-deoxy-β-D-ribofuranosyl]-1,3,2′,4″-tetra(desamino)-1,3,2′,4″-tetraazido-6,2″,3″,6″-tetra-*O*-benzoyl-6′,7′-oxazolidino-apramycin (46): To a stirred solution of **44** (364 mg, 1.11 mmol) and **35** (508 mg, 0.47 mmol) in dichloromethane (10.5 mL) at room temperature with oven-dried 4Å molecular sieves was added $BF_3{\cdot}OEt_2$ (0.33 mL, 2.67 mmol). Additional $BF_3{\cdot}OEt_2$ (0.8 mL, 6.48 mmol) was added over the course of the reaction whenever progress stopped. After 23 h, the reaction was quenched with excess triethylamine. The reaction mixture was filtered through Celite®, diluted with ethyl acetate, washed with saturated aqueous sodium bicarbonate and brine, dried over Na_2SO_4, and concentrated to dryness. The residue (an 0.3:1 α:β mixture) was purified via silica gel chromatography, eluting with a gradient of 0.3-1.0% dichloromethane in methanol (Rf = 0.3 in 1.8% methanol in dichloromethane) to give the desired anomer **46** as a white solid (335 mg, 44%). $[\alpha]_D^{21}$ = +54.5 (*c* 0.47, $CHCl_3$); ^{1}H NMR (600 MHz, $CDCl_3$) δ 8.21 – 8.16 (m, 2H, Ar), 8.13 – 8.08 (m, 2H, Ar), 8.08 – 8.03 (m, 2H, Ar), 8.01 – 7.96 (m, 2H, Ar), 7.65 (ddq, *J* = 9.3, 5.8, 1.3 Hz, 2H,

Ar), 7.61 – 7.56 (m, 2H, Ar), 7.54 (tdd, *J* = 7.4, 4.3, 1.7 Hz, 4H, Ar), 7.48 – 7.41 (m, 4H, Ar), 6.02 (t, *J* = 10.1 Hz, 1H, H3’’), 5.73 (d, *J* = 3.7 Hz, 1H, H1’’), 5.52 (d, *J* = 3.6 Hz, 1H, H1’), 5.31 (s, 1H, H1’’’), 5.23 – 5.17 (m, 2H, H6, H2’’), 4.99 (d, *J* = 4.4 Hz, 1H, H2’’’), 4.84 (d, *J* = 5.2 Hz, 1H, H8’), 4.77 (dd, *J* = 7.1, 3.6 Hz, 1H, H6’), 4.70 (dd, *J* = 12.1, 2.5 Hz, 1H, H6’’), 4.65 (dd, *J* = 12.1, 5.4 Hz, 1H, H6’’), 4.27 (dd, *J* = 10.3, 3.6 Hz, 1H, H5’), 4.10 (ddd, *J* = 10.6, 5.4, 2.5 Hz, 1H, H5’’), 3.99 (ddd, *J* = 7.9, 5.6, 3.2 Hz, 1H, H4’’’), 3.90 (t, *J* = 10.1 Hz, 1H, H4’’), 3.83 (t, *J* = 9.1 Hz, 1H, H5), 3.80 – 3.76 (m, 2H, H4, H7’), 3.65 (dd, *J* = 7.9, 4.4 Hz, 1H, H3’’’), 3.60 (ddd, *J* = 12.5, 10.2, 4.4 Hz, 1H, H1), 3.55 (dd, *J* = 11.0, 4.3 Hz, 1H, H4’), 3.50 – 3.42 (m, 2H, H3, H5’’’), 3.34 (dd, *J* = 13.2, 5.7 Hz, 1H, H5’’’), 3.16 (dt, *J* = 13.1, 4.2 Hz, 1H, H2’), 3.03 (ddd, *J* = 13.2, 5.5, 4.2 Hz, 1H, C*H*$_2$CH$_2$O), 3.00 – 2.95 (m, 1H, C*H*$_2$CH$_2$O), 2.94 (s, 3H, N-CH$_3$), 2.92 (m, 2H, CH$_2$O), 2.51 (dt, *J* = 13.2, 4.6 Hz, 1H, H2eq), 1.86 (s, 3H, CH$_3$CO), 1.83 – 1.78 (m, 1H, H3’eq), 1.72 (q, *J* = 12.6 Hz, 1H, H2ax), 1.36 (dt, *J* = 12.8, 11.5 Hz, 1H, H3’ax); ^{13}C NMR (150 MHz, CDCl$_3$) δ 169.9 (CH$_3$*C*O), 166.1, 1656.0, 165.7, 164.7 (Ph*C*O), 157.0 (NC=O), 133.9, 133.8, 133.7, 130.3, 130.0, 129.8, 129.3, 129.0, 128.8, 128.8, 128.7, 128.7, 128.6, 128.5 (Ar), 107.2 (C1’’’), 99.5 (C8’), 96.7 (C1’), 95.5 (C1’’), 80.1 (C5), 80.0 (C4’’’), 77.9 (C4), 77.8 (C3’’’), 74.6 (C6), 73.3 (C2’’’), 71.4 (C6’, C2’’), 70.5 (C3’’), 69.8 (C5’’), 69.4 (*C*H$_2$O), 66.4 (C5’), 65.8 (C4’), 63.4 (C6’’), 61.0 (C4’’), 60.3 (C7’), 58.9 (C1), 58.3 (C3), 56.2 (C2’), 52.3 (C5’’’), 50.4 (*C*H$_2$CH$_2$O), 31.5 (C2), 30.2 (N-CH$_3$), 29.0 (C3’), 20.30 (*C*H$_3$CO); ESI-HRMS: m/z calcd. for $C_{59}H_{59}N_{19}O_{20}Na$ $[M+Na]^+$ 1376.4076; found, 1376.4038. Although not isolated pure, the minor α-anomer was identified in the crude reaction mixture by the following diagnostic signals: δ 4.88 (d, *J* = 3.6 Hz, 1H), 4.66 (t, *J* = 2.7 Hz, 1H), 2.83 (s, 3H).

5-*O*-[5-Amino-3-*O*-(2-aminoethyl)-5-deoxy-β-D-ribofuranosyl] apramycin heptaacetate salt (31): To a stirred solution of **46** (130 mg, 0.097 mmol) in 1,4-dioxane (5 mL)

was added aqueous NaOH (3N, 5 mL), and the reaction mixture was heated to reflux. After 6 h, the reaction mixture was cooled to 55 °C and trimethylphosphine (1M in THF, 0.5 mL) was added. After 4 h, the reaction mixture was neutralized with glacial acetic acid and concentrated to dryness. The crude residue was dissolved in minimal aqueous acetic acid (10%) and purified using a CM Sephadex C25 column, eluting with 0.1-1.2% NH_4OH in water to give **31** as a white solid (58 mg, 53%); $[\alpha]_D^{21}$ = +72.5 (*c* 0.7, H_2O); ^{1}H NMR (900 MHz, D_2O) δ 5.75 (d, *J* = 3.8 Hz, 1H, H1'), 5.43 (d, *J* = 4.0 Hz, 1H, H1''), 5.37 (d, *J* = 1.5 Hz, 1H, H1'''), 5.13 (d, *J* = 8.6 Hz, 1H, H8'), 4.51 (t, *J* = 2.8 Hz, 1H, H6'), 4.38 (dd, *J* = 4.6, 1.5 Hz, 1H, H2'''), 4.16 (td, *J* = 7.7, 4.0 Hz, 1H, H4'''), 4.01 (dd, *J* = 7.3, 4.6 Hz, 1H, H3'''), 3.92 – 3.85 (m, 4H, H4, H5, H5'', H4'), 3.83 (t, *J* = 10.0 Hz, 1H, H3''), 3.81 – 3.77 (m, 2H, C*H*$_2$O, H6''), 3.77 – 3.74 (m, 1H C*H*$_2$O), 3.72 (dd, *J* = 12.5, 4.7 Hz, 1H, H6''), 3.66 – 3.61 (m, 3H, H5', H2'', H6), 3.56 (dt, *J* = 12.8, 4.3 Hz, 1H, H2'), 3.31 (m, 2H, H3, H5'''), 3.28 (dd, *J* = 8.6, 2.8 Hz, 1H, H7'), 3.23 (ddd, *J* = 12.5, 10.5, 4.1 Hz, 1H, H1), 3.17 (m, 4H, C*H*$_2$CH$_2$O, H5''', H4''), 2.70 (s, 3H, N-CH$_3$), 2.32 – 2.28 (m, 2H, H3'eq, H2eq), 1.95 (q, *J* = 11.9 Hz, 1H, H3ax), 1.85 (s, 21H, H$_3$CCO), 1.68 (q, *J* = 12.6 Hz, 1H, H2ax); ^{13}C NMR (226 MHz, D_2O) δ 181.0 (H$_3$C*C*O), 109.0 (C1'''), 94.5 (C1'), 93.3 (C1''), 93.0 (C8'), 83.4 (C5), 79.2 (C3'''), 77.14 (C4'''), 75.5 (C4), 72.8 (C2'''), 72.33 (C6), 70.3 (C2''), 69.9 (C5''), 69.6 (C5'), 68.8 (C3''), 66.06 (C4'), 66.03 (*C*H$_2$O), 62.8 (C6'), 60.4 (C6''), 59.7 (C7'), 52.1 (C4''), 50.3 (C1), 48.9 (C3), 47.9 (C2'), 42.2 (C5'''), 39.3 (*C*H$_2$CH$_2$O), 30.2 (N-CH$_3$), 29.3 (C2), 27.5 (C3'), 22.98 (H$_3$*C*CO); ESI-HRMS: m/z calcd. for $C_{28}H_{56}N_7O_{14}$ $[M+H]^+$ 714.3885; found, 714.3868.

6,3',4',2'',3''',4'''-Hexa-*O*-acetyl -5''-carboxy-1,3,2',6',2''',6'''-hexadesamino-1,3,2',6',2''',6'''-hexatrifluoroacetamidoneomycin (95). To a stirred solution of **94** (1.13 g, 0.95 mmol) in pyridine (9.5 mL) was added trityl chloride (560 mg, 1.9 mmol). Additional trityl chloride (2.04 g, 7.3 mmol) was added over the course of the reaction as progress slowed. After 52 h, Ac_2O (5 mL) and DMAP (30 mg, 0.25 mmol) were added. After 16 h, the reaction was quenched with H_2O,

diluted with EtOAc, and washed with 1 N HCl, saturated aqueous $NaHCO_3$, and brine. The organic layer was dried over Na_2SO_4 and concentrated to dryness, after which the crude product was purified through silica gel chromatography (0-10% MeOH in DCM). The resulting solid (1.31 g) was dissolved in DCM (14 mL) and $FeCl_3{\cdot}6H_2O$ (418 mg, 1.55 mmol) was added. After 2 h, the reaction was diluted with EtOAc and washed with water. The organic layer was dried over Na_2SO_4 and concentrated to dryness, after which the crude product was purified through silica gel chromatography (0-10% MeOH in DCM). A portion (246 mg) of the resulting solid (624 mg) was dissolved in MeCN:H_2O (1.7 mL, 1:1) and cooled to 0 °C, after which $NaHCO_3$ (28 mg, 0.33 mmol), BAIB (150 mg, 0.47 mmol) and TEMPO (14 mg, 0.09 mmol) were added. After 3 h, the reaction mixture was cooled to 0 °C and quenched with saturated aqueous $Na_2S_2O_3$. The reaction mixture was diluted with EtOAc and washed with brine, after which the organic layer was dried over Na_2SO_4 and concentrated to dryness. The crude product was purified via silica gel chromatography (0-20% MeOH in DCM, R_f = 0.1 in 6% MeOH in DCM) to give **95** (181 mg, 33% over four steps) as a white solid. $[\alpha]_D^{23}$ = +9.3 (*c* = 1.0, EtOAc); ^{1}H NMR (900 MHz, MeOD) δ 6.45 (s, 1H, H1'), 5.43 (d, *J* = 5.2 Hz, 1H, H1''), 5.20 (dd, *J* = 11.0, 9.2 Hz, 1H, H3'), 5.02 – 5.00 (m, 2H, H1''', H3'''), 5.00 – 4.98 (m, 1H, H6), 4.88 – 4.84 (m, 2H, H4', H4'''), 4.82 – 4.80 (m, 1H, H2''), 4.57 (dd, *J* = 4.6, 2.9 Hz, 1H, H3''), 4.54 (d, *J* = 2.9 Hz, 1H, H4''), 4.31 (dd, *J* = 11.0, 3.9 Hz, 1H, H2'), 4.26 – 4.22 (m, 2H, H3, H5'''), 4.22 – 4.20 (m, 1H, H2'''), 4.18 (ddd, *J* = 12.6, 10.5, 4.4 Hz, 1H, H1), 4.10 (t, *J* = 8.8 Hz, 1H, H5), 4.02 (dt, *J* = 10.3, 3.4 Hz, 1H, H5'), 3.90 (dd, *J* = 10.2, 8.4 Hz, 1H, H4), 3.77 (dd, *J* = 14.6, 3.7 Hz, 1H, H6'a), 3.65 (dd, *J* = 13.9, 5.9 Hz, 1H, H6'''a), 3.44 – 3.38 (m, 2H, H6'b, H6'''b), 2.16 (s, 3H, CH_3CO), 2.14 (s, 3H, CH_3CO), 2.10 (s, 3H, CH_3CO), 2.07 (s, 3H, CH_3CO), 2.03 (q, *J* = 13.0 Hz, 1H, H2ax), 1.99 (s, 3H, CH_3CO), 1.97 (dt, *J* = 13.0, 4.5 Hz, 1H, H2eq), 1.93 (s, 3H, CH_3CO); ^{13}C NMR (226 MHz, MeOD) δ 172.1 (C5''), 170.6 ($CH_3\mathit{C}O$), 170.4 ($CH_3\mathit{C}O$), 170.3 ($CH_3\mathit{C}O$), 169.9 ($CH_3\mathit{C}O$), 169.2 ($CH_3\mathit{C}O$), 168.7 ($CH_3\mathit{C}O$), 162.2 – 153.8 (m, $CF_3\mathit{C}O$), 118.4 – 113.8 (m, $\mathit{C}F_3CO$), 107.1

(C1’’), 98.0 (C1’’’), 95.2 (C1’), 83.5 (C5), 80.9 (C4’’), 79.1 (C3’’), 75.8 (C4), 75.5 (C6), 75.0 (C2’’’), 71.6 (C5’’’), 70.6 (C3’), 68.7 (C4’), 68.0 (C3’’’), 67.6 (C5’), 65.6 (C4’’’), 51.4 (C2’), 49.0 (C3), 48.22 (C1), 48.15 (C2’’’), 39.2 (C6’’’), 38.8 (C6’), 30.6 (C2), 19.9 (*C*H_3CO), 19.2 (*C*H_3CO), 19.12 (*C*H_3CO), 19.09 (*C*H_3CO), 19.07 (*C*H_3CO), 19.0 (*C*H_3CO). ESI-HRMS: *m/z* calc for $C_{47}H_{50}N_6O_{26}F_{18}Na$ $[M+Na]^+$ 1479.23795, found 1479.2375.

6,3’,4’,2’’,3’’’,4’’’-Hexa-*O*-acetyl -1,3,2’,6’,2’’’,6’’’-hexadesamino-4’’-deshydroxymethyl-1,3,2’,6’,2’’’,6’’’-hexatrifluoroacetamidoneomycin (96). To a stirred solution of **95** (505 mg, 0.35 mmol) in THF (3.4 mL) at 0 °C covered in foil was added Et_3N (0.06 mL, 0.42 mmol) followed by 1-oxa-2-oxo-3-thiaindolizinium chloride (132 mg, 0.69 mmol). After 40 mins, *tert*-dodecyl thiol (0.41 mL, 1.99 mmol) was added and the reaction was exposed to white light. After 1 h, the reaction was diluted with EtOAc and washed with saturated $NaHCO_3$ and brine. The organic layer was dried over Na_2SO_4 and concentrated to dryness. The crude product was purified via silica gel chromatography (25-70% EtOAc in hexanes, R_f = 0.6 in 6% MeOH in DCM) to give **96** (205 mg, 42%) as an off-white solid. $[\alpha]_D^{23}$ = +16.9 (*c* = 1.0, EtOAc); ^{1}H NMR (900 MHz, MeOD) δ 5.65 (d, *J* = 3.8 Hz, 1H, H1’), 5.29 (d, *J* = 3.4 Hz, 1H, H1’’), 5.24 (dd, *J* = 11.0, 9.1 Hz, 1H, H3’), 5.03 – 4.97 (m, 2H, H6, H3’’’), 4.93 (dd, *J* = 10.2, 9.2 Hz, 1H, H4’), 4.91 (d, *J* = 2.0 Hz, 1H, H1’’’), 4.86 – 4.84 (m, 1H, H4’’’), 4.83 (dd, *J* = 5.2, 3.4 Hz, 1H, H2’’), 4.51 (q, *J* = 5.4 Hz, 1H, H3’’), 4.41 (dd, *J* = 10.9, 3.8 Hz, 1H, H2’), 4.30 – 4.24 (m, 1H, H3), 4.22 (td, *J* = 6.8, 1.7 Hz, 1H, H5’’’), 4.20 – 4.17 (m, 1H, H1), 4.17 – 4.15 (m, 1H, H2’’’), 4.10 – 4.07 (m, 3H, H5, H4’’a, H5’), 3.83 (dd, *J* = 10.2, 8.7 Hz, 1H, H4), 3.77 (dd, *J* = 10.0, 5.0 Hz, 1H, H4’’b), 3.63 (dd, *J* = 14.7, 4.1 Hz, 1H, H6’a), 3.53 – 3.48 (m, 3H, H6’b, H6’’’), 2.16 (s, 3H, CH_3CO), 2.13 (s, 3H, CH_3CO), 2.10 (s, 3H, CH_3CO), 2.06 (s, 3H, CH_3CO), 2.01 (s, 3H, CH_3CO), 2.01 – 1.97 (m, 2H, H2), 1.96 (s, 3H, CH_3CO); ^{13}C NMR (226 MHz, MeOD) δ 170.6 (CH_3*C*O), 170.3 (CH_3*C*O), 170.2 (CH_3*C*O), 169.9 (CH_3*C*O), 169.3 (CH_3*C*O), 168.7 (CH_3*C*O), 158.4 – 156.8 (m, CF_3*C*O), 118.4 – 113.8 (m, *C*F_3CO),

107.3 (C1’’), 97.7 (C1’’’), 95.7 (C1’), 82.3 (C5), 76.8 (C4), 75.7 (C3’’), 75.4 (C2’’), 74.9 (C6), 71.7 (C5’’’), 70.3 (C4’’), 70.2 (C3’), 69.1 (C4’), 68.1 (C3’’’), 67.9 (C5’), 65.8 (C4’’’), 51.6 (C2’), 48.9 (C3), 48.2 (C1), 48.1 (C2’’’), 39.2 (C6’), 39.1 (C6’’’), 30.9 (C2), 19.6 (*C*H_3CO), 19.2 (*C*H_3-CO), 19.1 (*C*H_3CO), 19.1 (*C*H_3CO), 19.0 (*C*H_3CO). ESI-HRMS: *m/z* calc for $C_{46}H_{50}N_6O_{24}F_{18}Na$ $[M+Na]^+$ 1435.24812, found 1435.2456.

4’’-Deshydroxymethylneomomycin hexaacetate salt (83). To a stirred solution of **96** (83 mg, 0.059 mmol) in MeOH (0.6 mL) was added $Mg(OMe)_2$ solution (0.6 mL, 6-10% by wt). After 17 h, the reaction was concentrated to dryness and redissolved in 0.5 mL dioxane and 0.5 mL 1 N NaOH. After 6 h, the reaction mixture was neutralized with AcOH and concentrated to dryness. The crude product was passed through a CM Sephadex C25 column, loading in 10% aqueous acetic acid and eluting with a gradient of 0.2-1.2% ammonium hydroxide in deionized water. The product-containing fractions were lyophilized in vacuo with glacial acetic acid to generate the peracetate salt of **83** (30.7 mg, 55% over 3 steps); $[\alpha]_D^{23}$ = +16.1 (*c* = 0.4, H_2O); ^{1}H NMR (600 MHz, D_2O) δ 5.81 (d, *J* = 4.0 Hz, 1H, H1’), 5.37 (d, *J* = 4.2 Hz, 1H, H1’’), 5.25 (d, *J* = 1.8 Hz, 1H, H1’’’), 4.57 (td, *J* = 4.9, 3.5 Hz, 1H, H3’’), 4.30 (m, 2H, H4’’a, H2’’), 4.24 (ddd, *J* = 6.4, 4.1, 1.5 Hz, 1H, H5’’’), 4.16 (t, *J* = 3.2 Hz, 1H, H3’’’), 4.00 (dd, *J* = 10.1, 3.5 Hz, 1H, H4’’b), 3.96 (ddd, *J* = 10.3, 7.2, 3.5 Hz, 1H, H5’), 3.88 (dd, *J* = 10.7, 9.0 Hz, 1H ,H3’), 3.79 (t, *J* = 9.0 Hz, 1H, H5), 3.77 – 3.71 (m, 2H, H4’’’, H4), 3.60 (dd, *J* = 10.6, 8.9 Hz, 1H, H6), 3.53 (dt, *J* = 3.1, 1.3 Hz, 1H, H2’’’), 3.43 – 3.27 (m, 5H, H6’’’, H6’a, H2’, H4’), 3.26 – 3.15 (m, 3H, H6’b, H3, H1), 2.26 (dt, *J* = 12.7, 4.3 Hz, 1H, H2eq), 1.85 (s, 18H, CH_3CO), 1.61 (q, *J* = 12.6 Hz, 1H, H2ax); ^{13}C NMR (151 MHz, D_2O) δ 181.1 (CH_3*C*O), 109.6 (C1’’), 96.3 (C1’’’), 95.3 (C1’), 84.7 (C5), 78.3 (C4), 77.4 (C3’’), 74.8 (C2’’), 73.0 (C6), 70.7 (C4’), 70.6 (C4’’), 70.2 (C5’’’), 69.1 (C5’), 69.0 (C3’), 67.6 (C3’’’), 67.3 (C4’’’), 53.5 (C2’), 50.9 (C2’’’), 50.0 (C1), 48.8 (C3), 40.3 (C6’’’), 40.1 (C6’),

30.2 (C2), 23.1 (*C*CH_3CO); ESI-HRMS: *m/z* calc for $C_{22}H_{44}N_6O_{12}Na$ $[M+Na]^+$ 607.29094, found 607.2903.

1,3,2',6',2''',6'''-Hexaazido-1,3,2',6',2''',6'''-hexadesamino-5"-*O*-(2,4,6-triisopropylbenzenesulfonyl)-neomycin (**98**). To a stirred solution of **97** (1.93 g, 2.50 mmol) in pyridine (11 mL) was added trisyl chloride (1.35 g, 4.45 mmol). Additional trisyl chloride (0.63 g, 2.08 mmol) was added as reaction progress was sluggish. After 40h, the reaction was quenched with water and diluted with EtOAc. The organic layer was washed with 1 N HCl, saturated $NaHCO_3$, and brine, dried over Na_2SO_4, and evaporated to dryness. The crude mixture was purified via flash chromatography (0-20% MeOH in DCM, R_f = 0.4 in 10% MeOH/DCM) to give the desired product **98** (1.58 g, 61%) as an off-white solid. $[\alpha]_D^{23}$ = +67.3 (*c* = 1.0, MeOH); ^{1}H NMR (900 MHz, MeOD) δ 7.30 (s, 2H, Ar), 5.99 (d, *J* = 3.9 Hz, 1H, H1'), 5.41 (d, *J* = 1.8 Hz, 1H, H1''), 5.07 (d, *J* = 1.8 Hz, 1H, H1'''), 4.34 (dd, *J* = 4.4, 1.8 Hz, 1H, H2''), 4.33 – 4.31 (m, 1H, H3''), 4.31 – 4.27 (m, 2H, H4'', H5''a), 4.25 (dd, *J* = 10.8, 8.0 Hz, 1H, H5''b), 4.19 (p, *J* = 6.9 Hz, 2H, C*H*$(CH_3)_2$), 4.16 (ddd, *J* = 9.3, 6.4, 2.3 Hz, 1H, H5'), 3.98 (ddd, *J* = 8.4, 4.7, 2.0 Hz, 1H, H5'''), 3.91 (t, *J* = 3.4 Hz, 1H, H3'''), 3.89 (dd, *J* = 10.5, 8.9 Hz, 1H, H3'), 3.69 (t, *J* = 8.9 Hz, 1H, H5), 3.65 – 3.62 (m, 2H, H4, H2'''), 3.56 (ddd, *J* = 12.4, 9.9, 4.5 Hz, 1H, H3), 3.53 – 3.43 (m, 4H, H1, H6'a, H6'b, H6'''a), 3.41 (t, *J* = 2.6 Hz, 1H, H4'''), 3.39 – 3.34 (m, 3H, H2', H4', H6), 3.28 (dd, *J* = 12.9, 4.7 Hz, 1H, H6'''b), 2.97 (p, *J* = 6.9 Hz, 1H, C*H*$(CH_3)_2$), 2.23 (dt, *J* = 12.9, 4.5 Hz, 1H, H2eq), 1.36 (q, *J* = 12.6 Hz, 1H, H2ax), 1.31 (s, 3H, CH(C*H*$_3)_2$), 1.30 (s, 3H, CH(C*H*$_3)_2$), 1.30 – 1.29 (m, 6H, CH(C*H*$_3)_2$), 1.29 – 1.29 (m, 6H, CH(C*H*$_3)_2$); ^{13}C NMR (226 MHz, MeOD) δ 154.0 (Ar), 150.9 (Ar), 128.9 (Ar), 128.5 (Ar), 127.8 (Ar), 123.7 (Ar), 110.3 (C1''), 98.3 (C1'''), 96.0 (C1'), 84.4 (C5), 78.9 (C4''), 76.6 (C6), 76.3 (C3''), 75.7 (C4), 74.1 (C5'''), 73.0 (C2''), 71.9 (C5'), 71.4 (C4'), 71.2 (C3'), 70.9 (C5''), 69.6 (C3'''), 68.1 (C4'''), 63.2 (C2'), 60.5 (C1), 60.2

(C2’’’), 60.0 (C3), 51.4 (C6’), 50.8 (C6’’’), 34.1 (*C*H(CH$_3$)$_2$), 31.7 (C2), 29.4 (*C*H(CH$_3$)$_2$), 23.8 (CH(*C*H$_3$)$_2$), 22.5 (CH(*C*H$_3$)$_2$). ESI-HRMS: *m/z* calc for $C_{38}H_{56}N_{18}O_{15}SNa$ $[M+Na]^+$ 1059.37854, found 1059.3806.

1,3,2’,6’,2’’’,6’’’-Hexaazido-1,3,2’,6’,2’’’,6’’’-hexadesamino-5”-deoxy-5’’-iodoneomycin (**99**). To a stirred solution of **98** (372 mg, 0.36 mmol) in DMF (2.8 mL) was added NaI (593 mg, 3.96 mmol) and the temperature was raised to 80 °C. After 45 h, the reaction was diluted with EtOAc and washed with water. The aqueous layer was washed twice with EtOAc and the combined organic layers were washed with brine, dried over Na_2SO_4, and concentrated to dryness. The crude solid was purified via flash chromatography (0-10% MeOH in DCM, R_f = 0.2 in 6% MeOH in DCM) to give the desired compound **99** (234 mg, 76%) as a white solid. $[\alpha]_D^{23}$ = +123.1 (*c* = 0.78, MeOH); ^{1}H NMR (900 MHz, MeOD) δ 6.14 (d, *J* = 3.9 Hz, 1H, H1’), 5.36 (d, *J* = 1.9 Hz, 1H, H1’’), 5.12 (d, *J* = 1.8 Hz, 1H, H1’’’), 4.43 (dd, *J* = 4.6, 2.0 Hz, 1H, H2’’), 4.25 (dd, *J* = 6.6, 4.6 Hz, 1H, H3’’), 4.17 – 4.12 (m, 2H, H4’’, H5’), 4.04 (ddd, *J* = 8.6, 4.4, 1.9 Hz, 1H, H5’’’), 3.96 (t, *J* = 3.3 Hz, 1H, H3’’’), 3.90 (dd, *J* = 10.4, 8.8 Hz, 1H, H3’), 3.71 – 3.68 (m, 3H, H5, H2’’’, H6’’’a), 3.66 (dd, *J* = 10.7, 2.9 Hz, 1H, H5’’a), 3.63 (dd, *J* = 9.9, 8.8 Hz, 1H, H4), 3.59 – 3.55 (m, 1H, H3), 3.53 (dd, *J* = 13.2, 2.3 Hz, 1H, H6’’’b), 3.48 – 3.43 (m, 2H, H1, H4’’’), 3.43 – 3.40 (m, 2H, H6’), 3.39 – 3.34 (m, 4H, H5’’b, H2’, H4’, H6), 2.23 (dt, *J* = 12.9, 4.4 Hz, 1H, H2eq), 1.36 (q, *J* = 12.6 Hz, 1H, H2ax); ^{13}C NMR (226 MHz, MeOD) δ 110.2 (C1’’), 98.6 (C1’’’), 95.9 (C1’), 85.2 (C5), 81.1 (C4’’), 79.7 (C3’’), 76.8 (C6), 75.7 (C4), 74.3 (C5’’’), 74.3 (C2’’’), 71.9 (C5’), 71.4 (C4’), 71.3 (C3’), 70.0 (C3’’’), 68.3 (C4’’’), 63.6 (C2’), 60.6 (C2’’’), 60.4 (C1), 60.1 (C3), 51.3 (C6’), 51.2 (C6’’’), 31.8 (C2), 6.9 (C5’’); ESI-HRMS: *m/z* calc for $C_{23}H_{33}N_{18}O_{12}INa$ $[M+Na]^+$ 903.14622, found 903.1454.

5’’-Deoxyneomycin hexaacetate salt (58). To a stirred solution of **99** (55 mg, 0.062 mmol) in dioxane/water (1:1, 2.4 mL) was added Pd on carbon (109 mg). The reaction was purged with H_2 and pressurized to 50 psi. After 17 h, the reaction was filtered through Celite and concentrated to dryness. The crude product was passed through a CM Sephadex C25 column, loading in 10% aqueous acetic acid and eluting with a gradient of 0.1-1.2% ammonium hydroxide in deionized water. The product-containing fractions were lyophilized in vacuo with glacial acetic acid to generate the peracetate salt of **58** (19.5 mg, 33%) as a white solid. $[\alpha]_D^{23}$ = +39.2 (*c* = 0.27, H_2O); ^{1}H NMR (900 MHz, D_2O) δ 5.83 (d, *J* = 4.0 Hz, 1H, H1’), 5.27 (d, *J* = 3.4 Hz, 1H, H1’’), 5.21 (d, *J* = 1.8 Hz, 1H, H1’’’), 4.30 (t, *J* = 4.1 Hz, 1H, H2’’), 4.27 – 4.22 (m, 1H, H5’’’), 4.18 (m, 2H, H4’’, H3’’), 4.15 (t, *J* = 3.2 Hz, 1H, H3’’’), 3.97 (ddd, *J* = 10.4, 7.4, 3.5 Hz, 1H, H5’), 3.85 (dd, *J* = 10.7, 9.1 Hz, 1H, H3’), 3.78 – 3.72 (m, 2H, H5, H4’’’), 3.64 (t, *J* = 9.5 Hz, 1H, H4), 3.55 (t, *J* = 9.8 Hz, 1H, H6), 3.50 (t, *J* = 2.1 Hz, 1H, H2’’’), 3.40 – 3.33 (m, 4H, H2’, H4’, H6’’’a, H6’a), 3.31 (dd, *J* = 13.7, 4.2 Hz, 1H, H6’’’b), 3.22 – 3.18 (m, 1H, H1), 3.18 (s, 1H, H6’b), 3.09 (ddd, *J* = 13.5, 9.9, 4.2 Hz, 1H, H3), 2.20 (dt, *J* = 12.8, 4.3 Hz, 1H, H2eq), 1.85 (s, 18H, CH_3CO), 1.53 (q, *J* = 12.6 Hz, 1H, H2eq), 1.33 (d, *J* = 6.0 Hz, 3H, H5’’); ^{13}C NMR (226 MHz, D_2O) δ 181.0 ($CH_3\mathit{C}O$), 110.2 (C1’’), 95.8 (C1’’’), 95.4 (C1’), 85.4 (C5), 80.7 (C3’’), 79.3 (C4), 78.1 (C4’’), 73.5 (C2’’), 73.1 (C6), 70.8 (C4’), 70.1 (C5’’’), 69.1 (C3’), 69.0 (C5’), 67.7 (C3’’’), 67.5 (C4’’’), 53.6 (C2’), 51.0 (C2’’’), 50.3 (C1), 48.9 (C3), 40.4 (C6’), 40.2 (C6’’’), 30.9 (C2), 23.0 ($\mathit{C}H_3CO$), 18.4 (C5’’). ESI-HRMS: *m/z* calc for $C_{23}H_{46}N_6O_{12}Na$ $[M+Na]^+$ 621.30659, found 621.3065.

1,3,2’,6’,2’’’,6’’’-Hexaazido-1,3,2’,6’,2’’’,6’’’-hexadesamino-5”-deoxy-5’’-pthtalimidoneomycin (**100).** To a stirred solution of **98** (562 mg, 0.54 mmol) in DMF (5.4 mL) was added 18-crown-6 (2.87 g, 10.9 mmol) and potassium phthalimide (1.069 g, 5.77 mmol) and the temperature was raised to 95 °C. After 41 h, the reaction was diluted with EtOAc and washed

with water. The aqueous layer was washed twice with EtOAc and the combined organic layer was washed with brine, dried over Na_2SO_4, and concentrated to dryness. The crude solid was purified via flash chromatography (0-10% MeOH in DCM, R_f = 0.2 in 6% MeOH in DCM) to give the desired compound **100** (243 mg, 50%) as a pale yellow solid. $[\alpha]_D^{23}$ = +75.8 (*c* = 1.0, MeOH); ^{1}H NMR (900 MHz, MeOD) δ 7.95 – 7.89 (m, 2H, Ar), 7.82 (m, 2H, Ar), 5.71 (d, *J* = 3.9 Hz, 1H, H1'), 5.34 (d, *J* = 1.9 Hz, 1H, H1''), 5.14 (d, *J* = 1.8 Hz, 1H, H1'''), 4.53 (dd, *J* = 6.3, 4.6 Hz, 1H, H3''), 4.43 (q, *J* = 5.8 Hz, 1H, H4''), 4.36 (dd, *J* = 4.6, 1.9 Hz, 1H, H2''), 4.20 (ddd, *J* = 9.9, 6.0, 2.3 Hz, 1H, H5'), 4.11 (dd, *J* = 14.2, 5.5 Hz, 1H, H5''a), 4.08 (dd, *J* = 14.2, 5.8 Hz, 1H, H5''b), 4.03 (ddd, *J* = 7.6, 5.3, 1.9 Hz, 1H, H5'''), 3.94 (t, *J* = 3.5 Hz, 1H, H3'''), 3.80 (dd, *J* = 10.5, 8.9 Hz, 1H, H3'), 3.69 – 3.64 (m, 2H, H2''', H6'''a), 3.58 (dd, *J* = 13.2, 2.3 Hz, 1H, H6'a), 3.54 (t, *J* = 9.1 Hz, 1H, H5), 3.51 – 3.46 (m, 3H, H3, H6'b, H6'''b), 3.44 (t, *J* = 2.6 Hz, 1H, H4'''), 3.39 – 3.35 (m, 2H, H1, H4'), 3.32 – 3.29 (m, 1H, H4), 3.24 (dd, *J* = 10.4, 3.9 Hz, 1H, H2'), 3.03 (t, *J* = 9.5 Hz, 1H, H6), 2.20 (dt, *J* = 12.8, 4.5 Hz, 1H, H2eq), 1.24 (q, *J* = 12.5 Hz, 1H, H2ax); ^{13}C NMR (226 MHz, MeOD) δ 168.6 (NCO), 133.9 (Ar), 132.2 (Ar), 123.0 (Ar), 109.5 (C1''), 98.5 (C1'''), 96.8 (C1'), 83.0 (C5), 78.9 (C4''), 78.4 (C3''), 76.6 (C4), 75.9 (C6), 73.8 (C5'''), 73.2 (C2''), 71.7 (C5'), 71.4 (C4'), 71.3 (C3'), 69.6 (C3'''), 68.3 (C4'''), 63.7 (C2'), 60.8 (C2'''), 60.6 (C1), 59.5 (C3), 51.5 (C6'), 50.9 (C6'''), 39.7 (C5''), 31.5 (C2); ESI-HRMS: *m/z* calc for $C_{31}H_{37}N_{19}O_{14}Na$ $[M+Na]^+$ 922.26596, found 922.2670.

5''-Amino-1,3,2',6',2''',6'''-hexaazido-1,3,2',6',2''',6'''-hexadesamino-5"-deoxyneomycin (101). To a stirred solution of **100** (217 mg, 0.24 mmol) in MeOH (2.4 mL) was added hydrazine hydrate (0.2 mL). After 3 h, the reaction was concentrated to dryness and purified via flash chromatography (0-40% MeOH in DCM, R_f = 0.18 in 40% MeOH in DCM) to give the desired compound **101** (136 mg, 73%) as a pale yellow solid. $[\alpha]_D^{23}$ = +103.5 (*c* = 0.45, MeOH);

^{1}H NMR (600 MHz, MeOD) δ 5.81 (d, *J* = 3.8 Hz, 1H, H1'), 5.40 (d, *J* = 1.2 Hz, 1H, H1''), 5.14 (d, *J* = 1.8 Hz, 1H, H1'''), 4.39 – 4.35 (m, 2H, H2'', H3''), 4.21 (ddd, *J* = 10.0, 5.8, 2.4 Hz, 1H, H5'), 4.11 (td, *J* = 7.1, 3.8 Hz, 1H, H4''), 4.06 (ddd, *J* = 8.8, 4.1, 1.9 Hz, 1H, H5'''), 3.97 (t, *J* = 3.3 Hz, 1H, H3'''), 3.93 (dd, *J* = 10.5, 8.8 Hz, 1H, H3'), 3.73 – 3.68 (m, 3H, H5, H2''', H6'''a), 3.63 (dd, *J* = 9.9, 8.9 Hz, 1H, H4), 3.59 – 3.51 (m, 2H, H3, H6'''b), 3.49 – 3.44 (m, 3H, H4''', H1, H6'a), 3.43 – 3.38 (m, 1H, H6), 3.38 – 3.34 (m, 2H, H4', H6'), 3.08 – 3.00 (m, 2H, H5''a, H2'), 2.87 (dd, *J* = 13.4, 7.4 Hz, 1H, H5''b), 2.26 (dt, *J* = 12.8, 4.4 Hz, 1H, H2eq), 1.40 (q, *J* = 12.4 Hz, 1H, H2ax); ^{13}C NMR (151 MHz, MeOD) δ 109.4 (C1''), 98.1 (C1'), 97.1 (C1'''), 83.9 (C5), 80.9 (C4''), 77.0 (C3''), 76.3 (C4, C6), 74.5 (C5'''), 73.5 (C2''), 71.9 (C5'), 71.3 (C4'), 70.4 (C3'), 69.8 (C3'''), 68.2 (C4'''), 62.8 (C2'), 60.6 (C1'), 60.2 (C2'''), 59.8 (C3), 51.2 (C6', C6'''), 44.0 (C5''), 31.6 (C2); ESI-HRMS: *m/z* calc for $C_{23}H_{36}N_{19}O_{12}$ $[M+H]^+$ 770.27853, found 770.2783.

5''-Amino-5''-deoxyneomycin heptaacetate salt (72). To a stirred solution of **101** (17 mg, 0.022 mmol) in dioxane/water (1:1, 1.2 mL) was added $Pd(OH)_2$ on carbon. (32 mg). The reaction was purged with H_2 and pressurized to 50 psi. After 26 h, the reaction was filtered through Celite and concentrated to dryness. The crude product was passed through a CM Sephadex C25 column, loading in 10% aqueous acetic acid and eluting with a gradient of 0.1-1.2% ammonium hydroxide in deionized water. The product-containing fractions were lyophilized in vacuo with glacial acetic acid to generate the peracetate salt of **72** (15.7 mg, 70%) as a white solid. $[\alpha]_D^{23}$ = +22.8 (*c* = 0.25, H_2O); ^{1}H NMR (600 MHz, D_2O) δ 5.70 (d, *J* = 3.7 Hz, 1H, H1'), 5.40 (d, *J* = 2.9 Hz, 1H, H1''), 5.25 (d, *J* = 1.8 Hz, 1H, H1'''), 4.43 (t, *J* = 5.7 Hz, 1H, H3''), 4.33 (dd, *J* = 5.3, 3.0 Hz, 1H, H2''), 4.25 (m, 2H, H4'', H5'''), 4.17 (t, *J* = 3.1 Hz, 1H, H3'''), 3.96 (ddd, *J* = 10.2, 7.0, 3.6 Hz, 1H, H5'), 3.87 (t, *J* = 9.2 Hz, 1H, H5), 3.82 – 3.76 (m, 3H, H4''', H3', H4), 3.64 (dd, *J* =

10.5, 9.2 Hz, 1H, H6), 3.53 (p, *J* = 1.3 Hz, 1H, H2’’’), 3.42 – 3.31 (m, 5H, H5’’a, H6’a, H6’’’, H4’), 3.27 – 3.18 (m, 2H), 3.17 – 3.12 (m, 2H, H2’, H5’’), 2.25 (dt, *J* = 12.7, 4.2 Hz, 1H, H2eq), 1.87 (s, 21H, CH_3CO), 1.60 (q, *J* = 12.6 Hz, 1H, H2ax); ^{13}C NMR (151 MHz, D_2O) δ 180.9 (CH_3CO), 108.6 (C1’’), 95.9 (C1’), 95.7 (C1’’’), 83.5 (C5), 77.7 (C4’’), 77.6 (C4), 77.2 (C3’’), 73.2 (C2’’), 72.5 (C6), 70.8 (C4’), 70.25 (C5’’’), 70.16 (C3’), 69.4 (C5’), 67.7 (C3’’’), 67.5 (C4’’’), 53.9 (C2’), 50.8 (C2’’’), 50.4 (C3), 49.1 (C1), 41.7 (C5’’), 40.4 (C6’’’), 40.2 (C6’), 30.2 (CH_3CO), 22.9 (C2); ESI-HRMS: *m/z* calc for $C_{23}H_{47}N_7O_{12}Na$ $[M+Na]^+$ 636.31749, found 636.3177.

5’’-Formamido-5’’-deoxyneomycin hexaacetate salt (84). To a stirred solution of **101** (29 mg, 0.035 mmol) in THF (1 mL) and Et_3N (0.19 mL, 1.33 mmol) was added acetic anhydride (0.04 mL, 0.4 mmol). After 1.5 h, the reaction was concentrated to dryness. The crude product was traken up in methanol (1.5 mL) and saturated aqueous $NaHCO_3$ (0.4 mL) was added. After 3 h, the reaction was concentrated to dryness, redissolved in EtOAc and washed with water, followed by concentration of the organic layer to dryness and coevaporation of the crude product three times with toluene. The crude product was taken up in dioxane:water (1:1, 1 mL) and $Pd(OH)_2$ on carbon (65 mg) was added. The reaction mixture was stirred under H_2 at 50 psi for 17h, filtered through Celite, and concentrated to dryness. The crude product was passed through a CM Sephadex C25 column, loading in 10% aqueous acetic acid and eluting with a gradient of 0.2-1.2% ammonium hydroxide in deionized water. The product-containing fractions were lyophilized in vacuo with glacial acetic acid to generate the peracetate salt of **84** (15.6 mg, 41% over 3 steps) as a white solid. $[\alpha]_D^{23}$ = +32.0 (*c* = 0.20, H_2O); ^1H NMR (900 MHz, D_2O) δ 8.09 (s, 1H, CHO), 5.72 (d, *J* = 3.8 Hz, 1H, H1’), 5.28 (d, *J* = 3.7 Hz, 1H, H1’’), 5.21 (d, *J* = 1.7 Hz, 1H, H1’’’), 4.34 (td, *J* = 5.3, 1.3 Hz, 1H, H3’’), 4.26 – 4.22 (m, 2H, H2’’, H5’’’), 4.19 (q, *J* = 5.3 Hz, 1H, H4’’), 4.15 (t, *J* = 3.0

Hz, 1H, H3’’’), 3.98 (ddd, *J* = 10.3, 7.3, 3.4 Hz, 1H, H5’), 3.82 (dd, *J* = 10.6, 9.0 Hz, 1H, H3’), 3.79 – 3.73 (m, 2H, H5, H4’’’), 3.66 (t, *J* = 9.4 Hz, 1H, H4), 3.60 (dd, *J* = 14.5, 4.2 Hz, 1H, H5’’a), 3.57 (dd, *J* = 10.6, 9.0 Hz, 1H, H6), 3.50 (dt, *J* = 2.8, 1.4 Hz, 1H, H2’’’), 3.44 (dd, *J* = 14.5, 6.3 Hz, 1H, H5’’b), 3.41 – 3.34 (m, 3H, H4, H6’a, H6’’’a), 3.31 (ddd, *J* = 13.7, 4.0, 1.4 Hz, 1H, H6’’’b), 3.27 (dd, *J* = 10.7, 3.9 Hz, 1H, H2’), 3.21 – 3.17 (m, 2H, H1, H6’b), 3.09 (ddd, *J* = 12.1, 9.9, 4.3 Hz, 1H, H3), 2.19 (dt, *J* = 12.8, 4.3 Hz, 1H, H2eq), 1.84 (s, 18H, CH_3CO) 1.53 (q, *J* = 12.6 Hz, 1H, H2ax); ^{13}C NMR (226 MHz, D_2O) δ 181.2 (CH_3CO), 165.0 (CHO), 109.6 (C1’’), 95.9 (C1’’’), 95.5 (C1’), 85.2 (C5), 80.0 (C4’’), 79.2 (C4), 77.2 (C3’’), 73.2 (C2’), 73.0 (C6), 70.8 (C4’), 70.2 (C5’’’), 69.4 (C3’), 69.1 (C5’), 67.7 (C3’’’), 67.4 (C4’’’), 53.8 (C2’), 50.8 (C2’’’), 50.2 (C1), 48.9 (C3), 40.5 (C6’), 40.1 (C6’’’), 39.8 (C5’’), 30.9 (C2), 23.1 (CH_3CO). ESI-HRMS: *m/z* calc for $C_{24}H_{47}N_7O_{13}Na$ $[M+Na]^+$ 664.31241, found 664.3121.

5’’-Acetamido-5’’-deoxyneomycin hexaacetate salt (85). To a stirred solution of **101** (73 mg, 0.095 mmol) in THF (1 mL) and Et_3N (0.19 mL, 1.33 mmol) was added acetic anhydride (0.04 mL, 0.4 mmol). After 2h, the reaction was quenched with methanol and concentrated to dryness. The crude product was taken up in methanol (1.5 mL) and sodium methoxide (32 mg, 0.59 mmol) was added. After 30 mins, Amberlyst-15H was added and the solution was filtered and evaporated to dryness after coevaporation with toluene. The crude product was taken up in dioxane:water (1:1, 3 mL) and $Pd(OH)_2$ on carbon (166 mg) was added. The reaction mixture was stirred under H_2 at 50 psi for 14h, filtered through Celite, and concentrated to dryness. The crude product was passed through a CM Sephadex C25 column, loading in 10% aqueous acetic acid and eluting with a gradient of 0.2-1.2% ammonium hydroxide in deionized water. The product-containing fractions were lyophilized in vacuo with glacial acetic acid to generate the peracetate salt of **85** (23.2 mg, 24% over 3 steps) as a white solid. $[\alpha]_D^{23}$ = +41.1 (*c* = 0.61, H_2O); ^1H NMR (600 MHz, D_2O) δ

5.73 (d, *J* = 3.8 Hz, 1H, H1'), 5.30 (d, *J* = 3.7 Hz, 1H, H1''), 5.22 (d, *J* = 1.8 Hz, 1H, H1''), 4.34 (t, *J* = 5.3 Hz, 1H, H3''), 4.25 (m, 2H, H2'', H5'''), 4.18 (m, 2H, H4'', H3'''), 4.00 (ddd, *J* = 10.3, 7.2, 3.5 Hz, 1H, H5'), 3.84 (dd, *J* = 10.7, 9.0 Hz, 1H, H3'), 3.80 – 3.76 (m, 2H, H5, H4'''), 3.69 (t, *J* = 9.4 Hz, 1H, H4), 3.62 – 3.54 (m, 2H, H5''a, H6), 3.52 (dt, *J* = 3.0, 1.3 Hz, 1H, H2'''), 3.43 – 3.35 (m, 4H, H5''b, H4', H6'a, H6'''a), 3.32 (dd, *J* = 13.7, 4.1 Hz, 1H, H6'''b), 3.29 – 3.25 (m, 1H, H2'), 3.25 – 3.19 (m, 2H, H3, H6'b), 3.16 – 3.07 (m, 1H, H3), 2.22 (dt, *J* = 12.7, 4.2 Hz, 1H, H2eq), 1.98 (s, 3H, NHAc), 1.87 (s, 18H, CH_3CO) 1.56 (q, *J* = 12.6 Hz, 1H, H2ax); ^{13}C NMR (151 MHz, D_2O) δ 180.9 (CH_3CO) 174.7 (NHAc), 109.6 (C1''), 95.8 (C1'''), 95.5 (C1'), 85.2 (C5), 80.2 (C4''), 79.1 (C4), 77.5 (C3''), 73.3 (C2''), 73.0 (C6), 70.8 (C4'), 70.2 (C5'''), 69.3 (C3'), 69.1 (C5'), 67.7 (C3'''), 67.4 (C4'''), 53.9 (C2'), 50.9 (C2''), 50.2 (C1), 48.9 (C3), 41.4 (C5''), 40.5 (C6'''), 40.1 (C6'), 30.8 (C2), 22.9 (CH_3CO) 22.1 (NHAc). ESI-HRMS: *m/z* calc for $C_{25}H_{49}N_7O_{13}Na$ $[M+Na]^+$ 678.32806, found 678.3290.

6,3',2'',3''',4'''-Penta-*O*-acetyl -4',6'-*O*-benzylidene-5''-carboxy-1,3,2',2''',6'''-pentadesamino-1,3,2',2''',6'''-pentatrifluoroacetamidoparomomycin (103). To a stirred solution of **102** (1.23 g, 1.04 mmol) in pyridine (10 mL) was added trityl chloride (2.88 g, 10.4 mmol). After 40 h, Ac_2O (3 mL) and DMAP (31 mg, 0.25 mmol) were added. After 24 h, the reaction was quenched with H_2O, diluted with EtOAc, and washed with 1 N HCl, saturated aqueous $NaHCO_3$, and brine. The organic layer was dried over Na_2SO_4 and concentrated to dryness, after which the crude product was purified through silica gel chromatography (0-10% MeOH in DCM). A portion (661 mg) of the resulting solid (1.52 g) was dissolved in DCM (4 mL) and $FeCl_3 \cdot 6H_2O$ (219 mg, 0.81 mmol) was added. After 20 mins, the reaction was diluted with EtOAc and washed with water. The organic layer was dried over Na_2SO_4 and concentrated to dryness, after which the crude product was purified through silica gel chromatography (0-10% MeOH in DCM). The resulting solid (392 mg) was dissolved in DCM (2 mL) and cooled to 0 °C, after which 2 mL H_2O, BAIB (239 mg, 0.70 mmol) and TEMPO (9.5

mg, 0.06 mmol) were added. After 24 h, the reaction mixture was cooled to 0 °C and quenched with saturated aqueous $Na_2S_2O_3$. The reaction mixture was diluted with EtOAc and washed with brine, after which the organic layer was dried over Na_2SO_4 and concentrated to dryness. The crude product was purified via silica gel chromatography (0-10% MeOH in DCM, R_f = 0.3 in 10% MeOH in DCM) to give **103** (236 mg, 36% over four steps) as an off-white solid. $[\alpha]_D^{23}$ = -0.5 (*c* = 0.45, MeOH); ^{1}H NMR (600 MHz, MeOD) δ 7.43 (m, 2H, Ar), 7.38 – 7.29 (m, 3H, Ar), 6.30 (d, *J* = 4.1 Hz, 1H, H1'), 5.55 (s, 1H, Benzylidene), 5.41 (d, *J* = 4.9 Hz, 1H, H1''), 5.31 (t, *J* = 10.1 Hz, 1H, H3'), 5.03 – 5.00 (m, 2H, H1''', H3'''), 4.98 (dd, *J* = 10.6, 9.2 Hz, 1H, H6), 4.89 – 4.86 (m, 1H, H4'''), 4.81 (t, *J* = 4.7 Hz, 1H, H2'''), 4.58 (dd, *J* = 4.6, 3.2 Hz, 1H, H3''), 4.53 (d, *J* = 3.2 Hz, 1H, H4''), 4.37 (dd, *J* = 10.6, 4.2 Hz, 1H, H2'), 4.30 (dd, *J* = 10.2, 4.8 Hz, 1H, H6'a), 4.27 – 4.15 (m, 4H, H1, H3, H2''', H5'''), 4.12 (t, *J* = 8.8 Hz, 1H, H5), 3.92 (dd, *J* = 10.2, 8.3 Hz, 1H, H4), 3.86 (td, *J* = 9.8, 4.9 Hz, 1H, H5'), 3.79 – 3.71 (m, 2H, H6'b, H4'), 3.67 (dd, *J* = 13.9, 5.6 Hz, 1H, H6'''a), 3.43 – 3.38 (m, 1H, H6'''b), 2.15 (s, 3H, CH_3CO), 2.13 (s, 3H, CH_3CO), 2.10 (s, 3H, CH_3CO), 2.07 (s, 3H, CH_3CO), 2.05 – 1.99 (m, 1H, H2ax), 1.98 (s, 3H, CH_3CO), 1.91 (dt, *J* = 12.8, 4.3 Hz, 1H, H2eq); ^{13}C NMR (151 MHz, MeOD) δ 172.1 (C5''), 170.6 (CH_3CO), 170.6 (CH_3CO), 170.5 (CH_3CO), 169.2 (CH_3CO), 168.8 (CH_3CO), 158.4 – 156.4 (m, CF_3CO), 137.5 (Ar), 128.7 (Ar), 127.7 (Ar), 126.2 (Ar), 119.4 – 112.4 (m, CF_3CO), 107.3 (C1''), 101.7 (Benzylidene), 97.9 (C1'''), 96.3 (C1'), 83.8 (C5), 80.7 (C4''), 79.1 (C4'), 79.0 (C3''), 76.4 (C4), 75.6 (C6), 75.0 (C2'''), 71.7 (C5'''), 69.7 (C3'), 68.02 (C6'), 67.96 (C3'''), 65.6 (C4'''), 63.0 (C5'), 52.1 (C2'), 49.0 (C3), 48.2 (C1), 48.1 (C2'''), 39.3 (C6'''), 30.6 (C2), 19.9 (CH_3CO), 19.3 (CH_3CO), 19.2 (CH_3CO), 19.1 (CH_3CO), 19.0 (CH_3CO); ESI-HRMS: *m/z* calc for $C_{50}H_{52}N_5O_{25}F_{15}Na$ $[M+Na]^+$ 1430.26041, found 1430.2594.

6,3',2'',3''',4'''-Penta-*O*-acetyl -4',6'-*O*-benzylidene -1,3,2',2''',6'''-pentadesamino-4''-deshydroxymethyl -1,3,2',2''',6'''-pentatrifluoroacetamidoparomomycin (104). To a stirred

solution of **103** (282 mg, 0.20 mmol) in THF (2.3 mL) at 0 °C covered in foil was added Et_3N (0.04 mL, 0.32 mmol) followed by 1-oxa-2-oxo-3-thiaindolizinium chloride (82 mg, 0.43 mmol). After 1 h, *tert*-dodecyl thiol (0.34 mL, 1.4 mmol) was added and the reaction was exposed to white light. After 30 mins, the reaction was diluted with EtOAc and washed with saturated $NaHCO_3$ and brine. The organic layer was dried over Na_2SO_4 and concentrated to dryness. The crude product was purified via silica gel chromatography (30-70% EtOAc in hexanes, R_f = 0.35 in 50% EtOAc in hexanes) to give **104** (128 mg, 47%) as an off-white solid. $[\alpha]_D^{23}$ = +1.0 (*c* = 0.8, MeOH); ^{1}H NMR (900 MHz, MeOD) δ 7.43 (m, 2H, Ar), 7.38 – 7.32 (m, 3H, Ar), 5.58 (s, 1H, Benzylidene), 5.51 (d, *J* = 3.6 Hz, 1H, H1'), 5.34 (t, *J* = 10.1 Hz, 1H, H3'), 5.28 (d, *J* = 3.1 Hz, 1H, H1''), 5.01 – 4.99 (m, 1H, H6), 4.98 (t, *J* = 3.4 Hz, 1H, H3'''), 4.91 (d, *J* = 2.1 Hz, 1H, H1'''), 4.86 – 4.83 (m, 2H, H2'', H4'''), 4.52 (q, *J* = 5.8 Hz, 1H, H3''), 4.42 (dd, *J* = 10.6, 4.1 Hz, 1H, H2''), 4.32 (dd, *J* = 10.3, 5.0 Hz, 1H, H6'a), 4.27 – 4.17 (m, 3H, H5''', H1, H3), 4.14 (t, *J* = 2.5 Hz, 1H, H2'''), 4.13 – 4.11 (m, 1H, H4''a), 4.11 – 4.09 (m, 1H, H5), 3.91 (td, *J* = 9.9, 4.9 Hz, 1H, H5'), 3.83 (dd, *J* = 10.2, 8.8 Hz, 1H, H4), 3.80 (t, *J* = 9.7 Hz, 1H, H4'), 3.78 – 3.71 (m, 2H, H4''b, H6'b), 3.55 – 3.48 (m, 2H, H6'''), 2.17 (s, 3H, CH_3CO), 2.13 (s, 3H, CH_3CO), 2.10 (s, 3H, CH_3CO), 2.06 (s, 3H, CH_3-CO), 2.00 (s, 3H, CH_3CO), 1.99 – 1.96 (m, 2H, H2); ^{13}C NMR (226 MHz, MeOD) δ 170.7 (CH_3*C*O), 170.3 (CH_3*C*O), 169.3 (CH_3*C*O), 168.7 (CH_3*C*O), 158.3 – 156.9 (m, CF_3*C*O), 137.4 (Ar), 128.7 (Ar), 127.7 (Ar), 126.1 (Ar), 121.5 – 112.6 (m, *C*F_3CO), 107.7 (C1''), 101.8 (Benzylidene), 97.6 (C1'''), 97.0 (C1'), 82.6 (C5), 79.0 (C4'''), 77.7 (C4'), 75.3 (C2''), 75.1 (C3''), 75.0 (C6), 71.7 (C5'''), 69.9 (C4''), 69.2 (C3'), 68.1 (C3'''), 68.0 (C6'), 65.7 (C4'''), 63.4 (C5'), 52.4 (C2'), 48.8 (C1), 48.1 (C3), 48.0 (C2'''), 39.2 (C6'''), 30.9 (C2), 19.6 (*C*H_3CO), 19.24 (*C*H_3CO), 19.15 (*C*H_3CO), 19.1 (*C*H_3CO), 19.0 (*C*H_3CO). ESI-HRMS: *m/z* calc for $C_{49}H_{52}N_5O_{23}F_{15}Na$ $[M+Na]^+$ 1386.27058, found 1386.2716.

4’’-Deshydroxymethylparomomycin pentaacetate salt (86). To a stirred solution of **104** (128 mg, 0.094 mmol) in MeOH (1 mL) was added $TsOH{\cdot}H_2O$ (22 mg, 0.11 mmol). After 3 h, the reaction was quenched with saturated aqueous $NaHCO_3$ and diluted with EtOAc. The organic layer was washed with saturated aqueous $NaHCO_3$ and brine, dried over Na_2SO_4, and concentrated to dryness. The crude product was purified via flash chromatography (50-80% EtOAc in hexanes). The resulting solid (71 mg) was dissolved in MeOH (0.6 mL) and $Mg(OMe)_2$ solution (0.6 mL, 6-10% by wt) was added. After 25 h, the reaction was concentrated to dryness and redissolved in 0.6 mL dioxane and 0.6 mL 1 N NaOH. After 4 h, the reaction mixture was neutralized with AcOH and concentrated to dryness. The crude product was passed through a CM Sephadex C25 column, loading in 10% aqueous acetic acid and eluting with a gradient of 0.2-1.2% ammonium hydroxide in deionized water. The product-containing fractions were lyophilized in vacuo with glacial acetic acid to generate the peracetate salt of **86** (16.8 mg, 83% over 3 steps) as a white solid. $[\alpha]_D^{23}$ = +17.7 (*c* = 0.6, H_2O); ^{1}H NMR (600 MHz, D_2O) δ 5.58 (d, *J* = 3.9 Hz, 1H, H1’), 5.34 (d, *J* = 4.2 Hz, 1H, H1’’), 5.25 (d, *J* = 1.8 Hz, 1H, H1’’’), 4.58 (td, *J* = 5.0, 3.8 Hz, 1H, H3’’), 4.28 (ddd, *J* = 8.1, 5.2, 3.2 Hz, 2H, H2’’, H4’’a), 4.24 (ddd, *J* = 6.8, 4.0, 1.6 Hz, 1H, H5’’’), 4.16 (t, *J* = 3.2 Hz, 1H, H3’’’), 3.98 (dd, *J* = 10.1, 3.7 Hz, 1H, H4’’b), 3.86 (dd, *J* = 12.3, 2.3 Hz, 1H, H6’a), 3.84 – 3.76 (m, 4H, H4, H5, H5’, H3’), 3.75 (dt, *J* = 3.1, 1.4 Hz, 1H, H4’’’), 3.69 (dd, *J* = 12.1, 6.6 Hz, 1H, H6’b), 3.62 (dd, *J* = 10.6, 8.8 Hz, 1H, H6), 3.53 (dt, *J* = 3.1, 1.3 Hz, 1H, H2’’’), 3.48 – 3.41 (m, 1H, H4’), 3.40 – 3.32 (m, 3H, H6’’’a, H2’, H3), 3.31 – 3.21 (m, 2H, H6’’’b, H1), 2.34 (dt, *J* = 12.7, 4.3 Hz, 1H, H2eq), 1.85 (s, 15H, CH_3CO) 1.69 (q, *J* = 12.6 Hz, 1H, H2ax); ^{13}C NMR (151 MHz, D_2O) δ 181.1 ($CH_3\mathit{C}O$), 109.7 (C1’’), 96.3 (C1’’’, C1’), 84.0 (C5), 79.4 (C4), 77.2 (C3’’), 74.6 (C2’’), 73.9 (C5’), 72.6 (C6), 70.5 (C4’’), 70.2 (C5’’’), 69.5 (C3’), 69.2 (C4’), 67.6 (C3’’’),

67.3 (C4’’’), 60.3 (C6’), 53.9 (C2’), 50.9 (C2’’’), 49.7 (C1), 49.2 (C3), 40.3 (C5’’’), 29.1 (C2), 23.0 (*C*H_3CO); ESI-HRMS: *m/z* calc for $C_{22}H_{44}N_5O_{13}$ $[M+H]^+$ 586.29301, found 586.2923.

1,3,2’,2’’’,6’’’-Pentaazido-4’,6’-*O*-benzylidene-1,3,2’,2’’’,6’’’-pentadesamino-5”-*O*-(2,4,6- triisopropylbenzenesulfonyl)-paromomycin (**106**). To a stirred solution of **105** (338 mg, 0.41 mmol) in pyridine (2 mL) was added trisyl chloride (259 mg, 0.85 mmol). Additional trisyl chloride (126 mg, 0.41 mmol) was added when progress halted. After 40h, the reaction was quenched with water and diluted with EtOAc. The organic layer was washed with 1 N HCl, saturated aqueous $NaHCO_3$, and brine, dried over Na_2SO_4, and concentrated to dryness. The crude mixture was purified via flash chromatography (0-15% MeOH in DCM, R_f = 0.5 in 10% MeOH/DCM) to give **106** as an off-white solid (235 mg, 53%). $[\alpha]_D^{23}$ = +52.9 (*c* = 1.0, EtOAc); ^{1}H NMR (600 MHz, MeOD) δ 7.55 – 7.49 (m, 2H, Ar), 7.40 – 7.33 (m, 3H, Ar), 7.32 (s, 2H, Ar), 6.00 (d, *J* = 3.9 Hz, 1H, H1’), 5.61 (s, 1H, Benzylidene), 5.41 (d, *J* = 2.0 Hz, 1H, H1’’), 5.09 (d, *J* = 1.8 Hz, 1H, H1’’’), 4.36 (dd, *J* = 4.3, 2.1 Hz, 1H, H2’’), 4.35 – 4.28 (m, 3H, H3’’, H4’’, H5’’a), 4.27 – 4.09 (m, 6H, H5’’b, C*H*$(CH_3)_2$, H6’a, H5’, H3’), 4.00 (ddd, *J* = 8.8, 4.3, 2.0 Hz, 1H, H5’’’), 3.92 (t, *J* = 3.4 Hz, 1H, H3’’’), 3.81 (t, *J* = 10.2 Hz, 1H, H6’b), 3.69 (t, *J* = 8.8 Hz, 1HH5), 3.66 – 3.59 (m, 3H, H2’’, H4, H3), 3.59 – 3.52 (m, 2H, H4’, H6’’a), 3.50 (dd, *J* = 10.1, 4.0 Hz, 1H, H2’), 3.45 (ddd, *J* = 12.3, 9.9, 4.4 Hz, 1H, H1), 3.42 (t, *J* = 2.6 Hz, 1H, H4’’), 3.40 – 3.34 (m, 1H, H6), 3.27 (dd, *J* = 13.0, 4.3 Hz, 1H, H6’’b), 2.98 (p, *J* = 6.9 Hz, 1H, C*H*$(CH_3)_2$), 2.23 (dt, *J* = 12.9, 4.4 Hz, 1H, H2eq), 1.40 (q, *J* = 12.5 Hz, 1H, H2ax), 1.32 (s, 3H, Me), 1.31 (s, 9H, Me), 1.30 (s, 3H, Me), 1.30 (s, 3H, Me), 1.29 (s, 3H, Me); ^{13}C NMR (151 MHz, MeOD) δ 154.1 (Ar), 150.9 (Ar), 137.8 (Ar), 128.9 (Ar), 128.6 (Ar), 127.7 (Ar), 126.2 (Ar), 123.7 (Ar), 110.5 (C1’’), 101.7 (Benzylidene), 98.4 (C1’’’), 97.0 (C1’), 84.7 (C5), 81.5 (C4), 79.0 (C4’’), 76.4 (C4), 76.24 (C6), 76.21 (C3’’), 74.4 (C5’’’), 73.0 (C2’’), 70.7 (C5’’), 69.6 (C3’’’), 68.7 (C3’), 68.5 (C6’), 68.2

(C4’’’), 64.0 (C2’), 63.1 (C5’), 60.5 (C2’’’), 60.15 (C1), 60.0 (C3), 50.94 (C6’’), 34.1 (*C*H(CH_3)$_2$), 31.70 (C2), 29.4 (*C*H(CH_3)$_2$), 23.81 (Me), 23.80 (Me), 22.54 (Me), 22.53 (Me). ESI-HRMS: *m/z* calc for $C_{45}H_{61}N_{15}O_{16}SNa$ $[M+Na]^+$ 1122.40336, found 1122.4009.

1,3,2’,2’’’,6’’’-Pentaazido-4’,6’-*O*-benzylidene-1,3,2’,2’’’,6’’’-pentadesamino-5”-deoxy-5’’-iodoparomomycin (107). To a stirred solution of **106** (582 mg, 0.53 mmol) in acetone (5.6 mL) was added NaI (764 mg, 5.10 mmol), and the reaction was heated to reflux. Additional NaI (786 mg, 5.24 mmol) was added as progress halted. After 44h, the reaction mixture was concentrated to dryness and purified via flash chromatography (0-20% MeOH in DCM, R_f = 0.5 in 10% MeOH/DCM) to give the desired product **107** (339 mg, 68%) as a white solid. $[\alpha]_D^{23}$ = +69.4 (*c* = 1.0, EtOAc); ^{1}H NMR (900 MHz, MeOD) δ 7.51 (dd, *J* = 7.4, 2.3 Hz, 2H, Ar), 7.42 – 7.32 (m, 3H, Ar), 6.12 (d, *J* = 4.0 Hz, 1H, H1’), 5.62 (s, 1H, Benzylidene), 5.36 (d, *J* = 2.0 Hz, 1H, H1’’), 5.14 (d, *J* = 1.8 Hz, 1H, H1’’’), 4.45 (dd, *J* = 4.6, 2.0 Hz, 1H, H2’’), 4.26 (dd, *J* = 6.6, 4.7 Hz, 1H, H3’’), 4.24 (dd, *J* = 10.2, 5.0 Hz, 1H, H6’a), 4.17 – 4.11 (m, 3H, H4’’, H3’, H5’), 4.05 (ddd, *J* = 8.8, 4.2, 1.9 Hz, 1H, H5’’’), 3.97 (t, *J* = 3.3 Hz, 1H, H3’’’), 3.79 (t, *J* = 10.2 Hz, 1H, H6’b), 3.74 – 3.69 (m, 3H, H4, H6’’’a, H2’’’), 3.68 (dd, *J* = 10.7, 2.9 Hz, 1H, H5’’a), 3.64 (dd, *J* = 9.9, 8.8 Hz, 1H, H5), 3.59 – 3.54 (m, 2H, H4’, H3), 3.49 (dd, *J* = 10.1, 4.0 Hz, 1H, H2’), 3.47 – 3.44 (m, 2H, H1, H4’’’), 3.42 (dd, *J* = 13.0, 4.2 Hz, 1H, H6’’’b), 3.40 – 3.36 (m, 2H, H5’’b, H6), 2.23 (dt, *J* = 12.9, 4.5 Hz, 1H, H2eq), 1.40 (q, *J* = 12.6 Hz, 1H, H2ax); ^{13}C NMR (226 MHz, MeOD) δ 137.7 (Ar), 128.6 (Ar), 127.7 (Ar), 126.2 (Ar), 110.2 (C1’’), 101.7 (Benzylidene), 98.5 (C1’’’), 96.8 (C1’), 85.1 (C5), 81.5 (C4’), 80.9 (C4’’), 79.4 (C3’’), 76.5 (C6), 76.2 (C4), 74.3 (C5’’’), 74.1 (C2’’), 69.8 (C3’’’), 68.7 (C3’), 68.4 (C6’), 68.2 (C4’’’), 64.2 (C2’), 63.0 (C5’), 60.5 (C1), 60.2 (C2’’’), 60.1 (C3), 51.2 (C6’’’), 31.7 (C2), 6.8 (C5’’). ESI-HRMS: *m/z* calc for $C_{30}H_{38}N_{13}O_{15}INa$ $[M+Na]^+$ 966.17014, found 966.1688.

5’’-Deoxyparomomycin pentaacetate salt (87). To a stirred solution of **107** (180 mg, 0.19 mmol) in $CHCl_3$/water (4:1, 2 mL) was added *p*-toluenesulfonic acid (65.2 mg, 0.34 mmol). After 2h, the reaction was quenched with saturated aqueous $NaHCO_3$ and diluted with EtOAc. The organic layer was washed with saturated aqueous $NaHCO_3$ and brine, dried over Na_2SO_4, and concentrated to dryness. The crude solid was triturated several times with dichloromethane to remove excess benzaldehyde and give the hydrolyzed product (141 mg). A portion of the crude solid (32 mg) was dissolved in dioxane/water (1:1, 1 mL) and $Pd(OH)_2$ on carbon (76 mg) was added. The reaction mixture was purged with H_2, pressurized to 50 psi, filtered through Celite after 24h, and concentrated to dryness. The crude product was passed through a CM Sephadex C25 column, loading in 10% aqueous acetic acid and eluting with a gradient of 0.2-1.2% ammonium hydroxide in deionized water. The product-containing fractions were lyophilized in vacuo with glacial acetic acid to generate the peracetate salt of **87** (19.1 mg, 57% over 2 steps). $[\alpha]_D^{23}$ = +32.8 (*c* = 1.0, H_2O). ^{1}H NMR (600 MHz, D_2O) δ 5.67 (d, *J* = 4.0 Hz, 1H, H1’), 5.25 (d, *J* = 3.4 Hz, 1H, H1’’), 5.22 (d, *J* = 1.8 Hz, 1H, H1’’’), 4.29 (dd, *J* = 5.2, 3.5 Hz, 1H, H2’’), 4.25 (ddd, *J* = 6.0, 4.2, 1.6 Hz, 1H, H5’’’), 4.21 (t, *J* = 5.4 Hz, 1H, H3’’), 4.19 – 4.15 (m, 2H, H3’’, H4’), 3.89 – 3.81 (m, 3H, H6’a, H5, H3’), 3.80 – 3.74 (m, 3H, H4, H4’’’, H5’), 3.69 (dd, *J* = 12.1, 6.5 Hz, 1H, H6’b), 3.61 (dd, *J* = 10.5, 9.0 Hz, 1H, H6), 3.52 (dt, *J* = 3.0, 1.4 Hz, 1H, H2’’’), 3.43 (t, *J* = 9.4 Hz, 1H, H4’), 3.39 – 3.33 (m, 3H, H6’’’a, H2’, H3), 3.31 (dd, *J* = 13.7, 4.2 Hz, 1H, H6’’’b), 3.25 (ddd, *J* = 12.5, 10.5, 4.2 Hz, 1H, H1), 2.35 (dt, *J* = 12.8, 4.3 Hz, 1H, H2eq), 1.86 (s, 15H, AcOH), 1.70 (q, *J* = 12.7 Hz, 1H, H2ax), 1.35 (d, *J* = 6.3 Hz, 3H, H5’’). ^{13}C NMR (151 MHz, D_2O) δ 181.0 (CH_3CO), 110.2 (C1’’), 96.0 (C1’), 95.6 (C1’’’), 84.5 (C4), 80.5 (C3’’), 79.1 (C5), 77.9 (C4’’), 73.8 (C5’), 73.3 (C2’’), 72.5 (C6), 70.1 (C5’’’), 69.4 (C3’), 69.3 (C4’), 67.7 (C3’’’), 67.4 (C4’’’),

60.3 (C6'), 53.8 (C2'), 50.9 (C2''), 49.8 (C1), 49.1 (C3), 40.4 (C6'''), 29.1 (C2), 23.0 (*C*H_3CO), 18.3 (C5''). ESI-HRMS: *m/z* calc for $C_{23}H_{45}N_5O_{13}Na$ $[M+Na]^+$ 622.29061, found 622.2912.

1,3,2',5'',2''',6'''-Hexaazido-4',6'-*O*-benzylidene-1,3,2',2''',6'''-pentadesamino-5''-deoxyparomomycin (108). To a stirred solution of **106** (164 mg, 0.15 mmol) in DMF (1.5 mL) was added NaN_3 (102 mg, 1.57 mmol) and the reaction was heated to 80 °C. After 15h, the reaction mixture was diluted with EtOAc and washed with water. The aqueous layer was extracted twice with EtOAc and the combined organic layers were washed with brine, dried over Na_2SO_4, and concentrated to dryness. The crude product was purified via flash chromatography (0-10% MeOH in DCM, R_f = 0.5 in 6% MeOH in DCM) to give the desired compound **108** (99 mg, 78%) as a glassy solid. $[\alpha]_D^{23}$ = +109.3 (*c* = 0.93, MeOH); ^{1}H NMR (900 MHz, MeOD) δ 7.53 – 7.50 (m, 2H, Ar), 7.39 – 7.35 (m, 3H, Ar), 5.98 (d, *J* = 4.1 Hz, 1H, H1'), 5.61 (s, 1H, Benzylidene), 5.40 (s, 1H, H1''), 5.14 (s, 1H, H1'''), 4.41 – 4.37 (m, 2H, H3'', H2''), 4.26 – 4.21 (m, 2H, H4'', H6'a), 4.17 (td, *J* = 10.0, 4.9 Hz, 1H, H5'), 4.12 (t, *J* = 9.7 Hz, 1H, H3'), 4.07 – 4.03 (m, 1H, H5'''), 3.96 (t, *J* = 3.4 Hz, 1H, H3'''), 3.78 (t, *J* = 10.2 Hz, 1H, H6'b), 3.72 – 3.66 (m, 4H, H5, H2''', H5''a, H6'''a), 3.63 (t, *J* = 9.4 Hz, 1H, H4), 3.58 – 3.50 (m, 3H, H4', H5''b, H3), 3.48 – 3.43 (m, 2H, H1, H4'''), 3.42 – 3.37 (m, 2H, H6'''b, H6), 3.31 (dd, *J* = 10.1, 4.0 Hz, 1H, H2'), 2.23 (dt, *J* = 13.2, 4.6 Hz, 1H, H2eq), 1.40 (q, *J* = 12.6 Hz, 1H, H2ax); ^{13}C NMR (226 MHz, MeOD) δ 137.7 (Ar), 128.6 (Ar), 127.7 (Ar), 126.2 (Ar), 110.2 (C1''), 101.7 (Benzylidene), 98.4 (C1'''), 97.2 (C1'), 84.3 (C5), 81.5 (C4'), 79.9 (C4''), 76.8 (C3''), 76.5 (C4), 76.2 (C6), 74.3 (C5'''), 73.1 (C2''), 69.7 (C3'''), 68.6 (C3'), 68.4 (C4'''), 68.2 (C6'), 64.2 (C2'), 63.1 (C5'), 60.5 (C1), 60.2 (C2'''), 59.9 (C3), 53.0 (C5'), 51.2 (C6'''), 31.7 (C2); ESI-HRMS: *m/z* calc for $C_{30}H_{38}N_{18}O_{13}Na$ $[M+Na]^+$ 881.27579, found 881.2767.

5’’-Amino-5’’-deoxyparomomycin hexaacetate salt (73). To a solution of **108** (44 mg, 0.051 mmol) in dioxane/water (1:1, 1 mL) was added $Pd(OH)_2$ on carbon. The reaction mixture was purged with H_2 and pressurized to 50 psi. Additional $Pd(OH)_2$ (40 mg) and 10% aqueous AcOH (1.0 mL) were added when progress halted. After 72 h, the reaction mixture was filtered through Celite and concentrated to dryness. The crude product was passed through a CM Sephadex C25 column, loading in 10% aqueous acetic acid and eluting with a gradient of 0.2-1.2% ammonium hydroxide in deionized water. The product-containing fractions were lyophilized in vacuo with glacial acetic acid to generate the peracetate salt of **73** (27 mg, 54%). $[\alpha]_D^{23}$ = +18.7 (*c* = 0.70, H_2O); ^{1}H NMR (900 MHz, D_2O) δ 5.49 (d, *J* = 3.7 Hz, 1H, H1’), 5.35 (d, *J* = 2.5 Hz, 1H, H1’’), 5.21 (d, *J* = 1.9 Hz, 1H, H1’’’), 4.43 (dd, *J* = 6.5, 5.1 Hz, 1H, H3’’), 4.34 (dd, *J* = 5.1, 2.5 Hz, 1H, H2’’), 4.25 – 4.20 (m, 2H, H5’’’, H4’’), 4.14 (t, *J* = 3.2 Hz, 1H, H3’’’), 3.84 – 3.80 (m, 2H, H5, H6’a), 3.75 (dt, *J* = 2.9, 1.3 Hz, 1H, H4’’’), 3.75 – 3.66 (m, 4H, H4, H6’b, H3’, H5’), 3.57 (t, *J* = 9.9 Hz, 1H, H6), 3.48 (dt, *J* = 3.0, 1.3 Hz, 1H, H2’’’), 3.39 (t, *J* = 9.3 Hz, 1H, H4’), 3.35 (ddd, *J* = 14.3, 9.8, 4.7 Hz, 2H, H5’’a, H6’’’a), 3.30 (dd, *J* = 13.7, 4.1 Hz, 1H, H6’’’b), 3.21 (ddd, *J* = 13.2, 9.7, 4.1 Hz, 1H, H1), 3.17 (ddd, *J* = 12.4, 10.4, 4.1 Hz, 1H, H3), 3.13 (dd, *J* = 13.5, 8.9 Hz, 1H, H5’’), 3.03 (dd, *J* = 10.4, 3.7 Hz, 1H, H2’), 2.23 (dt, *J* = 12.9, 4.3 Hz, 1H, H2eq), 1.83 (s, 16H, CH_3CO), 1.57 (q, *J* = 12.6 Hz, 1H, H2ax); ^{13}C NMR (226 MHz, D_2O) δ 181.3 (CH_3CO), 109.0 (C1’’), 96.4 (C1’), 95.6 (C1’’’), 83.1 (C5), 78.6 (C4), 77.5 (C4’’), 77.1 (C3’’), 73.7 (C5’), 73.0 (C2’’), 72.7 (C5), 70.9 (C3’), 70.3 (C5’’’), 69.4 (C4’), 67.8 (C3’’’), 67.5 (C4’’’), 60.3 (C6’), 54.2 (C2’), 50.9 (C2’’’), 50.1 (C3), 49.4 (C1), 41.7 (C5’’), 40.4 (C6’’’), 29.8 (C2), 23.2 (CH_3CO); ESI-HRMS: *m/z* calc for $C_{23}H_{46}N_6O_{13}Na$ $[M+Na]^+$ 637.30151, found 637.3020.

1,3,2’,6’-Tetraazido-1,3,2’,6’-tetradesaminoribostamycin (**109**). To a stirred solution of NaN_3 (12.95 g, 0.20 mol) in H_2O/DCM (1:1, 70 mL) at 0 °C was added Tf_2O (18.5 mL, 0.039 mol)

dropwise. After 2 h, the reaction mixture was neutralized with saturated aqueous $NaHCO_3$. The aqueous layer was extracted twice with DCM (60 mL) and the combined organic layers were set aside. To a stirred solution of **70** (5.05 g, 7.69 mmol) in H_2O (80 mL) at 0 °C were added Et_3N (11 mL) and $CuSO_4{\cdot}5H_2O$ (88 mg, 0.35 mmol). The above TfN_3 solution was added dropwise, followed by MeOH (260 mL). After 16 h, the reaction was concentrated in vacuo until only H_2O remained. The aqueous solution was then acidified to pH 1.5 with 4 N HCl and extracted ten times with EtOAc after addition of NaCl (50 mL increments). The combined organic layers were washed with saturated aqueous $NaHCO_3$ and brine, dried over Na_2SO_4, and concentrated to dryness. The crude product was then purified via silica gel chromatography (0-20% MeOH in DCM, R_f = 0.2 in 6% MeOH in DCM) to give **109** (3.59 g, 54%) as a light brown solid. $[\alpha]_D^{23}$ = +66.6 (*c* = 1.0, MeOH); ^{1}H NMR (900 MHz, MeOD) δ 5.81 (d, *J* = 3.8 Hz, 1H, H1'), 5.37 (d, *J* = 1.2 Hz, 1H, H1''), 4.19 (ddd, *J* = 10.0, 5.7, 2.4 Hz, 1H, H5'), 4.16 – 4.14 (m, 2H, H2'', H3''), 3.96 (td, *J* = 5.7, 3.3 Hz, 1H, H4''), 3.89 (dd, *J* = 10.5, 8.8 Hz, 1H, H3'), 3.80 (dd, *J* = 11.8, 3.3 Hz, 1H, H5''a), 3.71 – 3.65 (m, 3H, H5''b, H4, H5), 3.57 – 3.52 (m, 2H, H6'a, H3), 3.48 – 3.42 (m, 3H, H6'b, H6, H1), 3.38 – 3.35 (m, 1H, H4'), 3.12 (dd, *J* = 10.5, 3.8 Hz, 1H, H2'), 2.24 (dt, *J* = 12.6, 4.2 Hz, 1H, H2eq), 1.41 (q, *J* = 12.3 Hz, 1H, H2ax); ^{13}C NMR (226 MHz, MeOD) δ 107.9 (C1''), 97.0 (C1'), 83.5 (C5), 83.2 (C4'), 76.0 (C6), 75.8 (C4), 75.5 (C2''), 71.8 (C5'), 71.2 (C4'), 70.7 (C3'), 70.2 (C3''), 63.2 (C2'), 62.2 (C5''), 60.5 (C1), 59.8 (C3), 51.2 (C6'), 31.6 (C2). ESI-HRMS: *m/z* calc for $C_{17}H_{26}N_{12}O_{10}Na$ $[M+Na]^+$ 581.17871, found 581.1787.

1,3,2',6'-Tetraazido-1,3,2',6'-tetradesamino-5"-*O*-(2,4,6-triisopropylbenzenesulfonyl)-ribostamycin (**110**). To a stirred solution of **109** (1.39 g, 2.49 mmol) in pyridine (13 mL) was added trisyl chloride (1.52 g, 4.98 mmol). After 22 h, the reaction was quenched with water and diluted with EtOAc. The organic layer was washed with 1 N HCl,

saturated $NaHCO_3$, and brine, dried over Na_2SO_4, and evaporated to dryness. The crude mixture was purified via flash chromatography (0-10% MeOH in DCM, R_f = 0.7 in 10% MeOH/DCM) to give the desired product **110** (834 mg, 41%) as a white solid. $[\alpha]_D^{23}$ = +42.8 (*c* = 0.5, MeOH); ^{1}H NMR (900 MHz, MeOD) δ 7.32 (s, 2H, Ar), 5.96 (d, *J* = 3.8 Hz, 1H, H1'), 5.36 (d, *J* = 1.3 Hz, 1H, H1''), 4.24 – 4.18 (m, 4H, C*H*$(CH_3)_2$, H5''), 4.17 – 4.14 (m, 2H, H5', H2''), 4.08 (td, *J* = 7.2, 3.1 Hz, 1H, H4''), 4.04 (dd, *J* = 7.4, 4.6 Hz, 1H, H3''), 3.88 (dd, *J* = 10.4, 8.8 Hz, 1H, H4'), 3.66 (t, *J* = 8.9 Hz, 1H, H5), 3.62 (dd, *J* = 9.8, 8.8 Hz, 1H, H4), 3.57 – 3.53 (m, 1H, H3), 3.51 (dd, *J* = 13.3, 2.4 Hz, 1H, H6'a), 3.48 – 3.42 (m, 2H, H6'b, H1), 3.37 – 3.35 (m, 1H, H4'), 3.32 – 3.28 (m, 2H, H2', H6), 2.97 (hept, *J* = 7.0 Hz, 1H, CH(C*H*$_3)_2$), 2.23 (dt, *J* = 12.9, 4.5 Hz, 1H, H2eq), 1.38 – 1.32 (m, 1H, H2ax), 1.32 – 1.28 (m, 18H, CH(C*H*$_3)_2$); ^{13}C NMR (226 MHz, MeOD) δ 154.1 (Ar), 150.9 (Ar), 129.0 (Ar), 123.7 (Ar), 110.2 (C1''), 96.0 (C1'), 83.9 (C5), 80.0 (C4''), 76.5 (C6), 75.9 (C4), 74.8 (C2''), 71.9 (C5'), 71.3 (C4'), 71.1 (C3'), 70.8 (C3''), 70.7 (C5''), 63.3 (C2'), 60.6 (C3), 60.0 (C1), 51.4 (C6'), 34.1 (*C*H$(CH_3)_2$), 31.7 (C2), 29.4 (*C*H$(CH_3)_2$), 23.73 (CH(*C*H$_3)_2$), 23.71 (CH(*C*H$_3)_2$), 22.53 (CH(*C*H$_3)_2$), 22.5 (CH(*C*H$_3)_2$); ESI-HRMS: *m/z* calc for $C_{32}H_{48}N_{12}O_{12}SNa$ $[M+Na]^+$ 847.31276, found 847.3127.

1,3,2',6',5''-Pentaazido-1,3,2',6'-tetradesamino-5"-deoxyribostamycin (**111**). To a stirred solution of **110** (383 mg, 0.47 mmol) in DMF (4.7 mL) was added NaN_3 (590 mg, 9.08 mmol) and the reaction was heated to 95 °C. After 21 h, the reaction mixture was diluted with EtOAc and washed with water. The aqueous layer was extracted twice with EtOAc and the combined organic layers were washed with brine, dried over Na_2SO_4, and concentrated to dryness. The crude product was purified via flash chromatography (0-20% MeOH in DCM, R_f = 0.2 in 6% MeOH in DCM) to give **111** (200 mg, 74%) as a white solid. $[\alpha]_D^{23}$ = +90.4 (*c* = 1.0, MeOH); ^{1}H NMR (900 MHz, MeOD) δ 6.00 (d, *J* = 3.9 Hz, 1H, H1'), 5.35 (s, 1H, H1''), 4.21 – 4.19 (m, 1H,

H2’’), 4.18 (ddd, *J* = 9.9, 5.9, 2.3 Hz, 1H, H5’), 4.07 (dd, *J* = 7.3, 4.6 Hz, 1H, H3’’), 4.02 (td, *J* = 7.1, 3.0 Hz, 1H, H4’’), 3.88 (dd, *J* = 10.4, 8.8 Hz, 1H, H3’), 3.65 (t, *J* = 8.8 Hz, 1H, H5), 3.62 (t, *J* = 9.2 Hz, 1H, H4), 3.60 – 3.51 (m, 3H, H3, H6’a, H5’’a), 3.48 (dd, *J* = 13.1, 6.9 Hz, 1H, H5’’b), 3.46 – 3.41 (m, 2H, H1, H6’b), 3.35 (dd, *J* = 18.1, 8.9 Hz, 2H, H6, H4’), 3.19 (dd, *J* = 10.4, 3.9 Hz, 1H, H2’), 2.23 (dt, *J* = 12.9, 4.5 Hz, 1H, H2eq), 1.37 (q, *J* = 12.5 Hz, 1H, H2ax); ^{13}C NMR (226 MHz, MeOD) δ 110.1 (C1’’), 96.2 (C1’), 84.0 (C5), 81.0 (C4’’), 76.4 (C6), 76.0 (C4), 75.0 (C2’’), 71.8 (C5’), 71.4 (C3’’), 71.2 (C4’), 71.1 (C3’), 63.5 (C2’), 60.6 (C1), 59.9 (C3), 53.3 (C5’’), 51.2 (C5’), 31.7 (C2). ESI-HRMS: *m/z* calc for $C_{17}H_{25}N_{15}O_9Na$ $[M+Na]^+$ 616.18519, found 616.1866.

5’’-Amino-5’’-deoxyribostamycin pentaacetate salt (91). To a solution of **111** (102 mg, 0.17 mmol) in dioxane/water (1:1, 2 mL) was added Pd on carbon (192 mg). The reaction mixture was purged with H_2 and pressurized to 50 psi. After 19 h, the reaction mixture was filtered through Celite and concentrated to dryness. The crude product was passed through a CM Sephadex C25 column, loading in 10% aqueous acetic acid and eluting with a gradient of 0.2-1.2% ammonium hydroxide in deionized water. The product-containing fractions were lyophilized in vacuo with glacial acetic acid to generate the peracetate salt of **91** (41 mg, 31%). $[\alpha]_D^{23}$ = +31.8 (*c* = 1.0, H_2O); ^{1}H NMR (600 MHz, D_2O) δ 5.90 (d, *J* = 3.8 Hz, 1H, H1’), 5.33 (d, *J* = 1.6 Hz, 1H, H1’’), 4.13 (dd, *J* = 4.8, 1.6 Hz, 1H, H2’’), 4.09 (dd, *J* = 7.1, 4.8 Hz, 1H, H3’’), 4.06 – 4.01 (m, 2H, H4’’, H4), 3.96 – 3.88 (m, 3H, H5, H3’, H5’), 3.66 (dd, *J* = 10.5, 9.3 Hz, 1H, H6), 3.43 (t, *J* = 8.9 Hz, 1H, H4’), 3.41 – 3.38 (m, 2H, H2’, H3), 3.36 (dd, *J* = 13.7, 3.4 Hz, 1H, H6’a), 3.29 (dd, *J* = 13.5, 3.9 Hz, 1H, H5’’a), 3.27 – 3.22 (m, 2H, H6’b, H1), 3.11 (dd, *J* = 13.5, 8.1 Hz, 1H, H5’’b), 2.35 (dt, *J* = 12.6, 4.2 Hz, 1H, H2eq), 1.84 (s, 15H, CH_3CO), 1.80 – 1.72 (m, 1H, H2ax); ^{13}C NMR (151 MHz, D_2O) δ 180.5 (CH_3CO), 108.5 (C1’’), 93.7 (C1’), 83.3 (C5), 78.3 (C4’’), 74.8 (C2’’), 74.5

(C4), 71.9 (C6), 71.3 (C3’’), 70.2 (C4’, 5’), 68.5 (C3’), 53.1 (C2’), 50.1 (C1), 48.8 (C3), 41.9 (C5’’), 39.9 (C6’), 28.3 (C2), 22.7 (*C*H_3CO). ESI-HRMS: *m/z* calc for $C_{17}H_{36}N_5O_9$ $[M+H]^+$ 454.25075, found 454.2502.

REFERENCES

1. Antibiotic Resistance Threats in the United States. https://www.cdc.gov/drugresistance/biggest-threats.html (accessed April 2021).

2. Butler, M. S.; Blaskovich, M. A. T.; Cooper, M. A., Antibiotics in the Clinical Pipeline at the End of 2015. *J. Antibiotics* **2017,** *70*, 3-24.

3. Butler, M. S.; Paterson, D. L., Antibiotics in the Clinical Pipeline in October 2019. *J. Antibiotics* **2020,** *73*, 329-364.

4. Renwick, M. J.; Brogan, D. M.; Mossialos, E., A Systematic Review and Critical Assessment of Incentive Strategies for Discovery and Development of Novel Antibiotics. *J. Antibiotics* **2016,** *69*, 73-88.

5. Ventola, C. L., The Antibiotic Resistance Crisis: Part 1: Causes and Threats. *P&T* **2015,** *40*, 277-283.

6. Ventola, C. L., The Antibiotic Resistance Crisis: Part 2: Management Strategies and New Agents. *P&T* **2015,** *40*, 344-352.

7. Böttger, E. C.; Crich, D., Aminoglycosides: Time for the Resurrection of a Neglected Class of Antibacterials? *ACS Infect. Dis.* **2020,** *6*, 168-172.

8. IMI Mission and Objective. https://www.imi.europa.eu/about-imi/mission-objectives (accessed June 2021).

9. ENABLE: European Gram-Negative Antibacterial Engine. https://www.imi.europa.eu/projects-results/project-factsheets/enable (accessed June 2021).

10. CARB-X: Combating Antibiotic Resistant Bacteria. https://carb-x.org/about/overview/ (accessed June 2021).

11. About GARDP. https://gardp.org/who-we-are/about-gardp/ (accessed June 2021).

12. Anderson, R. J.; Groundwater, P. W.; Todd, A.; Worsley, A. J., *Antibacterail Agents: Chemistry, Mode of Action, Mechanism of Resistance, and Clinical Applications*. Wiley: 2012.

13. Breijyeh, Z.; Jubeh, B.; Karaman, R., Resistance of Gram-Negative Bacteria to Current Antibacterial Agents and Approaches to Resolve It. *Molecules* **2020,** *25*, 1340.

14. Muñoz, K. A.; Hergenrother, P. J., Facilitating Compound Entry as a Means to Discover Antibiotics for Gram-Negative Bacteria. *Acc. Chem. Res.* **2021,** *54*, 1322-1333.

15. *Global Priority List of Antibiotic-Resistant Bacteria to Guide Research, Discovery, and Development of New Antibiotics*. World Health Organization: 2019.

16. Woodruff, H. B., Selman A. Waksman, Winner of the 1952 Nobel Prize for Physiology or Medicine. *Appl. Environ. Microbiol.* **2014,** *80*, 2-8.

17. Daniel, T. M., The History of Tuberculosis. *Respir. Med.* **2006,** *100*, 1862-1870.

18. Becker, B.; Cooper, M. A., Aminoglycoside Antibiotics in the 21st Century. *ACS Chem Biol* **2013,** *8*, 105-15.

19. *Critically Important Antimicrobials for Human Medicine*. 6th ed.; World Health Organization: 2019.

20. Kato, T.; Yang, G.; Teo, Y.; Juskeviciene, R.; Perez-Fernandez, D.; Shinde, H. M.; Salian, S.; Bernet, B.; Vasella, A.; Böttger, E. C.; Crich, D., Synthesis and Antiribosomal Activities of 4′-O-, 6′-O-, 4″-O-, 4′,6′-O- and 4″,6″-O-Derivatives in the Kanamycin Series Indicate Differing Target Selectivity Patterns between the 4,5- and 4,6-Series of Disubstituted 2-Deoxystreptamine Aminoglycoside Antibiotics. *ACS Infect. Dis.* **2015,** *1*, 479-486.

21. Matsushita, T.; Sati, G. C.; Kondasinghe, N.; Pirrone, M. G.; Kato, T.; Waduge, P.; Kumar, H. S.; Sanchon, A. C.; Dobosz-Bartoszek, M.; Shcherbakov, D.; Juhas, M.; Hobbie, S. N.; Schrepfer, T.; Chow, C. S.; Polikanov, Y. S.; Schacht, J.; Vasella, A.; Böttger, E. C.; Crich, D., Design, Multigram Synthesis, and in Vitro and in Vivo Evaluation of Propylamycin: A Semisynthetic 4,5-Deoxystreptamine Class Aminoglycoside for the Treatment of Drug-Resistant Enterobacteriaceae and Other Gram-Negative Pathogens. *J. Am. Chem. Soc.* **2019,** *141*, 5051-5061.

22. Takahashi, Y.; Igarashi, M., Destination of Aminoglycoside Antibiotics in the 'Post-Antibiotic Era'. *J. Antibiotics* **2018,** *71*, 4-14.

23. Sucheck, S. J.; Wong, A. L.; Koeller, K. M.; Boehr, D. D.; Draker, K.-a.; Sears, P.; Wright, G. D.; Wong, C.-H., Design of Bifunctional Antibiotics that Target Bacterial rRNA and Inhibit Resistance-Causing Enzymes. *J. Am. Chem. Soc.* **2000,** *122*, 5230-5231.

24. Fosso, M. Y.; Li, Y.; Garneau-Tsodikova, S., New Trends in the Use of Aminoglycosides. *MedChemComm* **2014,** *5*, 1075-1091.

25. Pokrovskaya, V.; Belakhov, V.; Hainrichson, M.; Yaron, S.; Baasov, T., Design, Synthesis, and Evaluation of Novel Fluoroquinolone−Aminoglycoside Hybrid Antibiotics. *J. Med. Chem.* **2009,** *52*, 2243-2254.

26. Forge, A.; Schacht, J., Aminoglycoside Antibiotics. *Audiol. Neuroto.* **2000,** *5*, 3-22.

27. Mingeot-Leclercq, M. P.; Glupczynski, Y.; Tulkens, P. M., Aminoglycosides: Activity and Resistance. *Antimicrob. Agents Chemother.* **1999,** *43*, 727-737.

28. Li, X.-Z.; Plésiat, P.; Nikaido, H., The Challenge of Efflux-Mediated Antibiotic Resistance in Gram-Negative Bacteria. *Clin. Microbiol. Rev.* **2015,** *28*, 337-418.

29. Noeske, J.; Wasserman, M. R.; Terry, D. S.; Altman, R. B.; Blanchard, S. C.; Cate, J. H. D., High-Resolution Structure of the *Escherichia coli* Ribosome. *Nat. Struct. Mol. Biol.* **2015,** *22*, 336-341.

30. Schilling-Bartetzko, S.; Bartetzko, A.; Nierhaus, K. H., Kinetic and Thermodynamic Parameters for tRNA Binding to the Ribosome and for the Translocation Reaction. *J. Biol. Chem.* **1992,** *267*, 4703-4712.

31. Herzog, I. M.; Louzoun Zada, S.; Fridman, M., Effects of 5-O-Ribosylation of Aminoglycosides on Antimicrobial Activity and Selective Perturbation of Bacterial Translation. *J. Med. Chem.* **2016,** *59*, 8008-8018.

32. Arya, D. P., *Aminoglycoside Antibiotics: From Chemical Biology to Drug Discovery*. Wiley: 2007.

33. Carter, A. P.; Clemons, W. M.; Brodersen, D. E.; Morgan-Warren, R. J.; Wimberly, B. T.; Ramakrishnan, V., Functional Insights from the Structure of the 30S Ribosomal Subunit and its Interactions with Antibiotics. *Nature* **2000,** *407*, 340-348.

34. Feldman, M. B.; Terry, D. S.; Altman, R. B.; Blanchard, S. C., Aminoglycoside Activity Observed on Single Pre-Translocation Ribosome Complexes. *Nat. Chem. Biol.* **2010,** *6*, 54-62.

35. Shandrick, S.; Zhao, Q.; Han, Q.; Ayida, B. K.; Takahashi, M.; Winters, G. C.; Simonsen, K. B.; Vourloumis, D.; Hermann, T., Monitoring Molecular Recognition of the Ribosomal Decoding Site. *Angew. Chem. Int. Ed.* **2004,** *43*, 3177-3182.

36. Kaul, M.; Barbieri, C. M.; Pilch, D. S., Fluorescence-Based Approach for Detecting and Characterizing Antibiotic-Induced Conformational Changes in Ribosomal RNA: Comparing Aminoglycoside Binding to Prokaryotic and Eukaryotic Ribosomal RNA Sequences. *J. Am. Chem. Soc.* **2004,** *126*, 3447-3453.

37. Ogle, J. M.; Ramakrishnan, V., Structural Insights into Translational Fidelity. *Annu. Rev. Biochem.* **2005,** *74*, 129-177.

38. Peske, F.; Savelsbergh, A.; Katunin, V. I.; Rodnina, M. V.; Wintermeyer, W., Conformational Changes of the Small Ribosomal Subunit During Elongation Factor G-Dependent tRNA-mRNA Translocation. *J. Mol. Biol.* **2004,** *343*, 1183-1194.

39. Kohanski, M. A.; Dwyer, D. J.; Hayete, B.; Lawrence, C. A.; Collins, J. J., A Common Mechanism of Cellular Death Induced by Bactericidal Antibiotics. *Cell* **2007,** *130*, 797-810.

40. Davis, B. D.; Chen, L. L.; Tai, P. C., Misread Protein Creates Membrane Channels: An Essential Step in the Bactericidal Action of Aminoglycosides. *Proc. Natl. Acad. Sci.* **1986,** *83*, 6164-6168.

41. Bryan, L. E.; Kwan, S., Roles of Ribosomal Binding, Membrane Potential, and Electron Transport in Bacterial Uptake of Streptomycin and Gentamicin. *Antimicrob. Agents Chemother.* **1983,** *23*, 835-845.

42. Matt, T.; Ng, C. L.; Lang, K.; Sha, S.-H.; Akbergenov, R.; Shcherbakov, D.; Meyer, M.; Duscha, S.; Xie, J.; Dubbaka, S. R.; Perez-Fernandez, D.; Vasella, A.; Ramakrishnan, V.; Schacht, J.; Böttger, E. C., Dissociation of Antibacterial Activity and Aminoglycoside Ototoxicity in the 4-Monosubstituted 2-Deoxystreptamine Apramycin. *Proc. Natl. Acad. Sci.* **2012,** *109*, 10984-10989.

43. Contrepois, A.; Brion, N.; Garaud, J. J.; Faurisson, F.; Delatour, F.; Levy, J. C.; Deybach, J. C.; Carbon, C., Renal Disposition of Gentamicin, Dibekacin, Tobramycin, Netilmicin, and Amikacin in Humans. *Antimicrob. Agents Chemother.* **1985,** *27*, 520-524.

44. Janknegt, R., Aminoglycoside Monitoring in the Once- or Twice-Daily Era. *Pharm. World. Sci.* **1993,** *15*, 151-155.

45. Priuska, E. M.; Schacht, J., Formation of Free Radicals by Gentamicin and Iron and Evidence for an Iron/Gentamicin Complex. *Biochem. Pharmacol.* **1995,** *50,* 1749-1752.

46. Giuliano, R. A.; Paulus, G. J.; Verpooten, G. A.; Pattyn, V. M.; Pollet, D. E.; Nouwen, E. J.; Laurent, G.; Carlier, M.-B.; Maldague, P.; Tulkens, P. M.; De Broe, M. E., Recovery of Cortical Phospholipidosis and Necrosis After Acute Gentamicin Loading in Rats. *Kidney Int.* **1984,** *26,* 838-847.

47. Kishore, B. K.; Kállay, Z.; Lambricht, P.; Laurent, G.; Tulkens, P. M., Mechanism of Protection Afforded by Polyaspartic Acid Against Gentamicin-Induced Phospholipidosis. I. Polyaspartic Acid Binds Gentamicin and Displaces it From Negatively Charged Phospholipid Layers In Vitro. *J. Pharmacol. Exp. Ther.* **1990,** *255,* 867-874.

48. Fausti, S. A.; Rappaport, B. Z.; Schechter, M. A.; Frey, R. H.; Ward, T. T.; Brummett, R. E., Detection of Aminoglycoside Ototoxicity by High-Frequency Auditory Evaluation: Selected Case Studies. *Am. J. Otolaryngol.* **1984,** *5,* 177-182.

49. Boettcher, F. A.; Henderson, D.; Gratton, M. A.; Danielson, R. W.; Byrne, C. D., Synergistic Interactions of Noise and Other Ototraumatic Agents. *Ear Hearing* **1987,** *8,* 192-212.

50. Henley, C. M.; Schacht, J., Pharmacokinetics of Aminoglycoside Antibiotics in Blood, Inner-Ear Fluids and Tissues and Their Relationship to Ototoxicity. *Audiology* **1988,** *27,* 137-146.

51. Lesniak, W.; Pecoraro, V. L.; Schacht, J., Ternary Complexes of Gentamicin with Iron and Lipid Catalyze Formation of Reactive Oxygen Species. *Chem. Res. Toxicol.* **2005,** *18,* 357-364.

52. Jiang, H.; Sha, S.-H.; Schacht, J., Rac/Rho Pathway Regulates Actin Depolymerization Induced by Aminoglycoside Antibiotics. *J. Neurosci. Res.* **2006,** *83,* 1544-1551.

53. Hobbie, S. N.; Pfister, P.; Brüll, C.; Westhof, E.; Böttger, E. C., Analysis of the Contribution of Individual Substituents in 4,6-Aminoglycoside-Ribosome Interaction. *Antimicrob. Agents Chemother.* **2005,** *49*, 5112-5118.

54. Matt, T.; Akbergenov, R.; Shcherbakov, D.; Böttger, E. C., The Ribosomal A-site: Decoding, Drug Target, and Disease. *Isr. J. Chem.* **2010,** *50*, 60-70.

55. Hobbie, S. N.; Bruell, C.; Kalapala, S.; Akshay, S.; Schmidt, S.; Pfister, P.; Böttger, E. C., A Genetic Model to Investigate Drug–Target Interactions at the Ribosomal Decoding Site. *Biochimie* **2006,** *88*, 1033-1043.

56. Hobbie, S. N.; Akshay, S.; Kalapala, S. K.; Bruell, C. M.; Shcherbakov, D.; Böttger, E. C., Genetic Analysis of Interactions with Eukaryotic rRNA Identify the Mitoribosome as Target in Aminoglycoside Ototoxicity. *Proc. Natl. Acad. Sci.* **2008,** *105*, 20888-20893.

57. Hobbie, S. N.; Bruell, C. M.; Akshay, S.; Kalapala, S. K.; Shcherbakov, D.; Böttger, E. C., Mitochondrial Deafness Alleles Confer Misreading of the Genetic Code. *Proc. Natl. Acad. Sci.* **2008,** *105*, 3244-3249.

58. Macfarlane, E. L. A.; Kwasnicka, A.; Hancock, R. E. W., Role of *Pseudomonas aeruginosa* PhoP-PhoQ in Resistance to Antimicrobial Cationic Peptides and Aminoglycosides. *Microbiol.* **2000,** *146*, 2543-2554.

59. Fernández, L.; Gooderham, W. J.; Bains, M.; McPhee, J. B.; Wiegand, I.; Hancock, R. E. W., Adaptive Resistance to the "Last Hope" Antibiotics Polymyxin B and Colistin in *Pseudomonas aeruginosa* is Mediated by the Novel Two-Component Regulatory System ParR-ParS. *Antimicrob. Agents Chemother.* **2010,** *54*, 3372-3382.

60. Nowicki, E. M.; O'Brien, J. P.; Brodbelt, J. S.; Trent, M. S., Extracellular Zinc Induces Phosphoethanolamine Addition to *Pseudomonas aeruginosa* Lipid A via the ColRS Two-Component System. *Mol. Microbiol.* **2015,** *97*, 166-178.

61. Murakami, S.; Nakashima, R.; Yamashita, E.; Yamaguchi, A., Crystal Structure of Bacterial Multidrug Efflux Transporter AcrB. *Nature* **2002,** *419*, 587-593.

62. Yu, E. W.; Aires, J. R.; Nikaido, H., AcrB Multidrug Efflux Pump of *Escherichia coli*: Composite Substrate-Binding Cavity of Exceptional Flexibility Generates Its Extremely Wide Substrate Specificity. *J. Bacteriol.* **2003,** *185*, 5657-5664.

63. Poole, K., Efflux-Mediated Antimicrobial Resistance. *J. Antimicrob. Chemother.* **2005,** *56*, 20-51.

64. Prammananan, T.; Sander, P.; Brown, B. A.; Frischkorn, K.; Onyi, G. O.; Zhang, Y.; Böttger, E. C.; Wallace, R. J., Jr., A Single 16S Ribosomal RNA Substitution Is Responsible for Resistance to Amikacin and Other 2-Deoxystreptamine Aminoglycosides in *Mycobacterium abscessus* and *Mycobacterium chelonae*. *J. Infect. Dis.* **1998,** *177*, 1573-1581.

65. Recht, M. I.; Douthwaite, S.; Puglisi, J. D., Basis for Prokaryotic Specificity of Action of Aminoglycoside Antibiotics. *EMBO J.* **1999,** *18*, 3133-3138.

66. Doi, Y.; Wachino, J.-I.; Arakawa, Y., Aminoglycoside Resistance: The Emergence of Acquired 16S Ribosomal RNA Methyltransferases. *Infect. Dis. Clin. North Am.* **2016,** *30*, 523-537.

67. González-Zorn, B.; Teshager, T.; Casas, M.; Porrero, M.; Moreno, M.; Courvalin, P.; Domínguez, L., *armA* and Aminoglycoside Resistance in *Escherichia coli*. *Emerg. Infect. Dis.* **2005,** *11*, 954.

68. Shaw, K. J.; Rather, P. N.; Hare, R. S.; Miller, G. H., Molecular Genetics of Aminoglycoside Resistance Genes and Familial Relationships of the Aminoglycoside-Modifying Enzymes. *Microbiol. Rev.* **1993,** *57*, 138-163.

69. Vakulenko, S. B.; Mobashery, S., Versatility of Aminoglycosides and Prospects for Their Future. *Clin. Microbiol. Rev.* **2003,** *16*, 430-450.

70. Wright, G. D., Aminoglycoside-Modifying Enzymes. *Curr. Opin. Microbiol.* **1999,** *2*, 499-503.

71. Ramirez, M. S.; Tolmasky, M. E., Aminoglycoside Modifying Enzymes. *Drug Resist. Update* **2010,** *13*, 151-171.

72. Sunada, A.; Nakajima, M.; Ikeda, Y.; Kondo, S.; Hotta, K., Enzymatic 1-*N*-Acetylation of Paromomycin by an Actinomycete Strain #8 with Multiple Aminoglycoside Resistance and Paromomycin Sensitivity. *J. Antibiot.* **1999,** *52*, 809-14.

73. Cameron, F. H.; Groot Obbink, D. J.; Ackerman, V. P.; Hall, R. M., Nucleotide Aequence of the AAD(2′) Aminoglycoside Adenylyltransferase Determinant aadB . Evolutionary Relationship of this Region with Those Surrounding aadA in R538-1 and dhfrll in R388. *Nucleic Acid Res.* **1986,** *14*, 8625-8635.

74. Garneau-Tsodikova, S.; Labby, K. J., Mechanisms of Resistance to Aminoglycoside Antibiotics: Overview and Perspectives. *Medchemcomm* **2016,** *7* (1), 11-27.

75. *Regional Outbreak of New Delhi Metallo-beta-lactamase Producing Carbapenen-resistant Enterobacteriaceae, Italy, 2018−2019,*. ECDC European Centre for Disease Prevention and Control, ECDC, Stockholm, 2019.

76. Kumarasamy, K. K.; Toleman, M. A.; Walsh, T. R.; Bagaria, J.; Butt, F.; Balakrishnan, R.; Chaudhary, U.; Doumith, M.; Giske, C. G.; Irfan, S.; Krishnan, P.; Kumar,

A. V.; Maharjan, S.; Mushtaq, S.; Noorie, T.; Paterson, D. L.; Pearson, A.; Perry, C.; Pike, R.; Rao, B.; Ray, U.; Sarma, J. B.; Sharma, M.; Sheridan, E.; Thirunarayan, M. A.; Turton, J.; Upadhyay, S.; Warner, M.; Welfare, W.; Livermore, D. M.; Woodford, N., Emergence of a New Antibiotic Resistance Mechanism in India, Pakistan, and the UK: A Molecular, Biological, and Epidemiological Study. *Lancet Infect. Dis.* **2010,** *10*, 597-602.

77. Allen, N. E.; Alborn, W. E.; Hobbs, J. N.; Kirst, H. A., 7-Hydroxytropolone: An Inhibitor of Aminoglycoside-2"-O-Adenylyltransferase. *Antimicrob. Agents Chemother.* **1982,** *22*, 824-831.

78. Galani, I.; Souli, M.; Daikos, G. L.; Chrysouli, Z.; Poulakou, G.; Psichogiou, M.; Panagea, T.; Argyropoulou, A.; Stefanou, I.; Plakias, G.; Giamarellou, H.; Petrikkos, G., Activity of Plazomicin (ACHN-490) against MDR clinical isolates of *Klebsiella pneumoniae*, *Escherichia coli*, and *Enterobacter spp*. from Athens, Greece. *J. Chemother.* **2012,** *24*, 191-194.

79. Aggen, J. B.; Armstrong, E. S.; Goldblum, A. A.; Dozzo, P.; Linsell, M. S.; Gliedt, M. J.; Hildebrandt, D. J.; Feeney, L. A.; Kubo, A.; Matias, R. D.; Lopez, S.; Gomez, M.; Wlasichuk, K. B.; Diokno, R.; Miller, G. H.; Moser, H. E., Synthesis and Spectrum of the Neoglycoside ACHN-490. *Antimicrob. Agents Chemother.* **2010,** *54*, 4636-4642.

80. Sonousi, A.; Sarpe, V. A.; Brilkova, M.; Schacht, J.; Vasella, A.; Böttger, E. C.; Crich, D., Effects of the 1-*N*-(4-Amino-2 S-hydroxybutyryl) and 6'-*N*-(2-Hydroxyethyl) Substituents on Ribosomal Selectivity, Cochleotoxicity, and Antibacterial Activity in the Sisomicin Class of Aminoglycoside Antibiotics. *ACS Infect. Dis.* **2018,** *4*, 1114-1120.

81. Kang, A. D.; Smith, K. P.; Eliopoulos, G. M.; Berg, A. H.; McCoy, C.; Kirby, J. E., In vitro Apramycin Activity Against Multidrug-Resistant *Acinetobacter baumannii* and *Pseudomonas aeruginosa*. *Diagn. Microbiol. Infect. Dis.* **2017,** *88*, 188-191.

82. Juhas, M.; Widlake, E.; Teo, J.; Huseby, D. L.; Tyrrell, J. M.; Polikanov, Y. S.; Ercan, O.; Petersson, A.; Cao, S.; Aboklaish, A. F.; Rominski, A.; Crich, D.; Böttger, E. C.; Walsh, T. R.; Hughes, D.; Hobbie, S. N., In Vitro Activity of Apramycin Against Multidrug-, Carbapenem- and Aminoglycoside-Resistant *Enterobacteriaceae* and *Acinetobacter baumannii*. *J. Antimicrob. Chemother.* **2019,** *74*, 944-952.

83. Smith, K. P.; Kirby, J. E., Evaluation of Apramycin Activity Against Carbapenem-Resistant and -Susceptible Strains of *Enterobacteriaceae*. *Diagn. Microbiol. Infect. Dis.* **2016,** *86*, 439-441.

84. Press Release 24th November, 2020. https://www.linkedin.com/feed/update/urn:li:activity:6736865575634513920 (accessed July 2021).

85. First-In-Human Study of Apramycin. https://clinicaltrials.gov/ct2/show/NCT04105205 (accessed April 2021).

86. Thompson, R. Q.; Presti, E. A., Nebramycin, a New Broad-Spectrum Antibiotic Complex. III. Isolation and Chemical-Physical Properties. *Antimicrob. Agents Chemother.* **1967,** *7*, 332-40.

87. Ose, E. E. Treatment of Swine Dysentary with Apramycin. US Patent 3876767, 1975.

88. Stark, W. M.; Hoehn, M. M.; Knox, N. G., Nebramycin, a New Broad-Spectrum Antibiotic Complex. I. Detection and Biosynthesis. *Antimicrob. Agents Chemother.* **1967,** *7*, 314-23.

89. Wick, W. E.; Welles, J. S., Nebramycin, a New Broad-Spectrum Antibiotic Complex. IV. In Vitro and In Vivo Laboratory Evaluation. *Antimicrob. Agents Chemother.* **1967,** *7*, 341-8.

90. Dowling, P. M., Aminoglycosides and Aminocyclitols. In *Antimicrobial Therapy in Veterenary Medicine*, 5th ed.; Giguère, S.; Prescott, J. F.; Dowling, P. M., Eds. Wiley-Blackwell: Chichester, U.K., 2013; pp 233-255.

91. Mandhapati, A. R.; Shcherbakov, D.; Duscha, S.; Vasella, A.; Böttger, E. C.; Crich, D., Importance of the 6′-Hydroxy Group and Its Configuration for Apramycin Activity. *ChemMedChem* **2014,** *9*, 2074-2083.

92. Matt, T.; Ng, C. L.; Lang, K.; Sha, S.-H.; Akbergenov, R.; Shcherbakov, D.; Meyer, M.; Duscha, S.; Xie, J.; Dubbaka, S. R.; Perez-Fernandez, D.; Vasella, A.; Ramakrishnan, V.; Schacht, J.; Böttger, E. C., Dissociation of Antibacterial Activity and Aminoglycoside Ototoxicity in the 4-Monosubstituted 2-Deoxystreptamine Apramycin. *Proc. Natl. Acad. Sci.* **2012,** *109*, 10984-10989.

93. Perez-Fernandez, D.; Shcherbakov, D.; Matt, T.; Leong, N. C.; Kudyba, I.; Duscha, S.; Boukari, H.; Patak, R.; Dubbaka, S. R.; Lang, K.; Meyer, M.; Akbergenov, R.; Freihofer, P.; Vaddi, S.; Thommes, P.; Ramakrishnan, V.; Vasella, A.; Böttger, E. C., 4′-O-Substitutions Determine Selectivity of Aminoglycoside Antibiotics. *Nat. Commun.* **2014,** *5*, 3112.

94. Ryden, R.; Moore, B. J., The In Vitro Activity of Apramycin, A New Aminocyclitol Antibiotic. *J. Antimicrob. Chemother*. **1977,** *3*, 609-13.

95. Ishikawa, M.; García-Mateo, N.; Čusak, A.; López-Hernández, I.; Fernández-Martínez, M.; Müller, M.; Rüttiger, L.; Singer, W.; Löwenheim, H.; Kosec, G.; Fujs, Š.; Martínez-Martínez, L.; Schimmang, T.; Petković, H.; Knipper, M.; Durán-Alonso, M. B., Lower Ototoxicity and Absence of Hidden Hearing Loss Point to Gentamicin C1a and Apramycin as Promising Antibiotics for Clinical Use. *Sci. Rep.* **2019,** *9*, 2410.

96. Brennan-Krohn, T.; Kirby, J. E., Synergistic Combinations and Repurposed Antibiotics Active Against the Pandrug-Resistant *Klebsiella pneumoniae* Nevada Strain. *Antimicrob. Agents Chemother.* **2019,** *63*, e01374-19.

97. Holbrook, S. Y. L.; Garneau-Tsodikova, S., Evaluation of Aminoglycoside and Carbapenem Resistance in a Collection of Drug-Resistant *Pseudomonas aeruginosa* Clinical Isolates. *Microb. Drug Resist.* **2018,** *24*, 1020-1030.

98. Kang, A. D.; Smith, K. P.; Berg, A. H.; Truelson, K. A.; Eliopoulos, G. M.; McCoy, C.; Kirby, J. E., Efficacy of Apramycin against Multidrug-Resistant *Acinetobacter baumannii* in the Murine Neutropenic Thigh Model. *Antimicrob. Agents Chemother.* **2018,** *62*.

99. Truelson, K. A.; Brennan-Krohn, T.; Smith, K. P.; Kirby, J. E., Evaluation of Apramycin Activity Against Methicillin-Resistant, Methicillin-Sensitive, and Vancomycin-Intermediate *Staphylococcus aureus* Clinical Isolates. *Diagn. Microbiol. Infect. Dis.* **2018,** *92*, 168-171.

100. Riedel, S.; Vijayakumar, D.; Berg, G.; Kang, A. D.; Smith, K. P.; Kirby, J. E., Evaluation of Apramycin Against Spectinomycin-Resistant and -Susceptible Strains of *Neisseria gonorrhoeae*. *J. Antimicrob. Chemother.* **2019,** *74* (5), 1311-1316.

101. Kirst, H. A.; Truedell, B. A. 1-*N*--Acylated and 1-*N*-Alkylated Derivatives of 4-*O*-Substituted-2-Deoxystreptamine Aminoglycosides. US Patent 4,468,512, 1984.

102. Kirst, H. A.; Truedell, B. A. 2'-*N*-Acylated and 2'-*N*-Alkylated Derivatives of 4-*O*-Substituted-2-Deoxystreptamine Aminoglycosides. US Patent 4,468,513, 1984.

103. Allen, N. E.; Alborn, W. E.; Kirst, H. A.; Toth, J. E., Comparison of Aminoglycoside Antibiotics with Respect to Uptake and Lethal Activity in *Escherichia coli*. *J. Med. Chem.* **1987,** *30*, 333-340.

104. Kuniaki, T.; Kohji, A.; Hideaki, T.; Takao, H.; Masahiko, A.; Mitsuhiro, K., Total Synthesis of Aminoglycoside Antibiotics, Apramycin and Saccharocin (KA-5685). *Bull. Chem. Soc. Jpn.* **1984,** *57*, 529-538.

105. Sarpe, V. A.; Pirrone, M. G.; Haldimann, K.; Hobbie, S. N.; Vasella, A.; Crich, D., Synthesis of Saccharocin from Apramycin and Evaluation of its Ribosomal Slectivity. *MedChemComm* **2019,** *10*, 554-558.

106. Awata, M.; Satoi, S.; Muto, N.; Hayashi, M.; Sagai, H.; Sakakibara, H., Saccharocin, a New Aminoglycoside Antibiotic. Fermentation, Isolation, Characterization and Structural Study. *J. Antibiot.* **1983,** *36*, 651-5.

107. Kirst, H. A. 4"-*N*-(Substituted)-Apramycin Antibiotic Derivatives and Intermediates Therefor. US Patent 4,360,665, 1982.

108. Kirst, H. A. 7-*N*-Substituted Apramycin Antibiotic Derivatives and Intermediates Therefor. US Patent 4,458,065, 1984.

109. Igarashi, K.; Honma, T. Aprosamine Derivatives. US Patent 4,362,866, 1982.

110. Kirst, H. A. 6"-(Substituted)-Apramycin Antibiotic Derivatives and Intermediates and Starting Materials Therefor. US Patent 4,379,917, 1983.

111. Igarashi, K.; Honma, T.; Sugawara, T. 5-Deoxyapramycin. US Patent 4,358,585, 1982.

112. Takahashi, Y.; Umemura, E.; Ida, T.; Igarashi, M.; Nagai, H. Novel Aminoglycoside Antibiotic Effective Against Multidrug-Resistant Bacteria and a Pharmaceutical Composition Containing the Same. WO Patent Appl. 2017/018258 A1, 2017.

113. Abe, Y.; Nakagawa, S.; Naito, T.; Kawaguchi, H., Synthesis and Activity of 6-*O*-(3-Amino-3-Deoxy-α-D-Glucopyranosyl)- and 5-*O*-(β-D-Ribofuranosyl)Apramycins. *J. Antibiotics* **1981,** *34*, 1434-1446.

114. Sonousi, A.; Quirke, J. C. K.; Waduge, P.; Janusic, T.; Gysin, M.; Haldimann, K.; Xu, S.; Hobbie, S. N.; Sha, S.-H.; Schacht, J.; Chow, C. S.; Vasella, A.; Böttger, E. C.; Crich, D., An Advanced Apralog with Increased in vitro and in vivo Activity toward Gram-negative Pathogens and Reduced ex vivo Cochleotoxicity. *ChemMedChem* **2021,** *16*, 335-339.

115. Quirke, J. C. K.; Rajasekaran, P.; Sarpe, V. A.; Sonousi, A.; Osinnii, I.; Gysin, M.; Haldimann, K.; Fang, Q.-J.; Shcherbakov, D.; Hobbie, S. N.; Sha, S.-H.; Schacht, J.; Vasella, A.; Böttger, E. C.; Crich, D., Apralogs: Apramycin 5-*O*-Glycosides and Ethers with Improved Antibacterial Activity and Ribosomal Selectivity and Reduced Susceptibility to the Aminoacyltranserferase (3)-IV Resistance Determinant. *J. Am. Chem. Soc.* **2020,** *142*, 530-544.

116. Alper, P. B.; Hendrix, M.; Sears, P.; Wong, C.-H., Probing the Specificity of Aminoglycoside−Ribosomal RNA Interactions with Designed Synthetic Analogs. *J. Am. Chem. Soc.* **1998,** *120*, 1965-1978.

117. Sonousi, A. Synthesis of Netilmicin and Apramycin Derivatives for the Treatment of Multidrug-Resistant Infectious Diseases. Wayne State University, Detroit, MI, 2017.

118. Zada, S. L.; Baruch, B. B.; Simhaev, L.; Engel, H.; Fridman, M., Chemical Modifications Reduce Auditory Cell Damage Induced by Aminoglycoside Antibiotics. *J. Am. Chem. Soc.* **2020,** *142*, 3077-3087.

119. de Armas, P.; Francisco, C. G.; Suarez, E., Fragmentation of Carbohydrate Anomeric Alkoxy Radicals. Tandem β-Fragmentation-Cyclization of Alcohols. *J. Am. Chem. Soc.* **1993,** *115*, 8865-8866.

120. Taha, H. A.; Richards, M. R.; Lowary, T. L., Conformational Analysis of Furanoside-Containing Mono- and Oligosaccharides. *Chem. Rev.* **2013,** *113*, 1851-1876.

121. VanRheenen, V.; Cha, D. Y.; Hartley, W. M., Catalytic Osmium Tetroxide Oxidation of Olefins: *cis*-1,2-Cyclohexanediol. *Org. Syn. Coll. Vol.* **1988,** *6*, 342-348.

122. Borch, R. F., Reductive Amination with Sodium Cyanoborohydride. *Org. Syn. Coll. Vol.* **1988,** *6*, 499-501.

123. Pathak, R.; Perez-Fernandez, D.; Nandurdikar, R.; Kalapala, S. K.; Böttger, E. C.; Vasella, A., Synthesis and Evaluation of Paromomycin Derivatives Modified at C(4′). *Helv. Chim. Acta* **2008,** *91*, 1533-1552.

124. Raluy, E.; Pàmies, O.; Diéguez, M., Modular Furanoside Phosphite-Phosphoroamidites, a Readily Available Ligand Library for Asymmetric Palladium-Catalyzed Allylic Substitution Reactions. Origin of Enantioselectivity. *Adv. Synth. Catal.* **2009,** *351*, 1648-1670.

125. Demko, Z. P.; Sharpless, K. B., An Intramolecular [2 + 3] Cycloaddition Route to Fused 5-Heterosubstituted Tetrazoles. *Org. Lett.* **2001,** *3*, 4091-4094.

126. Hobbie, S. N.; Kalapala, S. K.; Akshay, S.; Bruell, C.; Schmidt, S.; Dabow, S.; Vasella, A.; Sander, P.; Böttger, E. C., Engineering the rRNA Decoding Site of Eukaryotic Cytosolic Ribosomes in Bacteria. *Nucleic Acids Res.* **2007,** *35*, 6086-6093.

127. Hobbie, S. N.; Kaiser, M.; Schmidt, S.; Shcherbakov, D.; Janusic, T.; Brun, R.; Böttger, E. C., Genetic Reconstruction of Protozoan rRNA Decoding Sites Provides a Rationale for Paromomycin Activity against Leishmania and Trypanosoma. *PLOS Neglected Trop. Dis.* **2011,** *5*, e1161.

128. Sonousi, A.; Sarpe, V. A.; Brilkova, M.; Schacht, J.; Vasella, A.; Böttger, E. C.; Crich, D., Effects of the 1-*N*-(4-Amino-2*S*-hydroxybutyryl) and 6′-*N*-(2-Hydroxyethyl) Substituents on Ribosomal Selectivity, Cochleotoxicity, and Antibacterial Activity in the Sisomicin Class of Aminoglycoside Antibiotics. *ACS Infect. Dis.* **2018,** *4*, 1114-1120.

129. Zárate, S. G.; De la Cruz Claure, M. L.; Benito-Arenas, R.; Revuelta, R.; Santana, A. G.; Bastida, A., Overcoming Aminoglycoside Enzymatic Resistance: Design of Novel Antibiotics and Inhibitors. *Molecules* **2018,** *23*, 284.

130. Umezawa, S.; Tsuchiya, T.; Muto, R.; Nishimura, Y.; Umezawa, H., Synthesis of 3'-Deoxykanamycin Effective Against Kanamycin-Resistant *Escherichia coli* and *Pseudomonas aeruginosa*. *J. Antibiot.* **1971,** *24*, 274-6.

131. Hooper, I. R., The Naturally Occurring Aminoglycoside Antibiotics. In *Aminoglycoside Antibiotics*, Umezawa, H.; Hooper, I. R., Eds. Springer, Berlin, Heidelberg, 1982; Vol. 62.

132. Courvalin, P.; Davies, J., Plasmid-Mediated Aminoglycoside Phosphotransferase of Broad Substrate Range That Phosphorylates Amikacin. *Antimicrob. Agents Chemother.* **1977,** *11*, 619-624.

133. Yamamoto, H.; Kondo, S.; Maeda, K.; Umezawa, H., Synthesis of 5"-Lividomycin A and its Amino Derivative. *J. Antibiotics* **1982,** *25*, 487-488.

134. Torii, T.; Tsuchiya, T.; Umezawa, S.; Umezwa, H., Synthesis of 5"-Deoxy-5"-fluorolividomycin B. *Bull. Chem. Soc. Jpn.* **1983,** *56*, 1522-1526.

135. Fridman, M.; Belakhov, V.; Yaron, S.; Baasov, T., A New Class of Branched Aminoglycosides: Pseudo-Pentasaccharide Derivatives of Neomycin B. *Org. Lett.* **2003,** *5*, 3575-3578.

136. Bastida, A.; Hidalgo, A.; Chiara, J. L.; Torrado, M.; Corzana, F.; Pérez-Cañadillas, J. M.; Groves, P.; Garcia-Junceda, E.; Gonzalez, C.; Jimenez-Barbero, J.; Asensio, J. L., Exploring the Use of Conformationally Locked Aminoglycosides as a New Strategy to Overcome Bacterial Resistance. *J. Am. Chem. Soc.* **2006,** *128*, 100-116.

137. Swayze, E. E.; Hanessian, S.; Szychowski, J.; Adhikari, S. S.; Pachamuthu, K.; Wang, X.; Migawa, M. T.; Griffey, R. H. Antibacterial 4,5-Substituted Aminoglycoside Analogs Having Multiple Substituents. Patent No. US20080293649, 2008.

138. Kudyba, I.; Fernandez, D. P.; Böttger, E. C.; Vasella, A., Synthesis of Paromomycin Derivatives Modified at C(5″) to Selectively Target Bacterial rRNA. *Carbohydr. Res.* **2007,** *342*, 499-519.

139. Asako, T.; Yoshioka, K.; Mabuchi, H.; Hiraga, K., Chemical Transformation of 3'-Chloro-3'-deoxyaminoglycosides into New Cyclic Pseudo-trisaccharides. *Heterocycles* **1978,** *11*, 197-2002.

140. Blount, K. F.; Zhao, F.; Hermann, T.; Tor, Y., Conformational Constraint as a Means for Understanding RNA-Aminoglycoside Specificity. *J. Am. Chem. Soc.* **2005,** *127*, 9818-9829.

141. Barbieri, C. M.; Kaul, M.; Bozza-Hingos, M.; Zhao, F.; Tor, Y.; Hermann, T.; Pilch, D. S., Defining the Molecular Forces That Determine the Impact of Neomycin on Bacterial Protein Synthesis: Importance of the 2-Amino Functionality. *Antimicrob. Agents Chemother.* **2007,** *51*, 1760-1769.

142. Hayashi, T.; Saeki, H.; Takeda, N.; Ohki, E., I-N-Alkyl Analogs Of Butirosin. *J. Antibiotics* **1979,** *32*, 1280-1287.

143. Narita, Y.; Masuyoshi, S.; Yamasaki, T.; Naito, T.; Kawaguchi, H., Synthesis and Activity of Butirosin Derivatives with 5"-Amidino and 5"-Guanidino Substituents. *J. Antibiotics* **1991,** *44*, 86-92.

144. Umezawa, S.; Tsuchiya, T.; Ikeda, D.; Umezawa, H., Synthesis of 3',4'-Dideoxy and 3',4',5"-Trideoxyribostamycin Active Against Kanamycin-Resistant *E Coli* and *P Aeruginosa*. *J. Antibiotics* **1972,** *25*, 613-616.

145. Hanessian, S.; Massé, R.; Capmeau, M. L., Aminoglycoside Antibiotics: Synthesis of 5"-Amino-5"-deoxyneomycin and 5"-Amino-5"-deoxyparomomycin. *J. Antibiot.* **1977,** *30*, 893-6.

146. Zhang, J.; Chiang, F.-I.; Wu, L.; Czyryca, P. G.; Li, D.; Chang, C.-W. T., Surprising Alteration of Antibacterial Activity of 5″-Modified Neomycin against Resistant Bacteria. *J. Med. Chem.* **2008,** *51*, 7563-7573.

147. Watkins, D.; Kumar, S.; Green, K. D.; Arya, D. P.; Garneau-Tsodikova, S., Influence of Linker Length and Composition on Enzymatic Activity and Ribosomal Binding of Neomycin Dimers. *Antimicrob. Agents Chemother.* **2015,** *59*, 3899-905.

148. Jin, Y.; Watkins, D.; Degtyareva, N. N.; Green, K. D.; Spano, M. N.; Garneau-Tsodikova, S.; Arya, D. P., Arginine-Linked Neomycin B Dimers: Synthesis, rRNA Binding, and Resistance Enzyme Activity. *MedChemComm* **2016,** *7*, 164-169.

149. Thamban Chandrika, N.; Garneau-Tsodikova, S., Comprehensive Review of Chemical Strategies for the Preparation of New Aminoglycosides and their Biological Activities. *Chem. Soc. Rev.* **2018,** *47*, 1189-1249.

150. Lubriks, D.; Zogota, R.; Sarpe, V. A.; Matsushita, T.; Sati, G. C.; Haldimann, K.; Gysin, M.; Böttger, E. C.; Vasella, A.; Suna, E.; Hobbie, S. N.; Crich, D., Synthesis and Antibacterial Activity of Propylamycin Derivatives Functionalized at the 5″- and Other Positions with a View to Overcoming Resistance Due to Aminoglycoside Modifying Enzymes. *ACS Infect. Dis.* **2021**, doi:10.1021/acsinfecdis.1c00158.

151. Shalev, M.; Baasov, T., When Proteins Start to Make Sense: Fine-Tuning of Aminoglycosides for PTC Suppression Therapy. *MedChemComm* **2014,** *5*, 1092-1105.

152. Sati, G. C.; Sarpe, V. A.; Furukawa, T.; Mondal, S.; Mantovani, M.; Hobbie, S. N.; Vasella, A.; Böttger, E. C.; Crich, D., Modification at the 2′-Position of the 4,5-Series of 2-

Deoxystreptamine Aminoglycoside Antibiotics To Resist Aminoglycoside Modifying Enzymes and Increase Ribosomal Target Selectivity. *ACS Infect. Dis.* **2019,** *5*, 1718-1730.

153. François, B.; Russell, R. J. M.; Murray, J. B.; Aboul-ela, F.; Masquida, B.; Vicens, Q.; Westhof, E., Crystal Structures of Complexes Between Aminoglycosides and Decoding A Site Oligonucleotides: Role of the Number of Rings and Positive Charges in the Specific Binding Leading to Miscoding. *Nucleic Acids Res.* **2005,** *33*, 5677-5690.

154. Kaul, M.; Pilch, D. S., Thermodynamics of Aminoglycoside−rRNA Recognition: The Binding of Neomycin-Class Aminoglycosides to the A Site of 16S rRNA. *Biochemistry* **2002,** *41*, 7695-7706.

155. Kaul, M.; Barbieri, C. M.; Kerrigan, J. E.; Pilch, D. S., Coupling of Drug Protonation to the Specific Binding of Aminoglycosides to the A Site of 16S rRNA: Elucidation of the Number of Drug Amino Groups Involved and their Identities. *J. Mol. Biol.* **2003,** *326*, 1373-1387.

156. Kiviniemi, A.; Virta, P.; Lönnberg, H., Solid-Supported Synthesis and Click Conjugation of 4′-C-Alkyne Functionalized Oligodeoxyribonucleotides. *Bioconj. Chem.* **2010,** *21*, 1890-1901.

157. Ding, X.; Wang, W.; Kong, F., Detritylation of Mono- and Di-saccharide Derivatives Using Ferric Chloride Hydrate. *Carbohydr. Res.* **1997,** *303*, 445-448.

158. Epp, J. B.; Widlanski, T. S., Facile Preparation of Nucleoside-5‘-carboxylic Acids. *J. Org. Chem.* **1999,** *64*, 293-295.

159. Barton, D. H. R.; Crich, D.; Motherwell, W. B., New and Improved Methods for the Radical Decarboxylation of Acids. *J. Chem. Soc., Chem. Commun.* **1983**, 939-941.

160. Greenberg, W. A.; Priestley, E. S.; Sears, P. S.; Alper, P. B.; Rosenbohm, C.; Hendrix, M.; Hung, S.-C.; Wong, C.-H., Design and Synthesis of New Aminoglycoside Antibiotics

Containing Neamine as an Optimal Core Structure: Correlation of Antibiotic Activity with in Vitro Inhibition of Translation. *J. Am. Chem. Soc.* **1999,** *121*, 6527-6541.

161. Sen, S. E.; Roach, S. L., A Convenient Two-Step Procedure for the Synthesis of Substituted Allylic Amines from Allylic Alcohols. *Synthesis* **1995,** *1995*, 756-758.

162. Krimen, L., Acetic Formic Anhydride. *Org. Synth.* **1970,** *50*, 1.

163. Hu, X.; Zhang, W.; Carmichael, I.; Serianni, A. S., Amide Cis−Trans Isomerization in Aqueous Solutions of Methyl N-Formyl-D-glucosaminides and Methyl N-Acetyl-D-glucosaminides: Chemical Equilibria and Exchange Kinetics. *J. Am. Chem. Soc.* **2010,** *132*, 4641-4652.

164. LaPlanche, L. A.; Rogers, M. T., *cis* and *trans* Configurations of the Peptide Bond in N-Monosubstituted Amides by Nuclear Magnetic Resonance. *J. Am. Chem. Soc.* **1964,** *86*, 337-341.

165. Sati, G. C. Addressing The Threat Of Multidrug Resistant Infectious Diseases By Synthesis Of Novel Aminoglycoside Antibiotics. Wayne State University, Detroit, MI, 2018.

166. Pawar, D. M.; Khalil, A. A.; Hooks, D. R.; Collins, K.; Elliott, T.; Stafford, J.; Smith, L.; Noe, E. A., *E* and *Z* Conformations of Esters, Thiol Esters, and Amides. *J. Am. Chem. Soc.* **1998,** *120*, 2108-2112.

167. Baasov, T.; Pokrovskaya, V.; Belakhov, V.; Hainrichson, M. Conjugated Antimicrobial Agents. WO Patent Appl. 2010/113151, 2010.

168. Pathak, R.; Böttger, E. C.; Vasella, A., Design and Synthesis of Aminoglycoside Antibiotics to Selectively Target 16S Ribosomal RNA Position 1408. *Helv. Chim. Acta* **2005,** *88*, 2967-2985.

169. Corzana, F.; Cuesta, I.; Freire, F.; Revuelta, J.; Torrado, M.; Bastida, A.; Jiménez-Barbero, J.; Asensio, J. L., The Pattern of Distribution of Amino Groups Modulates the Structure

and Dynamics of Natural Aminoglycosides: Implications for RNA Recognition. *J. Am. Chem. Soc.* **2007,** *129*, 2849-2865.

170. Fourmy, D.; Recht, M. I.; Blanchard, S. C.; Puglisi, J. D., Structure of the A site of *Escherichia coli* 16S Ribosomal RNA Complexed with an Aminoglycoside Antibiotic. *Science* **1996,** *274*, 1367-71.

171. Huisgen, R.; Walz, H., Die Elektrischen Momente der Aliphatischen Lactame und die Konfiguration der Säureamidgruppe. *Chem. Ber.* **1956,** *89*, 2616-2629.

172. Bordwell, F. G.; Fried, H. E., Heterocyclic Aromatic Anions with 4n + 2 π-Electrons. *J. Org. Chem.* **1991,** *56*, 4218-4223.

173. Wright, G. D.; Thompson, P. R., Aminoglycoside Phosphotransferases: Proteins, Structure, and Mechanism. *Front. Biosci.* **1999,** *4*, D9-21.

174. Wang, L.-X.; Davis, B. G., Realizing the Promise of Chemical Glycobiology. *Chem. Sci.* **2013,** *4*, 3381-3394.

175. Winstein, S.; Clippinger, E.; Fainberg, A. H.; Heck, R.; Robinson, G. C., Salt Effects and Ion Pairs in Solvolysis and Related Reactions. III. Common Ion Rate Depression and Exchange of Anions during Acetolysis. *J. Am. Chem. Soc.* **1956,** *78*, 328-335.

176. Phan, T. B.; Nolte, C.; Kobayashi, S.; Ofial, A. R.; Mayr, H., Can One Predict Changes from S_N1 to S_N2 Mechanisms? *J. Am. Chem. Soc.* **2009,** *131*, 11392-11401.

177. Adero, P. O.; Amarasekara, H.; Wen, P.; Bohé, L.; Crich, D., The Experimental Evidence in Support of Glycosylation Mechanisms at the S_N1–S_N2 Interface. *Chem. Rev.* **2018,** *118*, 8242-8284.

178. Rhind-Tutt, A. J.; Vernon, C. A., Mechanisms of Reactions in the Sugar Series. Part II. Nucleophilic Substitution in 2,3,4,6-Tetra-*O*-Methylglycopyranosyl Chlorides. *J. Chem. Soc.* **1960**, 4637-4644.

179. Lucas, T. J.; Schuerch, C., Methanolysis as a Model Reaction for Oligosaccharide Synthesis of Some 6-Substituted 2,3,4-Tri-*O*-Benzyl-D-Galactopyranosyl Derivatives. *Carbohydr. Res.* **1975,** *39*, 39-45.

180. Lemieux, R. U.; Hendriks, K. B.; Stick, R. V.; James, K., Halide Ion Catalyzed Glycosidation Reactions. Syntheses of α-Linked Disaccharides. *J. Am. Chem. Soc.* **1975,** *97*, 4056-4062.

181. Eby, R.; Schuerch, C., The Use of 1-*O*-Tosyl-D-Glucopyranose Derivatives in α-D-Glucoside Synthesis. *Carbohydr. Res.* **1974,** *34*, 79-90.

182. Wallace, J. E.; Schroeder, L. R., Koenigs–Knorr Reactions. Part II. A Mechanistic Study of Mercury(II) Cyanide-Promoted Reactions of 2,3,4,6-Tetra-*O*-Methyl-α-D-Glucopyranosyl Bromide with Cyclohexanol in Benzene–Nitromethane. *J. Chem. Soc. Perkin Trans. 2* **1976**, 1632-1636.

183. Crich, D., Mechanism of a Chemical Glycosylation. *Acc. Chem. Res.* **2010,** *43*, 1144-1153.

184. Horenstein, N. A., Mechanisms for Nucleophilic Aliphatic Substitution at Glycosides. In *Adv. Phys. Org. Chem.*, Richard, J. P., Ed. Academic Press: 2006; Vol. 41, pp 275-314.

185. Jeanneret, R. A.; Johnson, S. E.; Galan, M. C., Conformationally Constrained Glycosyl Donors as Tools to Control Glycosylation Outcomes. *J. Org. Chem.* **2020,** *85*, 15801-15826.

186. Bohé, L.; Crich, D., A Propos of Glycosyl Cations and the Mechanism of Chemical Glycosylation; the Current State of the Art. *Carbohydr. Res.* **2015,** *403*, 48-59.

187. Walvoort, M. T. C.; van der Marel, G. A.; Overkleeft, H. S.; Codée, J. D. C., On the Reactivity and Selectivity of Donor Glycosides in Glycochemistry and Glycobiology: Trapped Covalent Intermediates. *Chem. Sci.* **2013,** *4*, 897-906.

188. Hosoya, T.; Kosma, P.; Rosenau, T., Contact Ion Pairs and Solvent-Separated Ion Pairs from D-Mannopyranosyl and D-Glucopyranosyl Triflates. *Carbohydr. Res.* **2015,** *401*, 127-131.

189. Crich, D., En Route to the Transformation of Glycoscience: A Chemist's Perspective on Internal and External Crossroads in Glycochemistry. *J. Am. Chem. Soc.* **2021,** *143*, 17-34.

190. Zhang, Z.; Ollmann, I. R.; Ye, X.-S.; Wischnat, R.; Baasov, T.; Wong, C.-H., Programmable One-Pot Oligosaccharide Synthesis. *J. Am. Chem. Soc.* **1999,** *121*, 734-753.

191. Fraser-Reid, B.; Cristóbal López, J., Armed-Disarmed Effects in Carbohydrate Chemistry: History, Synthetic and Mechanistic Studies. In *Reactivity Tuning in Oligosaccharide Assembly*, 2010/12/02 ed.; Fraser-Reid, B.; Cristóbal López, J., Eds. Springer, Berlin, Heidelberg: 2011; Vol. 301, pp 1-29.

192. Hettikankanamalage, A. A.; Lassfolk, R.; Ekholm, F. S.; Leino, R.; Crich, D., Mechanisms of Stereodirecting Participation and Ester Migration from Near and Far in Glycosylation and Related Reactions. *Chem. Rev.* **2020,** *120*, 7104-7151.

193. Kirmse, W.; Mrotzeck, U., Zerfall von 2-Oxa-5- und -6-Norbornandiazonium-Ionen. *Chem. Ber.* **1988,** *121*, 485-492.

194. Lambert, J. B.; Mark, H. W., Increased Electron Demand in the Solvolysis of Secondary 2-Norbornyl Tosylates. *J. Am. Chem. Soc.* **1978,** *100*, 2501-2505.

195. Crich, D.; Yang, F., Phenylthiomethyl Glycosides: Convenient Synthons for the Formation of Azidomethyl and Glycosylmethyl Glycosides and Their Derivatives. *Angew. Chem. Int. Ed.* **2009,** *48*, 8896-8899.

196. Chenault, H. K.; Chafin, L. F., Hydrolysis of *O*-Isopropenyl Glucopyranosides Involves *C*-Protonation and Alkenyl Ether Cleavage and Exhibits a Kinetic Influence of Anomeric Configuration. *J. Org. Chem.* **1994,** *59*, 6167-6169.

197. Chenault, H. K.; Chafin, L. F., Mechanism of Hydrolysis of Isopropenyl Glucopyranosides. Spectroscopic Evidence Concerning the Greater Reactivity of the α Anomer. *J. Org. Chem.* **1998,** *63*, 833-840.

198. Overend, W. G.; Rees, C. W.; Sequeira, J. S., Reactions at Position 1 of Carbohydrates. The Acid-Catalysed Hydrolysis of Glycosides. *J. Chem. Soc.* **1962**, 3429-3440.

199. Cocker, D.; Sinnott, M. L., Generation of Glycopyranosyl Cations in the Spontaneous Hydrolyses of 2,4-Dinitrophenyl Glycopyranosides. Evidence for the General Intermediacy of Glycopyranosyl Cations in the Acid-Catalysed Hydrolyses of Methyl Glycopyranosides. *J. Chem. Soc. Perkin Trans. 2* **1975**, 1391-1395.

200. Namchuk, M. N.; McCarter, J. D.; Becalski, A.; Andrews, T.; Withers, S. G., The Role of Sugar Substituents in Glycoside Hydrolysis. *J. Am. Chem. Soc.* **2000,** *122*, 1270-1277.

201. Bohé, L.; Crich, D., A Propos of Glycosyl Cations and the Mechanism of Chemical Glycosylation. *C. R. Chim.* **2011,** *14*, 3-16.

202. Rakhmankulov, D. L.; Akhmatdinov, R. T.; Kantor, E. A., Alkoxycarbenium Ions. *Russ. Chem. Rev.* **1984,** *53*, 888-899.

203. Matsumoto, K.; Ueoka, K.; Suzuki, S.; Suga, S.; Yoshida, J.-i., Direct and Indirect Electrochemical Generation of Alkoxycarbenium Ion Pools from Thioacetals. *Tetrahedron* **2009,** *65*, 10901-10907.

204. Saito, K.; Ueoka, K.; Matsumoto, K.; Suga, S.; Nokami, T.; Yoshida, J.-i., Indirect Cation-Flow Method: Flash Generation of Alkoxycarbenium Ions and Studies on the Stability of Glycosyl Cations. *Angew. Chem. Int. Ed.* **2011,** *50*, 5153-5156.

205. Bohé, L.; Crich, D., Glycosyl Cations Out on Parole. *Nat. Chem.* **2016,** *8*, 99-100.

206. Martin, A.; Arda, A.; Désiré, J.; Martin-Mingot, A.; Probst, N.; Sinaÿ, P.; Jiménez-Barbero, J.; Thibaudeau, S.; Blériot, Y., Catching Elusive Glycosyl Cations in a Condensed Phase with HF/SbF_5 Superacid. *Nat. Chem.* **2016,** *8*, 186-191.

207. L. Douglas, N.; V. Ley, S.; Lücking, U.; L. Warriner, S., Tuning Glycoside Reactivity: New Tool for Efficient Oligosaccharide Synthesis. *J. Chem. Soc. Perkin Trans. 1* **1998,** (1), 51-66.

208. Zhao, H.; Pan, Q.; Zhang, W.; Carmichael, I.; Serianni, A. S., DFT and NMR Studies of $^{2}J_{COH}$, $^{3}J_{HCOH}$, and $^{3}J_{CCOH}$ Spin-Couplings in Saccharides: C−O Torsional Bias and H-Bonding in Aqueous Solution. *J. Org. Chem.* **2007,** *72*, 7071-7082.

209. Roën, A.; Padrón, J. I.; Vázquez, J. T., Hydroxymethyl Rotamer Populations in Disaccharides. *J. Org. Chem.* **2003,** *68*, 4615-4630.

210. Bock, K.; Duus, J. Ø., A Conformational Study of Hydroxymethyl Groups in Carbohydrates Investigated by ^{1}H NMR Spectroscopy. *J. Carbohydr. Chem.* **1994,** *13*, 513-543.

211. Pirrone, M. G.; Matsushita, T.; Vasella, A.; Crich, D., Stereospecific Synthesis of Methyl 2-amino-2,4-dideoxy-6*S*-deuterio-α-D-*xylo*-hexopyranoside and methyl 2-amino-2,4-dideoxy-6*S*-deuterio-4-propyl-α-D-glucopyranoside: Side Chain Conformation of the Novel Aminoglycoside Antibiotic Propylamycin. *Carbohydr. Res.* **2020,** *491*, 107984.

212. Jensen, H. H.; Nordstrøm, L. U.; Bols, M., The Disarming Effect of the 4,6-Acetal Group on Glycoside Reactivity: Torsional or Electronic. *J. Am. Chem. Soc.* **2004,** *126*, 9205-9213.

213. Woods, R. J.; Andrews, C. W.; Bowen, J. P., Molecular Mechanical Investigations of the Properties of Oxocarbenium Ions. 2. Application to Glycoside Hydrolysis. *J. Am. Chem. Soc.* **1992,** *114*, 859-864.

214. Miljković, M.; Yeagley, D.; Deslongchamps, P.; Dory, Y. L., Experimental and Theoretical Evidence of Through-Space Electrostatic Stabilization of the Incipient Oxocarbenium Ion by an Axially Oriented Electronegative Substituent During Glycopyranoside Acetolysis. *J. Org. Chem.* **1997,** *62*, 7597-7604.

215. Dharuman, S.; Crich, D., Determination of the Influence of Side-Chain Conformation on Glycosylation Selectivity Using Conformationally Restricted Donors. *Chem. Eur. J.* **2016,** *22*, 4535-4542.

216. Jensen, H. H.; Bols, M., Stereoelectronic Substituent Effects. *Acc. Chem. Res.* **2006,** *39*, 259-265.

217. Smith, D. M.; Woerpel, K. A., Electrostatic Interactions in Cations and their Importance in Biology and Chemistry. *Org. Biomol. Chem.* **2006,** *4*, 1195-1201.

218. Fraser-Reid, B.; Wu, Z.; Andrews, C. W.; Skowronski, E.; Bowen, J. P., Torsional Effects in Glycoside Reactivity: Saccharide Couplings Mediated by Acetal Protecting Groups. *J. Am. Chem. Soc.* **1991,** *113*, 1434-1435.

219. Jensen, H. H.; Nordstrøm, L. U.; Bols, M., The Disarming Effect of the 4,6-Acetal Group on Glycoside Reactivity: Torsional or Electronic. *J. Am. Chem. Soc.* **2004,** *126*, 9205-9213.

220. Crich, D.; Sun, S., Direct Synthesis of β-Mannopyranosides by the Sulfoxide Method. *J. Org. Chem.* **1997,** *62*, 1198-1199.

221. Moumé-Pymbock, M.; Furukawa, T.; Mondal, S.; Crich, D., Probing the Influence of a 4,6-O-Acetal on the Reactivity of Galactopyranosyl Donors: Verification of the Disarming Influence of the *trans–gauche* Conformation of C5–C6 Bonds. *J. Am. Chem. Soc.* **2013,** *135*, 14249-14255.

222. Pirrone, M. G.; Gysin, M.; Haldimann, K.; Hobbie, S. N.; Vasella, A.; Crich, D., Predictive Analysis of the Side Chain Conformation of the Higher Carbon Sugars: Application to the Preorganization of the Aminoglycoside Ring 1 Side Chain for Binding to the Bacterial Ribosomal Decoding A Site. *J. Org. Chem.* **2020,** *85*, 16043-16059.

223. Kancharla, P. K.; Crich, D., Influence of Side Chain Conformation and Configuration on Glycosyl Donor Reactivity and Selectivity as Illustrated by Sialic Acid Donors Epimeric at the 7-Position. *J. Am. Chem. Soc.* **2013,** *135*, 18999-19007.

224. Dhakal, B.; Crich, D., Synthesis and Stereocontrolled Equatorially Selective Glycosylation Reactions of a Pseudaminic Acid Donor: Importance of the Side Chain Conformation, and Regioselective Reduction of Azide Protecting Groups. *J. Am. Chem. Soc.* **2018,** *140*, 15008-15015.

225. Popik, O.; Dhakal, B.; Crich, D., Stereoselective Synthesis of the Equatorial Glycosides of Legionaminic Acid. *J. Org. Chem.* **2017,** *82*, 6142-6152.

226. McDonnell, C.; López, O.; Murphy, P. V.; Fernández Bolaños, J. G.; Hazell, R. G.; Bols, M., Conformational Effects on Glycoside Reactivity: Study of the High Reactive Conformer of Glucose. *J. Am. Chem. Soc.* **2004,** *126*, 12374-12385.

227. Pedersen, C. M.; Marinescu, L. G.; Bols, M., Conformationally Armed Glycosyl Donors: Reactivity Quantification, New Donors and One Pot Reactions. *Chem. Commun.* **2008**, 2465-2467.

228. Jensen, H. H.; Pedersen, C. M.; Bols, M., Going to Extremes: "Super" Armed Glycosyl Donors in Glycosylation Chemistry. *Chem. Eur, J.* **2007,** *13*, 7576-7582.

229. Pedersen, C. M.; Marinescu, L. G.; Bols, M., Glycosyl Donors in Unusual Conformations - Influence on Selectivity and Reactivity. *Comptes Rendus Chimie* **2011,** *14*, 17-43.

230. Pedersen, C. M.; Nordstrom, L. U.; Bols, M., "Super Armed" Glycosyl Donors: Conformational Arming of Thioglycosides by Silylation *J. Am. Chem. Soc.* **2007,** *129*, 9222-9235.

231. Heuckendorff, M.; Premathilake, H. D.; Pornsuriyasak, P.; Madsen, A. O.; Pedersen, C. M.; Bols, M.; Demchenko, A. V., Superarming of Glycosyl Donors by Combined Neighboring and Conformational Effects. *Org. Lett.* **2013,** *15*, 4904-4907.

232. Okada, Y.; Mukae, T.; Okajimia, K.; Taira, M.; Fujita, M.; Yamada, H., Highly β-Selective *O*-Glucosidation Due to the Restricted Twist-Boat Conformation. *Org. Lett.* **2007,** *9*, 1573-1576.

233. Okada, Y.; Nagata, O.; Taira, M.; Yamada, H., Highly β-Selective and Direct formation of 2-*O*-Glycosylated Glucosides by ring Restriction into Twist Boat. *Org. Lett.* **2007,** *9*, 2755-2758.

234. Crich, D.; Sun, S., Direct Chemical Synthesis of β-Mannopyranosides and Other Glycosides via Glycosyl Triflates. *Tetrahedron* **1998,** *54*, 8321-8348.

235. Crich, D.; Chandrasekera, N. S., Mechanism of 4,6-*O*-Benzylidene-Directed β-Mannosylation as Determined by α-Deuterium Kinetic Isotope Effects. *Angew. Chem. Int. Ed.* **2004,** *43*, 5386-5389.

236. Crich, D.; Cai, W., Chemistry of 4,6-*O*-Benzylidene-D-glycopyranosyl Triflates: Contrasting Behavior between the Gluco and Manno Series. *J. Org. Chem.* **1999,** *64*, 4926-4930.

237. Bousquet, E.; Khitri, M.; Lay, L.; Nicotra, F.; Panza, L.; Russo, G., Capsular Polysaccharide of *Streptococcus pneumoniae* Type 19F: Synthesis of the Repeating Unit. *Carbohydr. Res.* **1998,** *311*, 171-181.

238. Crich, D.; Vinogradova, O., On the Influence of the C2−O2 and C3−O3 Bonds in 4,6-*O*-Benzylidene-Directed β-Mannopyranosylation and α-Glucopyranosylation. *J. Org. Chem.* **2006,** *71*, 8473-8480.

239. Crich, D.; Li, L., 4,6-O-Benzylidene-Directed β-Mannopyranosylation and α-Glucopyranosylation: The 2-Deoxy-2-fluoro and 3-Deoxy-3-fluoro Series of Donors and the Importance of the O2−C2−C3−O3 Interaction. *J. Org. Chem.* **2007,** *72*, 1681-1690.

240. Huang, M.; Garrett, G. E.; Birlirakis, N.; Bohé, L.; Pratt, D. A.; Crich, D., Dissecting the Mechanisms of a Class of Chemical Glycosylation Using Primary ^{13}C Kinetic Isotope Effects. *Nat. Chem.* **2012,** *4*, 663-667.

241. Santana, A. G.; Montalvillo-Jiménez, L.; Díaz-Casado, L.; Corzana, F.; Merino, P.; Cañada, F. J.; Jiménez-Osés, G.; Jiménez-Barbero, J.; Gómez, A. M.; Asensio, J. L., Dissecting the Essential Role of Anomeric β-Triflates in Glycosylation Reactions. *J. Am. Chem. Soc.* **2020,** *142*, 12501-12514.

242. Adero, P. O.; Furukawa, T.; Huang, M.; Mukherjee, D.; Retailleau, P.; Bohé, L.; Crich, D., Cation Clock Reactions for the Determination of Relative Reaction Kinetics in

Glycosylation Reactions: Applications to Gluco- and Mannopyranosyl Sulfoxide and Trichloroacetimidate Type Donors. *J. Am. Chem. Soc.* **2015,** *137*, 10336-10345.

243. Amyes, T. L.; Jencks, W. P., Lifetimes of Oxocarbenium Ions in Aqueous Solution from Common Ion Inhibition of the Solvolysis of α-Azido Ethers by Added Azide Ion. *J. Am. Chem. Soc.* **1989,** *111*, 7888-7900.

244. Horenstein, B. A.; Bruner, M., The N-Acetyl Neuraminyl Oxecarbenium Ion Is an Intermediate in the Presence of Anionic Nucleophiles. *J. Am. Chem. Soc.* **1998,** *120*, 1357-1362.

245. Griller, D.; Ingold, K. U., Free-Radical Clocks. *Acc. Chem. Res.* **1980,** *13*, 317-323.

246. Crich, D.; Sharma, I., Is Donor−Acceptor Hydrogen Bonding Necessary for 4,6-O-Benzylidene-directed β-Mannopyranosylation? Stereoselective Synthesis of β-C-Mannopyranosides and α-C-Glucopyranosides. *Org. Lett.* **2008,** *10*, 4731-4734.

247. El-Badri, M. H.; Willenbring, D.; Tantillo, D. J.; Gervay-Hague, J., Mechanistic Studies on the Stereoselective Formation of β-Mannosides from Mannosyl Iodides Using α-Deuterium Kinetic Isotope Effects. *J. Org. Chem.* **2007,** *72*, 4663-4672.

248. Chan, J.; Sannikova, N.; Tang, A.; Bennet, A. J., Transition-State Structure for the Quintessential S_N2 Reaction of a Carbohydrate: Reaction of α-Glucopyranosyl Fluoride with Azide Ion in Water. *J. Am. Chem. Soc.* **2014,** *136*, 12225-12228.

249. Kwan, E. E.; Park, Y.; Besser, H. A.; Anderson, T. L.; Jacobsen, E. N., Sensitive and Accurate ^{13}C Kinetic Isotope Effect Measurements Enabled by Polarization Transfer. *J. Am. Chem. Soc.* **2017,** *139*, 43-46.

250. Park, Y.; Harper, K. C.; Kuhl, N.; Kwan, E. E.; Liu, R. Y.; Jacobsen, E. N., Macrocyclic Bis-Thioureas Catalyze Stereospecific Glycosylation Reactions. *Science* **2017,** *355*, 162.

251. Gouliaras, C.; Lee, D.; Chan, L.; Taylor, M. S., Regioselective Activation of Glycosyl Acceptors by a Diarylborinic Acid-Derived Catalyst. *J. Am. Chem. Soc.* **2011,** *133*, 13926-13929.

252. Bennett, C. S., Glycosyl Sulfonates Beyond Triflates. *Chem. Rec.* **2021,** *21*, 1-11.

253. Zhuo, M.-H.; Wilbur, D. J.; Kwan, E. E.; Bennett, C. S., Matching Glycosyl Donor Reactivity to Sulfonate Leaving Group Ability Permits S_N2 Glycosylations. *J. Am. Chem. Soc.* **2019,** *141*, 16743-16754.

254. Issa, J. P.; Lloyd, D.; Steliotes, E.; Bennett, C. S., Reagent Controlled β-Specific Dehydrative Glycosylation Reactions with 2-Deoxy-Sugars. *Org. Lett.* **2013,** *15*, 4170-4173.

255. Ling, J.; Bennett, C. S., Versatile Glycosyl Sulfonates in β-Selective C-Glycosylation. *Angew. Chem. Int. Ed.* **2020,** *59*, 4304-4308.

256. Schjoldager, K. T.; Narimatsu, Y.; Joshi, H. J.; Clausen, H., Global View of Human Protein Glycosylation Pathways and Functions. *Nat. Rev. Mol. Cell. Biol.* **2020,** *21*, 729-749.

257. Menger, F. M., Enzyme Reactivity from an Organic Perspective. *Acc. Chem. Res.* **1993,** *26*, 206-212.

258. Kitaoka, M.; Hayashi, K., Carbohydrate-Processing Phosphorolytic Enzymes. *Trends Glycosci. Glycotechnol.* **2002,** *14*, 35-50.

259. Compain, P., Multivalent Effects in Glycosidase Inhibition: The End of the Beginning. *Chem. Rec.* **2020,** *20*, 10-22.

260. Tedaldi, L.; Wagner, G. K., Beyond Substrate Analogues: New Inhibitor Chemotypes for Glycosyltransferases. *MedChemComm* **2014,** *5*, 1106-1125.

261. Videira, P. A.; Marcelo, F.; Grewal, R. K., Glycosyltransferase Inhibitors: A Promising Strategy to Pave a Path from Laboratory to Therapy. *Carbohydr. Chem.* **2018,** *43*, 135-158.

262. Gloster, T. M.; Davies, G. J., Glycosidase Inhibition: Assessing Mimicry of the Transition State. *Org. Biomol. Chem.* **2010,** *8*, 305-320.

263. Henrissat, B., A Classification of Glycosyl Hydrolases Based on Amino Acid Sequence Similarities. *Biochem. J.* **1991,** *280*, 309-316.

264. Yip, V. L. Y.; Thompson, J.; Withers, S. G., Mechanism of GlvA from *Bacillus subtilis*: A Detailed Kinetic Analysis of a 6-Phospho-α-Glucosidase from Glycoside Hydrolase Family 4. *Biochemistry* **2007,** *46*, 9840-9852.

265. Yip, V. L. Y.; Withers, S. G., Mechanistic Analysis of the Unusual Redox-elimination Sequence employed by *Thermotoga maritima* Bg1T: A 6-Phospho-β-glucosidase from Glycoside Hydrolase Family 4. *Biochemistry* **2006,** *45*, 571-580.

266. Liu, Q. P.; Sulzenbacher, G.; Yuan, H.; Bennett, E. P.; Pietz, G.; Saunders, K.; Spence, J.; Niudelman, E.; Levery, s. B.; White, T.; Neveu, J. M.; Lane, W. S.; Bourne, Y.; Olsson, M. L.; Henrissat, B., Bacterial Glycosidases for the Production of Universal Red Blood Cells. *Nat. Biotechnol.* **2007,** *25*, 454-464.

267. Rojas-Cervellera, V.; Ardèvol, A.; Boero, M.; Planas, A.; Rovira, C., Formation of a Covalent Glycosyl–Enzyme Species in a Retaining Glycosyltransferase. *Chem. Eur. J.* **2013,** *19*, 14018-14023.

268. Soya, N.; Fang, Y.; Palcic, M. M.; Klassen, J. S., Trapping and Characterization of Covalent Intermediates of Mutant Retaining Glycosyltransferases. *Glycobiology* **2010,** *21*, 547-552.

269. Lee, S. S.; Hong, S. Y.; Errey, J. C.; Izumi, A.; Davies, G. J.; Davis, B. G., Mechanistic Evidence for a Front-Side, S_Ni-Type Reaction in a Retaining Glycosyltransferase. *Nat. Chem. Biol.* **2011,** *7*, 631-638.

270. Ardèvol, A.; Iglesias-Fernández, J.; Rojas-Cervellera, V.; Rovira, C., The Reaction Mechanism of Retaining Glycosyltransferases. *Biochem. Soc. Trans.* **2016,** *44*, 51-60.

271. Mestrom, L.; Przypis, M.; Kowalczykiewicz, D.; Pollender, A.; Kumpf, A.; Marsden, S. R.; Bento, I.; Jarzębski, A. B.; Szymańska, K.; Chruściel, A.; Tischler, D.; Schoevaart, R.; Hanefeld, U.; Hagedoorn, P.-L., Leloir Glycosyltransferases in Applied Biocatalysis: A Multidisciplinary Approach. *Int. J. Mol. Sci.* **2019,** *20*, 5263.

272. Bissaro, B.; Monsan, P.; Fauré, R.; O'Donohue, Michael J., Glycosynthesis in a Waterworld: New Insight into the Molecular Basis of Transglycosylation in Retaining Glycoside Hydrolases. *Biochem. J.* **2015,** *467*, 17-35.

273. Nakai, H.; Kitaoka, M.; Svensson, B.; Ohtsubo, K. i., Recent Development of Phosphorylases Possessing Large Potential for Oligosaccharide Synthesis. *Curr. Opin. Chem. Biol.* **2013,** *17*, 301-309.

274. Dahlquist, F. W.; Rand-Meir, T.; Raftery, M. A., Application of Secondary α-Deuterium Kinetic Isotope Effects to Studies of Enzyme Catalysis. Glycoside Hydrolysis by Lysozyme and β-Glucosidase. *Biochemistry* **1969,** *8*, 4214-4221.

275. Dahlquist, F. W.; Rand-Meir, T.; Raftery, M. A., Demonstration of Carbonium Ion Intermediate During Lysozyme Catalysis. *Proc. Natl. Acad. Sci.* **1968,** *61*, 1194-1198.

276. Sinnott, M. L., *Carbohydrate Chemistry and Biochemistry*. The Royal Society of Chemistry: Cambridge, UK, 2008.

277. Kempton, J. B.; Withers, S. G., Mechanism of *Agrobacterium* β-Glucosidase: Kinetic Studies. *Biochemistry* **1992,** *31*, 9961-9.

278. Zechel, D. L.; Withers, S. G., Glycosidase Mechanisms: Anatomy of a Finely Tuned Catalyst. *Acc. Chem. Res.* **2000,** *33*, 11-18.

279. Tanaka, Y.; Tao, W.; Blanchard, J. S.; Hehre, E. J., Transition State Structures for the Hydrolysis of α-D-Glucopyranosyl Fluoride by Retaining and Inverting Reactions of Glycosylases. *J. Biol. Chem.* **1994,** *269*, 32306-32312.

280. Murray, B. W.; Wittmann, V.; Burkart, M. D.; Hung, S.-C.; Wong, C.-H., Mechanism of Human α-1,3-Fucosyltransferase V: Glycosidic Cleavage Occurs Prior to Nucleophilic Attack. *Biochemistry* **1997,** *36*, 823-831.

281. Thompson, A. J.; Dabin, J.; Iglesias-Fernández, J.; Ardèvol, A.; Dinev, Z.; Williams, S. J.; Bande, O.; Siriwardena, A.; Moreland, C.; Hu, T.-C.; Smith, D. K.; Gilbert, H. J.; Rovira, C.; Davies, G. J., The Reaction Coordinate of a Bacterial GH47 α-Mannosidase: A Combined Quantum Mechanical and Structural Approach. *Angew. Chem. Int. Ed.* **2012,** *51*, 10997-11001.

282. Jeng, W.-Y.; Wang, N.-C.; Lin, C.-T.; Chang, W.-J.; Liu, C.-I.; Wang, A. H.-J., High-resolution Structures of *Neotermes koshunensis* β-glucosidase Mutants Provide Insights into the Catalytic Mechanism and the Synthesis of Glucoconjugates. *Acta Crystallogr., Sect. D: Biol. Crystallogr.* **2012,** *68*, 829-838.

283. Compain, P.; Martin, O. R., *Iminosugars: From Synthesis to Therapeutic Applications*. Wiley: Chichester, 2007; p 467.

284. Compain, P., Multivalent Effect in Glycosidase Inhibition: The End of the Beginning. *Chem. Rec.* **2020,** *20*, 10-22.

285. Asano, N., Glycosidase Inhibitors: Update and Perspectives on Practical Use. *Glycobiology* **2003,** *13* (10), 93R-104R.

286. Sauvage, E.; Terrak, M., Glycosyltransferases and Transpeptidases/Penicillin-Binding Proteins: Valuable Targets for New Antibacterials. *Antibiotics* **2016,** *5*, 12.

287. Kajimoto, T.; Node, M., Synthesis of Glycosyltransferase Inhibitors. *Synthesis* **2009**, 3179-3210.

288. Lombard, V.; Golaconda, R. H.; Drula, E.; Coutinho, P. M.; Henrissat, B., The Carbohydrate-Active Enzymes Database (CAZy) in 2013. *Nucleic Acids Res.* **2013,** *42*, D490-D495.

289. Davies, G. J.; Wilson, K. S.; Henrissat, B., Nomenclature for Sugar-Binding Subsites in Glycosyl Hydrolases. *Biochem. J.* **1997,** *321*, 557-559.

290. Quirke, J. C. K.; Crich, D., Glycoside Hydolases Restrict the Side Chain Conformation of their Substrates to Gain Additional Transition State Stabilization. *J. Am. Chem. Soc.* **2020,** *142*, 16965-16973.

291. Quirke, J. C. K.; Crich, D., Side Chain Conformation Restriction in the Catalysis of Glycosidic Bond Formation by Leloir Glycosyltransferases, Glycoside Phosphorylases, and Transglycosidases. *ACS Catal.* **2021,** *11*, 5069-5078.

292. Jongkees, S. A. K.; Withers, S. G., Unusual Enzymatic Glycoside Cleavage Mechanisms. *Acc. Chem. Res.* **2014,** *47*, 226-235.

293. Agirre, J.; Iglesias-Fernández, J.; Rovira, C.; Davies, G. J.; Wilson, K. S.; Cowtan, K. D., Privateer: Software for the Conformational Validation of Carbohydrate Structures. *Nat. Struct. Mol. Biol.* **2015,** *22*, 833-834.

294. Hudson, K. L.; Bartlett, G. J.; Diehl, R. C.; Agirre, J.; Gallagher, T.; Kiessling, L. L.; Woolfson, D. N., Carbohydrate–Aromatic Interactions in Proteins. *J. Am. Chem. Soc.* **2015,** *137*, 15152-15160.

295. McMahon, C. M.; Isabella, C. R.; Windsor, I. W.; Kosma, P.; Raines, R. T.; Kiessling, L. L., Stereoelectronic Effects Impact Glycan Recognition. *J. Am. Chem. Soc.* **2020,** *142*, 2386-2395.

296. Agirre, J.; Davies, G.; Wilson, K.; Cowtan, K., Carbohydrate Anomalies in the PDB. *Nat. Chem. Biol.* **2015,** *11*, 303-303.

297. Amarasekara, H.; Dharuman, S.; Kato, T.; Crich, D., Synthesis of Conformationally-Locked cis- and trans-Bicyclo[4.4.0] Mono-, Di-, and Trioxadecane Modifications of Galacto- and Glucopyranose; Experimental Limiting $^{3}J_{H,H}$ Coupling Constants for the Estimation of Carbohydrate Side Chain Populations and Beyond. *J. Org. Chem.* **2018,** *83*, 881-897.

298. Sobala, Ł.; Speciale, G.; Zhu, S.; Raich, L.; Sannikova, N.; Thompson, A.; Hakki, Z.; Lu, D.; Shamsi, S.; Lewis, A.; Rojas-Cervellera, V.; Bernardo-Seisdedos, G.; Zhang, Y.; Millet, O.; Jiménez-Barbero, J. s.; Bennett, A.; Sollogoub, M.; Rovira, C.; Davies, G.; Williams, S., An Epoxide Intermediate in Glycosidase Catalysis. *ACS Cent. Sci.* **2020,** *6*, 760-770.

299. Uitdehaag, J. C. M.; Kalk, K. H.; van der Veen, B. A.; Dijkhuizen, L.; Dijkstra, B. W., The Cyclization Mechanism of Cyclodextrin Glycosyltransferase (CGTase) as Revealed by a γ-Cyclodextrin-CGTase Complex at 1.8-Å Resolution. *J. Biol. Chem.* **1999,** *274*, 34868-34876.

300. Leemhuis, H.; Uitdehaag, J. C. M.; Rozeboom, H. J.; Dijkstra, B. W.; Dijkhuizen, L., The Remote Substrate Binding Subsite −6 in Cyclodextrin-glycosyltransferase Controls the Transferase Activity of the Enzyme via an Induced-fit Mechanism. *J. Biol. Chem.* **2002,** *277*, 1113-1119.

301. Uitdehaag, J. C. M.; Mosi, R.; Kalk, K. H.; van der Veen, B. A.; Dijkhuizen, L.; Withers, S. G.; Dijkstra, B. W., X-ray Structures Along the Reaction Pathway of Cyclodextrin

Glycosyltransferase Elucidate Catalysis in the α-Amylase Family. *Nat. Struct. Biol.* **1999,** *6*, 432-436.

302. Qian, X.; Palcic, M. M., Glycosyl Transferase Inhibitors. In *Carbohydrates in Chemistry and Biology. Part II: Biology of Saccharides*, Ernst, B.; Hart, G. W.; Sinay, P., Eds. Wiley-VCH: Weinheim, 2000; Vol. 3, pp 293-312.

303. Zechel, D. L.; Withers, S. G., Glycosyl Transferase Mechanisms. In *Comprehensive Natural Products Chemistry*, Barton, D. H. R.; Nakanishi, K.; Meth-Cohn, O., Eds. Pergamon: Oxford, 1999; Vol. 5, pp 279-314.

304. Lazarus, M. B.; Jiang, J.; Gloster, T. M.; Zandberg, W. F.; Whitworth, G. E.; Vocadlo, D. J.; Walker, S., Structural Snapshots of the Reaction Coordinate for *O*-GlcNAc Transferase. *Nat. Chem. Biol.* **2012,** *8*, 966-968.

305. Namchuk, M. N.; Withers, S. G., Mechanism of *Agrobacterium* β-glucosidase: Kinetic Analysis of the Role of Noncovalent Enzyme/Substrate Interactions. *Biochemistry* **1995,** *34*, 16194-16202.

306. Wolfenden, R.; Snider, M.; Ridgway, C.; Miller, B., The Temperature Dependence of Enzyme Rate Enhancements. *J. Am. Chem. Soc.* **1999,** *121*, 7419-7420.

307. Snider, M. J.; Gaunitz, S.; Ridgway, C.; Short, S. A.; Wolfenden, R., Temperature Effects on the Catalytic Efficiency, Rate Enhancement, and Transition State Affinity of Cytidine Deaminase, and the Thermodynamic Consequences for Catalysis of Removing a Substrate "Anchor". *Biochemistry* **2000,** *39*, 9746-9753.

308. Preiswerk, N.; Beck, T.; Schulz, J. D.; Milovník, P.; Mayer, C.; Siegel, J. B.; Baker, D.; Hilvert, D., Impact of Scaffold Rigidity on the Design and Evolution of an Artificial Diels-Alderase. *Proc. Natl. Acad. Sci.* **2014,** *111*, 8013-8018.

309. Campbell, A. P.; Tarasow, T. M.; Massefski, W.; Wright, P. E.; Hilvert, D., Binding of a High-Energy Substrate Conformer in Antibody Catalysis. *Proc. Natl. Acad. Sci.* **1993,** *90*, 8663-8667.

310. Page, M. I.; Jencks, W. P., Entropic Contributions to Rate Accelerations in Enzymic and Intramolecular Reactions and the Chelate Effect. *Proc. Natl. Acad. Sci.* **1971,** *68*, 1678-1683.

311. Ngoje, P.; Crich, D., Stereocontrolled Synthesis of the Equatorial Glycosides of 3-Deoxy-D-manno-oct-2-ulosonic Acid: Role of Side Chain Conformation. *J. Am. Chem. Soc.* **2020,** *142*, 7760-7764.

312. Dhakal, B.; Crich, D., Synthesis and Stereocontrolled Equatorially Selective Glycosylation Reactions of a Pseudaminic Acid Donor: Importance of the Side-Chain Conformation and Regioselective Reduction of Azide Protecting Groups. *J. Am. Chem. Soc.* **2018,** *140*, 15008-15015.

313. Ovchinnikova, O. G.; Mallette, e.; Koizumi, A.; Lowary, T. L.; Kimber, M. S.; Whitfield, C., Bacterial β-Kdo Glycosyltransferases Represent a New Glycosyltransferase Family (GT99). *Proc. Natl. Acad. Sci.* **2016,** *113*, E3120-E3129.

314. Gagnon, S. M. L.; Meloncelli, P. J.; Zheng, R. B.; Haji-Ghassemi, O.; Johal, A. R.; Borisova, S. N.; Lowary, T. L.; Evans, S. V., High Resolution Structures of the Human ABO(H) Blood Group Enzymes in Complex with Donor Analogs Reveal That the Enzymes Utilize Multiple Donor Conformations to Bind Substrates in a Stepwise Manner. *J. Biol. Chem.* **2015,** *290*, 27040-27052.

315. Quirke, J. C. K.; Crich, D., GH47 and Other Glycoside Hydrolases Catalyze Glycosidic Bond Cleavage with the Assistance of Substrate Super-Arming at the Transition State. *ACS Catal.* **2021,** *11*, 10308-10315.

316. Kuntz, D. A.; Liu, H.; Bols, M.; Rose, D. R., The Role of the Active Site Zn in the Catalytic Mechanism of the GH38 Golgi α-Mannosidase II: Implications from Noeuromycin Inhibition. *Biocatal. Biotransformation* **2006,** *24*, 55-61.

317. Rovira, C.; Males, A.; Davies, G. J.; Williams, S. J., Mannosidase Mechanism: At the Intersection of Conformation and Catalysis. *Curr. Opin. Struct. Biol.* **2020,** *62*, 79-92.

318. Lipscomb, W. N.; Sträter, N., Recent Advances in Zinc Enzymology. *Chem. Rev.* **1996,** *96*, 2375-2434.

319. Mock, W. L.; Freeman, D. J.; Aksamawati, M., Fluxionate Lewis Acidity of the Zn^{2+} Ion in Carboxypeptidase A. *Biochem. J.* **1993,** *289*, 185-193.

320. Kumar, A.; Blakemore, J. D., On the Use of Aqueous Metal-Aqua pKa Values as a Descriptor of Lewis Acidity. *Inorg. Chem.* **2021,** *60*, 1107-1115.

321. Perrin, D. D., *Ionisation Constants of Inorganic Acids and Bases in Aqueous Solution*. Pergamon: 1982.

322. Imberty, A.; Mitchell, E. P.; Wimmerová, M., Structural Basis of High-Affinity Glycan Recognition by Bacterial and Fungal Lectins. *Curr. Opin. Struct. Biol.* **2005,** *15*, 525-534.

323. Zhu, Y.; Suits, M. D. L.; Thompson, A. J.; Chavan, S.; Dinev, Z.; Dumon, C.; Smith, N.; Moremen, K. W.; Xiang, Y.; Siriwardena, A.; Williams, S. J.; Gilbert, H. J.; Davies, G. J., Mechanistic Insights Into a Ca^{2+}-Dependent Family of Alpha-Mannosidases in a Human Gut Symbiont. *Nat. Chem. Biol.* **2010,** *6*, 125-132.

324. Okuyama, M.; Yoshida, T.; Hondoh, H.; Mori, H.; Yao, M.; Kimura, A., Catalytic Role of the Calcium Ion in GH97 Inverting Glycoside Hydrolase. *FEBS Lett.* **2014,** *588*, 3213-3217.

325. Kayakiri, H.; Takase, S.; Shibata, T.; Okamoto, M.; Terano, H.; Hashimoto, M.; Tada, T.; Koda, S., Structure of Kifunensine, A New Immunomodulator Isolated from an Actinomycete. *J. Org. Chem.* **1989,** *54*, 4015-4016.

326. Males, A.; Raich, L.; Williams, S. J.; Rovira, C.; Davies, G. J., Conformational Analysis of the Mannosidase Inhibitor Kifunensine: A Quantum Mechanical and Structural Approach. *ChemBioChem* **2017,** *18*, 1496-1501.

327. Shah, N.; Kuntz, D. A.; Rose, D. R., Comparison of Kifunensine and 1-Deoxymannojirimycin Binding to Class I and II α-Mannosidases Demonstrates Different Saccharide Distortions in Inverting and Retaining Catalytic Mechanisms. *Biochemistry* **2003,** *42*, 13812-13816.

328. Karaveg, K.; Moremen, K. W., Energetics of Substrate Binding and Catalysis by Class 1 (Glycosylhydrolase Family 47) α-Mannosidases Involved in N-Glycan Processing and Endoplasmic Reticulum Quality Control*. *J. Biol. Chem.* **2005,** *280*, 29837-29848.

329. Larsson, A. M.; Bergfors, T.; Dultz, E.; Irwin, D. C.; Roos, A.; Driguez, H.; Wilson, D. B.; Jones, T. A., Crystal Structure of *Thermobifida fusca* Endoglucanase Cel6A in Complex with Substrate and Inhibitor: The Role of Tyrosine Y73 in Substrate Ring Distortion. *Biochemistry* **2005,** *44*, 12915-12922.

330. Pravdić, N.; Danilov, B.; Fletcher, H. G., The oxidation of partially protected 2-acetamido-2-deoxypyranoses with silver carbonate on celite. *Carbohydr. Res.* **1974,** *36*, 167-180.

331. Zamyatina, A.; Gronow, S.; Oertelt, C.; Puchberger, M.; Brade, H.; Kosma, P., Efficient Chemical Synthesis of the Two Anomers of ADP-L-glycero- and D-glycero-D-manno-Heptopyranose Allows the Determination of the Substrate Specificities of Bacterial Heptosyltransferases. *Angew. Chem. Int. Ed.* **2000,** *39*, 4150-4153.

332. Gronow, S.; Oertelt, C.; Ervelä, E.; Zamyatina, A.; Kosma, P.; Skurnik, M.; Holst, O., Characterization of the Physiological Substrate for Lipopolysaccharide Heptosyltransferases I and II. *J. Endotoxin Res.* **2001,** *7*, 263-70.

333. Grizot, S.; Salem, M.; Vongsouthi, V.; Durand, L.; Moreau, F.; Dohi, H.; Vincent, S.; Escaich, S.; Ducruix, A., Structure of the *Escherichia coli* Heptosyltransferase WaaC: Binary Complexes with ADP and ADP-2-deoxy-2-fluoro Heptose. *J. Mol. Biol.* **2006,** *363*, 383-394.

334. Gloster, T. M.; Madsen, R.; Davies, G. J., Dissection of Conformationally Restricted Inhibitors Binding to a β-Glucosidase. *ChemBioChem* **2006,** *7*, 738-742.

335. Gloster, T. M.; Meloncelli, P.; Stick, R. V.; Zechel, D.; Vasella, A.; Davies, G. J., Glycosidase Inhibition: An Assessment of the Binding of 18 Putative Transition-State Mimics. *J. Am. Chem. Soc.* **2007,** *129*, 2345-2354.